frontiers | Research Topics

Genetic and epigenetic aspects of non-coding RNAs in physiology and disease

Edited by
Amanda Salviano-Silva, Ticiana D. J. Farias, Angelica Beate Winter Boldt and Gabriel Adelman Cipolla

Published in
Frontiers in Genetics

ISSN 1664-8714
ISBN 978-2-83251-130-5
DOI 10.3389/978-2-83251-130-5

About Frontiers

Frontiers is more than just an open access publisher of scholarly articles: it is a pioneering approach to the world of academia, radically improving the way scholarly research is managed. The grand vision of Frontiers is a world where all people have an equal opportunity to seek, share and generate knowledge. Frontiers provides immediate and permanent online open access to all its publications, but this alone is not enough to realize our grand goals.

Frontiers journal series

The Frontiers journal series is a multi-tier and interdisciplinary set of open-access, online journals, promising a paradigm shift from the current review, selection and dissemination processes in academic publishing. All Frontiers journals are driven by researchers for researchers; therefore, they constitute a service to the scholarly community. At the same time, the *Frontiers journal series* operates on a revolutionary invention, the tiered publishing system, initially addressing specific communities of scholars, and gradually climbing up to broader public understanding, thus serving the interests of the lay society, too.

Dedication to quality

Each Frontiers article is a landmark of the highest quality, thanks to genuinely collaborative interactions between authors and review editors, who include some of the world's best academicians. Research must be certified by peers before entering a stream of knowledge that may eventually reach the public - and shape society; therefore, Frontiers only applies the most rigorous and unbiased reviews. Frontiers revolutionizes research publishing by freely delivering the most outstanding research, evaluated with no bias from both the academic and social point of view. By applying the most advanced information technologies, Frontiers is catapulting scholarly publishing into a new generation.

What are Frontiers Research Topics?

Frontiers Research Topics are very popular trademarks of the *Frontiers journals series*: they are collections of at least ten articles, all centered on a particular subject. With their unique mix of varied contributions from Original Research to Review Articles, Frontiers Research Topics unify the most influential researchers, the latest key findings and historical advances in a hot research area.

Find out more on how to host your own Frontiers Research Topic or contribute to one as an author by contacting the Frontiers editorial office: frontiersin.org/about/contact

Genetic and epigenetic aspects of non-coding RNAs in physiology and disease

Topic editors

Amanda Salviano-Silva — University Medical Center Hamburg-Eppendorf, Germany
Ticiana D. J. Farias — University of Colorado Anschutz Medical Campus, United States
Angelica Beate Winter Boldt — Federal University of Paraná, Brazil
Gabriel Adelman Cipolla — Federal University of Paraná, Brazil

Citation

Salviano-Silva, A., Farias, T. D. J., Boldt, A. B. W., Adelman Cipolla, G., eds. (2023). *Genetic and epigenetic aspects of non-coding RNAs in physiology and disease*. Lausanne: Frontiers Media SA. doi: 10.3389/978-2-83251-130-5

The authors declare that the research was conducted in the absence of any commercial or financial relationships that could be construed as a potential conflict of interest.

Table of contents

frontiers | Frontiers in Genetics

TYPE Editorial
PUBLISHED 09 December 2022
DOI 10.3389/fgene.2022.1078405

OPEN ACCESS

EDITED AND REVIEWED BY
William C. Cho,
QEH, Hong Kong SAR, China

*CORRESPONDENCE
Amanda Salviano-Silva,
a.salvianodasilva@uke.de

†These authors contributed equally to this work and share first authorship

SPECIALTY SECTION
This article was submitted to RNA, a section of the journal Frontiers in Genetics

RECEIVED 24 October 2022
ACCEPTED 02 December 2022
PUBLISHED 09 December 2022

CITATION
Adelman Cipolla G, Farias TD-J, Boldt ABW and Salviano-Silva A (2022), Editorial: Genetic and epigenetic aspects of non-coding RNAs in physiology and disease.
Front. Genet. 13:1078405.
doi: 10.3389/fgene.2022.1078405

Editorial: Genetic and epigenetic aspects of non-coding RNAs in physiology and disease

Gabriel Adelman Cipolla[1†], Ticiana D. -J. Farias[2†], Angelica Beate Winter Boldt[1†] and Amanda Salviano-Silva[3*†]

[1]Department of Genetics, Federal University of Parana, Curitiba, Brazil, [2]Department of Biomedical Informatics, School of Medicine, University of Colorado Anschutz Medical Campus, Aurora, CO, United States, [3]Department of Neurosurgery, University Medical Center Hamburg-Eppendorf, Hamburg, Germany

KEYWORDS

non-coding RNA, miRNA, lncRNA, circRNA, gene expression

Editorial on the Research Topic
Genetic and epigenetic aspects of non-coding RNAs in physiology and disease

The non-coding genomic regions harbor many regulatory sites and genes expressing functional RNAs without protein-coding features, the so-called non-coding RNAs (ncRNAs). Many ncRNAs have important roles in tissue development and homeostasis, and their deregulation has been increasingly associated with pathological conditions. Among the main classes of ncRNAs with regulatory functions, microRNAs (miRNAs) and long non-coding RNAs (lncRNAs) seem to stand out as those most investigated in the pathological context, followed by circular RNAs (circRNAs). Sequence and/or epigenetic status variations have been shown to influence ncRNA gene expression and/or secondary structure, consequently interfering with the expression, availability and/or function of their molecular targets. This Research Topic aimed at stimulating knowledge production on this cutting edge field of investigation, and includes eight original and two review articles exploring the genetic aspects of ncRNAs in physiological states and pathological conditions.

The first article published in this topic reported pioneer information on the levels of ncRNAs in extracellular vesicles (EVs) from anterior pituitary of Duroc swine model obtained by RNA sequencing (RNA-seq) analysis. The authors identified 416 miRNAs, 16,232 lncRNAs, and 495 circRNAs expressed in swine anterior pituitary EVs, predicted signaling pathways and discussed their potential crosstalk with messenger RNAs (mRNAs) as in competing endogenous RNA (ceRNA) networks (Xiong et al.). A second work also focusing on EVs aimed at revealing the profile and predicting the roles of circRNAs in acute ischemic stroke (AIS). To this end, researchers quantified the levels of circRNAs in exosomes obtained from the plasma of individuals after an AIS episode. Compared to controls, they detected differential levels of 198 circRNAs, out of which roughly half were predicted to possess a translational ability and impact focal

adhesion, tight junctions, and endocytosis. In addition, a few circRNAs predicted to take part in molecular pathways relevant for AIS were also proposed as potential biomarkers (Yang et al.). In another study with Brazilian patients, EV-miRNAs previously identified as breast cancer biomarkers in serum (miR-320a and miR-4433b-5p) presented high specificity and sensitivity as cell-free miRNAs and in biopsies. This was also true for lower levels of miR-150-5p and higher levels of miR-142-5p in tissue, according to TCGA. In this work, the researchers finally propose combinations of these four miRNAs to distinguish breast cancer patients from controls (Carvalho et al.). Furthermore, differentially expressed miRNAs enriched in leukemia pathogenesis pathways separate acute lymphoblastic leukemia (ALL) from myeloid leukemia (AML) and control individuals. Upregulated miRNA levels in ALL patients was positively correlated with soluble Human Leukocyte Antigen G molecule (sHLA-G) levels, suggesting the potential post-transcriptional regulation of an immuno-regulatory HLA-G and its role in modifying the immune response to subtypes of leukemia (Almeida et al.).

In their review, Ruffo et al. summarized the main results from RNA-seq studies concerning miRNAs, lncRNAs and circRNAs in neurodegenerative diseases, with a special focus on amyotrophic lateral sclerosis (Ruffo et al.). The second review article within this Research Topic addressed the host-virus molecular battlefield. Specifically, the authors presented an overview of the interplay between host miRNAs and HIV molecules or host genes somehow important in the viral cycle. As this remains an underexplored field, they also reviewed the broader literature for miRNAs that regulate, in the context of different diseases, HIV-associated genes. As discussed by the authors, this may be important to exploit microRNA-regulated pathways as potential therapeutic targets against HIV infection (Chinniah et al.). Also on the topic of human viral infections, the pioneering study by Carvalho-Silva et al. revealed the changes in miRNA levels from plasma of patients in the acute and recovery phases of Zika virus (ZIKV) infection. Interestingly, the authors found most differentially quantified miRNAs with lower levels in the ZIKV acute phase in comparison to the recovery phase or to the absence of infection. They highlight miR-142-3p as an example of a miRNA with lower levels in plasma of patients in the acute phase and with important roles in ZIKV infection or in immune responses (Carvalho-Silva et al.). Importantly, human papillomavirus (HPV) infection is recurrent in penile cancer (PeCa) cases and may downregulate two important tumor-suppressor genes *TP53* and *RB1*. Da Silva et al. observed that miRNAs upregulated in PeCa tumor samples potentially interact with *TP53* and *RB1* mRNAs contributing to their low expression. In addition, differentially expressed miRNAs were found to be located in high-risk HPV16 genotype integration sites of the host's genome, likely influencing the miRNA and target-gene regulation role in cancer pathogenesis (Da Silva et al.). Another cancer with a strong environmental factor is lung cancer. By studying lung squamous cell carcinoma (LUSC) in patients with an undeniable smoking history, Zhang et al. comprehensively analyzed the value of a set of lncRNAs to predict clinical aspects, prognosis, and tumor microenvironment, aiming on optimizing clinical decision making and prompting personalized therapy (Zhang et al.).

Finally, in an RNA-seq analysis of the myocardium tissue of a diabetic cardiomyopathy (DCM) rat model, Xi et al. found 355 lncRNAs and 828 mRNAs to be aberrantly expressed in DCM. Five lncRNAs - including the validated transcript XR_001842089 - were predicted in ceRNA network analysis to have maximum connections with differentially expressed mRNAs, being the AURKB, MELK and CDK1 transcripts their main potential targets in DCM development. According to the authors, these lncRNAs may have clinical relevance for DCM, as they are associated with fibrosis, energy metabolism of cardiac myocytes, and cell proliferation pathways (Xi et al.).

In conclusion, the regulation of gene expression involving ncRNAs in health and disease has a pivotal role in the maintenance of appropriate physiological conditions or sustained inflammation and tumoral processes. Their importance in different diseases cannot be underestimated. However, there is still a long way to firmly establish their causal roles in health and disease, and functional as well as clinical studies are especially needed to confirm their prognostic and diagnostic value. This article collection enables the reader to build new working hypotheses in order to overcome this challenge and achieve a deeper understanding of the physiological/pathological roles of ncRNAs, in addition to their increasing value as accessible biomarkers in different diseases.

Author contributions

All authors listed have made a substantial, direct, and intellectual contribution to the work and approved it for publication.

Conflict of interest

The authors declare that the research was conducted in the absence of any commercial or financial relationships that could be construed as a potential conflict of interest.

Publisher's note

frontiers in Genetics

ORIGINAL RESEARCH
published: 29 November 2021
doi: 10.3389/fgene.2021.772753

An Exploration of Non-Coding RNAs in Extracellular Vesicles Delivered by Swine Anterior Pituitary

*Jiali Xiong[1], Haojie Zhang[2], Bin Zeng[1], Jie Liu[1], Junyi Luo[1], Ting Chen[1], Jiajie Sun[1], Qianyun Xi[1] and Yongliang Zhang[1]**

[1]Guangdong Provincial Key Lab of Agro-Animal Genomics and Molecular Breeding, College of Animal Science, National Engineering Research Center for Breeding Swine Industry, South China Agricultural University, Guangzhou, China, [2]College of Animal Science and Technology, Guangxi University, Nanning, China

Extracellular vesicles are lipid bilayer-delimited particles carrying proteins, lipids, and small RNAs. Previous studies have demonstrated that they had regulatory functions both physiologically and pathologically. However, information remains inadequate on extracellular vesicles from the anterior pituitary, a key endocrine organ in animals and humans. In this study, we separated and identified extracellular vesicles from the anterior pituitary of the Duroc swine model. Total RNA was extracted and RNA-seq was performed, followed by a comprehensive analysis of miRNAs, lncRNAs, and circRNAs. Resultantly, we obtained 416 miRNAs, 16,232 lncRNAs, and 495 circRNAs. Furthermore, GO and KEGG enrichment analysis showed that the ncRNAs in extracellular vesicles may participate in regulating intracellular signal transduction, cellular component organization or biogenesis, small molecule binding, and transferase activity. The cross-talk between them also suggested that they may play an important role in the signaling process and biological regulation. This is the first report of ncRNA data in the anterior pituitary extracellular vesicles from the duroc swine breed, which is a fundamental resource for exploring detailed functions of extracellular vesicles from the anterior pituitary.

Keywords: anterior pituitary extracellular vesicles, miRNA, lncRNA, circRNA, cross-talk

OPEN ACCESS

Edited by:
Amanda Salviano-Silva, University Medical Center Hamburg-Eppendorf, Germany

Reviewed by:
Gabriela Canalli Kretzschmar, Federal University of Paraná, Brazil
Liang Zhang, City University of Hong Kong, Hong Kong SAR, China

****Correspondence:***
Yongliang Zhang
zhangyl@scau.edu.cn

Specialty section:
This article was submitted to RNA, a section of the journal Frontiers in Genetics

Received: *08 September 2021*
Accepted: *01 November 2021*
Published: *29 November 2021*

Citation:
Xiong J, Zhang H, Zeng B, Liu J, Luo J, Chen T, Sun J, Xi Q and Zhang Y (2021) An Exploration of Non-Coding RNAs in Extracellular Vesicles Delivered by Swine Anterior Pituitary. Front. Genet. 12:772753. doi: 10.3389/fgene.2021.772753

INTRODUCTION

The pituitary gland is often regarded as the "master gland", coordinating the complex functions of multiple endocrine glands along with the hypothalamus (Barkhoudarian 2017). The anterior glandular lobe of the pituitary, namely, the anterior pituitary, is a very important organ of the endocrine system that regulates several physiological processes including cell generation cycle, stress response, growth, reproduction, bone metabolism, and lactation (Schally et al., 1977; Weiss et al., 1978; Lin et al., 1983; Rocha et al., 2003; Takeuchi, 2009). It accounts for 80% of the entire pituitary

Abbreviations: ACTH, adrenocorticotropin hormone; ceRNAs, competitive endogenous RNAs; circRNA, circular RNA; FSH, follicle-stimulating hormone; FSHB, follicle stimulating hormone subunit beta; GH, growth hormone; GH1, growth hormone 1; GHR, growth hormone receptor; GNRHR, gonadotropin releasing hormone receptor; GHRHR, growth hormone releasing hormone receptor; GO, Gene ontology; KEGG, Kyoto Encyclopedia of Genes and Genomes; LH, luteinizing hormone: LHB, luteinizing hormone subunit beta; lncRNA, long non-coding RNA; miRNA, microRNA; ncRNA, Non-coding RNA; POMC, proopiomelanocortin; POU1F1, POU class 1 homeobox 1; PRL, prolactin; PRLHR, prolactin releasing hormone receptor; PRLR, prolactin receptor; TSH, thyroid-stimulating hormone.

gland and secretes six major hormones, including growth hormone (GH), prolactin (PRL), adrenocorticotropin hormone (ACTH), thyroid-stimulating hormone (TSH), luteinizing hormone (LH), and follicle-stimulating hormone (FSH), which are crucial to our physiological wellbeing (Nelson 2005; Le Tissier et al., 2012). These hormones target the adrenal gland, liver, bone, thyroid, breast, ovary, and testes, which are themselves regulated by the negative feedback of the hypothalamus and these target organs (Schally et al., 1977; Lin et al., 1983; Barkhoudarian, 2017).

Extracellular vesicles (EVs) are a type of nano-scale vesicles that can be secreted by most eukaryotic cells (van Niel et al., 2018; Jiang et al., 2021). EVs usually have cup- or round-shaped phospholipid bilayers under transmission electron microscopy, and are mainly spherical in body fluids. They are present in various tissues and biological fluids including blood, dendritic cells, lymphocytes, epithelial cells, red blood cells, stem cells, hepatocytes, and various tumor cells (Raposo et al., 1996; Zitvogel et al., 1998; Wolfers et al., 2001; Blanchard et al., 2002; Keller et al., 2006; Cabili et al., 2011; Regev-Rudzki et al., 2013; Han et al., 2016; Ibrahim et al., 2016), carrying a cargo of biological molecules of their origin, including proteins, lipids, mRNAs, microRNAs (miRNAs), long non-coding RNAs (lncRNAs), and circular RNAs (circRNAs) (Zitvogel et al., 1998; Thery et al., 2002; Keller et al., 2006; Koppers-Lalic et al., 2014). Latest data from Exocarta database show that 9,769 proteins, 3,408 mRNAs, and 2,838 miRNAs have been identified in EVs of different cellular origin (http://www.Exocarta.org). EVs were previously considered to be a waste of protein produced during cell metabolism (Johnston, 1992) until researchers found in the 1990s that they have immunoregulatory functions and can be an important cell regulatory factor (Raposo et al., 1996). More and more evidence showed that EVs have multiple functions in intercellular communication, which can be involved in the material transfer, signal transduction, and immune response regulation (Natasha et al., 2014; Pan et al., 2017; Raghu, 2016; Gang et al., 2018). Recently, Zhang et al. reported that pituitary tumor EVs inhibit the growth of pituitary adenoma by transmitting lncRNA H19 (Zhang et al., 2019).

Non-coding RNA (ncRNA) is a variety of functional RNA molecules that would not be translated into proteins. MiRNA is a type of small ncRNA and can negatively regulate the expression of its target gene expression at the post-transcriptional level (Bartel, 2018; Bartel, 2004; Doench et al., 2004). MiRNAs can participate in regulating the development of the pituitary gland (Calin et al., 2002; Bottoni et al., 2005; Amaral et al., 2009; Mao et al., 2010; Zhang et al., 2010; Nemoto et al., 2012; Schneeberger et al., 2012; Choi et al., 2013; Nemoto et al., 2013; Ye et al., 2013; Zhang et al., 2013a; Lannes et al., 2015). LncRNA is another type of ncRNA, defined as transcripts with longer than 200 nucleotides (Esteller, 2011). Researches indicated that lncRNAs play an important part in various biological processes (Li et al., 2015a; Mattick and Rinn 2015) and function in pituitary adenomas and normal anterior pituitary (Chunharojrith et al., 2015; Li et al., 2015b; Han et al., 2017; Fu et al., 2018). CircRNA is a class of single-stranded RNA that forms a covalently closed continuous loop. They were categorized as ncRNA, but more recently, they have been shown to code for proteins and could serve as miRNA sponges and compete with miRNAs to bind target mRNAs (Hansen et al., 2013; Memczak et al., 2013; Pamudurti et al., 2017). Many studies characterize circular RNAs by sorting through vast collections of RNA sequencing data (Salzman et al., 2012; Jeck et al., 2013; Memczak et al., 2013; Boeckel et al., 2015). Recently, Li et al. identified 6,113 circRNAs from the muscle of prenatal and postnatal sheep through RNA-seq (Li et al., 2017b), and some other studies have reported about circRNAs in pituitary adenomas (Liu et al., 2009; Wang et al., 2018).

As an important endocrine organ, there were very limited information about the secretion of EVs in the anterior pituitary gland. In this study, we extracted and identified EVs from the anterior pituitary of Duroc swine breed for the first time, and we also explored its ncRNAs. This study will provide a basis for further exploration of the functions of pituitary EVs.

MATERIALS AND METHODS

Sample Collection and EV Isolation

This study used three healthy male swine (Duroc) at 60 days of age, which were purchased from the Jintuan farm of JIADA GROUP (Zhaoqing, Guangdong, China). An endotracheal tube (30 cm length, 8 mm ID) was used to anesthetize the pigs with isoflurane (4.5% of tidal volume by mask) (Jantzen et al., 2011). Then, the pigs were euthanized by exsanguination under a surgical plane of the isoflurane anesthesia (Laber et al., 2016). The pituitary glands were removed, and the anterior lobe was immediately dissected under sterile conditions, rinsed in phosphate-buffered saline (PBS), and transferred to Hanks' balanced salt solution. The anterior pituitary tissue was cut up into 1 mm^3 pieces and cultured in serum-free Dulbecco's modified Eagle's medium/nutrient mixture F12 (DMEM/F12) (Gibco, US) supplemented with 100 U/ml penicillin and 100 μg/ml streptomycin (Gibco, US). Forty-eight hours later, the conditioned media (CM) was harvested and centrifuged at 300×g for 10 min to pellet debris and cells. The supernatant was transferred to a fresh tube, and EVs were isolated using an Exoquick EV Isolation Kit (SBI System Biosciences, CA, United States) according to the manufacturer's instructions as described previously (Chugh et al., 2013; Umezu et al., 2013; Li et al., 2016; Raoof et al., 2018; Tara et al., 2018; Junling et al., 2019; Li et al., 2019; Ling et al., 2019), and the samples were stored at −80°C for use.

Electron Microscopic Analysis of EVs

A drop of EV suspension (about 10 μL) was fixed on a formvar-coated copper grid for 2 min, washed briefly in ultrapure water, negatively stained with 1% uranyl acetate, and observed by transmission electron microscopy (TEM; JEM-2000EX; Jeol, Tokyo, Japan) at an acceleration voltage of 80 kV.

Nanoparticle Trafficking Analysis

The size distribution of EVs was analyzed by tracking particles and sized automatically based on Brownian motion and the

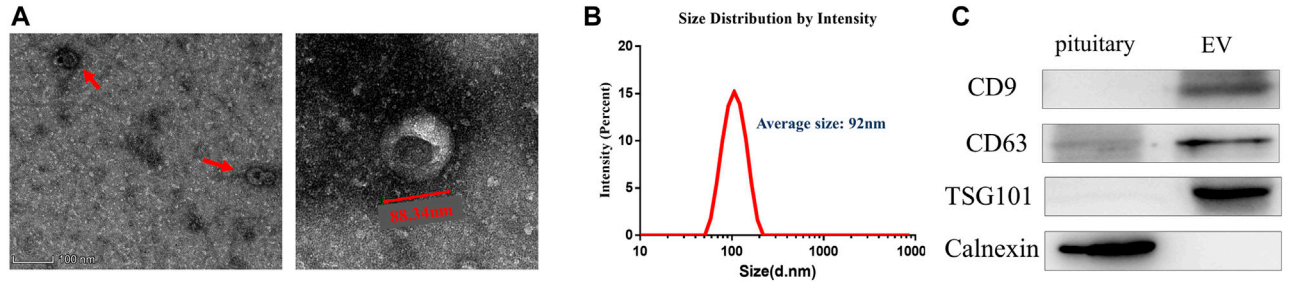

FIGURE 1 | Isolation and identification of EVs from anterior pituitary of Duroc swine. **(A)** Transmission electron microscopy analysis. Wide-field **(left)** and close-up **(right). (B)** Size distribution analysis of EVs. **(C)** EVs confirmed by Western blot with three positive markers CD9, CD63, and TSG101.

diffusion coefficient using Zetasizer (Malvern Panalytical, Malvern, United Kingdom) at 25°C.

BCA Protein Assay, SDS-PAGE, and Western Blot Analyses

Total protein content was assayed using the Pierce BCA Protein Assay Kit (ThermoScientific, Waltham, MA) according to the manufacturer's instructions. The proteins were measured using a FluorChem M Fluorescent Imaging System (ProteinSimple, Santa Clara, CA), separated by SDS-PAGE (10%), and transferred to a polyvinylidene difluoride membrane (Millipore, Billerica, MA). We used three positive markers (CD9, CD63, and TSG101) for Western blots. After blocking with 5% skim milk for 2 h, the membranes were incubated overnight at 4°C with specific antibodies against CD9, CD63 (1:1,000; Sangon Biotech, China), and TSG101 (1:1,000; Zen Biotech, China). We applied horseradish peroxidase–conjugated goat anti-rabbit IgG (H + L; 1:50,000; Jackson ImmunoResearch, West Grove, PA) as a secondary antibody for 1 h at room temperature.

Total RNA Extraction, RNA-Seq Library Preparation, and Sequencing

We extracted total RNA from EV suspension samples using Trizol reagent (Invitrogen, Carlsbad, CA) according to the manufacturer's instruction. RNA quantity and quality were assessed using an RNA 6000 Nano Lab-Chip Kit and Agilent 2,100 Bioanalyzer (Agilent Technologies, Inc., Santa Clara, CA) with RNA integrity number >7.0. A total amount of 3 μg total RNA per sample was used as input material for the small RNA library. Sequencing libraries were generated using NEBNext® Multiplex Small RNA Library Prep Set for Illumina® (NEB, United States). After cluster generation, the library preparations were sequenced on an Illumina Hiseq 2,500/2000 platform and 50 bp single-end reads were generated at the Novogene Bioinformatics Institute (Beijing, China). A total amount of 2 μg RNA per sample was used as input material for the Library preparation for lncRNA sequencing. The libraries were sequenced on an Illumina Hiseq 2,500 platform, and 125 bp paired-end reads were generated. The circRNA in the whole transcriptome project was analyzed in lncRNA sequencing, and no separate library was built.

qRT-PCR

RNA was extracted from EVs using Trizol reagent, and RNA concentration was detected by a spectrophotometer (Nanodrop 2000; Thermo Fisher). Total RNA (1 μg) was reverse-transcribed into cDNA using the PrimeScript™ RT reagent Kit with gDNA Eraser (Takara). U6 was used as control. The 2-ΔΔCT method was applied to determine relative miRNA expression levels.

Sequence Data Analysis

For small RNA sequencing, the workflow is shown in additional **Figure 1A**. Raw reads in fastq format were filtered through custom perl and python scripts at first. Clean reads were obtained by removing reads with poly-N, 5′ adapter contaminants, poly A or T or G or C, those without 3' adapter or the insert tag, and low-quality reads from raw data. Q20, Q30, and GC (Q20 and Q30 are Phred scores, which represent sequencing quality, and GC represents the percentage of bases G and C in the sequencing) content of the clean data were calculated at the same time. High-quality data were used for subsequent analyses. The small RNA tags were mapped to reference sequence by Bowtie (Langmead et al., 2009) without mismatch to analyze their expression and distribution on the reference. Mapped small RNA tags were used for searching known miRNA. Mirbase20.0 was used as reference, and modified software mirdeep2 (Friedlander et al., 2012) and srna-tools-cli (http://srna-tools.cmp.uea.ac.uk/) were used to obtain the potential miRNA and draw secondary structures. The characteristics of the hairpin structure of miRNA precursor can be used to predict novel miRNA. The available software miREvo (Wen et al., 2012) and mirdeep2 (Friedlander et al., 2012) were collaboratively used to predict novel miRNA by analyzing the secondary structure, the Dicer cleavage site, and the minimum free energy of the small RNA tags unannotated in the former steps.

For lncRNA sequencing, the workflow is shown in additional **Figure 1B**. Raw reads in fastq format were firstly processed through in-house perl scripts. Then, we obtained clean reads by removing low-quality reads and those containing adapters and poly-N from the raw data. At the same time, Q20, Q30, and GC content of the clean data were calculated. Index of the reference genome was built using bowtie2 v2.2.8 and paired-end clean reads were aligned to the reference genome using HISAT2 v2.0.4 (Langmead and Salzberg, 2012). The mapped reads of each sample were assembled by StringTie (v1.3.3) in a reference-

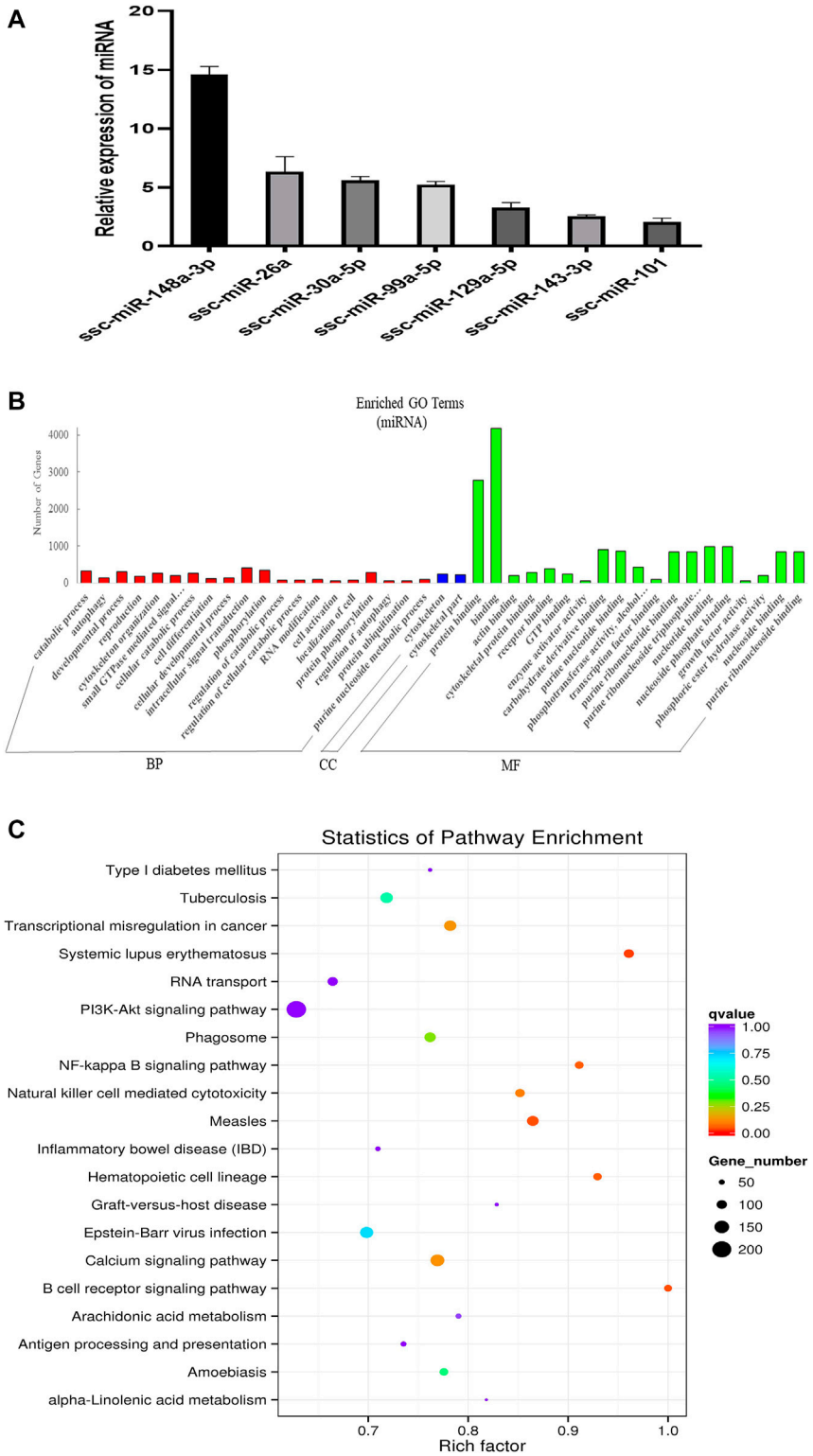

FIGURE 2 | Overview and analysis of small RNA deep sequencing data in EVs. **(A)** Identification of candidate miRNAs. **(B)** Gene ontology (GO) annotation analysis. **(C)** Kyoto Encyclopedia of Genes and Genomes (KEGG) pathway analysis enrichment analysis of miRNA's target genes. BP, biological process; CC, cellular component; MF, molecular function.

based approach (Pertea et al., 2016). After evaluating the quality of original data produced, we set up a series of strict screening conditions according to its structural and functional characteristics based on the results of transcriptome splicing. Through the five steps screening of exon number, transcript length, known transcript annotations, transcript expression, and coding potential. The screened lncRNAs were regarded as the final candidate lncRNA set for subsequent analysis. Then, we use three types of coding potential analysis software, CNCI (Sun et al., 2013), CPC2 (Kang et al., 2017), and Pfam-scan (Punta et al., 2012), to distinguish lncRNA from mRNA. The intersecting results of each software were defined, and those that were determined to be noncoding were designated as candidate lncRNA. We used Cufflink (v2.1.1) to calculate fragments per kilobase million (FPKM) for both lncRNA and coding genes (Trapnell et al., 2010). The transcript expression levels (FPKM value) were expressed as fragments per kilobase of transcript per million mapped reads values. For circRNA sequencing, the workflow is also shown in additional **Figure 1B**. Quality control was carried out with the same procedures at first. Reference genome and gene model annotation files were downloaded from the genome website (NCBI Datasets) directly. Index of the reference genome was built using bowtie2 v2.2.8, and paired-end clean reads were aligned to the reference genome using Bowtie (Langmead et al., 2009). The circRNAs were detected and identified using find_circ (Memczak et al., 2013) and CIRI2 (Gao et al., 2018). Circos software was used to construct the circos figure, and the raw counts were normalized using TPM (Zhou and Zhang, 2010). We used KOBAS (Mao et al., 2005) software to test the statistical enrichment of the target gene candidates in Kyoto Encyclopedia of Genes and Genomes (KEGG) pathways. On the other hand, using miRanda, we performed ceRNA analysis, screened miRNAs and selected mRNAs, lncRNAs, and circRNAs that potentially target the miRNA and have negative expression correlations. Cytoscape software was used to construct the lncRNA-miRNA-gene and circRNA-miRNA-gene networks.

RESULTS

Isolation and Identification of EVs From Anterior Pituitary of Duroc Swine

EVs were isolated from Duroc swine anterior pituitary (additional **Figure 2**). We detected the purified vesicles using transmission electron microscopy which showed that their size and cup-shaped morphology (**Figure 1A**) are typical characteristics of EVs. Then, we used Zetasizer to analyze their size distribution and found that the vesicles' average size was about 92 nm (**Figure 1B**). EVs were further confirmed by Western blot with positive common surface markers CD9, CD63, and TSG101 (**Figure 1C**).

Overview and analysis of small RNA deep sequencing data in EVs

In order to explore the ncRNA expression profiles of the EVs, we used RNA-seq analyses to characterize the ncRNA from normal anterior of three 60-day-old Duroc swine. We obtained 12778982 (EV_1), 15668033 (EV_2), and 15353011 (EV_3) clean reads that were screened from small RNA (sRNA) for subsequent analysis after quality evaluation (additional file 1: **Supplementary Table S1**). Meanwhile, the length distribution of the obtained total sRNA fragments were analyzed (additional **Figure 3**). In general, sRNAs ranged from 18 to 35 nt in length and the majority of the miRNA reads were about 22 nt. A total of 416 miRNAs were obtained from samples, 343 of which are known miRNAs and 73 are newly predicted miRNAs (additional file 2: **Supplementary Table S2**). Of these known miRNAs, 61 miRNAs were highly expressed (1,000 < average signals ≤ 10,000), and, in particular, 46 miRNAs were extremely highly expressed in EVs (average signals ≥10,000). We randomly selected a few candidate highly expressed miRNAs, and their relative expression levels were consistent with the sequencing results (**Figure 2A**). To further characterize the regulatory roles of miRNAs in the anterior pituitary EVs, miRNA target prediction, Gene Ontology (GO), and Kyoto Encyclopedia of Genes and Genomes (KEGG) annotation analyses were performed. A total of 25,516 target genes for the 416 miRNAs were predicted. Our GO annotation indicated that these predicted target genes were significantly enriched in intracellular signal transduction, phosphorylation, catabolic process, developmental process, the component of cytoskeletal part, binding, protein binding, and nucleotide-binding (**Figure 2B**). The KEGG pathway analysis results revealed that the genes were associated with several pathways, including NF-kappa B signaling pathway, Calcium signaling pathway and B cell receptor signaling pathway (**Figure 2C**). These findings suggest that miRNA in anterior pituitary EVs may be involved in regulating intracellular signal transduction and immune metabolism.

Overview and bioinformatics analysis of lncRNA deep sequencing data in EVs

LncRNA is a class of RNA molecules with transcript lengths over 200 nt and does not encode proteins. We set the filter criteria according to its characteristics and counted the number of transcripts screened per step (additional **Figure 4A**). For lncRNA prediction, CPC and CNCI were used for potential coding ability detection, and PFAM, a protein database, was used for protein annotation information analysis and potential coding ability detection (additional **Figure 4B**). Resultantly, 15,545 novel lncRNAs and 687 annotated lncRNAs (additional file 3: **Supplementary Table S3**) were identified respectively. We classified different types of lncRNA (lincRNA, anti-sense_lncRNA, and intronic_lncRNA), and results showed that the percentage of intronic_lncRNA was the highest (**Figure 3A**). The structure and sequence conservation of lncRNAs and mRNAs were also compared and analyzed. We found that lncRNAs were shorter in length in the transcript (additional **Figure 4C**) and their genes tended to contain fewer exons (**Figure 3B**). Most of the mRNAs had longer open reading frames than lncRNAs (additional **Figure 4D**). The transcript expression levels of lncRNAs were higher than that of mRNAs (additional **Figure 4E**), and we also got the same perception by comparing the FPKM of EVs from the different samples (additional **Figure 4F**). We investigated the possible functions

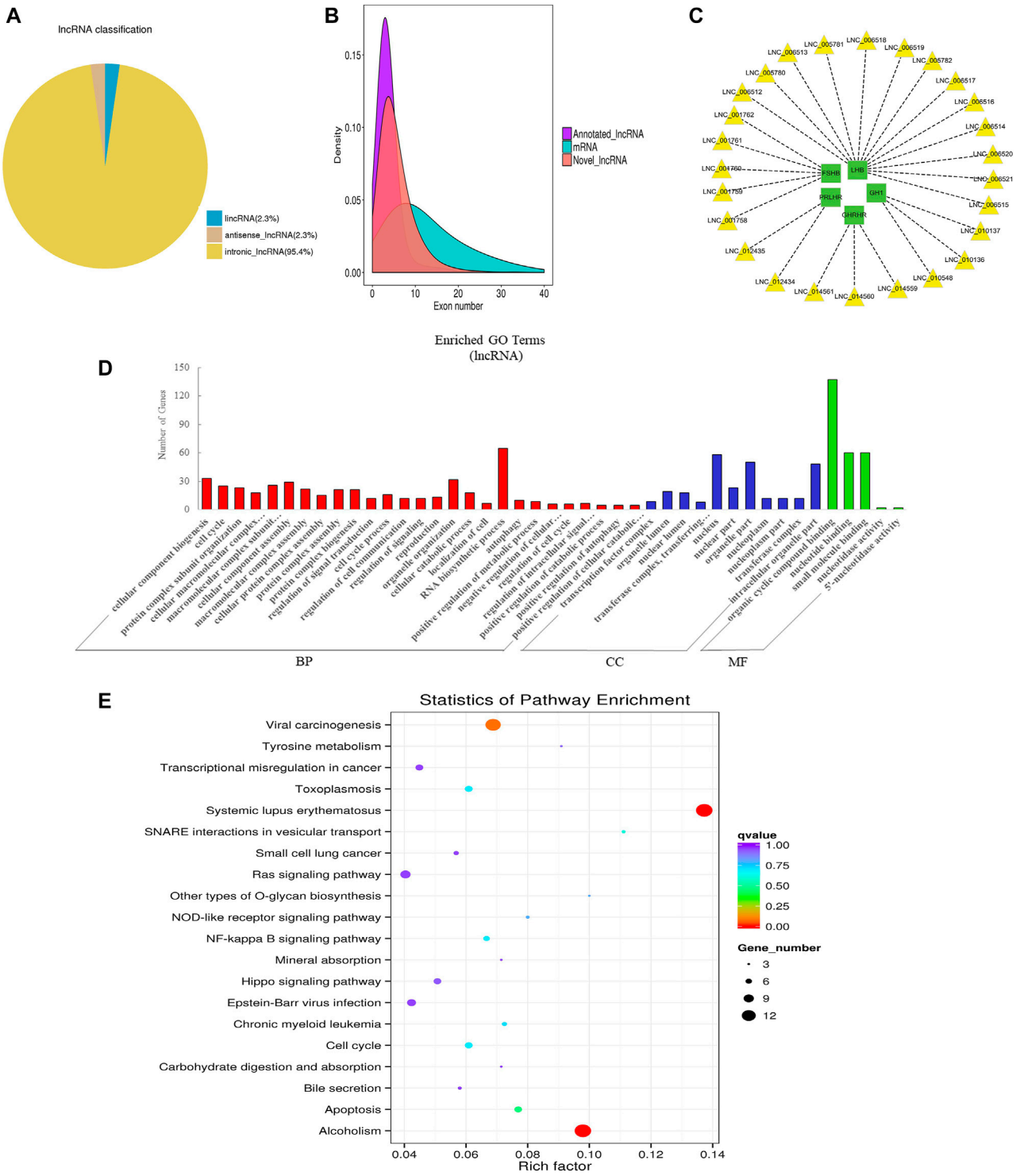

FIGURE 3 | Overview and bioinformatics analysis of lncRNA deep sequencing data in EVs. **(A)** LncRNA type distribution map. **(B)** Number density map of LncRNA and mRNA exons. **(C)** lncRNA-mRNA co-expression (green and yellow represent genes and lncRNAs respectively). **(D)** GO annotation analysis. **(E)** KEGG pathway analysis enrichment analysis. BP, biological process; CC, cellular component; MF, molecular function.

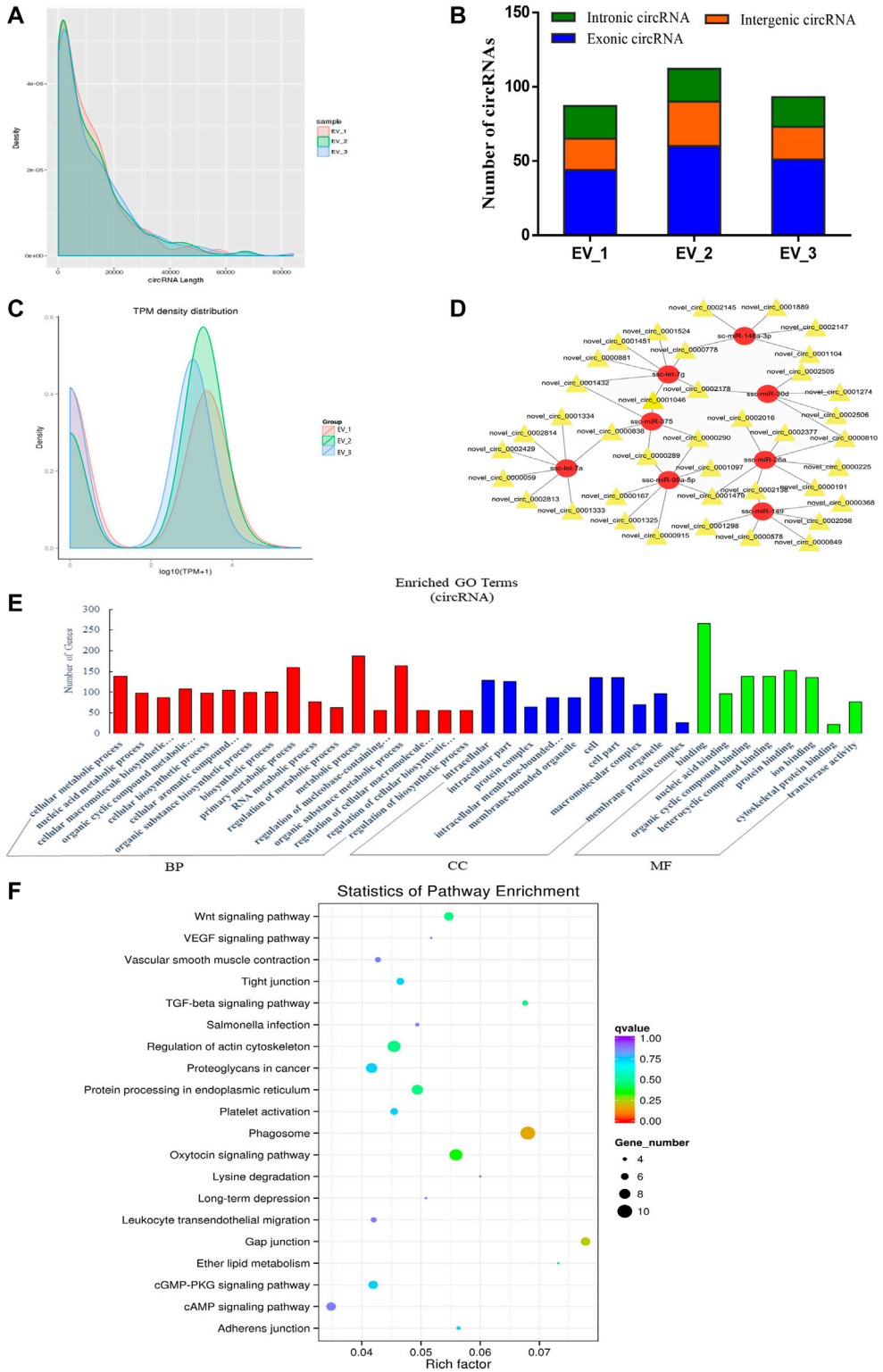

FIGURE 4 | Overview and bioinformatics analysis of circRNA deep sequencing data in EVs. **(A)** The length distribution of circRNAs for all samples. **(B)** The source of circRNAs for all samples, showing the numbers of exonic, intronic and intergenic circRNAs of each sample. **(C)** TPM density map, showing consistency between samples. **(D)** The network of circRNA-miRNA co-expression (red and yellow represent miRNA and circRNA respectively). **(E)** GO annotation analysis **(F)** KEGG pathway analysis enrichment analysis. BP, biological process; CC, cellular component; MF, molecular function.

of the lncRNAs by searching for protein-coding genes 100 kb upstream and downstream of all identified lncRNAs to predict the potential *cis*-regulatory targets of lncRNAs (Bao et al., 2018). A total of 16,439 protein-coding genes were predicted for 9,524 lncRNAs. A number of lncRNAs were found to co-express with pituitary-specific genes including growth hormone 1 (*GH1*), growth hormone-releasing hormone receptor (*GHRHR*), prolactin-releasing hormone receptor (*PRLHR*), follicle-stimulating hormone subunit beta (*FSHB*), and luteinizing hormone subunit beta (*LHB*) (**Figure 3C**). Some other lncRNAs co-expressed with genes involved in EVs' marker protein, protein transport, and docking such as *CD63*, *CD81*, *TSG101*, *Rab27A*, *Rab27B*, and *UBL3*. GO annotation indicated that the predicted target genes of lncRNAs were significantly enriched in cellular component biogenesis, organelle organization, RNA biosynthetic process, the cellular component of nucleus and organelle part, organic cyclic compound binding, nucleotide binding, and small molecule binding (**Figure 3D**). KEGG pathway analysis revealed that these genes were associated with Systemic lupus erythematosus, alcoholism, apoptosis, cell cycle, and NF-kappa B signaling pathway (**Figure 3E**). These data indicated that lncRNAs in EVs of the anterior pituitary could participate in the immune regulation and growth process of organisms.

Overview and bioinformatics analysis of circRNA deep sequencing data in EVs

After evaluating the data output quality, we obtained 495 novel circRNAs (additional file 4: **Supplementary Table S4**) and then counted the length distribution and the source of the circRNAs for all samples (**Figure 4A**). It showed that the length of the circRNAs is mostly scattered in a range of less than 10000 nt and the sources of the circRNAs mostly from the intergenic area compared with the exon and intron area (**Figure 4B**). The expression levels of all circRNAs were statistically analyzed and normalized by TPM (**Figure 4C**). TPM density distribution allows overall inspection of gene expression patterns in samples, and the results showed large overlap areas which meant a consistency between samples (Zhou et al., 2010). We then constructed a circRNA-miRNA co-expression network based on the RNA-seq results. CircRNA could inhibit the function of miRNA by combining it with miRNA (Hansen et al., 2013). Therefore, the analysis of miRNA binding sites on the identified circRNAs helps to further study the function of circRNAs. Then, we used miRanda to predict the miRNA binding sites of cleaved circRNAs and eventually focused on those circRNAs that combined with highly expressed miRNAs in the pituitary and EVs from the anterior pituitary. A network map was constructed containing 39 circRNAs, 8 miRNAs, and 49 relationships (**Figure 4D**). In order to explore the potential functions of the circRNAs in EVs from the anterior pituitary, we performed GO and KEGG pathway enrichment analysis. The results showed that the enriched GO terms were mainly associated with metabolic process, cellular biosynthetic process, binding, and transferase activity (**Figure 4E**) and the KEGG pathways were mainly enriched in Phagosome, gap junction, the Wnt signaling pathway, regulation of actin cytoskeleton, and protein processing in endoplasmic reticulum (**Figure 4F**). These findings indicated that circRNAs in EVs of the anterior pituitary could regulate the cellular metabolic and biosynthetic process.

Analysis of crosstalk in lncRNA-miRNA-mRNA relationship in EVs

Recent studies suggested that lncRNAs could function as endogenous miRNA sponges to prevent miRNA from binding to reduce the regulatory effect of miRNAs on their target mRNA (Cai and Cullen, 2007; Wang et al., 2010; Tay et al., 2014). To further analyze the crosstalk between lncRNA, miRNA, and mRNA, we predicted their interaction and further focused on the competitive endogenous RNAs (ceRNAs) relative with pituitary function. A network was drawn with 97 lncRNAs that could sponge 11 miRNAs to regulate 10 pituitary-specific genes including *GH1*, *GHRHR*, *PRLHR*, *FSHB*, *LHB*, proopiomelanocortin (*POMC*), growth hormone receptor (*GHR*), prolactin receptor (*PRLR*), gonadotropin-releasing hormone receptor (*GNRHR*), and POU class 1 homeobox 1 (*POU1F1*) (**Figure 5A**). We also performed GO enrichment analysis, which revealed 273 significantly enriched terms in the categories of biological process, molecular function, and cellular components, and we showed a part of terms with lots of gene numbers (**Figure 5B**). Its annotation indicated that they participated in intracellular signal transduction, cellular component organization or biogenesis, RNA metabolic process, localization, regulation of the metabolic process, binding, and regulation of catalytic activity which suggested that they were involved in the body's basic biological regulation.

Analysis of crosstalk in circRNA-miRNA-mRNA relationship in EVs

The current studies have proved that circRNAs could act as ceRNAs to compete for miRNA-binding sites to affect the function of miRNAs (Hansen et al., 2013; Thomas and Saetrom, 2014). Therefore, the analysis of interactions between miRNAs and circRNAs is helpful for further study. Similarly, we mainly concerned the ceRNAs relative to pituitary function in the constructed potential circRNA–miRNA–mRNA associations. The resultant network was comprised of 188 edges among 11 miRNAs, 58 circRNAs, and 10 pituitary-specific genes including *GH1*, *POMC*, *GHR*, *GHRHR*, *PRLR*, *LHB*, *PRLHR*, *FSHB*, *GNRHR*, and *POU1F1* (**Figure 6A**). For the potential functions of the associated ncRNAs in EVs from the anterior pituitary, we conducted GO enrichment analysis which revealed 265 significantly enriched terms. Some terms enriched a high number of genes (**Figure 6B**). Our GO annotation indicated that they were involved in intracellular signal transduction, cellular component organization or biogenesis, transport, protein binding, hydrolase activity, and phosphotransferase activity. These findings suggested that the network in circRNA-miRNA-mRNA relationship in EVs played an important role in the process of biosynthetic and information transmission.

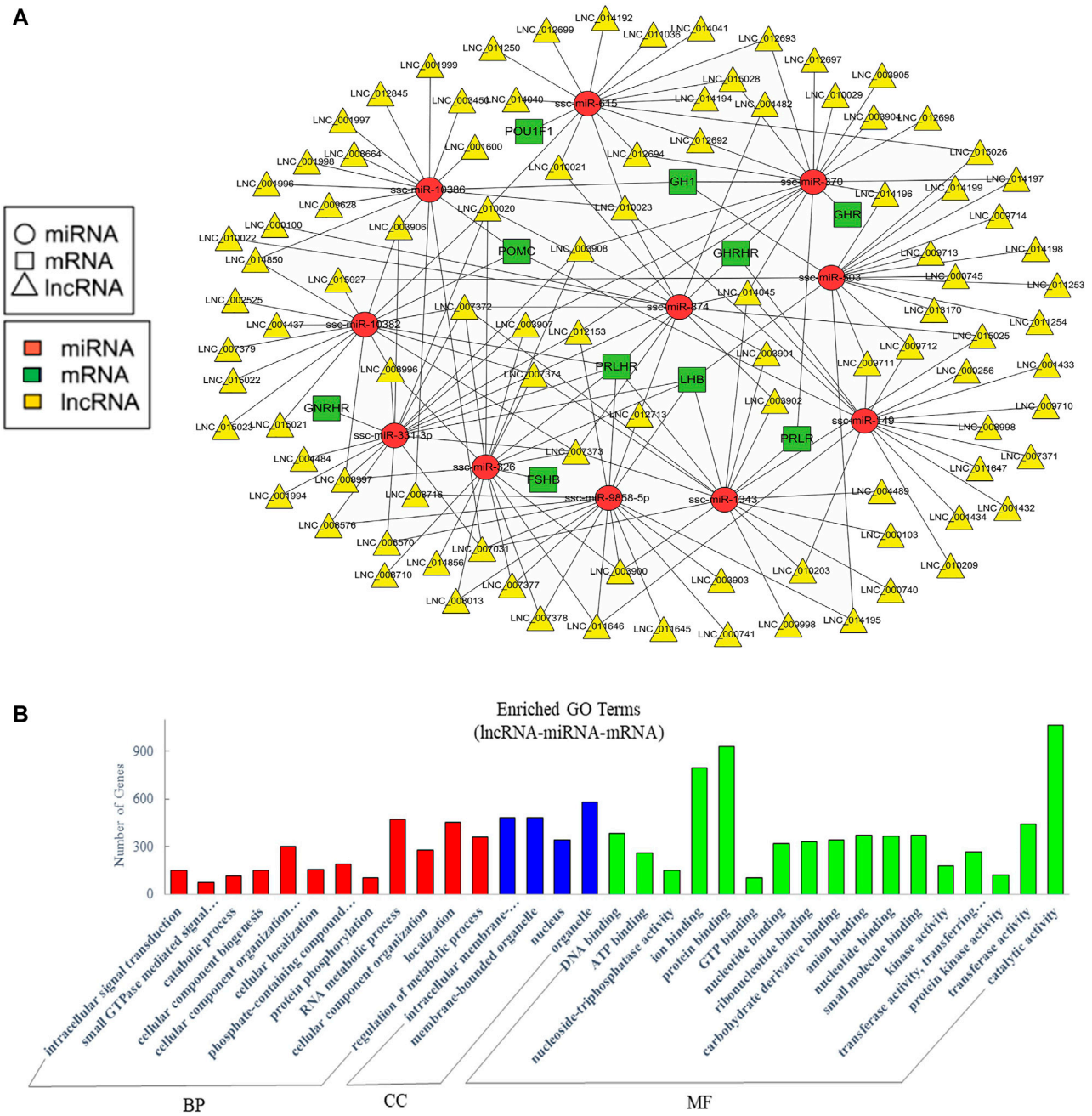

FIGURE 5 | Analysis of crosstalk in lncRNA-miRNA-mRNA relationship in EVs. **(A)** The ceRNA network of lncRNA, miRNA and pituitary-specific genes. **(B)** GO annotation analysis. GO analysis show significantly enriched terms ($p < 0.05$) in the categories of biological process, cellular components, and molecular function. BP, biological process; CC, cellular components; MF, molecular function.

DISCUSSION

EVs contain plentiful cargoes including proteins, lipids, and nucleic acids which are specifically sorted and packaged, and contents packed are cell type-specific (Hessvik and Llorente, 2018). More and more evidence indicated that EVs can transfer important cargoes such as miRNA, mRNA, and proteins from cell to cell *via* membrane vesicle delivery, thereby being a new approach of intracellular or organ-to organ communication (Théry et al., 2002; Mathivanan et al., 2010; Tan et al., 2013; Javeed and Mukhopadhyay, 2017). Studies have reported that EVs can mediate the transmission of information between endothelial cells, smooth muscle cells, cardiomyocytes, stem cells, and fibroblasts (Hergenreider et al., 2012; Bang et al., 2014; Wang et al., 2014). Hepatocyte-derived EVs could act as potential biomarkers of liver disease and

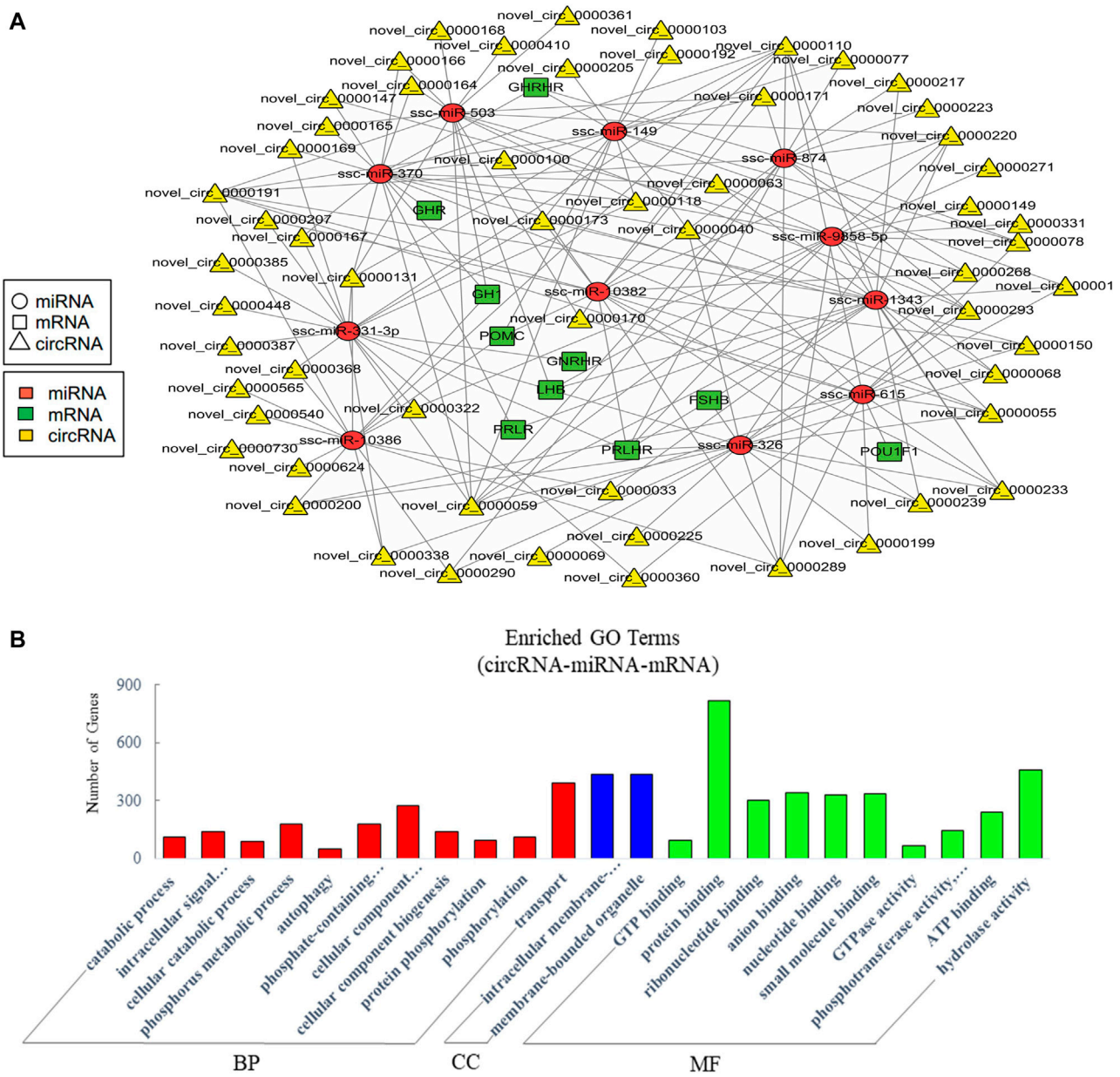

FIGURE 6 | Analysis of crosstalk in circRNA-miRNA-mRNA relationship in EVs. **(A)** The ceRNA network of circRNA, miRNA, and pituitary-specific genes. **(B)** GO annotation analysis, showing significantly enriched terms ($p < 0.05$) in the categories of biological process, cellular components, and molecular function. BP = biological process; CC = cellular components; MF = molecular function.

promote cell proliferation and liver regeneration (Bala et al., 2012; Nojima et al., 2015). EVs secreted by skeletal muscle contain proteins and miRNAs that can be transferred to adjacent muscle cells (Pedersen and Febbraio, 2012). EVs from the adipose tissue could mediate activation of macrophage-induced insulin resistance and are regarded as the main immune regulator secreted by insulin resistance factors (Deng et al., 2009; Kranendonk et al., 2014). As an important endocrine gland, whether the pituitary gland produces EVs and its cargos remains unclear up to date.

Firstly, considering that the pig pituitary is small and difficult to obtain, we used the Exoquick Isolation Kit to isolate the EVs, then identified them using transmission electron microscopy and western blot detection of CD9, CD63, TSG101, and Calnexin, followed by RNA extraction and sequencing. The Venn diagrams of miRNAs, lncRNAs, and circRNAs were drawn through analysis to show the distributions of numbers among three samples (additional **Figure 5**). A total of 416 miRNAs were obtained from samples, 343 of which are known miRNAs and 73 are newly predicted miRNAs. Our research group has revealed

the expression of miRNAs in porcine anterior pituitary cells and found that miRNAs could regulate the hormone secretion from the anterior pituitary (Qi et al., 2015, Ye, et al., Ye et al., 2013). Interestingly, we found most of the top 20 miRNAs such as miR-7, miR-375, let-7a, let-7c, miR-26a, miR-30a, let-7g, miR-30days, miR-127, miR-151, miR-21, miR-149, miR-99a, and miR-143 in EVs are also highly expressed in the porcine pituitary (Yuan et al., 2015). Various studies also revealed several of their enrichment in metabolisms and functions. MiR-7 is abundant in the pituitary of mice (Bak et al., 2008) and pigs (Ye et al., 2015; He et al., 2018). Research showed that miR-7 might play an important role in the hypothalamic–pituitary–gonadal (HPG) axis and be involved in body growth by acting on the pituitary *GHRHR* in pigs (Zhang et al., 2013a; He et al., 2018). MiR-375 could regulate pituitary pro-opiomelanocortin (*POMC*) expression (Zhang et al., 2013b). Let-7f-5p was a highly expressed miRNA of the let-7 family in the pituitary (Wu et al., 2017). Mir-26a plays an important role in cell cycle control by modulating protein kinase C delta (Erica et al., 2013). MiR-200b could stimulate luteinizing hormone (LH) levels by targeting *ZEB1* (Hasuwa et al., 2013). KEGG and GO analysis suggest that miRNAs in EVs of the anterior pituitary could regulate intracellular signal transduction, phosphorylation, catabolism, and development.

CeRNAs regulate gene expression by competitively binding to microRNAs (Salmena et al., 2011). Recent studies have shown that the interaction of the miRNA seed region with mRNA is not unidirectional, but that the pool of mRNAs, lncRNA (Cesana et al., 2011), and circRNA (Hansen, et al., Memczak, et al.) competes for the same library of miRNA to regulate miRNA activity (Tay et al., 2011). These ceRNAs act as molecular sponges for miRNA through their miRNA binding sites to inhibit target genes of the respective miRNA family. Unlike miRNAs, the function of lncRNAs and circRNAs is poorly understood in pig pituitary.

There are a large number of studies that have identified the role of lncRNA in pituitary function. Researches have shown that the anterior pituitary lncRNA of rats plays an important role in hormone and reproduction development and regulation (Han et al., 2017). MIR205HG enabled to regulate the secretion of GH and PRL in anterior pituitary (Du et al., 2019). LncRNA C5orf66-AS1 suppressed the development and invasion of pituitary null cell adenomas (Yu et al., 2017). LncRNA RPSAP52 was verified to act as miRNA sponge to promote cell growth (D'Angelo et al., 2019). In our study, some lncRNAs could co-express with pituitary-specific genes like *GH1*, *GHRHR*, *PRLHR*, *FSHB*, and *LHB*. Some other lncRNAs could co-express with genes involved in EVs' marker protein, protein transport, and docking such as *CD63*, *CD81*, *TSG101*, *Rab27A*, *Rab27B*, and *UBL3*. On the other hand, the signal of a two-circRNA was found to be able to predict tumor recurrence in clinically non-functioning pituitary adenoma (Guo et al., 2019). Another study reported that thousands of sheep genes could express circRNAs in the pituitary gland (Li et al., 2017a). Regarding circRNA, in this article, we determined numerous circRNAs that interact with highly expressed miRNAs both in EVs and the pituitary, participating in the biologic functions of the pituitary gland. Our results suggests that ceRNAs in EVs from the anterior pituitary may take part in the cellular metabolic and biosynthetic process and the cross-talk between mRNA, miRNA, lncRNA, and circRNA may be involved in the regulation of pituitary endocrine functions and signaling process. Since EVs are composed of complicated groups with different size and contents, methods for extraction and purification of them are still in development. The extraction kit used in this study is well accepted nowadays, though it has potential limitations and we will further verify and explore the function of obtained ncRNAs in subsequent research.

On the whole, our study is the first exploration of the expression of ncRNAs in EVs delivered by the anterior pituitary in Duroc swine model. MiRNAs, lncRNAs, and circRNAs of EVs from the anterior pituitary may act as novel regulators of pituitary development and endocrine regulation. These findings provided an insight into EVs derived from the anterior pituitary and are helpful to explore the potential functions of EV cargoes.

DATA AVAILABILITY STATEMENT

The original contributions presented in the study are publicly available in NCBI under accession number PRJNA644768.

ETHICS STATEMENT

The animal study was reviewed and approved by the Institutional Animal Care and Use Committee of South China Agricultural University, China. All animal experimentation complied with the laboratory animal management and welfare regulations approved by the Standing Committee of Guangdong People's Congress (Guangzhou), China. Ethical code number: SCAU-AEC-2010-0416.

AUTHOR CONTRIBUTIONS

YZ, QX, and JS conceived and designed the experiments; JX performed experiments and analyzed the data. HZ, BZ, JL, JL, and TC contributed reagents, materials, and analysis tools. JX wrote the paper. YZ revised the paper. All authors read and approved the final manuscript.

FUNDING

The research was supported by grants from the National Natural Science Foundation of China (31802156, 32072814, 32072812), and the Key Project of Guangdong Provincial Nature Science Foundation (2021A1515011310, 2020A1515010062). The funders had no role in study design, sample collection and analysis, decision to publish, or preparation of the manuscript.

SUPPLEMENTARY MATERIAL

The Supplementary Material for this article can be found online at: https://www.frontiersin.org/articles/10.3389/fgene.2021.772753/full#supplementary-material

REFERENCES

Amaral, F. C., Torres, N., Saggioro, F., Neder, L., Machado, H. R., Silva, W. A., Jr., et al. (2009). Micrornas Differentially Expressed in Acth-Secreting Pituitary Tumors. *J. Clin. Endocrinol. Metab.* 94, 320–323. doi:10.1210/jc.2008-1451

Bak, M., Silahtaroglu, A., Moller, M., Christensen, M., Rath, M. F., Skryabin, B., et al. (2008). Microrna Expression in the Adult Mouse central Nervous System. *RNA* 14, 432–444. doi:10.1261/rna.783108

Bala, S., Petrasek, J., Mundkur, S., Catalano, D., Levin, I., Ward, J., et al. (2012). Circulating Micrornas in Exosomes Indicate Hepatocyte Injury and Inflammation in Alcoholic, Drug-Induced, and Inflammatory Liver Diseases. *Hepatology* 56, 1946–1957. doi:10.1002/hep.25873

Bang, C., Batkai, S., Dangwal, S., Gupta, S. K., Foinquinos, A., Holzmann, A., et al. (2014). Cardiac Fibroblast-Derived Microrna Passenger Strand-Enriched Exosomes Mediate Cardiomyocyte Hypertrophy. *J. Clin. Invest.* 124, 2136–2146. doi:10.1172/jci70577

Bao, Z., Yang, Z., Huang, Z., Zhou, Y., Cui, Q., and Dong, D. (2018). Lncrnadisease 2.0: An Updated Database of Long Non-coding Rna-Associated Diseases. *Nuclc Acids Res.* 47, D1034–D1037. doi:10.1093/nar/gky905:

Barkhoudarian, G., and Kelly, D. F. 2017, The Pituitary Gland: Anatomy, Physiology, and its Function as the Master Gland. *Cushing's Disease*, 1–41. doi:10.1016/b978-0-12-804340-0.00001-2

Bartel, D. P. (2018). Metazoan MicroRNAs. *Cell* 173, 20–51. doi:10.1016/j.cell.2018.03.006

Bartel, D. P. (2004). Micrornas: Genomics, Biogenesis, Mechanism, and Function Cell. *Cell* 116, 281–297. doi:10.1016/s0092-8674(04)00045-5

Blanchard, N., Lankar, D., Faure, F., Regnault, A., Dumont, C., Raposo, G., et al. (2002). TCR Activation of Human T Cells Induces the Production of Exosomes Bearing the TCR/CD3/ζ Complex. *J. Immunol.* 168, 3235–3241. doi:10.4049/jimmunol.168.7.3235

Boeckel, J.-N., Jaé, N., Heumüller, A. W., Chen, W., Boon, R. A., Stellos, K., et al. (2015). Identification and Characterization of Hypoxia-Regulated Endothelial Circular RNA. *Circ. Res.* 117, 884–890. doi:10.1161/circresaha.115.306319

Bottoni, A., Piccin, D., Tagliati, F., Luchin, A., Zatelli, M. C., and degli Uberti, E. C. (2005). Mir-15a and Mir-16-1 Down-Regulation in Pituitary Adenomas. *J. Cel. Physiol.* 204, 280–285. doi:10.1002/jcp.20282

Cabili, M. N., Trapnell, C., Goff, L., Koziol, M., Tazon-Vega, B., Regev, A., et al. (2011). Integrative Annotation of Human Large Intergenic Noncoding Rnas Reveals Global Properties and Specific Subclasses. *Genes Dev.* 25, 1915–1927. doi:10.1101/gad.17446611

Cai, X., and Cullen, B. R. (2007). The Imprinted H19 Noncoding RNA Is a Primary microRNA Precursor. *Rna* 13, 313–316. doi:10.1261/rna.351707

Calin, G. A., Dumitru, C. D., Shimizu, M., Bichi, R., Zupo, S., Noch, E., et al. (2002). Nonlinear Partial Differential Equations and Applications: Frequent Deletions and Down-Regulation of Micro- RNA Genes miR15 and miR16 at 13q14 in Chronic Lymphocytic Leukemia. *Proc. Natl. Acad. Sci.* 99, 15524–15529. doi:10.1073/pnas.242606799

Cesana, M., Cacchiarelli, D., Legnini, I., Santini, T., Sthandier, O., Chinappi, M., et al. (2011). A Long Noncoding RNA Controls Muscle Differentiation by Functioning as a Competing Endogenous RNA. *Cell* 147, 358–369. doi:10.1016/j.cell.2011.09.028

Choi, J.-W., Kang, S.-M., Lee, Y., Hong, S.-H., Sanek, N. A., Young, W. S., et al. (2013). Microrna Profiling in the Mouse Hypothalamus Reveals Oxytocin-Regulating Microrna. *J. Neurochem.* 126, 331–337. doi:10.1111/jnc.12308

Chugh, P. E., Sin, S.-H., Ozgur, S., Henry, D. H., Menezes, P., Griffith, J., et al. (2013). Systemically Circulating Viral and Tumor-Derived Micrornas in Kshv-Associated Malignancies. *Plos Pathog.* 9, e1003484. doi:10.1371/journal.ppat.1003484

Chunharojrith, P., Nakayama, Y., Jiang, X., Kery, R. E., Ma, J., De La Hoz Ulloa, C. S., et al. (2015). Tumor Suppression by Meg3 Lncrna in a Human Pituitary Tumor Derived Cell Line. *Mol. Cell Endocrinol.* 416, 27–35. doi:10.1016/j.mce.2015.08.018

D'Angelo, D., Mussnich, P., Sepe, R., Raia, M., Del Vecchio, L., Cappabianca, P., et al. (2019). Rpsap52 Lncrna Is Overexpressed in Pituitary Tumors and Promotes Cell Proliferation by Acting as Mirna Sponge for Hmga Proteins. *J. Mol. Med. (Berl)* 97, 1019–1032. doi:10.1007/s00109-019-01789-7

Deng, Z.-b., Poliakov, A., Hardy, R. W., Clements, R., Liu, C., Liu, Y., et al. (2009). Adipose Tissue Exosome-like Vesicles Mediate Activation of Macrophage-Induced Insulin Resistance. *Diabetes* 58, 2498–2505. doi:10.2337/db09-0216

Doench, J. G., Peterson, C. P., and Sharp, P. A. (2004). The Functions of Animal Micrornas. *Nature* 431, 350–355. doi:10.1038/nature02871

Du, Q., Hoover, A. R., Dozmorov, I., Raj, P., Khan, S., Molina, E., et al. (2019). Mir205hg Is a Long Noncoding Rna that Regulates Growth Hormone and Prolactin Production in the Anterior Pituitary *Dev. Cell* 49, 618–631.e5. doi:10.1016/j.devcel.2019.03.012

Erica, G., Federico, T., Carlo, F., Daniela, M., Mariella, M., Maria, R. A., et al. (2013). Mir-26a Plays an Important Role in Cell Cycle Regulation in Acth-Secreting Pituitary Adenomas by Modulating Protein Kinase Cλ. *Endocrinology* 154, 690-1700. doi:10.1210/en.2012-2070

Esteller, M. (2011). Non-coding Rnas in Human Disease. *Nat. Rev. Genet.* 12, 861–874. doi:10.1038/nrg3074

Friedländer, M. R., Mackowiak, S. D., Li, N., Chen, W., and Rajewsky, N. (2012). Mirdeep2 Accurately Identifies Known and Hundreds of Novel Microrna Genes in Seven Animal Clades. *Nucleic Acids Res.* 40, 37–52. doi:10.1093/nar/gkr688

Fu, D., Zhang, Y., and Cui, H. (2018). Long noncoding rna ccat2 is activated by e2f1 and exerts oncogenic properties by interacting with pttg1 in pituitary adenomas. *Am. J. Cancer Res.* 8, 245–255.

Gang, C., Huang, A. C, Wei, Z., Gao, Z., Min, W., Wei, X., et al. (2018). Exosomal Pd-L1 Contributes to Immunosuppression and Is Associated with Anti-pd-1 Response. *Nature* 560, 382–386. doi:10.1038/s41586-018-0392-8

Gao, Y., Zhang, J., and Zhao, F. (2018). Circular RNA Identification Based on Multiple Seed Matching. *Circular rna identification based Mult. seed matching Brief Bioinform* 19, 803–810. doi:10.1093/bib/bbx014

Guo, J., Wang, Z., Miao, Y., Shen, Y., Li, M., Gong, L., et al. (2019). A two-circRNA S-ignature P-redicts T-umour R-ecurrence in C-linical N-on-functioning P-ituitary A-denoma. *Oncol. Rep.* 41, 113–124. doi:10.3892/or.2018.6851

Han, C., Sun, X., Liu, L., Jiang, H. Y., Shen, Y., Xu, X. Y., et al. (2016). Exosomes and Their Therapeutic Potentials of Stem Cells. *Stem Cells. Inter.* 2016, 1-11. doi:10.1155/2016/7653489

Han, D.-X., Sun, X.-L., Fu, Y., Wang, C.-J., Liu, J.-B., Jiang, H., et al. (2017). Identification of Long Non-coding Rnas in the Immature and Mature Rat Anterior Pituitary. *Sci. Rep.* 7, 17780. doi:10.1038/s41598-017-17996-6

Hansen, T. B., Jensen, T. I., Clausen, B. H., Bramsen, J. B., Finsen, B., Damgaard, C. K., et al. (2013). Natural Rna Circles Function as Efficient Microrna Sponges. *Nature* 495, 384–388. doi:10.1038/nature11993

Hasuwa, H., Ueda, J., Ikawa, M., and Okabe, M. (2013). Mir-200b and Mir-429 Function in Mouse Ovulation and Are Essential for Female Fertility. *Science* 341, 71–73. doi:10.1126/science.1237999

He, J., Zhang, J., Wang, Y., Liu, W., Gou, K., Liu, Z., et al. (2018). Mir-7 Mediates the Zearalenone Signaling Pathway Regulating Fsh Synthesis and Secretion by Targeting Fos in Female Pigs. *Endocrinology* 159, 2993–3006. doi:10.1210/en.2018-00097

Hergenreider, E., Heydt, S., Tréguer, K., Boettger, T., Horrevoets, A. J. G., Zeiher, A. M., et al. (2012). Atheroprotective Communication between Endothelial Cells and Smooth Muscle Cells through Mirnas. *Nat. Cell Biol* 14, 249–256. doi:10.1038/ncb2441

Hessvik, N. P., and Llorente, A. (2018). Current Knowledge on Exosome Biogenesis and Release. *Cell. Mol. Life Sci.* 75, 193–208. doi:10.1007/s00018-017-2595-9

Ibrahim, S. H., Hirsova, P., Tomita, K., Bronk, S. F., Werneburg, N. W., Harrison, S. A., et al. (2016). Mixed Lineage Kinase 3 Mediates Release of C-X-C Motif Ligand 10-bearing Chemotactic Extracellular Vesicles from Lipotoxic Hepatocytes. *Hepatology* 63, 731–744. doi:10.1002/hep.28252

Jantzen, A. E., Lane, W. O., Gage, S. M., Haseltine, J. M., Galinat, L. J., Jamiolkowski, R. M., et al. (2011). Autologous Endothelial Progenitor Cell-Seeding Technology and Biocompatibility Testing for Cardiovascular Devices in Large Animal Model. *J. Vis. Exp.* 55, e3197. doi:10.3791/3197

Javeed, N., and Mukhopadhyay, D. (2017). Exosomes and Their Role in the Micro-/macro-environment:A Comprehensive Review. *J. Biomed. Res.* 31, 386. doi:10.7555/jbr.30.20150162

Jeck, W. R., Sorrentino, J. A., Wang, K., Slevin, M. K., Burd, C. E., Liu, J., et al. (2013). Circular Rnas Are Abundant, Conserved, and Associated with Alu Repeats. *RNA* 19, 141–157. doi:10.1261/rna.035667.112

Jiang, X., You, L., Zhang, Z., Cui, X., Zhong, H., Sun, X., et al. (2021). Biological Properties of Milk-Derived Extracellular Vesicles and Their Physiological Functions in Infant. *Front. Cell Dev. Biol.* 9, 693534. doi:10.3389/fcell.2021.693534

Johnstone, R. M. (1992). Maturation of Reticulocytes: Formation of Exosomes as a Mechanism for Shedding Membrane Proteins. *Biochem. Cell Biol.* 70, 179–190. doi:10.1139/o92-028

Kang, Y.-J., Yang, D.-C., Kong, L., Hou, M., Meng, Y.-Q., Wei, L., et al. (2017). Cpc2: A Fast and Accurate Coding Potential Calculator Based on Sequence Intrinsic Features. *Nucleic Acids Res.* 45, W12–W16. doi:10.1093/nar/gkx428

Keller, S., Sanderson, M. P., Stoeck, A., and Altevogt, P. (2006). Exosomes: From Biogenesis and Secretion to Biological Function. *Immunol. Lett.* 107, 102–108. doi:10.1016/j.imlet.2006.09.005

Koppers-Lalic, D., Hackenberg, M., Bijnsdorp, I. V., van Eijndhoven, M. A. J., Sadek, P., Sie, D., et al. (2014). Nontemplated Nucleotide Additions Distinguish the Small RNA Composition in Cells from Exosomes. *Cell Rep.* 8, 1649–1658. doi:10.1016/j.celrep.2014.08.027

Kranendonk, M. E. G., Visseren, F. L. J., van Balkom, B. W. M., Nolte-'t Hoen, E. N. M., van Herwaarden, J. A., de Jager, W., et al. (2014). Human Adipocyte Extracellular Vesicles in Reciprocal Signaling between Adipocytes and Macrophages. *Obesity* 22, 1296–1308. doi:10.1002/oby.20679

Laber, K., Newcomer, C. E., Decelle, T., Everitt, J. I., Guillen, J., and Brønstad, A. (2016). Recommendations for Addressing Harm-Benefit Analysis and Implementation in Ethical Evaluation - Report from the Aalas-Felasa Working Group on Harm-Benefit Analysis - Part 2. *Lab. Anim.* 50, 21–42. doi:10.1177/0023677216642397

Langmead, B., and Salzberg, S. L. (2012). Fast Gapped-Read Alignment with Bowtie 2. *Nat. Methods* 9, 357–359. doi:10.1038/nmeth.1923

Langmead, B., Trapnell, C., Pop, M., and Salzberg, S. L. (2009). Ultrafast and Memory-Efficient Alignment of Short DNA Sequences to the Human Genome. *Genome Biol.* 10, R25. doi:10.1186/gb-2009-10-3-r25

Lannes, J., L'Hôte, D., Garrel, G., Laverrière, J.-N., Cohen-Tannoudji, J., and Quérat, B. (2015). Rapid Communication: A Microrna-132/212 Pathway Mediates Gnrh Activation of Fsh Expression. *Mol. Endocrinol.* 29, 364–372. doi:10.1210/me.2014-1390

Le Tissier, P. R., Hodson, D. J., Lafont, C., Fontanaud, P., Schaeffer, M., and Mollard, P. (2012). Anterior Pituitary Cell Networks. *Front. Neuroendocrinology* 33, 252–266. doi:10.1016/j.yfrne.2012.08.002

Li, C. H., Gao, Y., Wang, S., Xu, F. F., Dai, L. S., Jiang, H., et al. (2015a). Expression Pattern of Jmjd1c in Oocytes and its Impact on Early Embryonic Development. *Genet. Mol. Res.* 14, 18249–18258. doi:10.4238/2015.december.23.12

Li, C., Li, X., Ma, Q., Zhang, X., Cao, Y., Yao, Y., et al. (2017a). Genome-wide Analysis of Circular Rnas in Prenatal and Postnatal Pituitary Glands of Sheep. *Sci. Rep.* 7, 16143. doi:10.1038/s41598-017-16344-y

Li, C., Li, X., Yao, Y., Ma, Q., Ni, W., Zhang, X., et al. (2017b). Genome-wide Analysis of Circular RNAs in Prenatal and Postnatal Muscle of Sheep. *Oncotarget* 8, 97165–97177. doi:10.18632/oncotarget.21835

Li, L., Cao, B., Liang, X., Lu, S., Luo, H., Wang, Z., et al. (2019). Microenvironmental Oxygen Pressure Orchestrates an Anti- and Pro-tumoral γδ T Cell Equilibrium via Tumor-Derived Exosomes. *Oncogene* 38, 2830–2843. doi:10.1038/s41388-018-0627-z

Li, L., Li, C., Wang, S., Wang, Z., Jiang, J., Wang, W., et al. (2016). Exosomes Derived from Hypoxic Oral Squamous Cell Carcinoma Cells Deliver miR-21 to Normoxic Cells to Elicit a Prometastatic Phenotype. *Cancer Res.* 76, 1770–1780. doi:10.1158/0008-5472.can-15-1625

Li, L., Lu, S., Liang, X., Cao, B., Wang, S., Jiang, J., et al. (2019). Γδtdes: An Efficient Delivery System for Mir-138 with Anti-tumoral and Immunostimulatory Roles on Oral Squamous Cell Carcinoma. *Mol. Thera. - Nuc. Acids.* 14, 101-113. doi:10.1016/j.omtn.2018.11.009

Li, Z., Li, C., Liu, C., Yu, S., and Zhang, Y. (2015b). Expression of the Long Non-coding RNAs MEG3, HOTAIR, and MALAT-1 in Non-functioning Pituitary Adenomas and Their Relationship to Tumor Behavior. *Pituitary* 18, 42–47. doi:10.1007/s11102-014-0554-0

Lin, M. T., Ho, L. T., and Uang, W. N. (1983). Effects of Anterior Pituitary Hormones and Their Releasing Hormones on Physiological and Behavioral Functions in Rats. *J. Steroid Biochem.* 19, 433–438. doi:10.1016/b978-0-08-030771-8.50062-0

Liu, Z., Liu, Y., Fang, W., Chen, W., Li, C., and Xiao, Z. (2009). Establishment of Differential Expression Profiles from Invasive and Non-invasive Pituitary Adenomas. 34: 569–575.

Mao, X., Cai, T., Olyarchuk, J. G., and Wei, L. (2005). Automated Genome Annotation and Pathway Identification Using the Kegg Orthology (Ko) as a Controlled Vocabulary. *Bioinformatics* 21, 3787–3793. doi:10.1093/bioinformatics/bti430

Mao, Z.-G., He, D.-S., Zhou, J., Yao, B., Xiao, W.-W., Chen, C.-H., et al. (2010). Differential Expression of Micrornas in Gh-Secreting Pituitary Adenomas. *Diagn. Pathol.* 5, 79. doi:10.1186/1746-1596-5-79

Mathivanan, S., Ji, H., and Simpson, R. J. (2010). Exosomes: Extracellular Organelles Important in Intercellular Communication. *J. Proteomics* 73, 1907–1920. doi:10.1016/j.jprot.2010.06.006

Mattick, J. S., and Rinn, J. L. (2015). Discovery and Annotation of Long Noncoding Rnas. *Nat. Struct. Mol. Biol.* 22, 5–7. doi:10.1038/nsmb.2942

Memczak, S., Jens, M., Elefsinioti, A., Torti, F., Krueger, J., Rybak, A., et al. (2013). Circular Rnas Are a Large Class of Animal Rnas with Regulatory Potency. *Nature* 495, 333–338. doi:10.1038/nature11928

Natasha, G., Gundogan, B., Tan, A., Farhatnia, Y., Wu, W., Rajadas, J., et al. (2014). Exosomes as Immunotheranostic Nanoparticles. *Clin. Ther.* 36, 820–829. doi:10.1016/j.clinthera.2014.04.019

Nelson, R. J. (2005). *An Introduction to Behavioral Endocrinology. An Introduction to Behavioral Endocrinology*. Massachusetts, US: Sinauer Associates.

Nemoto, T., Mano, A., and Shibasaki, T. (2012). Increased Expression of Mir-325-3p by Urocortin 2 and its Involvement in Stress-Induced Suppression of Lh Secretion in Rat Pituitary. *Am. J. Physiology-Endocrinology Metab.* 302, E781–E787. doi:10.1152/ajpendo.00616.2011

Nemoto, T., Mano, A., and Shibasaki, T. (2013). Mir-449a Contributes to Glucocorticoid-Induced Crf-R1 Downregulation in the Pituitary during Stress. *Mol. Endocrinol.* 27, 1593–1602. doi:10.1210/me.2012-1357

Nojima, H., Freeman, C. M., Schuster, R. M., Japtok, L., Kleuser, B., Edwards, M. J., et al. (2015). Hepatocyte Exosomes Mediate Liver Repair and Regeneration via Sphingosine-1-Phosphate. *J. Hepatol.*, S0168827815005310.

Nordgren, T. M., Heires, A. J., Zempleni, J., Swanson, B. J., Wichman, C., and Romberger, D. J. (2018). Bovine Milk-Derived Extracellular Vesicles Enhance Inflammation and Promote M1 Polarization Following Agricultural Dust Exposure in Mice. *J. Nutr. Biochem.* 64, 110–120. doi:10.1016/j.jnutbio.2018.10.017

Pamudurti, N. R., Bartok, O., Jens, M., Ashwal-Fluss, R., Stottmeister, C., Ruhe, L., et al. (2017). Translation circrnas *Mol. Cell* 66, 9–21. doi:10.1016/j.molcel.2017.02.021

Pan, L., Liang, W., Fu, M., Huang, Z.-h., Li, X., Zhang, W., et al. (2017). Exosomes-mediated Transfer of Long Noncoding Rna Zfas1 Promotes Gastric Cancer Progression. *J. Cancer Res. Clin. Oncol.* 143, 991–1004. doi:10.1007/s00432-017-2361-2

Pedersen, B. K., and Febbraio, M. A. (2012). Muscles, Exercise and Obesity: Skeletal Muscle as a Secretory Organ. *Nat. Rev. Endocrinol.* 8, 457–465. doi:10.1038/nrendo.2012.49

Pertea, M., Kim, D., Pertea, G. M., Leek, J. T., and Salzberg, S. L. (2016). Transcript-level Expression Analysis of RNA-Seq Experiments with HISAT, StringTie and Ballgown. *Nat. Protoc.* 11, 1650–1667. doi:10.1038/nprot.2016.095

Punta, M., Coggill, P. C., Eberhardt, R. Y., Mistry, J., Tate, J., Boursnell, C., et al. (2012). The Pfam Protein Families Database. *Nucleic Acids Res.* 40, D290–D301. doi:10.1093/nar/gkr1065

Qi, Q.-E., Xi, Q.-Y., Ye, R.-S., Chen, T., Cheng, X., Li, C.-Y., et al. (2015). Alteration of the miRNA Expression Profile in Male Porcine Anterior Pituitary Cells in Response to GHRH and CST and Analysis of the Potential Roles for miRNAs in Regulating GH. *Growth Horm. IGF Res.* 25, 66–74. doi:10.1016/j.ghir.2014.12.002

Raghu, K. (2016). The Biology and Function of Exosomes in Cancer. *J. Clin. Invest.* 126, 1208–1215. doi:10.1172/JCI81135

Raoof, R., Bauer, S., El Naggar, H., Connolly, N. M. C., Brennan, G. P., Brindley, E., et al. (2018). Dual-center, Dual-Platform Microrna Profiling Identifies Potential Plasma Biomarkers of Adult Temporal Lobe Epilepsy. *EBioMedicine* 38, 127–141. doi:10.1016/j.ebiom.2018.10.068

Raposo, G., Nijman, H. W., Stoorvogel, W., Liejendekker, R., Harding, C. V., Melief, C. J., et al. (1996). B Lymphocytes Secrete Antigen-Presenting Vesicles. *J. Exp. Med.* 183, 1161–1172. doi:10.1084/jem.183.3.1161

Regev-Rudzki, N., Wilson, D. W., Carvalho, T. G., Sisquella, X., Coleman, B. M., Rug, M., et al. (2013). Cell-Cell Communication between Malaria-Infected Red Blood Cells via Exosome-like Vesicles. *Cell* 153, 1120–1133. doi:10.1016/j.cell.2013.04.029

Rocha, K. t. M., Forti, F. b. L., Lepique, A. P., and Armelin, H. A. (2003). Deconstructing the Molecular Mechanisms of Cell Cycle Control in a Mouse Adrenocortical Cell Line: Roles of ACTH. *Microsc. Res. Tech.* 61, 268–274. doi:10.1002/jemt.10336

Salmena, L., Poliseno, L., Tay, Y., Kats, L., and Pandolfi, P. P. (2011). A Cerna Hypothesis: The Rosetta Stone of a Hidden Rna Language? *Cell* 146, 353–358. doi:10.1016/j.cell.2011.07.014

Salzman, J., Gawad, C., Wang, P. L., Lacayo, N., and Brown, P. O. (2012). Circular Rnas Are the Predominant Transcript Isoform from Hundreds of Human Genes in Diverse Cell Types. *PLoS One* 7, e30733. doi:10.1371/journal.pone.0030733

Schally, A. V., Kastin, A. J., and Arimura, A. (1977). Hypothalamic Hormones: The Link between Brain and Body.

Schneeberger, M., Altirriba, J., García, A., Esteban, Y., Castaño, C., García-Lavandeira, M., et al. (2012). Deletion of miRNA Processing Enzyme Dicer in POMC-Expressing Cells Leads to Pituitary Dysfunction, Neurodegeneration and Development of Obesity. *Mol. Metab.* 2, 74–85. doi:10.1016/j.molmet.2012.10.001

Sun, L., Luo, H., Bu, D., Zhao, G., Yu, K., Zhang, C., et al. (2013). Utilizing Sequence Intrinsic Composition to Classify Protein-Coding and Long Non-coding Transcripts. *Nucleic Acids Res.* 41, e166. doi:10.1093/nar/gkt646

Takeuchi, Y. (2009). Hormones and Osteoporosis Update. Possible Roles of Pituitary Hormones, TSH and FSH, for Bone Metabolism. *Clin. Calcium* 19, 977–983.

Tan, A., Rajadas, J., and Seifalian, A. M. (2013). Exosomes as Nano-Theranostic Delivery Platforms for Gene Therapy. *Adv. Drug Deliv. Rev.* 65, 357–367. doi:10.1016/j.addr.2012.06.014

Tay, Y., Kats, L., Salmena, L., Weiss, D., Tan, S. M., Ala, U., et al. (2011). Coding-Independent Regulation of the Tumor Suppressor PTEN by Competing Endogenous mRNAs. *Cell* 147, 344–357. doi:10.1016/j.cell.2011.09.029

Tay, Y., Rinn, J., and Pandolfi, P. P. (2014). The Multilayered Complexity of Cerna Crosstalk and Competition. *Nature* 505, 344–352. doi:10.1038/nature12986

Théry, C., Zitvogel, L., and Sebastian, A. (2002). Exosomes: Composition, Biogenesis and Function Nature. *Rev. Immunol.* 28, 569–579. doi:10.1038/nri855

Thomas, L. F., and Sætrom, P. (2014). Circular Rnas Are Depleted of Polymorphisms at Microrna Binding Sites. *Bioinformatics* 30, 2243–2246. doi:10.1093/bioinformatics/btu257

Trapnell, C., Williams, B. A., Pertea, G., Mortazavi, A., Kwan, G., van Baren, M. J., et al. (2010). Transcript Assembly and Quantification by Rna-Seq Reveals Unannotated Transcripts and Isoform Switching during Cell Differentiation. *Nat. Biotechnol.* 28, 511–515. doi:10.1038/nbt.1621

Umezu, T., Ohyashiki, K., Kuroda, M., and Ohyashiki, J. H. (2013). Leukemia Cell to Endothelial Cell Communication via Exosomal miRNAs. *Oncogene* 32, 2747–2755. doi:10.1038/onc.2012.295

van Niel, G., D'Angelo, G., and Raposo, G. (2018). Shedding Light on the Cell Biology of Extracellular Vesicles. *Nat. Rev. Mol. Cell Biol* 19, 213–228. doi:10.1038/nrm.2017.125

Wang, J., Liu, X., Wu, H., Ni, P., Gu, Z., Qiao, Y., et al. (2010). Creb Up-Regulates Long Non-coding Rna, Hulc Expression through Interaction with Microrna-372 in Liver Cancer. *Nucleic Acids Res.* 38, 5366–5383. doi:10.1093/nar/gkq285

Wang, J., Wang, D., Wan, D., Ma, Q., Liu, Q., Li, J., et al. (2018). Circular RNA in Invasive and Recurrent Clinical Nonfunctioning Pituitary Adenomas: Expression Profiles and Bioinformatic Analysis. *World Neurosurg.* 117, e371–e386. doi:10.1016/j.wneu.2018.06.038

Wang, X., Huang, W., Liu, G., Cai, W., Millard, R. W., Wang, Y., et al. (2014). Cardiomyocytes Mediate Anti-angiogenesis in Type 2 Diabetic Rats through the Exosomal Transfer of Mir-320 into Endothelial Cells. *J. Mol. Cell Cardiol.* 74, 139–150. doi:10.1016/j.yjmcc.2014.05.001

Weiss, S., Bergland, R., Page, R., Turpen, C., and Hymer, W. C. (1978). Pituitary Cell Transplants to the Cerebral Ventricles Promote Growth of Hypophysectomized Rats. *Exp. Biol. Med.* 159, 409–413. doi:10.3181/00379727-159-40359

Wen, M., Shen, Y., Shi, S., and Tang, T. (2012). Mirevo: An Integrative Microrna Evolutionary Analysis Platform for Next-Generation Sequencing Experiments. *Bmc Bioinformatics* 13, 140. doi:10.1186/1471-2105-13-140

Wolfers, J., Lozier, A., Raposo, G., Regnault, A., Théry, C., Masurier, C., et al. (2001). Tumor-derived Exosomes Are a Source of Shared Tumor Rejection Antigens for Ctl Cross-Priming. *Nat. Med.* 7, 297–303. doi:10.1038/85438

Wu, N., Zhu, Q., Chen, B., Gao, J., Xu, Z., and Li, D. (2017). High-throughput Sequencing of Pituitary and Hypothalamic Microrna Transcriptome Associated with High Rate of Egg Production. *BMC Genomics* 18, 255. doi:10.1186/s12864-017-3644-3

Ye, R.-S., Li, M., Qi, Q.-E., Cheng, X., Chen, T., Li, C.-Y., et al. (2015). Comparative Anterior Pituitary Mirna and Mrna Expression Profiles of Bama Minipigs and Landrace Pigs Reveal Potential Molecular Network Involved in Animal Postnatal Growth. *PLoS One* 10, e0131987. doi:10.1371/journal.pone.0131987

Ye, R. S., Xi, Q. Y., Qi, Q., Cheng, X., Chen, T., Li, H., et al. (2013). Differentially Expressed Mirnas after Gnrh Treatment and Their Potential Roles in Fsh Regulation in Porcine Anterior Pituitary Cell. *Plos One* 8, e57156. doi:10.1371/journal.pone.0057156

Yu, G., Li, C., Xie, W., Wang, Z., Gao, H., Cao, L., et al. (2017). Long Non-coding Rna C5orf66-As1 Is Downregulated in Pituitary Null Cell Adenomas and Is Associated with Their Invasiveness. *Oncol. Rep.* 38, 1140–1148. doi:10.3892/or.2017.5739

Yuan, B., Han, D. X., Dai, L. S., Gao, Y., Ding, Y., Yu, X. F., et al. (2015). A Comprehensive Expression Profile of Micrornas in Rat's Pituitary. *Int. J. Clin. Exp. Med.* 8, 13289–13295.

Zhang, J., Han, X., Zhao, Y., Xue, X., and Fan, S. (2019). Mouse Serum Protects against Total Body Irradiation-Induced Hematopoietic System Injury by Improving the Systemic Environment after Radiation. *Free Radic. Biol. Med.* 131, 382–392. doi:10.1016/j.freeradbiomed.2018.12.021

Zhang, L., Cai, Z., Wei, S., Zhou, H., Zhou, H., Jiang, X., et al. (2013a). Microrna Expression Profiling of the Porcine Developing Hypothalamus and Pituitary Tissue. *Ijms* 14, 20326–20339. doi:10.3390/ijms141020326

Zhang, N., Lin, J.-k., Chen, J., Liu, X.-f., Liu, J.-l., Luo, H.-s., et al. (2013b). Microrna 375 Mediates the Signaling Pathway of Corticotropin-Releasing Factor (Crf) Regulating Pro-opiomelanocortin (Pomc) Expression by Targeting Mitogen-Activated Protein Kinase 8. *J. Biol. Chem.* 288, 10361–10373. doi:10.1074/jbc.m112.425504

Zhang, Y., Liu, Y. T., Tang, H., Xie, W. Q., Yao, H., Gu, W. T., et al. (2019). Exosome-transmitted Lncrna H19 Inhibits the Growth of Pituitary Adenoma. *J. Clin. Endocrinol. Metab.* 104, 6345–6356. doi:10.1210/jc.2019-00536

Zhang, Z., Florez, S., Gutierrez-Hartmann, A., Martin, J. F., and Amendt, B. A. (2010). Micrornas Regulate Pituitary Development, and Microrna 26b Specifically Targets Lymphoid Enhancer Factor 1 (Lef-1), Which Modulates Pituitary Transcription Factor 1 (Pit-1) Expression. *J. Biol. Chem.* 285, 34718–34728. doi:10.1074/jbc.m110.126441

Zhou, L., Chen, J., Li, Z., Li, X., Hu, X., Huang, Y., et al. (2010). Integrated Profiling of Micrornas and Mrnas: Micrornas Located on xq27.3 Associate with clear Cell Renal Cell Carcinoma. *PLoS One* 5, e15224. doi:10.1371/journal.pone.0015224

Zhou, L., and Zhang, Z. (2010). Trusted Channels with Password-Based Authentication and Tpm-Based Attestation. Proceedings of the 2010 International Conference on Communications and Mobile Computing, Shenzhen, China, April 12-14, 2010 (IEEE). doi:10.1109/cmc.2010.232

Zitvogel, L., Regnault, A., Lozier, A., Wolfers, J., Flament, C., Tenza, D., et al. (1998). Eradication of Established Murine Tumors Using a Novel Cell-free Vaccine: Dendritic Cell Derived Exosomes. *Nat. Med.* 4, 594–600. doi:10.1038/nm0598-594

Conflict of Interest: The authors declare that the research was conducted in the absence of any commercial or financial relationships that could be construed as a potential conflict of interest.

Publisher's Note: All claims expressed in this article are solely those of the authors and do not necessarily represent those of their affiliated organizations, or those of the publisher, the editors, and the reviewers. Any product that may be evaluated in this article, or claim that may be made by its manufacturer, is not guaranteed or endorsed by the publisher.

frontiers in Genetics

REVIEW
published: 02 December 2021
doi: 10.3389/fgene.2021.784996

Deregulation of ncRNA in Neurodegenerative Disease: Focus on circRNA, lncRNA and miRNA in Amyotrophic Lateral Sclerosis

Paola Ruffo[1]*, *Claudia Strafella*[2,3], *Raffaella Cascella*[2,3], *Valerio Caputo*[2,3], *Francesca Luisa Conforti*[1], *Sebastiano Andò*[1,4] and *Emiliano Giardina*[2,3]

[1]Medical Genetics Laboratory, Department of Pharmacy, Health and Nutritional Sciences, University of Calabria, Rende, Italy, [2]Genomic Medicine Laboratory UILDM, IRCCS Santa Lucia Foundation, Rome, Italy, [3]Medical Genetics Laboratory, Department of Biomedicine and Prevention, Tor Vergata University, Rome, Italy, [4]Centro Sanitario, University of Calabria, Arcavacata di Rende, Italy

Parallel and massive sequencing of total RNA samples derived from different samples are possible thanks to the use of NGS (Next Generation Sequencing) technologies. This allowed characterizing the transcriptomic profile of both cell and tissue populations, increasing the knowledge of the molecular pathological processes of complex diseases, such as neurodegenerative diseases (NDs). Among the NDs, Amyotrophic Lateral Sclerosis (ALS) is caused by the progressive loss of motor neurons (MNs), and, to date, the diagnosis is often made by exclusion because there is no specific symptomatologic picture. For this reason, it is important to search for biomarkers that are clinically useful for carrying out a fast and accurate diagnosis of ALS. Thanks to various studies, it has been possible to propose several molecular mechanisms associated with the disease, some of which include the action of non-coding RNA, including circRNAs, miRNAs, and lncRNAs which will be discussed in the present review. The evidence analyzed in this review highlights the importance of conducting studies to better characterize the different ncRNAs in the disease to use them as possible diagnostic, prognostic, and/or predictive biomarkers of ALS and other NDs.

Keywords: ncRNA, circRNA, lncRNA, miRNA, amyotrophic lateral sclerosis, RNA-seq, neurodegenerative disorders, NGS

OPEN ACCESS

Edited by:
Amanda Salviano-Silva, University Medical Center Hamburg-Eppendorf, Germany

Reviewed by:
Francesco Lotti, Columbia University, United States
Riccardo De Santis, The Rockefeller University, United States

***Correspondence:**
Paola Ruffo
paolaruffo.bio@gmail.com

Specialty section:
This article was submitted to RNA, a section of the journal Frontiers in Genetics

Received: *28 September 2021*
Accepted: *16 November 2021*
Published: *02 December 2021*

Citation:
Ruffo P, Strafella C, Cascella R, Caputo V, Conforti FL, Andò S and Giardina E (2021) Deregulation of ncRNA in Neurodegenerative Disease: Focus on circRNA, lncRNA and miRNA in Amyotrophic Lateral Sclerosis. Front. Genet. 12:784996. doi: 10.3389/fgene.2021.784996

INTRODUCTION

The accessibility to plenty of data concerning transcriptional factors, non-coding RNAs (ncRNAs), RNA editing, alternative splicing represented a crucial milestone for improving the knowledge of complex disorders (Liu et al., 2017). In particular, ncRNAs include small nucleolar RNAs (snoRNAs), small interfering RNAs (siRNAs), microRNAs (miRNAs), circular RNAs (circRNAs) and long-non-coding RNAs (lncRNAs). All of them have been extensively investigated as contributing factors in various metabolic processes such as programmed cell death, development and differentiation as well as in several transcriptional process and post-transcriptional modifications (Ma et al., 2020). In general, ncRNAs have been described as significant players in biological regulatory networks that, in turn, affect different protein effectors involved in the response to specific biological stimuli or in determining the future of the cell (Wang et al., 2019). Alternative

RNA splicing is a biochemical process in which introns are removed and remaining exons are bound, creating thereby different transcription isoforms of individual genes in order to increase the molecular diversity (Scotti and Swanson, 2016a; Bagyinszky et al., 2020; Elorza et al., 2021). In human cells, about 90–95% of genes are subjected to alternative splicing. Genetic mutations affecting such process can lead to the formation of abnormal transcripts or proteins with altered stability and function (Scotti and Swanson, 2016a; Elorza et al., 2021). In fact, several studies have established that mis-splicing is involved in various diseases such as cancer, muscular dystrophy, neurodegenerative diseases Ule and Blencowe, 2019; Srebrow and Kornblihtt, 2006; Scotti and Swanson, 2016b; Nik and Bowman, 2019.

NDs encompass a broad range of neurological disorders characterized by a progressive loss of neurons in specific areas of the brain or spinal cord. Although some family cases carry pathogenic mutations segregating with the disease, the etiology of NDs is often multifactorial, with the onset, progression and therapeutic response affected by a complex interaction among multiple genes, non-genetic factors and individual lifestyle (Strafella et al., 2018). GWAS studies found several SNPs correlated with the susceptibility to sporadic cases of NDs, although they are not sufficient to explain the complex phenotypes displayed by the affected individuals. In this context, the analysis of the transcriptome can add knowledge concerning the functional correlation between SNPs and clinical phenotypes (Sutherland et al., 2011). Several studies highlighted the advantages of running deep analyses of the transcriptome as a promising tool to implement the research on NDs, including the study of the role of ncRNAs and their impact on gene expression, neuronal function and viability in affected subjects. However, whether the deregulation of genes and transcriptional signatures are a cause or consequence of the onset of NDs is still a matter of debate (Costa et al., 2013).

Among NDs, Amyotrophic Lateral Sclerosis (ALS, also known as Lou Gehrig's disease) is caused by the progressive loss of MNs, resulting in the paralysis of voluntary muscles, muscle atrophy, stiffness, fasciculation and progressive difficulty swallowing, phonation and respiratory function (Hobson et al., 2016; Harrison et al., 2018n). Sporadic ALS (sALS) is the most common form of disease, accounting for about 90% of all cases. Family ALS (fALS), instead, affects about 10% of individuals and is inherited by an autosomal dominant pattern (Chen et al., 2013). The 40–55% of familial cases are due to pathogenic mutations in disease-associated genes, among which *SOD1*, *FUS*, *TARDBP* and *C9ORF72* are the most frequently involved (Perrone Benedetta e Franc, 2020). This disease has a very rapid course and, to date, the diagnosis is often made by exclusion because there is not a specific symptomatology framework. This is the reason why, it is important to research clinically useful biomarkers addressed to make a faster and more precise diagnosis of ALS, especially in cases where there are not genetic mutations or cases of affection within the family.

It is known that metabolomics studies have allowed the identification of various metabolites related to altered pathophysiology of ALS that could represent specific biomarkers alone or in concordance, identifying a specific metabolic signature for ALS. The identification of these signatures allows the development of personalized therapy. Glutamatergic excitotoxicity, stress and the progression of energy metabolism have been discovered, thanks to differential oxidative metabolomics experiments, as key factors leading to the degeneration of MNs. Such alterations have been observed both in affected patients and in disease models strengthening their role as biomarkers (Lanznaster et al., 2018).

In addition, many recent studies have focused on the role of neurofilaments (NFs) as biomarkers in ALS. NFs are cytoskeletal proteins and their levels improve in biological fluids in proportion to the axonal degree. The work conducted by Sun et al., 2020, confirmed that neurofilament reading chain (NFL) levels are promising prognostic biomarkers for monitoring disease severity and progression of ALS. There are several research groups that have confirmed the use of NFL as specific biomarkers of the disease (Tortelli et al., 2015; Forgrave et al., 2019; Verde et al., 2019; Benatar et al., 2020).

Up to date, the molecular mechanisms of ALS are not completely understood. ALS is a complex and multifactorial disease characterized by the involvement of several pathological processes. The most characteristic pathogenic mechanisms of ALS include axonal transport dysfunctions, apoptotic mechanisms, neuroinflammation, proteins aggregation and abnormal mitochondrial function (Krokidis and Vlamos, 2018a). Over the different molecular mechanisms which have been associated with ALS in the last years, some of which include the action of non-coding RNAs, including miRNAs, lncRNAs and circRNAs (Salta and De Strooper, 2017), which will be discussed in the present review.

The Use of RNA-SEQ Analysis for Elucidating ALS Mechanisms

The application of NGS technologies in the context of modern molecular medicine has provided many data from DNA or RNA samples, both in terms of qualitative and quantitative information, that have been essential for discovering primary and secondary molecular targets in the context of NDs. In general, the RNA-seq analysis can offer a complete and detailed analysis of the whole transcriptome and a list of Differential Expressed Genes (DEG), which are useful to understand how the different genes can be up-regulated or down-regulated in affected subjects compared to healthy controls (Costa et al., 2010). The DEG analysis can be further utilized to assess how molecular pathways are modified in pathological contexts compared to health conditions and to identify which transcriptional changes can be related to the onset and progression of specific disease conditions. Indeed, transcriptional changes have been described as a consequence of biological aging or in the etiopathogenesis of complex disorders, including NDs (Costa-Silva et al., 2017; Su et al., 2019). Today, different technologies for sequencing are available: bulk and single cells RNA-seq, Poly-A and ribo-minus RNA-seq experiments, short and long reads sequencing.

Bulk RNA-seq technologies have been extensively used to primarily study average gene expression on thousands of cells. The advent of single-cell RNA sequencing (scRNA-seq) offers unprecedented opportunities to explore gene expression profile at the single cell level leading to in-depth discoveries on the variability and dynamics of cellular expression. Currently available scRNA-seq approaches still have a major problem, as weakly expressed genes are not identified. Furthermore, since most current scRNA-seq methods primarily capture polyA + RNA, the development of protocols capable of capturing both polyA + and polyA- RNAs allows for a comprehensive investigation of coding and non-coding gene expression (Chen et al., 2019a).

Recently, RNA-seq methods, based on mRNA or ribo-minus based on NGS, are considered more accurate and comprehensive for transcriptome profiling (Wang et al., 2009). In eukaryotic cells, 80% of the total RNAs are ribosomal RNA (rRNA) while the remaining 5% are positive polyadenylate [poly (A) +] mRNA. The mRNA-seq (polyA-selected RNA-sequencing) and rmRNA-seq (ribo-minus RNA-sequencing) methods selectively remove a different set of RNA: negative poly (A) RNA and rRNA, respectively. This protocol enriches the transcripts of poly (A) + including mRNA and many non-coding RNAs and also reduces the amount of pre-mRNA. In contrast, depleted rRNA removes cytoplasmic and mitochondrial rRNA and thus includes poly (A) + mRNA, as well as non-coding RNA or protein-coding mRNA that are not polyadenylated (Chen et al., 20209). The comparison between these two RNA sequencing analyses: rmRNA-seq and mRNA-seq showed that rmRNA-seq can detect more transcripts including genes encoding proteins, ncRNA, snoRNA and snRNA, highlighting how this technology provides more in-depth data than those of mRNA-seq for the systematic profiling of transcriptomes. In particular, the rmRNA-seq method allows to obtain data on different polyA-orbimorphic transcripts such as transcripts of protein-coding genes (e.g. Histone, Heg1 and Dux), ncRNA, snoRNA, snRNA and new ncRNA. However, both technologies fail to identify a significant fraction of transcripts, considered potential NpA (non-polyA) or bimorphic transcripts, and these NpA transcripts are quite abundant in eukaryotic cells up to about 80% of the total transcribed sequences (Cui et al., 2010n).

Short-read sequencing is the method for detecting and quantifying the gene expression of the entire transcriptome. This sequencing technologies perform sequencing by synthesis (SBS) or ligation. Each strategy uses DNA polymerase or ligase enzymes for numerous strands of DNA in parallel, respectively. This method requires the identification of the newly sequenced nucleotides as they are incorporated, without interrupting the synthesis process [Genomics (26 luglio 2021), 2021]. The short-read sequencing has several advantages such as, it is cheaper and easier to implement than microarrays; generates comprehensive, high-quality data that identify quantitative expression levels well across the transcriptome; it is a robust method that exhibits high intra-platform and cross-platform correlations. However, errors may occur in the sample preparation phase and during computational analysis that negatively affects the ability to correctly identify and quantify the different expression isoforms of the gene (RNA sequencing: the teenage years, 2021). Moreover, this technology cannot sequence long stretches of DNA because the DNA strands must be fragmented and amplified before the sequencing process. A new approach is the use of long-read sequencing for obtaining the full-length sequence of the mRNA. This method allows labelling full-length cDNAs with unique molecular identifiers (UMIs), which are copied along the length of individual cDNA molecules before the preparation of a short-read RNA-seq library. Transcription isoforms can be reconstructed up to 4 kb. Comparing the two methods, long read shows much lower throughput and much higher error than short-read platforms that, in turn, show off greater fidelity given their increased use. However, long reads platoforms can capture multiple transcripts (RNA sequencing: the teenage years, 2021).

Most RNA-seq studies for ALS have been performed on mouse models or cultured cells derived from the spinal cord, brain stem and Central Nervous System (CNS) (Liu et al., 2020). ALS rodent models have been indispensable for developing hypotheses on how mutant SOD1 proteins induce MNs degeneration. In Wenting Liu et al., 2020, Single-cell RNA sequencing (scRNA-seq) has been performed on a transgenic mouse model of ALS (*SOD1**G93A), in particular at level of the brain stem region. The region of the brain stem has been deliberately chosen, as it is responsible for the oral-motor functions that are strongly affected by the disease. In fact, about 25% of ALS cases is characterized by progressive bulbar paralysis and maxillary muscle strength with consequences on chewing, swallowing and loss of ability to move (Riera-Punet et al., 2018). The results of the experiments highlighted the alteration of both genes and pathways already known and related to ALS, and those specific to the anatomical area of interest, such as the transport of toxins in the ependymal cells of the brainstem and the response to organophosphate in Schwann cells. Subsequently, the differentially expressed genes of the animal model were compared with the human GWAS highlighting an overlap of the two and, therefore, emphasizing that the discoveries made on murine models may be relevant to human disease (Liu et al., 2020). In another study, the identification of transcriptional changes and a high number of DEG confirmed the involvement of different types of glial cells in ALS. Animal models carrying *SOD1* mutation allowed identifying the involvement of the oligodendrocytes in the pathology, showing altered neurogenesis and nuclear envelope formation (Kang et al., 2013). At level of microglia, the immune pathway resulted to be altered, supporting the thesis that the progression of the disease is driven by changes affecting the immune-inflammatory response. Astrocytes and Schwann cells showed a significant number of DEGs and relevant transcriptomic alterations. Altogether, these evidences allow understanding that different types of cell play a specific role in the pathology that are worth to be clarified in order to devise targeted treatments. In ependymal cells, the presence of the genetic variant in *SOD1* is directly correlated in toxin transport and cell differentiation (Liu et al., 2020).

Other studies have been conducted on SALS post-mortem cortex samples and allowing distinctions into molecular subtypes

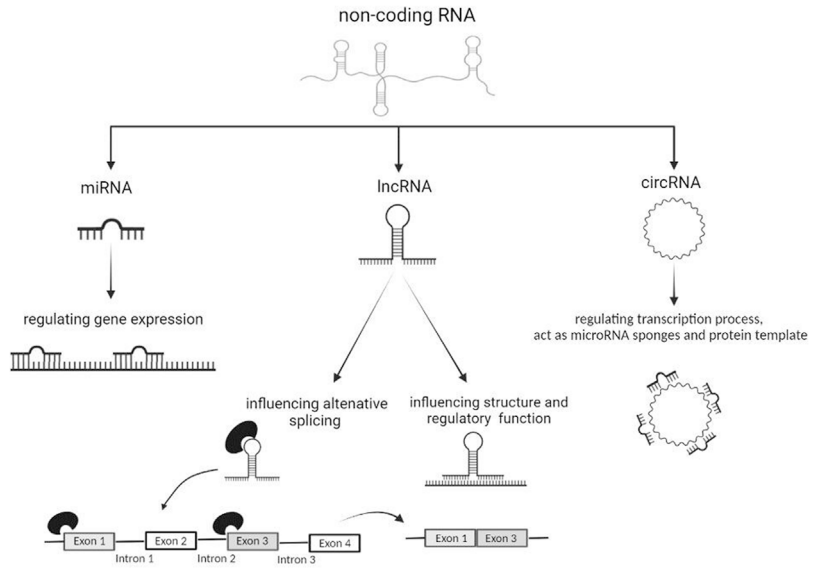

FIGURE 1 | The actions of miRNAs, lncRNAs and circRNAs on different molecular processes.

characterized by different combinations of genes and pathways deregulated (La Cognata et al., 2021). The existence of distinct molecular subtypes of ALS have also been highlighted in other works (Aronica et al., 2015). Thanks to these discoveries, it is possible to think of designing targeted and effective therapies specific to each patient. The study and evaluation of post-mortem brain tissue RNA samples reveal pathogenetic mechanisms at the end-stage of the disease and do not clarify whether the transcriptional differences are a cause or a consequence of the disease process. In this context, the use of iPSC (induced pluripotent stem cells) derived from ALS patients has provided important insights into the pathophysiology of the disease, encouraging researchers to consult the molecular heterogeneity of ALS and follow the course of degeneration.

The study conducted by Kiskinis et al., 2014 involved a combined approach of stem cell reprogramming and differentiation with genome engineering and RNA-seq to identify transcriptional and functional changes induced by the *SOD1*-A4V mutation in human MNs. The study demonstrates that the *SOD1*-A4V missense mutation causes a proapoptotic phenotype in cultured human NMs, limiting their long-term survival. Thanks to the use of RNA-seq technology, the transcriptional differences between human *SOD1* +/A4V and control MNs have been defined. The results show that MNs derived from patient-specific iPSC displayed disease hallmarks, such as defects in mitochondrial morphology and transport, oxidative and ER-related stress, and an activated UPR (unfolded protein response). Subsequent functional studies demonstrated that these perturbed pathways are consequences dependent on the presence of the *SOD1* A4V mutation (Kiskinis et al., 2014). Strongly altered signalling pathways in iPSC with *SOD1* mutation, were also found by Bhinge et al., 2017. In this study, iPSC lines were generated by correcting the point mutation in *SOD1* using CRISPR-Cas9 genome editing technology, in order to exclude the possibility of observing phenotypic differences due to genetic variation in iPSC lines. By comparing the observed phenotypes with those arising from post mortem tissues of patients with the disease or in rodent models, it was confirmed that the *in vitro* model reflects specific aspects of the disease. The analysis conducted with RNA-seq identified several pathways commonly dysregulated in ALS-affected MNs, such as the activation of cell cycle genes and p53 in *SOD1*-mutant MNs. Furthermore, pharmacological inhibition of the upregulated pathways, it was possible assisting to the activation of the AP1 pathway, through MAPK signalling, with consequent neurodegeneration of MNs. Further studies are needed to elucidate the mechanisms of neurodegeneration and also to provide phenotypic screens for searching new molecular targets (Bhinge et al., 2017).

Another RNA-seq analysis was conducted on peripheral blood mononuclear cells (PBMC) from sporadic and mutated patients with ALS (mutations in *FUS*, *TARDBP*, *SOD1* and *VCP* genes) and healthy controls allowing the characterization and comparison of the entire transcriptome of the PBMC content, both in terms of coding and non-coding RNAs. The aim of this work was the creation of a dataset for RNA profiling in ALS using a tissue that is easy to collect, manage and store (Zucca et al., 2019).

Spatial transcriptomics (ST) generates quantitative transcriptome RNA sequencing data through polyadenylated RNA capture on spatially bar-coded DNA capture probe arrays. In the study conducted by Miniati et al., 2019, ST is applied to spatially profile gene expression in lumbar spinal cord tissue sections from *SOD1*-G93A (ALS) and *SOD1*-WT (control) mice at presymptomatic time points, onset, symptomatic and end-stage. In addition, this technique has been used to profile gene expression in tissue sections of the

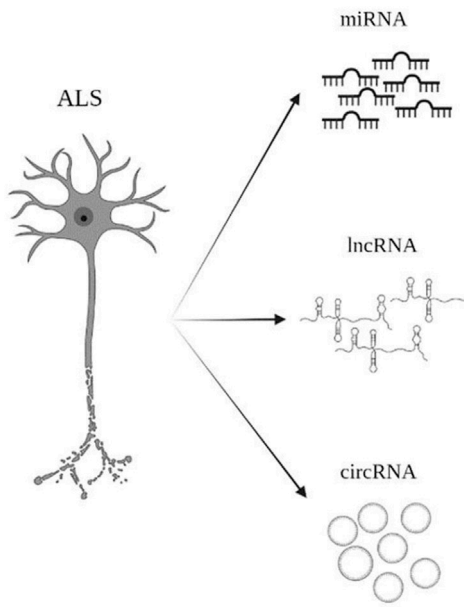

miRNA	Regulation	Target Gene
miR-151a-5p	Down	*ARHGDIA, OTUB1*
miR-199a-5p	Down	*DRAM1, BECN1*
miR-423-3p	Down	/
miR-338-3p	Up	*SLC1A2, AATK,PTPRT*
miR-206	Up	*GJA1, VEGFA*
miR-133a	Up	*TUBA4A, VAPB*
miR-335-5p	Down	*CASP-7, ICAM-1*
miR-129-5p	Up	*HMGB1*

lncRNA	Regulation	Target Gene
NEAT1	Up	*TDP-43, FUS/TLS*
MALAT1	Up	*SYNRG, ITSN2, AAK1, PICALM, and AP3B1*
MEG3	Up	*PAX6 AND DBX1*
ABCA12	Down	*SNCA,FBXW11*
DYRK2	Down	*BRCA1*
POTEM	Down	/

circRNA	Regulation	Genomic location
hsa_circ_0063411	Up	*TNRC6B*
hsa_circ_0023919	Down	*PICALM*
hsa_circ_0088036	Up	*SUSD1*
hsa-mir-9	Up	/

FIGURE 2 | An overview of the miRNA, lncRNA and circRNAs, mainly investigated in ALS.

accumulated spinal cord and post mortem cervical from sporadic lumbar or bulbar onset ALS patients. From the results obtained, it has been possible to distinguish the differences between the populations of microglia and astrocytes during the onset of the disease and the gene expression changes of the different transcriptional pathways. Furthermore, thanks to the procedure implemented, it has been possible to draw deductions from mouse models and then testing them in clinical samples (Spatiotemporal dynamics, 2021).

RNA Molecules as Biomarkers in ALS

A hallmark of NDs is protein aggregation and alterations in RNA metabolism (Kinoshita et al., 2021). The alterations affect all levels of gene regulation, from RNA synthesis to degradation, and have been associated with specific alterations in RNA-binding proteins (RBPs) and non-coding RNAs. These ncRNAs are stable constructs in body fluids where their presence and potential could serve as likely non-invasive biomarkers of NDs, including ALS (Competing EndogenousA, 2021). Among non-coding RNAs, the following subsections of the review will discuss the studies concerning the role of miRNAs, lncRNAs and circRNAs in ALS physiopathology and their potential application as disease biomarkers.

miRNAs

MicroRNAs (miRNAs) are small oligonucleotide sequences (about 19–22 base pairs) of single-stranded non-coding RNA, which play a crucial function by regulating gene expression at post-transcriptional level (**Figure 1**). The action of miRNAs has been suggested as a mechanism to regulate neuroinflammation in different NDs including ALS (Benigni et al., 2016; Bai et al., 2017a; Wang et al., 2020; Strafella et al., 2021a; Strafella et al., 2021b).

Several studies highlighted how altered biogenesis and expression of miRNAs can be responsible of the degeneration of spinal motor neurons, both in fALS and sALS (Olejniczak et al., 2018; MicroAs in amyotrophic, 2021; Vaz et al., 20217; Krokidis and Vlamos, 2018b). In addition, miRNAs have been found to exert a function in neuronal inflammation in ALS (Emde et al., 2015). Numerous works showed that miRNAs in affected subjects can cross the blood-brain barrier to reach the bloodstream and, thereby, could be utilized as biomarkers of disease (Saucier et al., 2019; Liu et al., 2021). Highly deregulated miRNAs have been associated with different degrees of disease progression. miR-151a-5p, miR-199a-5p and miR-423-3p were seen to be down-regulated in affected subjects, whereas miR-338-3p, miR-206 and miR-133a appeared up-regulated. Moreover, up-regulation of miR-199a-5p, miR-206, miR-133a correlated with a better prognosis and a slower course of disease (Dobrowolny et al., 2021). miR-338-3p is involved in ALS pathogenesis, not only in tissues directly related to the disease but also in the peripheral tissues such as blood, helping to evaluate the potential of such miRNAs as a novel class of genetic blood marker for sALS (De Felice et al., 2014). miR-199a-5p has been involved in the initial phase of ALS and has been found significantly down-regulated in the last phase of disease. In contrast, miR-206 has been supposed to mitigate the progression of the disease by enhancing the regeneration of the joints at neuromuscular level (Dobrowolny et al., 2021). miR-335-5p was found to be downregulated in ALS

patient serum, increasing oxidative stress, inhibiting caspase 3/7 apoptotic pathway, and deregulating neuronal degeneration (De Luna et al., 2020).

Recent studies have highlighted the presence of connections between miRNAs and RBPs, such as TDP-43 and FUS, with essential regulatory complexes such as Drosha in the nucleus and Dicer in the cytoplasm. Drosha complexes with DGCR8 have also been associated with TDP-43, suggesting a more complex dynamics than miRNAs and protein-related pathologies, especially in MNs. FUS gene localizes together with TDP-43 in the Drosha nuclear complex and the direct binding of FUS to the nascent pri-miRNAs allows to recruit Drosha to transcriptionally active sites for further processing of the pri-miRNAs themselves. Furthermore, FUS has been shown to promote gene silencing through direct binding to certain miRNA and mRNA targets. Mutations in this gene also impair the function of the AGO2 protein in the miRNA-induced silencing complex (miRISC) (Pham et al., 2020).

In subjects affected by fALS and sALS carrying *SOD1* mutation, the up-regulation of miR-129-5p revealed a direct action against the *ELAVL4* gene transcript (*Elav-Like RNA-Binding Protein 4*, 1p34, OMIM #168360). It is interesting to note that this transcript encodes HuD protein, which binds RNA and is mainly expressed at the neuronal level, where it is involved in many molecular processes, such as the control of neuronal life by promoting the translation of the mRNAs involved in axonal and neuronal formation. Experimental studies have shown how HuD is down-regulated in *SOD1* mutated samples; miR-129-5p acts positively against HuD by increasing its expression and preventing this protein from being degraded (Loffreda et al., 2020). Furthermore, *ELAVL4* have also been found deregulated in *in vitro* models carrying mutations in *FUS* gene downstream miR-375 deregulation (De Santis et al., 2017; Comparative interactomic, 2021; MutantS andL4 (H, 2021; Dell'Orco et al., 2021).

lncRNAs

Long non-coding RNAs (lncRNAs) consist of more than 200 nucleotides and are involved in the regulation of several biological functions (Ma et al., 2020). lncRNAs are characterized by a tissue-specific expression and play a modulatory role in the CNS by influencing epigenetic processes, post-translational and transcriptional regulation, alternative splicing and cell cycle (Yuan et al., 2020) (**Figure 1**). These constructs are well known to be associated with the pathogenesis of many NDs and a more detailed understanding of them could identify them as specific biomarkers of disease (Bhattacharyya et al., 2021).

RNA-seq analyses of sALS and fALS patients revealed the presence of lncRNAs differentially expressed both in blood mononuclear cells and in the spinal cord (Gagliardi et al., 2018). Several lncRNAs have been found both in MNs and in peripheral blood such as *NEAT1* (*Nuclear Paraspeckle Assembly Transcript 1*, 11q13.1, OMIM #612769), *MALAT1* (*Metastasis-Associated Lung Adenocarcinoma Transcript 1,* 11q13.1, OMIM # 607924) and *MEG3* (*Maternally Expressed Gene 3*, 14q32.2, OMIM # 605636). The RBPs associated with ALS have been shown to interact with NEAT1 and regulate its expression. Several studies have shown how NEAT1 binds FUS and TDP-43 by increasing the frequency by which paraspeckles (i.e.subnuclear bodies located in the interchromatin space of cells) are formed at the nuclear level and in MNs (Vangoor et al., 2021). Paraspeckles play a fundamental role in the control of gene expression thanks to the nuclear retention of modified RNA. Through this mechanism, paraspeckles can control gene expression during many cellular processes including differentiation, viral infection and stress responses (Fox and Lamond, 2010), as well as exert anti-apoptotic activity. An increase in the early stages of ALS could be related to an increase in the survival of MNs. Many studies have shown that RBP mutations influence the formation of paraspeckles leading to a more aggressive phenotype. Indeed, mutations in *FUS* result in lower paraspeckle production and dysregulation of *NEAT1* transcription (Vangoor et al., 2021) (Gagliardi et al., 2018). A study by Suzuki et al., 2019 correlated *NEAT1* expression to defects in the genesis of paraspeckle that cause neurodegeneration and neuronal death in ALS (Suzuki et al., 2019). Many disease-related genes can give rise to sense or anti-sense RNA that are then translated into proteins but play the role of lncRNAs. The anti-sense transcripts perform several functions such as the activation of RNA interference caused by the formation of double-stranded RNA created by the union of single complementary strands; transcriptional interference caused by the displacement of transcription factors in the promoter region; epigenetic regulation mediated by the recruitment of chromatin remodelling factors. Based on these different roles, the use of sensory oligonucleotides as a targeted therapy could be hypothesized. The *ATXN2* gene (*Ataxin 2*, 12q.24.1, OMIM #601517) has been associated with ALS because of its interaction with FUS and TDP-43, by which it has been supposed to contribute to the disease pathogenesis. Mutations in *ATXN2* can cause the production of antisense transcripts that are present in the tissues of ALS patients. *MALAT1* (OMIM * 607924) has shown a high affinity for TDP-43, whose binding result in a subsequent increased expression, whereas *MEG3* (OMIM * 605636) has been found down-regulated and displayed a lower binding of TDP-43. The different interactions of *FUS* and TDP-43 with different lncRNAs could be associated with degeneration of MNs in ALS, with a mislocalization of the genes themselves and impact on the distribution of MNs (Vangoor et al., 2021).

In Y. Yu, et al., 2021, six differentially-regulated lncRNAs emerged in peripheral leukocytes between sALS patient and control. Of them, lnc-ABCA12-3: 1, lnc-DYRK2-7: 1 and lnc-POTEM-4: 7 have been proposed as sALS markers. In particular, Lnc-DYRK2-7: 1 and lnc-POTEM-4: 7 have been specifically down-regulated in affected subjects compared to healthy controls (Yu et al., 2021).

circRNAs

RNA sequencing technology is currently the only method capable of providing a complete landscape of circRNAs throughout the body and in specific tissue areas (Philips et al., 2020). In particular, ribo-minus RNA-seq, has allowed identifying new change in circRNAs expression and also investigate the roles of these circRNAs in the condition of interest (Cooper et al., 2018). circRNAs are very stable regulating molecules within the cell as they are resistant to the action of exonucleases (Chen, 2016;

Xie et al., 2017). circRNAs can act as transcriptional regulators, miRNA sponges and protein template, although emerging evidence described them as protein decoys, scaffolds and recruiters (Zhou et al., 2020) (**Figure 1**). circRNAs are actively involved in the formation of muscle tissues (Legnini et al., 2017); synaptic formation and activity (Chen et al., 2019b); control of neuronal gene expression; neuronal differentiation and development of the CNS. circRNAs are ubiquitously present in many cell types, although they are particularly enriched at neuronal level (Zhou et al., 2020; Legnini et al., 2017; Chen et al., 2019b; D'Ambra et al., 2019).

Concerning circRNAs and ALS, a recent paper (Dolinar's article et al., 2019) presented the first differential expression analysis of circRNAs in patients with ALS diagnosis (Dolinar et al., 2019). The analysis was performed on leukocytes, considering that blood is an easily accessible biological source and therefore it is more suitable for diagnostic use.

The experiment results indicate hsa_circ_0063411, hsa_circ_0023919, hsa_circ_0088036 as potential blood biomarkers for ALS. Specifically, hsa_circ_0023919 is located within *PICALM* gene (*Phosphatidylinositol-binding Clathrin Assembly Protein*, 11q14.2, OMIM #603025) and presents two link sites for hsa-miR-9, which appeared up-regulated in patients with sALS (Vrabec et al., 2018). However, further studies are necessary to test the potential association between hsa_circ_0023919, hsa-miR-9 and the disease (Dolinar et al., 2019). Concerning hsa_circ_0063411, more in-depth and targeted studies are needed to evaluate the possible relationship with hsa-miR-647, given the presence of a link site for this miR on the circRNAs. There is no biological evidence regarding this circRNAs but its ligand, hsa-miR-647, has been found down-regulated in ALS patients (Bai et al., 2017b). The hsa_circ_0088036 is found within *SUSD1* gene (*Sushi domain containing 1*, 9q31.3, OMIM #607723), which has been associated with ALS (Dolinar et al., 2019). Levels of such circRNAs have been found up-regulated in ALS patients as well as in patients suffering from Rheumatoid Arthritis, for which hsa_circ_0088036 is already considered a biomarker (Group Therapy for Schizop, 2020d). Since these two disorders share some common mechanisms, it would be interesting to further investigate the role of hsa_circ_0088036 in ALS as well. In the study conducted by Dolinar et al., 2019, hsa_circ_0088036 and hsa_circ_0023919 were negatively associated with the age of onset of disease, whereas hsa_circ_0063411 was negatively associated with the duration of the disease and survival (Dolinar et al., 2019). This work has laid the foundations for considering circRNAs as diagnostic biomarkers, although further studies are needed to clarify their association with the pathology.

A direct role in regulating circRNAs production has been shown by *FUS* gene. In particular, the RNA-binding protein FUS has been identified as a novel regulator of circRNAs production and also a key player in controlling the expression of these transcripts in mouse MNs. In these *in vitro*-derived MNs there is a high number of circRNAs and a specific subclass is influenced by the levels of *FUS*, which can enhance or repress the back-slicing reaction. The analysis of the subcellular localization identified nuclear circRNAs species entirely derived from exonic sequences. The fact that *FUS* is involved in circRNAs biogenesis is important not only to elucidate its role in this process, but also to link the function of circRNAs to neurodegenerative processes (Errichelli et al., 2017).

CONCLUSION AND FUTURE PROSPECTIVE

The availability of NGS technologies allowed the massive and parallel sequencing of total RNA samples derived from a range of specimens. This enabled the characterization of the transcriptomic profile of several cell populations and tissues, providing a more detailed and accurate overview of complex traits and phenotypes. Several studies and experiments showed that the alteration of RNA metabolism, function, structure and localization of both coding and non-coding RNAs are involved in the onset and progression of ALS (Zucca et al., 2019). The use of RNA-seq analysis highlighted the existence of a wide class of ncRNAs (**Figure 2**), whose investigation is providing more and more insightful clues for improving the knowledge of disease and addressing the forthcoming research efforts towards the development of more effective clinical treatments and diagnostic protocols.

In this context, it is important to note that recent studies showed that lncRNA and mRNA can compete for binding to miRNAs and this interaction can play a role in different diseases, including ALS (Liu et al., 2021). The potential cross-talk between miRNA-lncRNA-mRNA can be investigated by means of competitive endogenous RNA (ceRNA) network analysis. This model allows assessing how the different ncRNAs can interact together and affect the molecular pathogenesis of disease (Sardina et al., 2017). On this subject, Liu et al. (2021) created a ceRNA network with the aim of making a molecular characterization of the ALS development and providing promising targets for clinical treatment. The study made it possible to understand that the regulation of MALAT1 plays an important role in the development of the disease. Furthermore, the *SYNRG*, *ITSN2*, *AAK1*, *PICALM* and *AP3B1* genes associated with ALS and regulated by MALAT1, have been found to play an important role in the pathogenesis of ALS. In particular, the discovery of the association between *AAK1* gene and ALS is of considerable interest, although further research is necessary to understand the correlation of this gene and the other ones with the disease (Liu et al., 2021).

In conclusion, the above-discussed recent findings emphasized that the future studies should be tailored to better characterize the pathophysiological role of the different ncRNAs and ceRNA networks in the disease, aiming to employ them as possible prognostic, predictive and/or diagnostic biomarkers for ALS and other NDs.

AUTHOR CONTRIBUTIONS

PR writing the review with the CS and VC support. RC, FC, SA, and EG contributed to manuscript design. All authors contributed to the manuscript review, read and approved the submitted version providing critical feedback that helped shape the text.

REFERENCES

Aronica, E., Baas, F., Iyer, A., ten Asbroek, A. L. M. A., Morello, G., Cavallaro, S., et al. (2015). Molecular Classification of Amyotrophic Lateral Sclerosis by Unsupervised Clustering of Gene Expression in Motor Cortex. *Neurobiol. Dis.* 74 (febbraio), 359–376. doi:10.1016/j.nbd.2014.12.002

Bagyinszky, E., Giau, V. V., and An, S. A. (2020). Transcriptomics in Alzheimer's Disease: Aspects and Challenges. *Ijms* 21, 3517. doi:10.3390/ijms21103517

Bai, X., Tang, Y., Yu, M., Wu, L., Liu, F., Ni, J., et al. (2017). Downregulation of Blood Serum microRNA 29 Family in Patients with Parkinson's Disease. *Sci. Rep.* 7 (1), 5411. doi:10.1038/s41598-017-03887-3

Bai, X., Tang, Y., Yu, M., Wu, L., Liu, F., Ni, J., et al. (2017). Downregulation of Blood Serum microRNA 29 Family in Patients with Parkinson's Disease. *Sci. Rep.* 7 (1), 5411. doi:10.1038/s41598-017-03887-3

Benatar, M., Zhang, L., Wang, L., Granit, V., Statland, J., Barohn, R., et al. (2020). Validation of Serum Neurofilaments as Prognostic and Potential Pharmacodynamic Biomarkers for ALS. *Neurology* 95, e59–69. doi:10.1212/WNL.0000000000009559

Benigni, M., Ricci, C., Jones, A. R., Giannini, F., Al-Chalabi, A., and Battistini, S. (2016). Identification of MiRNAs as Potential Biomarkers in Cerebrospinal Fluid from Amyotrophic Lateral Sclerosis Patients. *Neuromol Med.* 18, 551–560. doi:10.1007/s12017-016-8396-8

Bhattacharyya, N., Pandey, V., Bhattacharyya, M., and Dey, A. (2021). Regulatory Role of Long Non Coding RNAs (LncRNAs) in Neurological Disorders: From Novel Biomarkers to Promising Therapeutic Strategies. *Asian J. Pharm. Sci.* doi:10.1016/j.ajps.2021.02.006

Bhinge, A., Namboori, S. C., Zhang, X., VanDongen, A. M. J., Stanton, L. W., and Stanton, e. Lawrence. W. (2017). Genetic Correction of SOD1 Mutant IPSCs Reveals ERK and JNK Activated AP1 as a Driver of Neurodegeneration in Amyotrophic Lateral Sclerosis. *Stem Cel Rep.* 8 (4), 856–869. doi:10.1016/j.stemcr.2017.02.019

Chen, S., Sayana, P., Zhang, X., and Le, W. (2013). Genetics of Amyotrophic Lateral Sclerosis: An Update. *Mol. Neurodegeneration* 8, 28. doi:10.1186/1750-1326-8-28

Chen, G., Ning, B., and Shi, T. (2019). Single-Cell RNA-Seq Technologies and Related Computational Data Analysis. *Front. Genet.* 10, 317. doi:10.3389/fgene.2019.00317

Chen, B. J., Huang, S., and Janitz, M. (2019). Changes in Circular RNA Expression Patterns during Human Foetal Brain Development. *Genomics* 111 (4), 753–758. doi:10.1016/j.ygeno.2018.04.015

Chen, L., Yang, R., Kwan, T., Tang, C., Watt, S., Zhang, Y., et al. (20202020). Paired rRNA-Depleted and polyA-Selected RNA Sequencing Data and Supporting Multi-Omics Data from Human T Cells. *Sci. Data* 7, 376. doi:10.1038/s41597-020-00719-4

Chen, L.-L. (2016). The Biogenesis and Emerging Roles of Circular RNAs. *Nat. Rev. Mol. Cel Biol* 17 (4), 205–211. doi:10.1038/nrm.2015.32

Comparative interactomics analysis of different ALS-associated proteins identifies converging molecular pathways - PubMed (2021). Consultato. Available at: https://pubmed.ncbi.nlm.nih.gov/27164932/.

Competing Endogenous RNA Networks as Biomarkers in Neurodegenerative Diseases (2021). Consultato. Available at: https://www.ncbi.nlm.nih.gov/pmc/articles/PMC7765627/.

Cooper, D. A., Cortés-López, M., Miura, e. Pedro., and Miura, P. (2018). Genome-Wide circRNA Profiling from RNA-Seq Data. *Methods Mol. Biol. (Clifton, N.J.)* 1724, 27–41. doi:10.1007/978-1-4939-7562-4_3

Costa, V., Angelini, C., De Feis, I., and Ciccodicola, A. (2010). Uncovering the Complexity of Transcriptomes with RNA-Seq. *J. Biomed. Biotechnol.* 2010, 1–19. doi:10.1155/2010/853916

Costa, V., Aprile, M., Esposito, R., and Ciccodicola, A. (2013). RNA-seq and Human Complex Diseases: Recent Accomplishments and Future Perspectives. *Eur. J. Hum. Genet.* 21, 134–142. doi:10.1038/ejhg.2012.129

Costa-Silva, J., Domingues, D., and Lopes, F. M. (2017). RNA-seq Differential Expression Analysis: An Extended Review and a Software Tool. *PLOS ONE* 12, e0190152. doi:10.1371/journal.pone.0190152

Cui, P., Lin, Q., Ding, F., Xin, C., Gong, W., Zhang, L., et al. (2010n2010). A Comparison between Ribo-Minus RNA-Sequencing and PolyA-Selected RNA-Sequencing. *Genomics* 96 (5), 259–265. doi:10.1016/j.ygeno.2010.07.010

D'Ambra, E., Capauto, D., and Morlando, M. (2019). Exploring the Regulatory Role of Circular RNAs in Neurodegenerative Disorders. *Ijms* 20 (21), 5477. doi:10.3390/ijms20215477

De Felice, B., Annunziata, A., Fiorentino, G., Borra, M., Biffali, E., Coppola, C., et al. (2014). MiR-338-3p Is Over-expressed in Blood, CFS, Serum and Spinal Cord from Sporadic Amyotrophic Lateral Sclerosis Patients. *Neurogenetics* 15 (4), 243–253. doi:10.1007/s10048-014-0420-2

De Luna, N., Turon-SansTuron-Sans, J., Cortes-Vicente, E., Carrasco-Rozas, A., Illán-Gala, I., Dols-Icardo, O., et al. (2020). Downregulation of MiR-335-5P in Amyotrophic Lateral Sclerosis Can Contribute to Neuronal Mitochondrial Dysfunction and Apoptosis. *Sci. Rep.* 10 (1), 4308. doi:10.1038/s41598-020-61246-1

De Santis, R., Santini, L., Colantoni, A., Peruzzi, G., de Turris, V., Alfano, V., et al. (2017). FUS Mutant Human Motoneurons Display Altered Transcriptome and MicroRNA Pathways with Implications for ALS Pathogenesis. *Stem Cel Rep.* 9 (5), 1450–1462. doi:10.1016/j.stemcr.2017.09.004

Dell'Orco, M., Sardone, V., Gardiner, A. S., Pansarasa, O., Bordoni, M., Perrone-Bizzozero, N. I., et al. (2021). HuD Regulates SOD1 Expression during Oxidative Stress in Differentiated Neuroblastoma Cells and Sporadic ALS Motor Cortex. *Neurobiol. Dis.* 148 (gennaio 2021), 105211. doi:10.1016/j.nbd.2020.105211

Dobrowolny, G., Martone, J., Lepore, E., Casola, I., Petrucci, A., Inghilleri, M., et al. (2021). A Longitudinal Study Defined Circulating MicroRNAs as Reliable Biomarkers for Disease Prognosis and Progression in ALS Human Patients. *Cell Death Discov.* 7 (1), 4. doi:10.1038/s41420-020-00397-6

Dolinar, A., Koritnik, B., Glavač, D., and Ravnik-Glavač, M. (2019). Circular RNAs as Potential Blood Biomarkers in Amyotrophic Lateral Sclerosis. *Mol. Neurobiol.* 56, 8052–8062. doi:10.1007/s12035-019-1627-x

Elorza, A., Márquez, Y., Cabrera, J. R., Sánchez-Trincado, J. L., Santos-Galindo, M., Hernández, I. H., et al. (2021). Huntington's Disease-specific Mis-Splicing Unveils Key Effector Genes and Altered Splicing Factors. *Brain A J. Neurol.* 144, 2009–2023. marzo 2021. doi:10.1093/brain/awab087

Emde, A., Eitan, C., Liou, L. L., Libby, R. T., Rivkin, N., Magen, I., et al. (2015). Dysregulated Mi RNA Biogenesis Downstream of Cellular Stress and ALS -causing Mutations: a New Mechanism for ALS. *Embo J.* 34, 2633–2651. doi:10.15252/embj.201490493

Errichelli, L., Dini Modigliani, S., Laneve, P., Colantoni, A., Legnini, I., Capauto, D., et al. (2017). FUS Affects Circular RNA Expression in Murine Embryonic Stem Cell-Derived Motor Neurons. *Nat. Commun.* 8 (30 marzo 2017), 14741. doi:10.1038/ncomms14741

Forgrave, L. M., Ma, M., Best, J. R., and DeMarco, M. L. (2019). The Diagnostic Performance of Neurofilament Light Chain in CSF and Blood for Alzheimer's Disease, Frontotemporal Dementia, and Amyotrophic Lateral Sclerosis: A Systematic Review and Meta-analysis. *Alzheimer's Demen. Diagn. Assess. Dis. Monit.* 11, 730–743. doi:10.1016/j.dadm.2019.08.009

Fox, A. H., and Lamond, A. I. Cold Spring Harbor Perspectives in Biology 2, n. 7 (2010, Paraspeckles): a000687. doi:10.1101/cshperspect.a000687

Gagliardi, S., Zucca, S., Pandini, C., Diamanti, L., Bordoni, M., Sproviero, D., et al. (2018). Long Non-coding and Coding RNAs Characterization in Peripheral Blood Mononuclear Cells and Spinal Cord from Amyotrophic Lateral Sclerosis Patients. *Sci. Rep.* 8 (5 febbraio 2018), 2378. doi:10.1038/s41598-018-20679-5

Genomics (2021). Front Line. «Long-Read Sequencing vs Short-Read Sequencing». Front Line Genomics (Blog). https://frontlinegenomics.com/long-read-sequencing-vs-short-read-sequencing/.

Group Therapy for Schizophrenia (2020d2020). "Group therapy for schizophrenia: A meta-analysis": Correction to Burlingame et al. (2020). *Psychotherapy (Chic)* 57 (4), 597. doi:10.1037/pst0000354

Harrison, D., Mehta, P., van Es, M. A., Stommel, E., Drory, V. E., Nefussy, B., et al. (2018n2018). "ALS Reversals": Demographics, Disease Characteristics, Treatments, and Co-morbidities. *Amyotroph. Lateral Scler. Frontotemporal Degeneration* 19 (7), 495–499. 8. doi:10.1080/21678421.2018.1457059

Hobson, E. V., Harwood, C. A., McDermott, Christopher. J., Shaw, e. Pamela. J., McDermott, C. J., and Shaw, P. J. (2016). Clinical Aspects of Motor Neurone Disease. *Medicine* 44 (9), 552–556. doi:10.1016/j.mpmed.2016.06.004

Kang, S. H., Li, Y., Fukaya, M., Lorenzini, I., Cleveland, D. W., Ostrow, Lyle. W., et al. (2013). Degeneration and Impaired Regeneration of Gray Matter Oligodendrocytes in Amyotrophic Lateral Sclerosis. *Nat. Neurosci.* 16 (5), 571–579. doi:10.1038/nn.3357

Kinoshita, C., Kubota, N., and Aoyama, K. (2021). Interplay of RNA-Binding Proteins and microRNAs in Neurodegenerative Diseases. *Ijms* 2210, 5292. doi:10.3390/ijms22105292

Kiskinis, E., Sandoe, J., Williams, L. A., Boulting, G. L., Moccia, R., Wainger, B. J., et al. (2014). Pathways Disrupted in Human ALS Motor Neurons Identified through Genetic Correction of Mutant SOD1. *Cell Stem Cell* 14 (6), 781–795. doi:10.1016/j.stem.2014.03.004

Krokidis, M. G., and Vlamos, P. (2018). Transcriptomics in Amyotrophic Lateral Sclerosis. *Front. Biosci. (Elite Ed.* 10 (1), 103–121. doi:10.2741/e811

Krokidis, M. G., and Vlamos, e. Panagiotis. (2018). Transcriptomics in Amyotrophic Lateral Sclerosis. *Front. Biosci.* 10, 103–121. doi:10.2741/e811

La Cognata, V., Morello, G., Cavallaro, S., and Cavallaro, e. Sebastiano. (2021). Omics Data and Their Integrative Analysis to Support Stratified Medicine in Neurodegenerative Diseases. *Ijms* 22 (9), 4820. doi:10.3390/ijms22094820

Lanznaster, D., de Assis, D. R., Corcia, P., Pradat, P.-F., and Blasco, H. (2018). Metabolomics Biomarkers: A Strategy toward Therapeutics Improvement in ALS. *Front. Neurol.* 9, 1126. doi:10.3389/fneur.2018.01126

Legnini, I., Di Timoteo, G., Rossi, F., Morlando, M., Briganti, F., Sthandier, O., et al. (2017). Circ-ZNF609 Is a Circular RNA that Can Be Translated and Functions in Myogenesis. *Mol. Cel* 66 (1), 22–37.e9. doi:10.1016/j.molcel.2017.02.017

Liu, E. Y., Cali, C. P., and Lee, E. B. (2017). RNA Metabolism in Neurodegenerative Disease. *Dis. Models Mech.* 10 (5), 509–518. doi:10.1242/dmm.028613

Liu, W., Venugopal, S., Majid, S., Ahn, I. S., Diamante, G., Hong, J., et al. (2020). Single-Cell RNA-Seq Analysis of the Brainstem of Mutant SOD1 Mice Reveals Perturbed Cell Types and Pathways of Amyotrophic Lateral Sclerosis. *Neurobiol. Dis.* 141 (luglio 2020), 104877. doi:10.1016/j.nbd.2020.104877

Liu, D., Zuo, X., Zhang, P., Zhao, R., Lai, D., Chen, K., et al. (2021). The Novel Regulatory Role of LncRNA-MiRNA-MRNA Axis in Amyotrophic Lateral Sclerosis: An Integrated Bioinformatics Analysis. *Comput. Math. Methods Med.* 2021, 1–12. doi:10.1155/2021/5526179

Loffreda, A., Nizzardo, M., Arosio, A., Ruepp, M.-D., Calogero, R. A., Volinia, S., et al. (2020). MiR-129-5p: A Key Factor and Therapeutic Target in Amyotrophic Lateral Sclerosis. *Prog. Neurobiol.* 190 (1 luglio 2020), 101803. doi:10.1016/j.pneurobio.2020.101803

Ma, N., Tie, C., Yu, B., Zhang, W., and Wan, J. (2020). Identifying lncRNA-miRNA-mRNA Networks to Investigate Alzheimer's Disease Pathogenesis and Therapy Strategy. *Aging* 12 (3), 2897–2920. doi:10.18632/aging.102785

MicroRNAs in amyotrophic lateral sclerosis: from pathogenetic involvement to diagnostic biomarker and therapeutic agent development | SpringerLink (2021). Consultato. Available at: https://link.springer.com/article/10.1007/s10072-020-04773-z.

Mutant FUS and ELAVL4 (HuD) Aberrant Crosstalk in Amyotrophic Lateral Sclerosis - PubMed (2021). Consultato. Available at: https://pubmed.ncbi.nlm.nih.gov/31242416/.

Nik, S., and Bowman, T. V. (2019). Splicing and Neurodegeneration: Insights and Mechanisms. *WIREs RNA* 10 (4), e1532. doi:10.1002/wrna.1532

Olejniczak, M., Kotowska-Zimmer, A., and Krzyzosiak, W. (2018). Stress-induced Changes in miRNA Biogenesis and Functioning. *Cell. Mol. Life Sci.* 75 (2), 177–191. doi:10.1007/s00018-017-2591-0

Perrone Benedetta e Francesca Luisa Conforti (2020). Common Mutations of Interest in the Diagnosis of Amyotrophic Lateral Sclerosis: How Common Are Common Mutations in ALS Genes? *Expert Rev. Mol. Diagn.* 20 (7), 703–714. doi:10.1080/14737159.2020.1779060

Pham, J., Keon, M., Brennan, S., and Saksena, N. (2020). Connecting RNA-Modifying Similarities of TDP-43, FUS, and SOD1 with MicroRNA Dysregulation amidst A Renewed Network Perspective of Amyotrophic Lateral Sclerosis Proteinopathy. *Ijms* 21 (10), 3464. doi:10.3390/ijms21103464

Philips, A., Nowis, K., Stelmaszczuk, M., Jackowiak, P., Podkowiński, J., Handschuh, L., et al. (2020). Expression Landscape of circRNAs in *Arabidopsis thaliana* Seedlings and Adult Tissues. *Front. Plant Sci.* 11, 576581. doi:10.3389/fpls.2020.576581

Riera-Punet, N., Martinez-Gomis, J., Paipa, A., Povedano, M., and Peraire, M. (2018). Alterations in the Masticatory System in Patients with Amyotrophic Lateral Sclerosis. *J. Oral Facial Pain Headache* 32 (1), 84–90. doi:10.11607/ofph.1882

«RNA sequencing: the teenage years | Nature Reviews Genetics» (2021). . https://www.nature.com/articles/s41576-019-0150-2.Consultato

Salta, E., and De Strooper, B. (2017). Noncoding RNAs in Neurodegeneration. *Nat. Rev. Neurosci.* 18 (10), 627–640. doi:10.1038/nrn.2017.90

Sardina, D. S., Alaimo, S., Ferro, A., Pulvirenti, A., and Giugno, R. (2017). A Novel Computational Method for Inferring Competing Endogenous Interactions. *Brief Bioinform* 18 (6), bbw084–81. doi:10.1093/bib/bbw084

Saucier, D., Wajnberg, G., Roy, J., Beauregard, A.-P., Chacko, S., Crapoulet, N., et al. (2019). Identification of a Circulating MiRNA Signature in Extracellular Vesicles Collected from Amyotrophic Lateral Sclerosis Patients. *Brain Res.* 1708, 100–108. doi:10.1016/j.brainres.2018.12.016

Scotti, M. M., and Swanson, M. S. (2016). RNA Mis-Splicing in Disease. *Nat. Rev. Genet.* 17 (1), 19–32. doi:10.1038/nrg.2015.3

Scotti, M. M., and Swanson, M. S. (2016). RNA Mis-Splicing in Disease. *Nat. Rev. Genet.* 17 (1), 19–32. doi:10.1038/nrg.2015.3

Spatiotemporal dynamics of molecular pathology in amyotrophic lateral sclerosis (2021). Consultato. Available at: https://www.science.org/doi/10.1126/science.aav9776?url_ver=Z39.88-2003&rfr_id=ori:rid:crossref.org&rfr_dat=cr_pub%20%200pubmed.

Srebrow, A., and Kornblihtt, A. R. (2006). The Connection between Splicing and Cancer. *J. Cel Sci.* 119 (Pt 13), 2635–2641. (1 luglio 2006. doi:10.1242/jcs.03053

Strafella, C., Caputo, V., Galota, M. R., Zampatti, S., Marella, G., Mauriello, S., et al. (2018). Application of Precision Medicine in Neurodegenerative Diseases. *Front. Neurol.* 9, 701. doi:10.3389/fneur.2018.00701

Strafella, C., Caputo, V., Termine, A., Fabrizio, C., Ruffo, P., Potenza, S., et al. (2021). Genetic Determinants Highlight the Existence of Shared Etiopathogenetic Mechanisms Characterizing Age-Related Macular Degeneration and Neurodegenerative Disorders. *Front. Neurol.* 12 (2021), 626066. doi:10.3389/fneur.2021.626066

Strafella, C., Caputo, V., Termine, A., Assogna, F., Pellicano, C., Pontieri, F. E., et al. (2021). Immune System and Neuroinflammation in Idiopathic Parkinson's Disease: Association Analysis of Genetic Variants and miRNAs Interactions. *Front. Genet.* 12, 651971. doi:10.3389/fgene.2021.651971

Su, L., Chen, S., Zheng, C., Wei, H., and Song, X. (2019). Meta-Analysis of Gene Expression and Identification of Biological Regulatory Mechanisms in Alzheimer's Disease. *Front. Neurosci.* 13, 633. doi:10.3389/fnins.2019.00633

Sutherland, G. T., Janitz, M., and Kril, J. J. (2011). Understanding the Pathogenesis of Alzheimer's Disease: Will RNA-Seq Realize the Promise of Transcriptomics? *J. Neurochem.* 116 (6), 937–946. doi:10.1111/j.1471-4159.2010.07157.x

Suzuki, H., Shibagaki, Y., Hattori, S., and Matsuoka, M. (2019). C9-ALS/FTD-linked Proline-Arginine Dipeptide Repeat Protein Associates with Paraspeckle Components and Increases Paraspeckle Formation. *Cell Death Dis* 1010, 746. doi:10.1038/s41419-019-1983-5

Tortelli, R., Copetti, M., Ruggieri, M., Cortese, R., Capozzo, R., Leo, A., et al. (2015). Cerebrospinal Fluid Neurofilament Light Chain Levels: Marker of Progression to Generalized Amyotrophic Lateral Sclerosis. *Eur. J. Neurol.* 22, 215–218. doi:10.1111/ene.12421

Ule, J., and Blencowe, B. J. (2019). Alternative Splicing Regulatory Networks: Functions, Mechanisms, and Evolution. *Mol. Cel* 76, 329–345. doi:10.1016/j.molcel.2019.09.017

Vangoor, V. R., Gomes-DuartePasterkamp, A., and Pasterkamp, R. J. (2021). Long Non-coding RNAs in Motor Neuron Development and Disease. *J. Neurochem.* 156 (6), 777–801. doi:10.1111/jnc.15198

Vaz, A. R., Vizinha, D., Morais, H., Colaço, A. R., Loch-Neckel, G., Barbosa, M., et al. (20212021). Overexpression of MiR-124 in Motor Neurons Plays a Key Role in ALS Pathological Processes. *Ijms* 22 (11), 6128. doi:10.3390/ijms22116128

Verde, F., Steinacker, P., Weishaupt, J. H., Kassubek, J., Oeckl, P., Halbgebauer, S., et al. (2019). Neurofilament Light Chain in Serum for the Diagnosis of Amyotrophic Lateral Sclerosis. *J. Neurol. Neurosurg. Psychiatry* 90 (2), 157–164. doi:10.1136/jnnp-2018-318704

Vrabec, K., Boštjančič, E., Koritnik, B., Leonardis, L., Dolenc Grošelj, L., Zidar, J., et al. (2018). Differential Expression of Several MiRNAs and the Host Genes AATK and DNM2 in Leukocytes of Sporadic ALS Patients. *Front. Mol. Neurosci.* 11. doi:10.3389/fnmol.2018.00106

Wang, Z., Gerstein, M., and Snyder, M. (2009). RNA-seq: A Revolutionary Tool for Transcriptomics. *Nat. Rev. Genet.* 10 (1), 57–63. doi:10.1038/nrg2484

Wang, J., Zhu, S., Meng, N., He, Y., Lu, R., and Yan, G.-R. (2019). NcRNA-Encoded Peptides or Proteins and Cancer. *Mol. Ther.* 27 (10), 1718–1725. doi:10.1016/j.ymthe.2019.09.001

Wang, R., Li, Q., He, Y., Yang, Y., Ma, Q., and Li, C. (2020). miR-29c-3p Inhibits Microglial NLRP3 Inflammasome Activation by Targeting NFAT5 in Parkinson's Disease. *Genes Cells* 25 (6), 364–374. doi:10.1111/gtc.12764

Xie, L., Mao, M., Xiong, K., and Jiang, B. (2017). Circular RNAs: A Novel Player in Development and Disease of the Central Nervous System. *Front. Cel. Neurosci.* 11, 354. doi:10.3389/fncel.2017.00354

Yu, Y., Pang, D., Li, C., Gu, X., Chen, Y., Ou, R., et al. 2021, The Expression Discrepancy and Characteristics of Long Non-coding RNAs in Peripheral Blood Leukocytes from Amyotrophic Lateral Sclerosis Patients. doi:10.21203/rs.3.rs-565200/v2

Yuan, Q., Guo, X., Ren, Y., Wen, X., and Gao, L. (2020). Cluster Correlation Based Method for lncRNA-Disease Association Prediction. *BMC Bioinformatics* 21 (1), 180. doi:10.1186/s12859-020-3496-8

Zhou, W.-Y., Cai, Z.-R., Liu, J., Wang, D.-S., JuXu, H.-Q., and Xu, R.-H. (2020). Circular RNA: Metabolism, Functions and Interactions with Proteins. *Mol. Cancer* 19, 172. doi:10.1186/s12943-020-01286-3

Zucca, S., Gagliardi, S., Pandini, C., Diamanti, L., Bordoni, M., Sproviero, D., et al. (2019). RNA-seq Profiling in Peripheral Blood Mononuclear Cells of Amyotrophic Lateral Sclerosis Patients and Controls. *Sci. Data* 6 (5 febbraio 2019), 190006. doi:10.1038/sdata.2019.6

Conflict of Interest: The authors declare that the research was conducted in the absence of any commercial or financial relationships that could be construed as a potential conflict of interest.

Publisher's Note: All claims expressed in this article are solely those of the authors and do not necessarily represent those of their affiliated organizations, or those of the publisher, the editors and the reviewers. Any product that may be evaluated in this article, or claim that may be made by its manufacturer, is not guaranteed or endorsed by the publisher.

frontiers in Genetics

ORIGINAL RESEARCH
published: 14 March 2022
doi: 10.3389/fgene.2022.810974

Profile and Functional Prediction of Plasma Exosome-Derived CircRNAs From Acute Ischemic Stroke Patients

*Jie Yang[1,2], Junli Hao[3], Yapeng Lin[2], Yijia Guo[4], Ke Liao[4], Min Yang[2], Hang Cheng[2], Ming Yang[2] and Kejie Chen[5]**

[1]Department of Neurology, Sichuan Provincial People's Hospital, University of Electronic Science and Technology of China, Chengdu, China, [2]Department of Neurology, Clinical Medical College, The First Affiliated Hospital of Chengdu Medical College, Chengdu, China, [3]School of Bioscience and Technology, Chengdu Medical College, Chengdu, China, [4]International Clinical Research Center, Chengdu Medical College, Chengdu, China, [5]School of Public Health, Chengdu Medical College, Chengdu, China

Stroke is one of the major causes of death and long-term disability, of which acute ischemic stroke (AIS) is the most common type. Although circular RNA (circRNA) expression profiles of AIS patients have been reported to be significantly altered in blood and peripheral blood mononuclear cells, the role of exosome-containing circRNAs after AIS is still unknown. Plasma exosomes from 10 AIS patients and 10 controls were isolated, and through microarray and bioinformatics analysis, the profile and putative function of circRNAs in the plasma exosomes were studied. A total of 198 circRNAs were differentially quantified ($|\log2 \text{ fold change}| \geq 1.00$, $p < 0.05$) between AIS patients and controls. The levels of 12 candidate circRNAs were verified by qRT-PCR, and the quantities of 10 of these circRNAs were consistent with the data of microarray. The functions of host genes of differentially quantified circRNAs, including RNA and protein process, focal adhesion, and leukocyte transendothelial migration, were associated with the development of AIS. As a miRNA sponge, differentially quantified circRNAs had the potential to regulate pathways related to AIS, like PI3K-Akt, AMPK, and chemokine pathways. Of 198 differentially quantified circRNAs, 96 circRNAs possessing a strong translational ability could affect cellular structure and activity, like focal adhesion, tight junction, and endocytosis. Most differentially quantified circRNAs were predicted to bind to EIF4A3 and AGO2—two RNA-binding proteins (RBPs)—and to play a role in AIS. Moreover, four of ten circRNAs with verified levels by qRT-PCR (hsa_circ_0112036, hsa_circ_0066867, hsa_circ_0093708, and hsa_circ_0041685) were predicted to participate in processes of AIS, including PI3K-Akt, AMPK, and chemokine pathways as well as endocytosis, and to be potentially useful as diagnostic biomarkers for AIS. In conclusion, plasma exosome-derived circRNAs were significantly differentially quantified between AIS patients and controls and participated in the occurrence and progression of AIS by sponging miRNA/RBPs or translating into proteins, indicating that circRNAs from plasma exosomes could be crucial molecules in the pathogenesis of AIS and promising candidates as diagnostic biomarkers and therapeutic targets for the condition.

Keywords: circRNA, plasma exosome, profile, acute ischemic stroke, ceRNA

OPEN ACCESS

Edited by:
Gabriel Adelman Cipolla, Federal University of Paraná, Brazil

Reviewed by:
Jiankun Zang, Jinan University, China
Venkata Garikipati, The Ohio State University, United States

****Correspondence:***
Kejie Chen
ckj930@126.com

Specialty section:
This article was submitted to RNA, a section of the journal Frontiers in Genetics

Received: *08 November 2021*
Accepted: *31 January 2022*
Published: *14 March 2022*

Citation:
Yang J, Hao J, Lin Y, Guo Y, Liao K, Yang M, Cheng H, Yang M and Chen K (2022) Profile and Functional Prediction of Plasma Exosome-Derived CircRNAs From Acute Ischemic Stroke Patients. Front. Genet. 13:810974. doi: 10.3389/fgene.2022.810974

INTRODUCTION

As a common vascular disease, stroke is one of the major causes of death and long-term disability, challenging the current healthcare system worldwide (Hu et al., 2017; Szegedi et al., 2017). Of all stroke cases, ischemic stroke (IS) accounts for more than 80% of them (Benjamin et al., 2018). In humans, IS results from various factors or diseases, including hypertension, large-vessel atherosclerosis and rupture of an atherosclerotic plaque, cardioembolism, and lacunar infarcts induced by small-vessel disease. However, the underlying mechanism and relationship of these factors or diseases with stroke remain incompletely known, which restricts safer and more efficient treatment to stroke. To treat patients with IS, early reperfusion of blocked arteries is most frequently performed, even though it is constrained by a narrow time window and risk of bleeding (Snow, 2016; Alberts, 2017; Powers et al., 2018). Therefore, novel targets for diagnostics or therapeutics are urgently needed for patients with IS.

Exosomes, nanosized vesicles (~30–150 nm) with lipid bilayer membranes, are secreted by various cells and naturally present in the blood (Caby et al., 2005; Couzin, 2005; Raposo and Stoorvogel, 2013). When incorporating into target recipient cells, exosomes release cargos, like proteins, lipids, DNA, mRNAs, and noncoding RNAs (Hon et al., 2017; Skotland et al., 2017; Mousavi et al., 2019), into the cellular microenvironment of recipient cells (Cocucci et al., 2009; Simons and Raposo, 2009). Therefore, exosomes play a crucial role in cell-to-cell communication and intercellular signal transduction (Zhang et al., 2017) and are emerging as promising targets for the pathogenesis of diseases and potent tools for diagnosis and therapy. Among the various cargos in exosomes, circular RNA (circRNA) is attracting more attention due to its unique structure. CircRNAs are a class of noncoding RNAs with covalent bonds between 3′ head and 5′ tail ends to produce a circular pattern (Memczak et al., 2013), a more stable one than that of linear RNAs (Suzuki et al., 2006). Moreover, circRNAs are highly conserved and abundantly expressed in human cells (Rybak-Wolf et al., 2015) and characterized by distinct tissue-specific expression (Memczak et al., 2013). The high stability, evolutionary conservation, and abundance of circRNAs in various species endow them with numerous different potential functions in the regulation of gene expression, such as miRNA sponges, interactions with RNA-binding proteins (RBPs), or translation into proteins (Han et al., 2018). Consequently, circRNAs have been considered important biological regulators for understanding the molecular mechanisms of disease and identifying effective diagnostic biomarkers or therapeutic targets (Liu W. et al., 2017).

CircRNAs have been reported to be involved in the progression of many diseases, including Alzheimer's disease (Lukiw, 2013), cardiovascular diseases (Du et al., 2017a; Jiang et al., 2019), atherosclerosis (Burd et al., 2010), stroke (Peng et al., 2019; Li et al., 2021), and various cancers (Li et al., 2015; Yao et al., 2017). Recently, circRNAs have been considered to be potential biomarkers or targets for diagnosis or treatment of acute IS (AIS) (Lu et al., 2020; Zuo et al., 2020). CircUCK2, as a miRNA sponge, markedly reduced IS infarct volume and improved neurological impairment in the mouse model of focal cerebral ischemia and reperfusion (Chen W. et al., 2020), while circHECTD1 aggravated cerebral infarction volume and neuronal apoptosis in the mouse model of IS (Dai et al., 2021). Moreover, circRNAs exhibit dynamic expression patterns in a series of physiological and pathological conditions and possess important regulatory effects. Expression profiles of circRNAs from peripheral blood mononuclear cells and blood of patients with AIS are significantly different from those of controls (Li S. et al., 2020; Dong et al., 2020; Ostolaza et al., 2020).

However, the profile and regulatory network of circRNAs derived from plasma exosomes of patients with AIS remain unclear. In this prospective investigation, a case-controlled study was conducted, and the circRNA profile of plasma exosomes was compared between AIS patients and controls through microarray. By bioinformatics approaches, the functions and signaling pathways of differentially quantified circRNAs were analyzed. Based on the results of microarray, 12 circRNAs with high fold changes among differentially quantified circRNAs were chosen for validation by qRT-PCR, and their roles in the pathogenesis of AIS and diagnostic values for AIS were also explored. The data of the present study shed light on the possible roles of exosome-derived circRNAs in regulating the pathogenesis of AIS and provide new potential targets for diagnosis and therapy of AIS.

TABLE 1 | Demographic characteristics of AIS patients and controls.

Characteristics	AIS patients	Controls
Age (mean ± SD), year	75.80 ± 7.84	68.17 ± 10.97
Male, *n* (%)	5 (50%)	5 (50%)
Ethnic Han, *n* (%)	10 (100%)	10 (100%)
Time after onset (mean ± SD), hour	6.65 ± 4.37	—
Comorbidity, n (%)		
Hypertension	4 (40%)	0 (0%)
Diabetes	3 (30%)	0 (0%)
Coronary heart disease	4 (40%)	0 (0%)
Atrial fibrillation	2 (20%)	0 (0%)

—, *not applicable.*

MATERIALS AND METHODS

Study Subjects

Ten adult patients with AIS (five males and five females) were selected from the First Affiliated Hospital of Chengdu Medical College in 2020. AIS was diagnosed according to the Guidelines for the Prevention of Stroke in Patients with Stroke and Transient Ischemic Attack (Kernan et al., 2014). Ten controls approximately age-matched were enrolled from the health management center of the First Affiliated Hospital of Chengdu Medical College in 2020. The demographic description of AIS patients and controls is shown in **Table 1**. The investigation was approved by the Ethical Committee of First Affiliated Hospital of Chengdu Medical College. All study participants or their authorized representatives signed informed consent forms.

Inclusion criteria are as follows: (1) aged 50–90 years old, (2) within 24 h after onset, and (3) have agreed to sign the informed

consent. Exclusion criteria are as follows: (1) have received thrombolysis and/or thrombectomy treatment and (2) have other concomitant diseases, including acute infection, immune diseases, neurodegenerative diseases, and tumors.

Isolation and Characterization of Plasma Exosomes

Blood samples from 10 AIS patients and 10 controls included in the present study were collected into EDTA tubes by venipuncture. After centrifuging at 2,000 rcf for 15 min at room temperature, a clear top layer was harvested to a labeled tube (BS-50-M, Biosharp, China) and stored at −80°C. Plasma exosomes were isolated using the exoRNeasy Serum/Plasma Maxi kit (77064, Qiagen Sciences Inc., Germany) following the manufacturer's instruction. The resulting exosome pellet was suspended in PBS for further RNA or protein extraction. The exosome fraction isolated from plasma was characterized by western blot, nanoparticle tracking analysis (NTA), and transmission electron microscopy (TEM).

Western Blot

Plasma exosomes suspended in PBS were mixed with the same volume of RIPA lysis buffer, and exosome proteins were purified from each sample and separated by SDS-PAGE gel and then transferred to a polyvinylidene fluoride (PVDF) membrane. The membrane was blocked using 5% BSA and then treated with antibodies against CD63 (ab134045, Abcam, United Kingdom) or TSG101 (ab133586, Abcam, United Kingdom) at 4°C for 12 h. Horseradish peroxidase-conjugated secondary antibody (SBI, United States) was then applied, and the blots were developed with enhanced chemiluminescence reagents.

NTA

Isolated exosomes were diluted in PBS and analyzed using the ZetaView (S/N 17-310, Particle Metrix, Germany) with NTA software (ZetaView 8.04.02). Triplicate measurements were recorded for each sample. Size distribution and concentration profiles were averaged to derive the representative size distribution profiles.

TEM

Plasma exosomes suspended in PBS were fixed in 2% paraformaldehyde. The fixed sample was absorbed onto formvar-coated copper grids for 5 min at room temperature. After being rinsed in distilled water, samples were stained with methyl cellulose uranyl acetate for 1 min at room temperature. Excess liquid was wicked off the grid using filter paper, and grids were stored at room temperature until imaging. Imaging was performed using Tecnai G2 Spirit BioTwin (FEI, United States).

Total RNA Extraction From Plasma Exosomes

By exoRNeasy Serum/Plasma Maxi Kit (77064, Qiagen Sciences Inc., Germany), total RNA was extracted from plasma exosomes isolated from the 10 AIS patients and 10 controls following the manufacturer's recommendation. RNA integrity of total RNA was inspected by an Agilent Bioanalyzer 4200 (Agilent Technologies, Santa Clara, CA, United States) (data not shown).

TABLE 2 | The primer sequences of 12 differentially quantified circRNAs.

circRNA	Sequence (5′–3′)
hsa_circ_0131433	Forward: TCTGTGAGGTTCTTGATTTGGA
	Reverse: TCTTTTCCCTCTTGCCTTCC
hsa_circ_0123103	Forward: GAAATGCCGTGTGGAACTCT
	Reverse: TTCATGATCACTTGGGCAGT
hsa_circ_0112036	Forward: CACGAGAATTGAAGTGGGAGA
	Reverse: TGCATTTCGAGAGCAATGAG
hsa_circ_0050840	Forward: CTTGTCCACTCCGGCTAAAG
	Reverse: CTCCTGTTCATGTGGGGACT
hsa_circ_0077256	Forward: TTGAATGAGGGTCGCTGTCT
	Reverse: AGCTGCTAGTCAGTCACATTCG
hsa_circ_0113001	Forward: GACCAGGCAAGCTAGTGCTC
	Reverse: TTTGGAGCACTCTTCAAGTCC
hsa_circ_0092545	Forward: GAAATGGCAACTTTCCTCCA
	Reverse: CCACACAGCATCAGGTTTTG
hsa_circ_0041685	Forward: GACAGTCTCCAGGGAAAGCA
	Reverse: GCCTCCTGAATCTGAATTCCT
hsa_circ_0059662	Forward: ATCTCCTGTCCCCTGCTCAT
	Reverse: TGAGTCACCCCAACCTCTGT
hsa_circ_0032222	Forward: ACCTGTGTGGCCTGGTACAT
	Reverse: GTGTCAATGGCATCCTCCAC
hsa_circ_0093708	Forward: AACACAGCTGACTGGGTCCT
	Reverse: CAGCCTCTCTTCTCCAGGAA
hsa_circ_0066867	Forward: CCTGTTGGTTGCTCTTTTCA
	Reverse: TGATAGGTGGGACTGGAAGG

CircRNA Microarray Profiling

SurePrint G3 Human ceRNA microarray (4 × 180K, design ID: 085499) was made by Agilent Technologies and contained probes interrogating 84,569 circRNAs. Total RNAs were incubated with RNase R to eliminate linear RNAs. The enriched circRNAs were transcribed into fluorescent complementary RNA (cRNA), which then were hybridized onto the circRNA microarray. After hybridization, the signal of the circRNA microarray was scanned using the Agilent Microarray Scanner (Agilent Technologies Inc., Santa Clara, CA, United States).

Microarray Data Analysis

The scanned information was extracted using the Agilent Feature Extraction software 10.7 (Agilent Technologies Inc., Santa Clara, CA, United States). Raw data were normalized by quantile algorithm, R package "limma". Differentially quantified circRNAs were identified through volcano plot filtering. Hierarchical clustering analysis was conducted to display the circRNA profile pattern between patients with AIS and controls.

Validation of Selected Differentially Quantified circRNAs by qRT-PCR

The microarray results were verified by qRT-PCR using samples from the same subjects (10 AIS patients and 10 controls). Total RNA from plasma exosomes was incubated with RNase R to eliminate linear RNAs and reverse transcribed by RevertAid First-Strand cDNA Synthesis Kit (K1622, Thermo Scientific,

United States). CircRNA levels were determined by qRT-PCR *via* TB Green® *Premix Ex Taq*™ II (RR820Q, TaKaRa, Japan) with the BIO-RAD system (MiniOpticon, United States) according to the instruction of the manufacturer. The reaction system was 25 μl in volume and consisted of 12.5 μl of TB Green *Premix Ex Taq* II, 2 μl of cDNA, 1 μl of forward and reverse primers (10 μM), and 8.5 μl of RNase-free water. The optimum reaction conditions were as follows: 95°C for 30 s, followed by 40 cycles of 95°C for 5 s and 60°C for 30 s. Twelve circRNAs with high fold changes from the microarray results were chosen for validation by qRT-PCR with GAPDH as a normalization reference. The specific primers for target circRNAs are described in **Table 2** and synthesized by Sangon Biotech (Shanghai, China). The primers for GAPDH were purchased from Sangon Biotech (B662104, Sangon Biotech, China). All reactions were performed in triplicate. The threshold cycle (Ct) was determined using the default threshold settings, and the average Ct value was used to calculate the relative fold changes of the 12 circRNAs by the $2^{-\Delta\Delta Ct}$ method (Livak and Schmittgen, 2001).

Bioinformatics Analysis and Target Prediction

Host/target genes of differentially quantified circRNAs were illuminated by Gene Ontology (GO, http://www.geneontology.org/) and Kyoto Encyclopedia of Genes and Genomes (KEGG, http://kobas.cbi.pku.edu.cn/) analyses. Target miRNAs of circRNAs were predicted using miRanda (http://www.microrna.org/microrna/home.do) and TargetScan (http://www.targetscan.org/vert_72/). MiRNA response elements as regulators of mRNAs were predicted through TargetScan (http://www.targetscan.org/vert_72/) and microT-CDS (http://www.microrna.gr/microT-CDS). All circRNA–miRNA–mRNA interaction networks of differentially quantified circRNAs were visualized by Cytoscape 3.8.2. The tissue specificity of differentially quantified circRNAs was annotated *via* TSCD (http://gb.whu.edu.cn/TSCD/). The types and sites of RBPs binding to differentially quantified circRNAs were annotated by circinteractome (https://circinteractome.nia.nih.gov/). The probability of differentially quantified circRNAs coding for proteins was estimated by circBank (http://www.circbank.cn/), in which circRNAs with a coding probability >0.99 were analyzed.

Receiver Operating Characteristic Curve Analysis

The levels of differentially quantified circRNAs verified by qRT-PCR were applied to generate ROC curves for the 10 AIS patients and 10 controls. The area under the curve (AUC) was calculated to assess the predictive value of the selected circRNAs for AIS diagnosis.

Statistical Analysis

The differentially quantified circRNAs were defined as $|\log_2 \text{fold change}| \geq 1.00$ and $p < 0.05$. The *p*-value denotes the significance of GO and KEGG pathway analyses ($p < 0.05$). All statistical analyses were performed by SPSS (26.0, IBM, United States). All data were represented as the mean ± standard deviation ($\bar{X} \pm SD$). A *p*-value <0.05 was considered statistically significant.

RESULTS

Characterization of Plasma Exosome

The exosomes isolated from plasma of patients with AIS and controls had obvious detectable levels of CD63 and TSG101 by western blot (**Figure 1A**). The typical bilayer of exosomes was observed (**Figures 1B,C**) through TEM, and the median size of exosomes isolated from plasma was ~137 nm for controls and ~141 nm for patients with AIS (**Figures 1D,E**, respectively). These data confirmed that we successfully isolated plasma exosomes from blood.

Profile of CircRNAs Derived From Plasma Exosomes

The profile of 84,569 human circRNAs was generated by SurePrint G3 Human ceRNA microarray using plasma exosomes from patients with AIS and controls. After fold-change filtering, 198 circRNAs were differentially quantified between patients with AIS and controls, including 72 upregulated ($\log_2$ fold change ≥ 1.00, $p < 0.05$) and 126 downregulated ($\log_2$ fold change ≤ −1.00, $p < 0.05$) circRNAs. Hierarchical clustering of the levels between AIS patients and controls is illustrated in **Figure 2A**. The volcano plot showed that significant variation was observed in circRNA levels between AIS patients and controls (**Figure 2B**).

The distribution patterns of differentially quantified circRNAs in the chromosomes are shown in **Figure 3A**, indicating that the profile of circRNAs in patients with AIS was significantly different from that in controls. Moreover, the tissue-specific analysis showed that the differentially quantified circRNAs were mainly derived from the digestive system (esophagus, esophagogastric junction, intestine, and liver), the cardiovascular system (blood vessel and heart), and lungs (**Figure 3B**).

GO and KEGG Pathway Analyses of Host Genes of Differentially Quantified circRNAs

The different profiles of circRNAs between patients with AIS and controls could be the result of disordered expression of host genes generating circRNAs; thus, GO and KEGG pathway analyses were performed to evaluate the putative functions of host genes. According to the GO analysis shown in **Figure 4A**, the host genes of differentially quantified circRNAs, in the cellular component, were mainly involved in ribonucleoprotein (ribonucleoprotein complex, cytoplasmic ribonucleoprotein granule, and ribonucleoprotein granule) and cell junction (focal adhesion and cellsubstrate junction). The molecular functions related to host genes mainly included translation regulator activity and binding (ribosome,

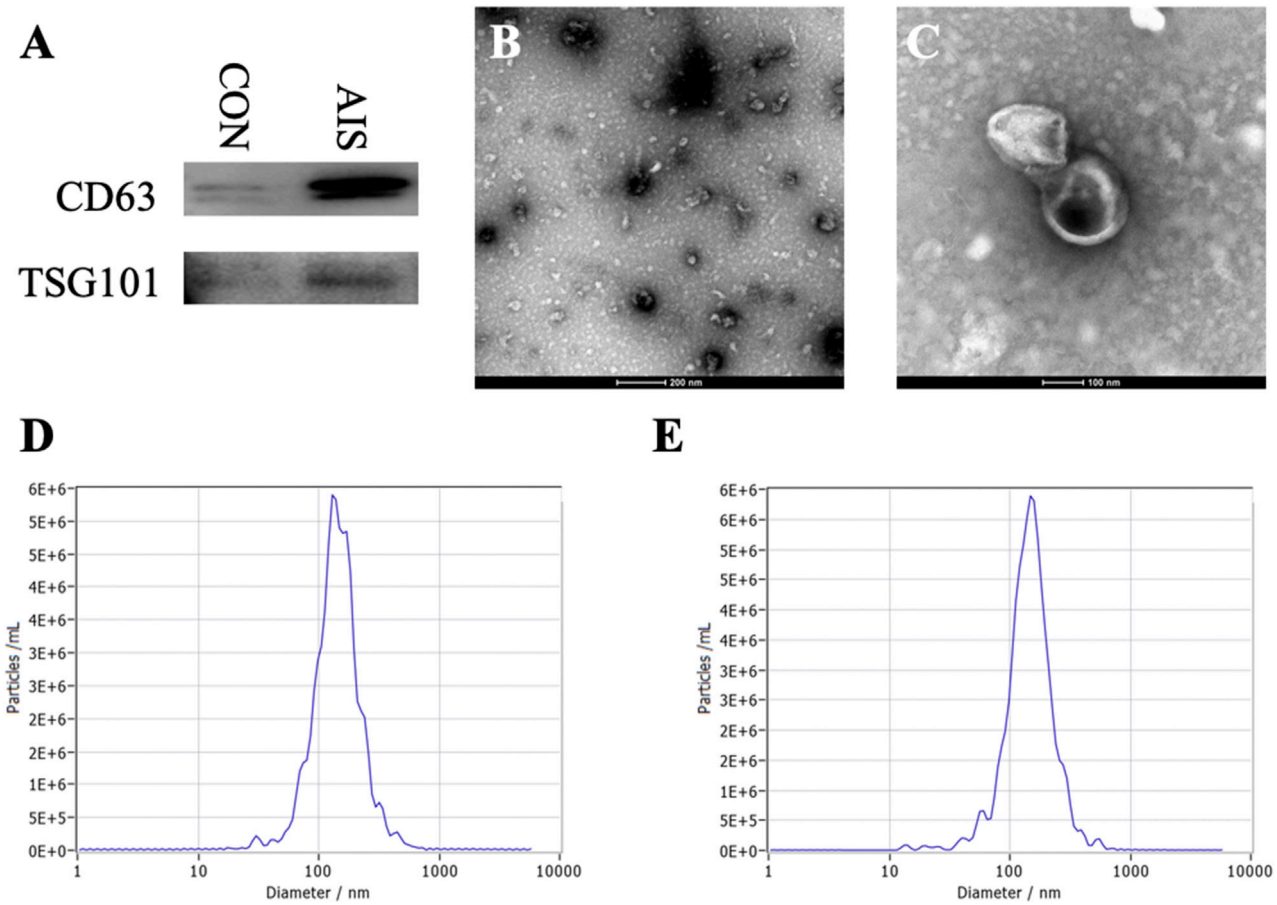

FIGURE 1 | Identification and characterization of plasma exosomes. **(A)** Detection of CD63 and TSG101 as exosome markers by western blot. **(B,C)** Representative images of transmission electron microscopy. **(D,E)** Representative size of exosomes from controls and AIS patients, respectively.

ribonucleoprotein, and cadherin), and the major biological processes of host genes were associated with RNA regulation. The KEGG analysis showed that intracellular physiological processes (like RNA transport and protein processing in endoplasmic reticulum) and intercellular interaction (like focal adhesion and leukocyte transendothelial migration) could be affected, indicating cellular functions disrupted in AIS (**Figure 4B**).

Validation of Levels of Differentially Quantified circRNAs

To validate the results from microarray, the levels of 12 differentially quantified circRNAs with high fold changes were determined using qRT-PCR. Among 12 selected differentially quantified circRNAs, the levels of 10 circRNAs were significantly different ($p < 0.05$) between AIS patients and controls, including five upregulated (hsa_circ_0066867, hsa_circ_0093708, hsa_circ_0032222, hsa_circ_0059662, and hsa_circ_0041685) and five downregulated (hsa_circ_0131433, hsa_circ_0123103, hsa_circ_0112036, hsa_circ_0113001, and hsa_circ_0050840) circRNAs (**Figures 5A,B**). The data showed that the levels of differentially quantified circRNAs by qRT-PCR were consistent with the results from microarray, supporting its reliability.

Predicted circRNA-miRNA-mRNA Networks of Differentially Quantified circRNAs

As one of the mechanisms regulating gene expression, circRNA sponges miRNA and represses the effects of miRNA on mRNA. The miRNAs predicted to be sponged by 198 differentially quantified circRNAs formed an intricate network (**Figure 5C**). To explore the potential pathways involved with the differentially quantified circRNAs, verified differentially quantified circRNAs, including five upregulated (hsa_circ_0066867, hsa_circ_0093708, hsa_circ_0032222, hsa_circ_0059662, and hsa_circ_0041685) and five downregulated (hsa_circ_0131433, hsa_circ_0123103, hsa_circ_0112036, hsa_circ_0113001, and hsa_circ_0050840) circRNAs, were analyzed. **Figure 5D** showed the predicted

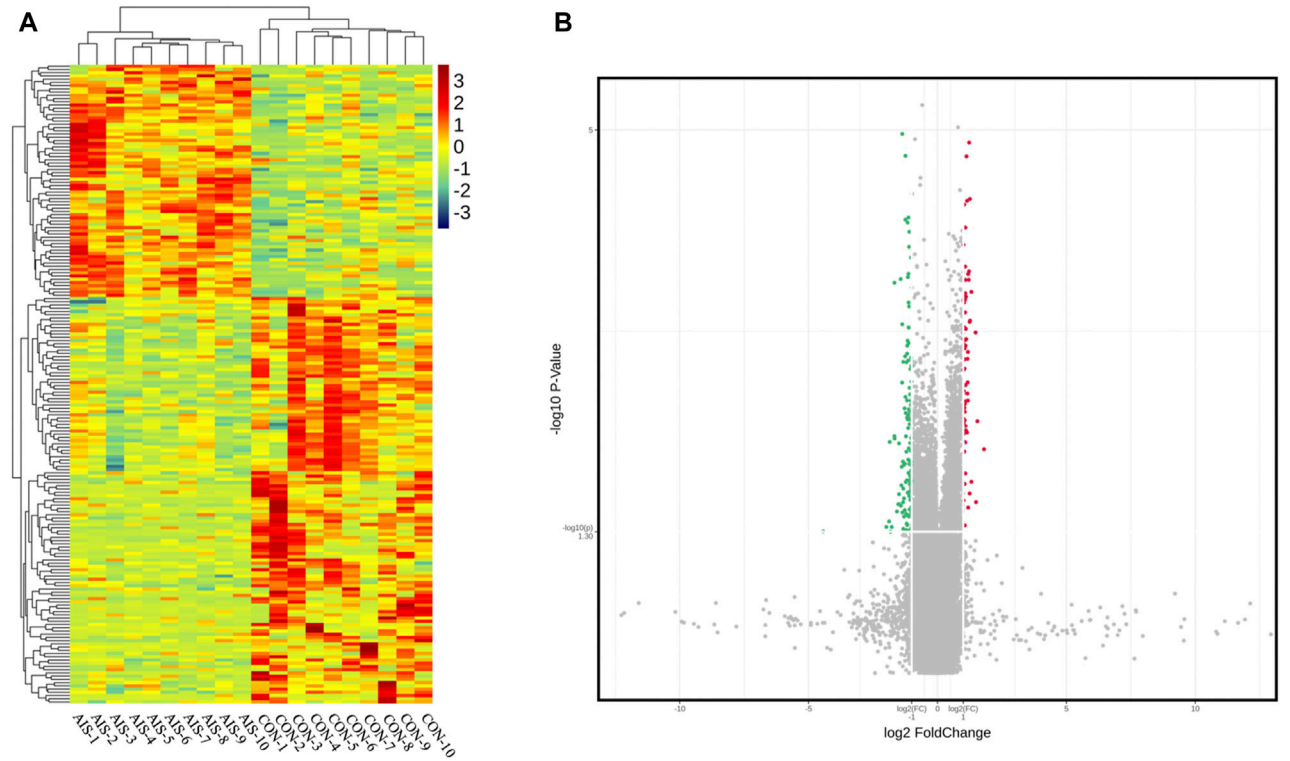

FIGURE 2 | CircRNA profiles of plasma exosomes from AIS patients (AIS) and controls (CON). **(A)** Heat map of circRNAs differentially quantified between AIS patients and controls. **(B)** Volcano plot of circRNA profiles between AIS patients and controls. Red dots represent significantly upregulated circRNAs (log_2 fold change ≥ 1.00 and $p < 0.05$, $n = 10$, independent two-sample *t*-test), and green dots represent significantly downregulated circRNAs (log_2 fold change ≤ −1.00 and $p < 0.05$, $n = 10$, independent two-sample *t*-test).

network of circRNA–miRNA–mRNA, suggesting that verified differentially quantified circRNAs could regulate the expression of various target genes by sponging multiple miRNAs.

GO and KEGG Pathway Analyses of Target Genes of Differentially Quantified circRNAs

Then, GO and KEGG pathway analyses of target genes of 10 differentially quantified circRNAs verified by qRT-PCR were performed to study the potential roles of these circRNAs in AIS. As to the cellular component of GO annotation, the target genes were enriched in the nucleus (nucleus, nucleoplasm, and nuclear lumen), organelle (intracellular/intracellular membrane-bounded/membrane-bounded organelle), and membrane (intrinsic/integral component of membrane) (**Figure 6A**). The molecular functions were mainly related to DNA binding and *cis*-regulatory region, and the biological processes were associated with the regulation of macromolecules and nucleic acids (RNA and DNA). The KEGG analysis showed that metabolic (AMPK signaling pathway and PI3K-Akt signaling pathway), endocrine-related (vasopressin-regulated water reabsorption, adrenergic signaling in cardiomyocytes, and relaxin signaling pathway), and inflammatory (chemokine signaling pathway) pathways were enriched (**Figure 6B**).

According to circRNA–miRNA–mRNA networks, by GO and KEGG analyses, several differentially quantified circRNAs verified by qRT-PCR were involved in processes and pathways related to AIS. Hsa_circ_0112036 sponging miR-24-3p and regulating the levels of STRADB/BCL2L11/CDKN1B and hsa_circ_0066867 impacting miR-182-5p-FOXO3 were predicted in the AMPK and PI3K-Akt pathways. Hsa_circ_0093708, *via* miR-4269-CREB5 or miR-4533-AQP4, and hsa_circ_0041685, *via* miR-4267-DCTN2, played roles in the vasopressin-regulated water reabsorption. Moreover, hsa_circ_0066867 or hsa_circ_0041685 potentially regulated chemokine signaling through miR-6737-5p-CCL2 or miR-3192-5p-CXCL12, respectively.

Coding Probability of Differentially Quantified circRNAs

Certain circRNAs could be translated into proteins and participate in many processes of diseases. Thus, the coding probability of the differentially quantified circRNAs was analyzed. Of all 198 differentially quantified circRNAs, 96 circRNAs had strong coding potential (coding probability > 0.99), indicating that these molecules, through translation, could contribute to the process of AIS (**Figure 7A**).

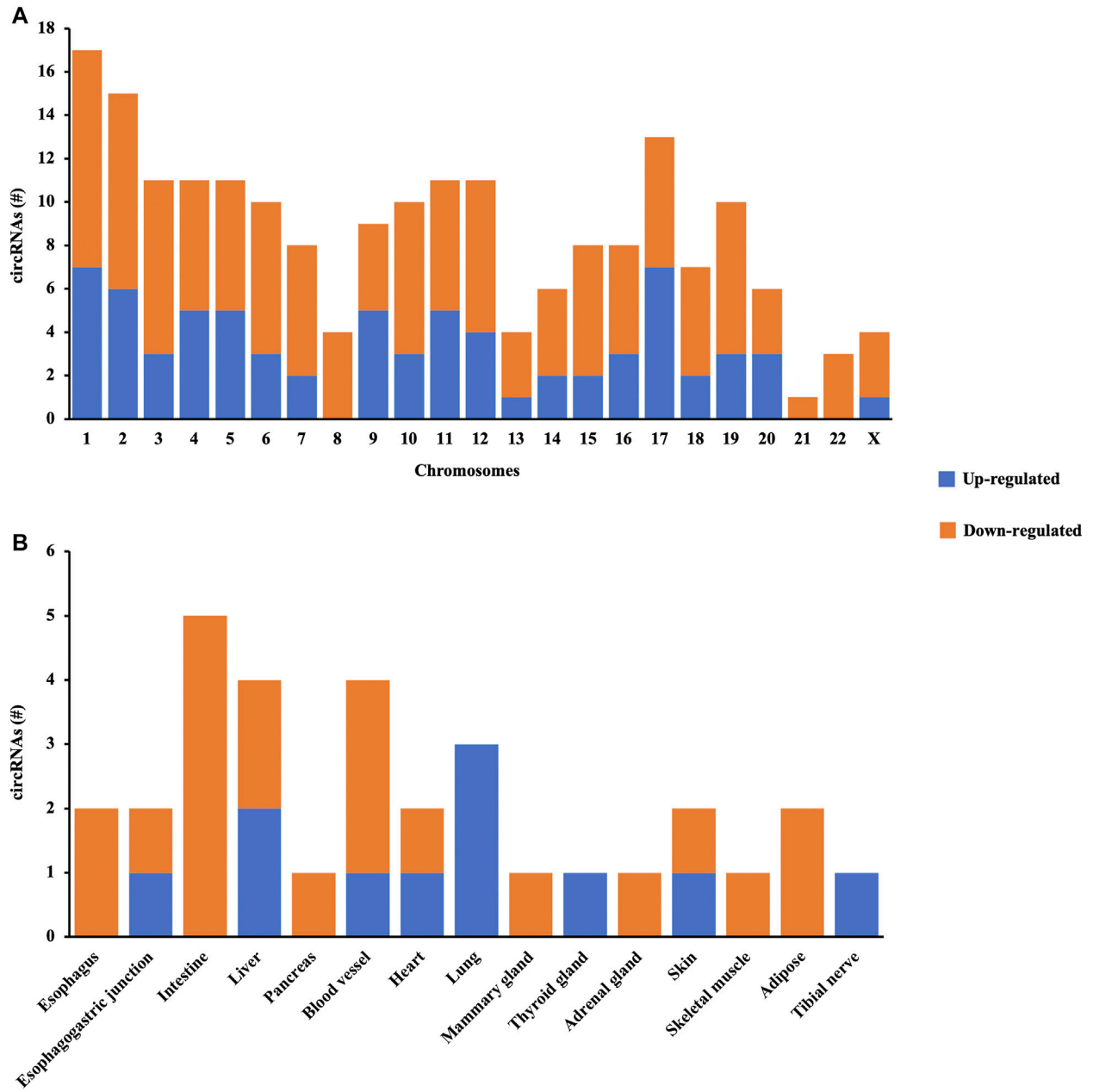

FIGURE 3 | Characterization of circRNA profiles between AIS patients and controls. **(A)** Bar diagram of the distribution of differentially quantified circRNAs in different chromosomes. **(B)** Top 15 tissue-specific distributions of differentially quantified circRNAs.

To further investigate the role of proteins translated from differentially quantified circRNAs with strong coding potential in AIS, GO, and KEGG pathway analyses for these proteins were performed. The results of GO analysis showed that cellular components were mainly located in the intracellular (cytoplasm and organelle) and extracellular (vesicle and exosome) compartments. The molecular functions of these proteins were related to RNA and protein binding (enzyme/cadherin/cell adhesion molecule binding), and the biological processes were mainly related to localization (protein and cell) and cellular homeostasis (cellular component organization, organelle assembly, microtubule-based process, and cytoskeleton organization) (**Figure 7B**). The KEGG pathway analysis showed that intracellular activities (endocytosis, RNA transport, phagosome, and protein processing in endoplasmic reticulum) and interactions between cells (focal adhesion and tight junction) could be affected by proteins predicted to be translated from circRNAs (**Figure 7C**). Of the 10 verified differentially quantified circRNAs, hsa_circ_0041685 was

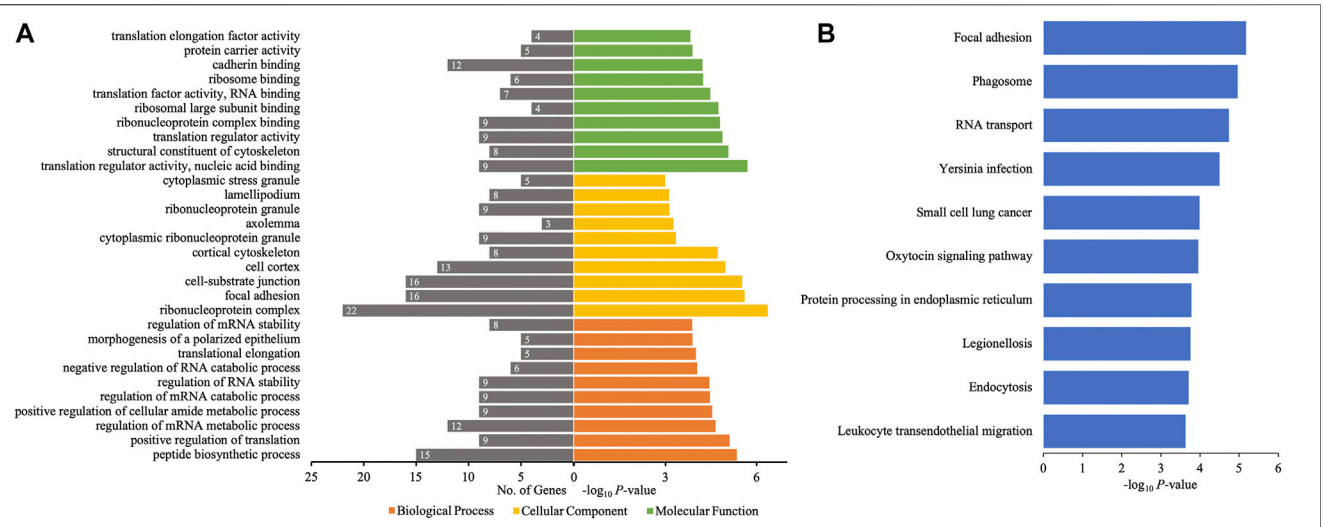

FIGURE 4 | GO annotations and KEGG pathway analyses for host genes of the differentially quantified circRNAs. **(A)** GO annotations. The GO analysis categorized the mRNAs into different groups under the theme of biological process, cellular component, and molecular function. The gene count for each GO category is listed on the left. **(B)** Top 10 KEGG pathways. The vertical axis indicates the pathway category, and the horizontal axis indicates the $-\log_{10} p$-value of a pathway (Fisher's exact test).

predicted to be translated into RABEP1 and to impact the process of endocytosis.

Prediction of RBPs Binding to Differentially Quantified circRNAs

Besides sponging miRNAs, circRNAs could bind to RBPs to regulate the expression of genes and processes of diseases. Among 38 RBPs, eukaryotic initiation factor 4A-3 (EIF4A3) had the highest count of binding sites for the differentially quantified circRNAs, while Argonaute 2 (AGO2) and fragile X mental retardation protein (FMRP) ranked second and third places, respectively. Moreover, of 198 differentially quantified circRNAs, 170 circRNAs were predicted to bind to EIF4A3, 89 circRNAs to bind to AGO2, and 65 circRNAs to bind to fused in sarcoma (FUS) (**Figure 8**).

Evaluation of Diagnostic Value of circRNAs in AIS With ROC Curve Analysis

ROC curve analysis was applied to evaluate the potential diagnostic value of the differentially quantified circRNAs derived from plasma exosomes. Based on the results of GO and KEGG analyses above, hsa_circ_0112036, hsa_circ_0066867, hsa_circ_0093708, and hsa_circ_0041685 were chosen for this analysis. The AUC of these four circRNAs ranged from 0.760 to 0.810 ($p < 0.05$), with the highest AUC found for hsa_circ_0112036 (AUC = 0.810) (**Figure 9**).

DISCUSSION

Stroke causes high mortality and disability rates globally (Hu et al., 2017). As the most common type of stroke, IS could be the result of various factors or diseases, including advanced age, smoking, hypertension, hyperlipidemia, and diabetes mellitus (Guzik and Bushnell, 2017). It has been reported that circRNA profiles of peripheral blood and peripheral blood mononuclear cells from patients with AIS were markedly different from those of controls (Li S. et al., 2020; Dong et al., 2020), indicating that circRNAs could be regulatory factors in AIS. However, it remains unknown whether circRNAs carried by exosomes mediate the signaling transduction and participate in the occurrence and progression of AIS. Hence, the present study aimed to elucidate the profile and potential function of circRNAs derived from plasma exosomes of patients with AIS.

By microarray, 198 differentially quantified circRNAs were found between patients with AIS and controls, evidencing that the profile of circRNAs derived from plasma exosomes was affected by AIS. CircRNAs are highly conserved and characterized by a stable structure and distinct tissue-specific expression (Memczak et al., 2013; Beermann et al., 2016). A tissue-specific circRNA database showed that the major origins of differentially quantified circRNAs with tissue specificity included the digestive system, the cardiovascular system, and lungs. The diseases contributing to AIS, like hypertension, atherosclerosis, and diabetes mellitus, cause marked impairment of the cardiovascular system, disrupting the expression of circRNAs (Wu et al., 2017; Zhao et al., 2020; Fu and Sun, 2021). The aberrant profile of circRNAs specific to the digestive system could be in part the result of the eating habits of patients with AIS. According to the latest literature, a high-fat diet could impair the colonic epithelium and alter the metabolic capacity of the microbiota, increasing the level of circulating trimethylamine N-oxide and the risk of atherosclerosis (Yoo and Zieba, 2021), which could partially explain the changes in the profile of circRNAs specific to the digestive system in AIS. Moreover, changes in the expression of lung-specific circRNAs could be

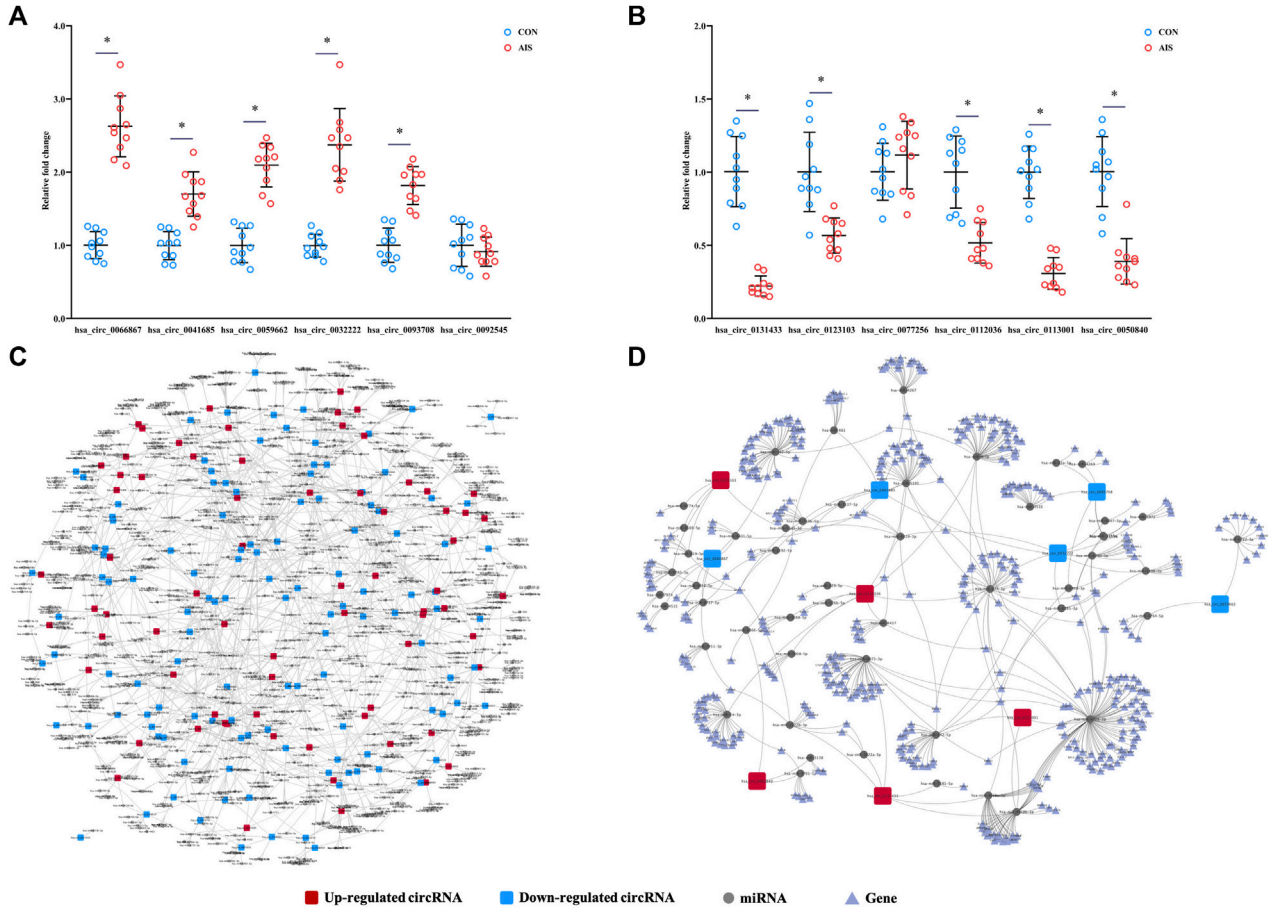

FIGURE 5 | Validation and network diagram of differentially quantified circRNAs. **(A,B)** Relative fold changes of 12 differentially quantified circRNAs using qRT-PCR ($n = 10$). *, $p < 0.05$. **(C)** Network of circRNA-miRNA of 198 differentially quantified circRNAs. **(D)** Network of circRNA-miRNA-mRNA of the 10 differentially quantified circRNAs verified by qRT-PCR.

contributing to the altered function of platelets in AIS. Platelet activation and platelet–leukocyte aggregation are independent determinants for AIS (Schmalbach et al., 2015). The lungs have been identified as a primary site of terminal platelet production and an organ with considerable hematopoietic potential (Lefrançais et al., 2017). This suggests that dysfunctional platelet from the lung could partially account for the association between aberrant expression of pulmonary circRNAs and AIS. These results indicate that, except for the well-known cardiovascular system, the digestive system and lungs could be non-negligible aspects in the pathogenesis of AIS.

Eukaryotic circRNAs are most commonly generated by back-splicing from pre-mRNAs of host genes—a process in which a downstream 5′ splice site joins with an upstream 3′ splice site—and regulate their expression *via* feedback (Memczak et al., 2013; Ashwal-Fluss et al., 2014; Lasda and Parker, 2014; Ragan et al., 2019). Thus, the profile of exosomal circRNAs could be an indicator of the expression profile of host genes. According to GO annotations of host genes, the ribosome and ribonucleoprotein could be impacted in AIS, disordering RNA translation/regulation and protein processing in the endoplasmic reticulum, which was highlighted by KEGG analysis. It has been reported that endoplasmic reticulum stress induced by abnormal protein processing takes place in atherosclerosis (Tabas, 2010; Huang et al., 2018) and hypertension (Naiel et al., 2019; Liu et al., 2020), for which the underlying mechanism could be the dysfunction of vascular endothelial cells by endoplasmic reticulum stress, like excessive apoptosis (Sun et al., 2015; Carlisle et al., 2016). Moreover, by KEGG pathway analysis, focal adhesion and leukocyte transendothelial migration were significantly enriched. Focal adhesions—contact points for the cell with the extracellular matrix—regulate communication of the cell with the surrounding extracellular environment and signaling of diverse cellular processes, including proliferation, migration, apoptosis, spreading, and differentiation (Carragher and Frame, 2004), also found in patients with large-artery atherosclerotic stroke by Xiao et al. (2021). There are a variety of molecules associated with focal adhesion, such as focal adhesion kinase (FAK), integrin, talin, and vinculin, and their activities are related to the development of hypertension (Sugimura et al., 2010; Sen et al., 2011; Jia et al., 2017), atherosclerosis (von Essen et al., 2016; Murphy et al., 2019),

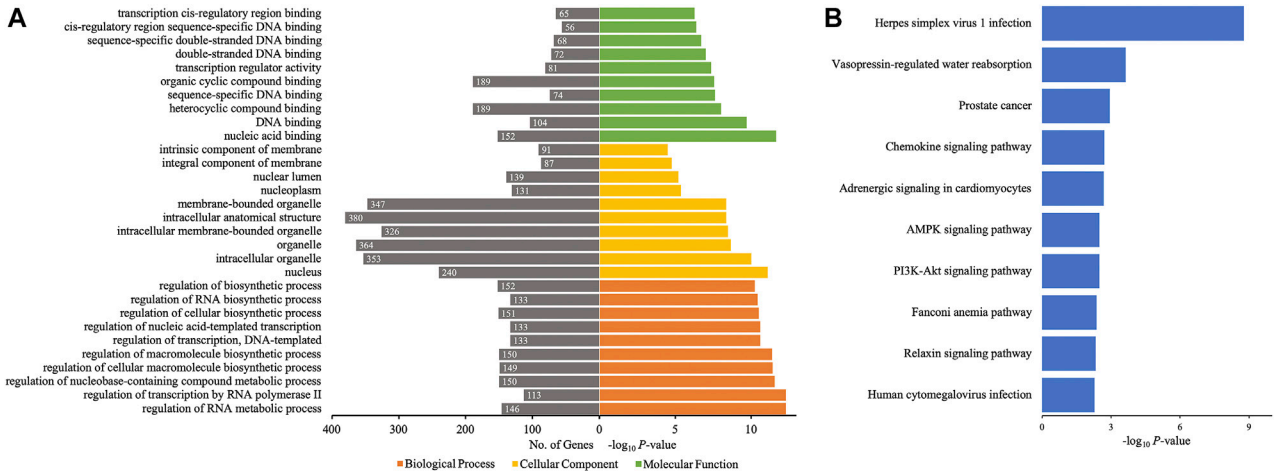

FIGURE 6 | GO annotations and KEGG pathway analyses for target genes of the 10 differentially quantified circRNAs verified by qRT-PCR. **(A)** GO annotations. The GO analysis categorized the mRNAs into different groups under the theme of biological process, cellular component, and molecular function. The gene count for each GO category is listed on the left. **(B)** Top 10 KEGG pathways. The vertical axis indicates the pathway category, and the horizontal axis indicates the $-\log_{10}$ *p*-value of a pathway (Fisher's exact test).

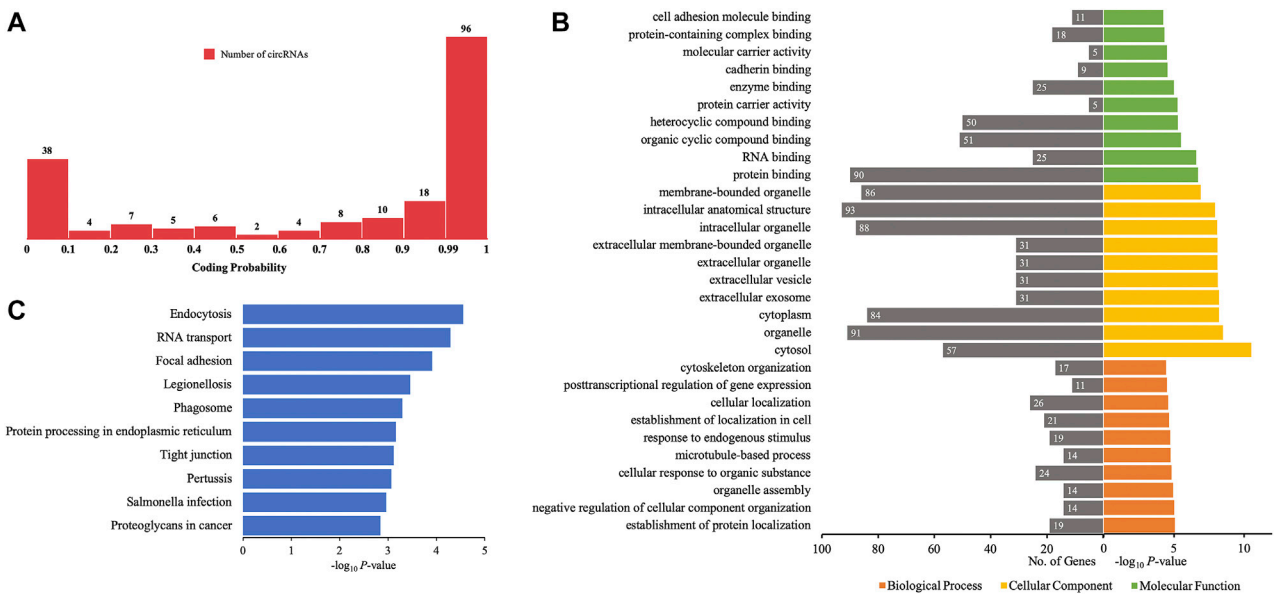

FIGURE 7 | GO annotations and KEGG pathway analyses for proteins potentially coded by differentially quantified circRNAs. **(A)** Distribution of the coding probability of differentially quantified circRNAs. **(B)** GO annotations. The GO analysis categorized the genes into different groups under the theme of biological process, cellular component, and molecular function. The gene count for each GO category is listed on the left. **(C)** Top 10 KEGG pathways. The vertical axis indicates the pathway category, and the horizontal axis indicates the $-\log_{10}$ *p*-value of a pathway (Fisher's exact test).

and thrombosis (Hitchcock et al., 2008), contributing to the progression of AIS. Moreover, leukocytes, especially monocytes, migrate from blood to the subendothelial space and form foam cells with lipoproteins, a key point to aggravate inflammation of the atherosclerotic plaque (Hansson and Libby, 2006; Gisterå and Hansson, 2017). Based on the data mentioned above, the diseases or factors causing AIS, including hypertension, atherosclerosis, and thrombosis, were significantly accompanied by altered profiles of host genes and circRNAs, demonstrating that circRNAs derived from plasma exosomes could be useful biomarkers to evaluate AIS or diseases/factors related to it. In addition, the data on GO and KEGG pathway analyses for host genes of differentially quantified circRNAs were different from those of previous research on blood of patients with AIS (Li S. et al., 2020), indicating that the profile of circRNAs from diverse origins was markedly distinct.

FIGURE 8 | Distribution of top 15 RBPs predicted to bind to differentially quantified circRNAs.

Though the function of most circRNAs remains unknown, a few circRNAs described in physiological and pathological processes generally act as miRNA/protein sponges or translate into proteins (Hansen et al., 2013; Zheng et al., 2016; Pamudurti et al., 2017). To evaluate the function of differentially quantified circRNAs found in the present study, by *in silico* analysis, the putative roles of exosome-derived circRNAs were predicted in AIS.

As miRNA sponges, circRNAs bind to miRNAs and consequently inhibit their function, which is a new mechanism in the regulation of miRNA activity and gene expression (Hansen et al., 2013; Memczak et al., 2013). In the present study, the interaction between differentially quantified circRNAs and miRNAs formed a complex network, suggesting that circRNAs could regulate various stages of AIS *via* sponging miRNAs. MiR-382-5p, containing binding sites for hsa_circ_0069594 and hsa_circ_0128924, is involved in the NFIA signaling regulating cholesterol homeostasis and inflammation (Hu et al., 2015). MiR-92a (potentially sponged by hsa_circ_0024722, hsa_circ_0059965, and hsa_circ_0062949) and miR-221/222 (potentially sponged by hsa_circ_0139214 and hsa_circ_0108959) participated in the course of atherosclerosis by targeting KLF2 mRNA, which modulates shear stress genes (Wu et al., 2011), and sustaining plaque stability (Bazan et al., 2015), respectively. Furthermore, miR-298 (potentially sponged by hsa_circ_0097102 and hsa_circ_0014293) exacerbated cerebral ischemia/reperfusion injury by targeting ACT1 mRNA (Sun et al., 2018), while miR-210 (potentially sponged by hsa_circ_0140265 and hsa_circ_0040760) targets CASP8AP2 mRNA and ISCU1/2 mRNA to suppress apoptosis and improve cerebral injury following AIS (Chan et al., 2009; Kim et al., 2009).

To explore the function of genes regulated by the circRNA–miRNA–mRNA interaction network, we performed GO and KEGG pathway analyses for the target genes of 10 differentially quantified circRNAs verified by qRT-PCR, including five upregulated (hsa_circ_0066867, hsa_circ_0093708, hsa_circ_0032222, hsa_circ_0059662, and hsa_circ_0041685) and five downregulated (hsa_circ_0131433, hsa_circ_0123103, hsa_circ_0112036, hsa_circ_0113001, and hsa_circ_0050840) circRNAs. The results showed that, as competing endogenous RNAs, differentially quantified circRNAs, through misregulating RNA and DNA, would impact cellular components, including the nucleus, organelle, and membrane, and modify the function and fate of cells/tissues. AIS induces neuron apoptosis (Jiang et al., 2018), while autophagy could rescue neurons from apoptosis and confer neuroprotection in AIS (Wang et al., 2012; Wang et al., 2014). These processes involved organelles, like the mitochondria and endoplasmic reticulum (Chen et al., 2002; Yorimitsu et al., 2006; Heath-Engel et al., 2008; Guan et al., 2018), and signaling pathways enriched by KEGG analysis, including PI3K-Akt and AMPK pathways (Sheng et al., 2010; Jiang et al., 2015; Hou et al., 2018; Wang et al., 2020). Similarly, Li et al. 2020b also predicted that circRNAs from the blood could regulate apoptosis in AIS. Based on the circRNA–miRNA–mRNA network,

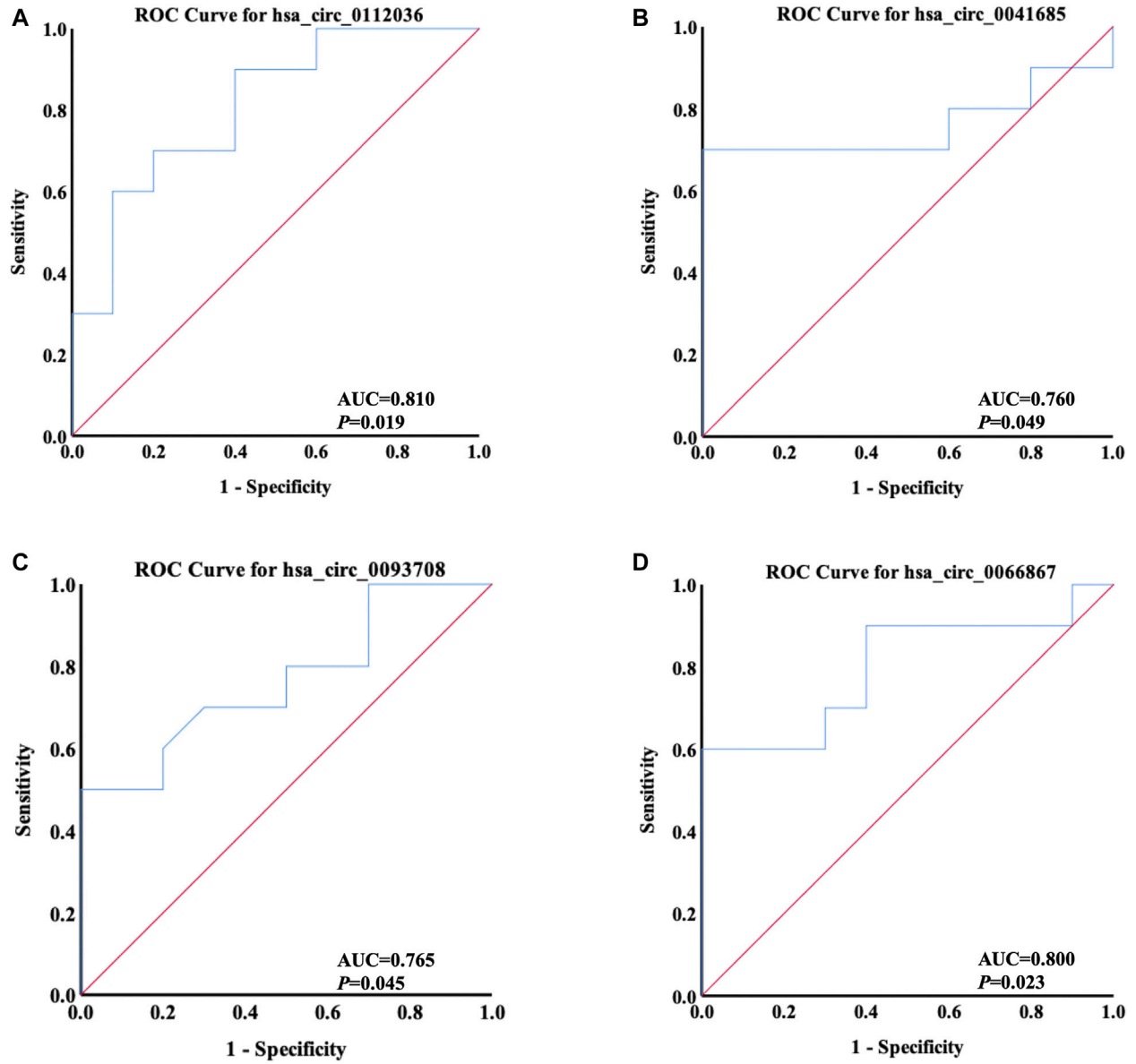

FIGURE 9 | ROC curves of four differentially quantified circRNAs verified by qRT-PCR, including **(A)** hsa_circ_0112036, **(B)** hsa_circ_0041685, **(C)** hsa_circ_0093708, and **(D)** hsa_circ_0066867 (*n* = 10). The red diagonal lines in the graphs represent the diagnostic threshold value of circRNAs for AIS (AUC = 0.500).

hsa_circ_0112036 and hsa_circ_0066867 have been predicted to regulate mRNAs related to AMPK and PI3K-Akt signaling, like STRADB, BCL2L11, CDKN1B, and FOXO3, and be involved with the process of AIS. Moreover, KEGG analysis highlighted pathways related to vasopressin-regulated water reabsorption and chemokine signaling. It has been reported that vasopressin is associated with stroke-related edema (Ameli et al., 2014) and that aquaporin 4 (AQP4), the most ubiquitous water channel in the central nervous system and abundantly expressed in astrocytes, participates in the vasopressin-regulated water reabsorption. Zheng et al. 2017 reported that astrocyte cell injury would be ameliorated by downregulation of AQP4 expression in cerebral IS. In the present study, the hsa_circ_0093708-miR-4533-AQP4 axis was predicted, and the increased level of hsa_circ_0093708 in plasma exosomes of AIS patients suggested that AIS patients may have upregulated the expression of AQP4 and, therefore, be prone to brain injury. Chemokine signaling was indispensable for leukocyte migration, which is a crucial event in the development of inflammation and atherosclerosis (Ruytinx et al., 2018; Yan et al., 2021). In this context, we found that hsa_circ_0066867 and hsa_circ_0041685, significantly increased in AIS patients, potentially regulate chemokine signaling through miR-6737-5p-CCL2 and miR-3192-5p-CXCL12, respectively. Previous studies showed that CCL2 promoted IS *via* chemokine signaling (Li L. et al., 2020) and that the level of serum CXCL12 was positively correlated with stroke severity (Liu

et al., 2015). Therefore, circRNAs from plasma exosomes could potentially prevent and/or assist in the treatment of AIS. Besides, the results on target genes of differentially quantified circRNAs were different from those of Dong et al. (2020), in which circRNAs of peripheral blood mononuclear cells from patients with AIS were involved in inflammation and immunity. We speculated that, compared with circRNAs from a single source, circRNAs from plasma exosomes originating from various cells/tissues could provide more comprehensive information as to AIS.

Since researchers found that certain proteins translated by circRNAs participate in the processes of human diseases (Yang et al., 2018; Zhang et al., 2018), a variety of circRNAs have been described as coding RNAs, and the resulting proteins may play biological roles in the emergence and progression of human diseases. The translational potential of differentially quantified circRNAs were assessed, and the functions of circRNA-translated proteins were also analyzed by GO and KEGG. We found that 96 of 198 differentially quantified circRNAs had strong translational potential. On one hand, the proteins that might be translated from differentially quantified circRNAs with translational potential may contribute to intracellular metabolic processes and functions of cells, including RNA binding, organelle assembly, microtubule-based process, and protein processing in the endoplasmic reticulum. On the other hand, these proteins were involved in the communication between cells *via* several ways, like endocytosis, phagosome, focal adhesion, and tight junction. Endocytosis—a ubiquitous physiological process mediating nutrient uptake, receptor internalization, and signaling, essential events for cell growth and survival—has been reported to cause neuronal death and exacerbate brain damage during AIS (Troulinaki and Tavernarakis, 2012; Tejeda et al., 2019; Diaz-Guerra, 2021). RABEP1 is an essential and rate-limiting component of the endosome fusion regulating early endosomal transport in endocytosis. Upregulated hsa_circ_0041685 might result in increased level of RABEP1 and accelerate endocytosis, playing a role in the development of AIS. Focal adhesion, predicted by GO and KEGG analyses of host genes as well, played an important role in various inducers of AIS, including hypertension (Jia et al., 2017), atherosclerosis (von Essen et al., 2016), and thrombosis (Hitchcock et al., 2008). Chen et al. reported that, in a mouse model, targeting of FAK could be a potential treatment for early IS (Chen et al., 2018). Tight junction is a selectively permeable barrier that generally represents the rate-limiting step of paracellular transport, and, as one of the pathophysiological features of AIS, loss of blood–brain barrier tight junction integrity results in vasogenic edema, hemorrhagic transformation, and increased mortality (Abdullahi et al., 2018; Yang et al., 2019). Thus, we suspected that exosome-derived circRNAs could be a new treatment approach to AIS. Furthermore, there were several events highlighted by GO and KEGG analyses of both host genes and proteins encoded by circRNAs, suggesting that disordered expression of host genes could affect the profile of circRNAs in AIS, and vice versa.

RBPs assemble the ribonucleoprotein complexes to bind RNA sequences by interacting with specific *cis*-regulatory elements and affect the expression and function of their target RNAs (Janga and Mittal, 2011). Increased evidence indicates that many circRNAs interact with RBPs (Hansen et al., 2013; Ashwal-Fluss et al., 2014; Abdelmohsen et al., 2017) and that the interactions between circRNAs and RBPs are also deemed to be an essential element involved in gene transcriptional regulation (Hansen et al., 2013; Memczak et al., 2013), circRNA translation (Yang et al., 2017), and RBP sponging (Du et al., 2017b). Therefore, the distribution of putative RBPs interacting with differentially quantified circRNAs was investigated in the present study. The data showed that the main RBPs binding to differentially quantified circRNAs were EIF4A3 and AGO2. EIF4A3, a core component of the exon junction complex, regulated neuronal cell injury by targeting cGLIS3 in AIS (Jiang et al., 2021). AGO2 is a critical component of the RNA-induced silencing complex and, as a consequence, a master regulator of miRNA-dependent gene silencing. AGO2-associated miRNA profiles were modified in the brain of a rat stroke model (Liu X. S. et al., 2017). Besides, RBPs can be critical factors for the promotion of circRNA transmission from cells (Janas et al., 2015) and can serve as intracellular inducers of circRNA loading in exosomes (O'Leary et al., 2017), which could assist circRNAs in mediating communication between cells *via* exosomes.

CircRNAs are stable and abundant and function as effective diagnostic biomarkers of stroke, like hsa_circ_0001599 (Li et al., 2021) and hsa_circ_0141720 (Chen Y. et al., 2020). In order to explore new circRNAs as potential biomarkers of AIS, ROC curves of four circRNAs (hsa_circ_0112036, hsa_circ_0066867, hsa_circ_0093708, and hsa_circ_0041685) predicted to play a role in the pathogenesis of AIS were analyzed. The data showed that the levels of the four circRNAs could significantly differentiate AIS patients from controls, with hsa_circ_0112036 possessing the highest AUC. These results indicated that the four circRNAs could be further explored as promising biomarkers for AIS diagnosis.

Taken together, the data of this study demonstrate that circRNAs derived from plasma exosomes were differentially quantified between AIS patients and controls. Importantly, these results revealed that exosomal circRNAs from plasma, especially hsa_circ_0112036, hsa_circ_0066867, hsa_circ_0093708, and hsa_circ_0041685, potentially participate in the progression of AIS *via* sponging miRNA/RBPs or encoding proteins, may be explored as biomarkers for the diagnosis of AIS, and may also be potential targets for therapeutic interventions. However, these findings are based on only 10 AIS patients and 10 controls, and more samples are necessary to assess and validate the data in the future.

DATA AVAILABILITY STATEMENT

The microarray datasets generated during the current study have been deposited in the NCBI Gene Expression Omnibus (GEO) repository and are accessible via GEO series accession number GSE195442 (https://www.ncbi.nlm.nih.gov/geo/query/acc.cgi?acc=GSE195442).

ETHICS STATEMENT

The investigation was approved by the Ethical Committee of the First Affiliated Hospital of Chengdu Medical College. The patients/participants provided their written informed consent to participate in this study.

AUTHOR CONTRIBUTIONS

JY, JH, and KC conceived the study; YG, KL, MY (sixth author), HC, and MY (eighth author) collected the samples; JH and YL performed isolation and characterization of plasma exosomes; JY, JH, and KC performed validation of circRNA levels by qRT-PCR; JY and KC analyzed the data and wrote the manuscript. All authors have read and agreed on the contents of the manuscript.

FUNDING

This study was supported by grants from the National Natural Science Foundation of China (81870940, 82171295), the Health Commission of Sichuan Province (18ZD008) and the Natural Science Foundation of Chengdu Medical College (CYZ17-06).

REFERENCES

Abdelmohsen, K., Panda, A. C., Munk, R., Grammatikakis, I., Dudekula, D. B., De, S., et al. (2017). Identification of HuR Target Circular RNAs Uncovers Suppression of PABPN1 Translation by CircPABPN1. *RNA Biol.* 14 (3), 361–369. doi:10.1080/15476286.2017.1279788

Abdullahi, W., Tripathi, D., and Ronaldson, P. T. (2018). Blood-brain Barrier Dysfunction in Ischemic Stroke: Targeting Tight Junctions and Transporters for Vascular protection. *Am. J. Physiology-Cell Physiol.* 315 (3), C343–c356. doi:10.1152/ajpcell.00095.2018

Alberts, M. J. (2017). Stroke Treatment with Intravenous Tissue-type Plasminogen Activator. *Circulation* 135 (2), 140–142. doi:10.1161/circulationaha.116.025724

Ameli, P. A., Ameli, N. J., Gubernick, D. M., Ansari, S., Mohan, S., Satriotomo, I., et al. (2014). Role of Vasopressin and its Antagonism in Stroke Related Edema. *J. Neurosci. Res.* 92 (9), 1091–1099. doi:10.1002/jnr.23407

Ashwal-Fluss, R., Meyer, M., Pamudurti, N. R., Ivanov, A., Bartok, O., Hanan, M., et al. (2014). circRNA Biogenesis Competes with Pre-mRNA Splicing. *Mol. Cel* 56 (1), 55–66. doi:10.1016/j.molcel.2014.08.019

Bazan, H. A., Hatfield, S. A., O'Malley, C. B., Brooks, A. J., Lightell, D., Jr., and Woods, T. C. (2015). Acute Loss of miR-221 and miR-222 in the Atherosclerotic Plaque Shoulder Accompanies Plaque Rupture. *Stroke* 46 (11), 3285–3287. doi:10.1161/strokeaha.115.010567

Beermann, J., Piccoli, M.-T., Viereck, J., and Thum, T. (2016). Non-coding RNAs in Development and Disease: Background, Mechanisms, and Therapeutic Approaches. *Physiol. Rev.* 96 (4), 1297–1325. doi:10.1152/physrev.00041.2015

Benjamin, E. J., Virani, S. S., Callaway, C. W., Chamberlain, A. M., Chang, A. R., Cheng, S., et al. (2018). Heart Disease and Stroke Statistics-2018 Update: A Report from the American Heart Association. *Circulation* 137 (12), e67–e492. doi:10.1161/cir.0000000000000558

Burd, C. E., Jeck, W. R., Liu, Y., Sanoff, H. K., Wang, Z., and Sharpless, N. E. (2010). Expression of Linear and Novel Circular Forms of an INK4/ARF-Associated Non-coding RNA Correlates with Atherosclerosis Risk. *Plos Genet.* 6 (12), e1001233. doi:10.1371/journal.pgen.1001233

Caby, M.-P., Lankar, D., Vincendeau-Scherrer, C., Raposo, G., and Bonnerot, C. (2005). Exosomal-like Vesicles Are Present in Human Blood Plasma. *Int. Immunol.* 17 (7), 879–887. doi:10.1093/intimm/dxh267

Carlisle, R. E., Werner, K. E., Yum, V., Lu, C., Tat, V., Memon, M., et al. (2016). Endoplasmic Reticulum Stress Inhibition Reduces Hypertension through the Preservation of Resistance Blood Vessel Structure and Function. *J. Hypertens.* 34 (8), 1556–1569. doi:10.1097/hjh.0000000000000943

Carragher, N. O., and Frame, M. C. (2004). Focal Adhesion and Actin Dynamics: a Place where Kinases and Proteases Meet to Promote Invasion. *Trends Cel Biol.* 14 (5), 241–249. doi:10.1016/j.tcb.2004.03.011

Chan, S. Y., Zhang, Y.-Y., Hemann, C., Mahoney, C. E., Zweier, J. L., and Loscalzo, J. (2009). MicroRNA-210 Controls Mitochondrial Metabolism during Hypoxia by Repressing the Iron-Sulfur Cluster Assembly Proteins ISCU1/2. *Cel Metab.* 10 (4), 273–284. doi:10.1016/j.cmet.2009.08.015

Chen, D., Wei, L., Liu, Z.-R., Yang, J. J., Gu, X., Wei, Z. Z., et al. (2018). Pyruvate Kinase M2 Increases Angiogenesis, Neurogenesis, and Functional Recovery Mediated by Upregulation of STAT3 and Focal Adhesion Kinase Activities after Ischemic Stroke in Adult Mice. *Neurotherapeutics* 15 (3), 770–784. doi:10.1007/s13311-018-0635-2

Chen, S.-D., Lee, J.-M., Yang, D.-I., Nassief, A., and Hsu, C. Y. (2002). Combination Therapy for Ischemic Stroke. *Am. J. Cardiovasc. Drugs* 2 (5), 303–313. doi:10.2165/00129784-200202050-00003

Chen, W., Wang, H., Feng, J., and Chen, L. (2020a). Overexpression of circRNA circUCK2 Attenuates Cell Apoptosis in Cerebral Ischemia-Reperfusion Injury via miR-125b-5p/GDF11 Signaling. *Mol. Ther. - Nucleic Acids* 22, 673–683. doi:10.1016/j.omtn.2020.09.032

Chen, Y., Wang, B., Liu, W., Xu, P., and Song, L. (2020b). Diagnostic Value of Serum Hsa_circ_0141720 in Patients with Acute Ischemic Stroke. *Clin. Lab.* 66 (8). doi:10.7754/Clin.Lab.2020.191266

Cocucci, E., Racchetti, G., and Meldolesi, J. (2009). Shedding Microvesicles: Artefacts No More. *Trends Cel Biol.* 19 (2), 43–51. doi:10.1016/j.tcb.2008.11.003

Couzin, J. (2005). The Ins and Outs of Exosomes. *Science* 308 (5730), 1862–1863. doi:10.1126/science.308.5730.1862

Dai, Q., Ma, Y., Xu, Z., Zhang, L., Yang, H., Liu, Q., et al. (2021). Downregulation of Circular RNA HECTD1 Induces Neuroprotection against Ischemic Stroke through the microRNA-133b/TRAF3 Pathway. *Life Sci.* 264, 118626. doi:10.1016/j.lfs.2020.118626

Diaz-Guerra, M. (2021). Excitotoxicity-induced Endocytosis as a Potential Target for Stroke Neuroprotection. *Neural Regen. Res.* 16 (2), 300–301. doi:10.4103/1673-5374.290892

Dong, Z., Deng, L., Peng, Q., Pan, J., and Wang, Y. (2020). CircRNA Expression Profiles and Function Prediction in Peripheral Blood Mononuclear Cells of Patients with Acute Ischemic Stroke. *J. Cel Physiol* 235 (3), 2609–2618. doi:10.1002/jcp.29165

Du, W. W., Yang, W., Chen, Y., Wu, Z.-K., Foster, F. S., Yang, Z., et al. (2017a). Foxo3 Circular RNA Promotes Cardiac Senescence by Modulating Multiple Factors Associated with Stress and Senescence Responses. *Eur. Heart J.* 38 (18), ehw001–1412. doi:10.1093/eurheartj/ehw001

Du, W. W., Zhang, C., Yang, W., Yong, T., Awan, F. M., and Yang, B. B. (2017b). Identifying and Characterizing circRNA-Protein Interaction. *Theranostics* 7 (17), 4183–4191. doi:10.7150/thno.21299

Fu, Y., Sun, C., Li, Q., Qian, F., Li, C., Xi, X., et al. (2021). Differential RNA Expression Profiles and Competing Endogenous RNA-Associated Regulatory Networks during the Progression of Atherosclerosis. *Epigenomics* 13 (2), 99–112. doi:10.2217/epi-2020-0252

Gisterå, A., and Hansson, G. K. (2017). The Immunology of Atherosclerosis. *Nat. Rev. Nephrol.* 13 (6), 368–380. doi:10.1038/nrneph.2017.51

Guan, R., Zou, W., Dai, X., Yu, X., Liu, H., Chen, Q., et al. (2018). Mitophagy, a Potential Therapeutic Target for Stroke. *J. Biomed. Sci.* 25 (1), 87. doi:10.1186/s12929-018-0487-4

Guzik, A., and Bushnell, C. (2017). Stroke Epidemiology and Risk Factor Management. *CONTINUUM: Lifelong Learn. NeurologyCerebrovascular Disease)* 23 (1), 15–39. doi:10.1212/con.0000000000000416

Han, B., Chao, J., and Yao, H. (2018). Circular RNA and its Mechanisms in Disease: From the Bench to the Clinic. *Pharmacol. Ther.* 187, 31–44. doi:10.1016/j.pharmthera.2018.01.010

Hansen, T. B., Jensen, T. I., Clausen, B. H., Bramsen, J. B., Finsen, B., Damgaard, C. K., et al. (2013). Natural RNA Circles Function as Efficient microRNA Sponges. *Nature* 495 (7441), 384–388. doi:10.1038/nature11993

Hansson, G. K., and Libby, P. (2006). The Immune Response in Atherosclerosis: a Double-Edged Sword. *Nat. Rev. Immunol.* 6 (7), 508–519. doi:10.1038/nri1882

Heath-Engel, H. M., Chang, N. C., and Shore, G. C. (2008). The Endoplasmic Reticulum in Apoptosis and Autophagy: Role of the BCL-2 Protein Family. *Oncogene* 27 (50), 6419–6433. doi:10.1038/onc.2008.309

Hitchcock, I. S., Fox, N. E., Prévost, N., Sear, K., Shattil, S. J., and Kaushansky, K. (2008). Roles of Focal Adhesion Kinase (FAK) in Megakaryopoiesis and Platelet Function: Studies Using a Megakaryocyte Lineage-specific FAK Knockout. *Blood* 111 (2), 596–604. doi:10.1182/blood-2007-05-089680

Hon, K. W., Abu, N., Ab Mutalib, N.-S., and Jamal, R. (2017). Exosomes as Potential Biomarkers and Targeted Therapy in Colorectal Cancer: A Mini-Review. *Front. Pharmacol.* 8, 583. doi:10.3389/fphar.2017.00583

Hou, Y., Wang, K., Wan, W., Cheng, Y., Pu, X., and Ye, X. (2018). Resveratrol Provides Neuroprotection by Regulating the JAK2/STAT3/PI3K/AKT/mTOR Pathway after Stroke in Rats. *Genes Dis.* 5 (3), 245–255. doi:10.1016/j.gendis.2018.06.001

Hu, X., De Silva, T. M., Chen, J., and Faraci, F. M. (2017). Cerebral Vascular Disease and Neurovascular Injury in Ischemic Stroke. *Circ. Res.* 120 (3), 449–471. doi:10.1161/circresaha.116.308427

Hu, Y.-W., Zhao, J.-Y., Li, S.-F., Huang, J.-L., Qiu, Y.-R., Ma, X., et al. (2015). RP5-833A20.1/miR-382-5p/NFIA-dependent Signal Transduction Pathway Contributes to the Regulation of Cholesterol Homeostasis and Inflammatory Reaction. *Atvb* 35 (1), 87–101. doi:10.1161/atvbaha.114.304296

Huang, A., Patel, S., McAlpine, C., and Werstuck, G. (2018). The Role of Endoplasmic Reticulum Stress-Glycogen Synthase Kinase-3 Signaling in Atherogenesis. *Ijms* 19 (6), 1607. doi:10.3390/ijms19061607

Janas, T., Janas, M. M., Sapoń, K., and Janas, T. (2015). Mechanisms of RNA Loading into Exosomes. *FEBS Lett.* 589 (13), 1391–1398. doi:10.1016/j.febslet.2015.04.036

Janga, S. C., and Mittal, N. (2011). Construction, Structure and Dynamics of post-transcriptional Regulatory Network Directed by RNA-Binding Proteins. *Adv. Exp. Med. Biol.* 722, 103–117. doi:10.1007/978-1-4614-0332-6_7

Jia, D., Zhu, Q., Liu, H., Zuo, C., He, Y., Chen, G., et al. (2017). Osteoprotegerin Disruption Attenuates HySu-Induced Pulmonary Hypertension through Integrin α V β 3/FAK/AKT Pathway Suppression. *Circ. Cardiovasc. Genet.* 10 (1), 1591. doi:10.1161/circgenetics.116.001591

Jiang, Q., Su, D.-Y., Wang, Z.-Z., Liu, C., Sun, Y.-N., Cheng, H., et al. (2021). Retina as a Window to Cerebral Dysfunction Following Studies with circRNA Signature during Neurodegeneration. *Theranostics* 11 (4), 1814–1827. doi:10.7150/thno.51550

Jiang, S., Guo, C., Zhang, W., Che, W., Zhang, J., Zhuang, S., et al. (2019). The Integrative Regulatory Network of circRNA, microRNA, and mRNA in Atrial Fibrillation. *Front. Genet.* 10, 526. doi:10.3389/fgene.2019.00526

Jiang, S., Li, T., Ji, T., Yi, W., Yang, Z., Wang, S., et al. (2018). AMPK: Potential Therapeutic Target for Ischemic Stroke. *Theranostics* 8 (16), 4535–4551. doi:10.7150/thno.25674

Jiang, T., Yu, J.-T., Zhu, X.-C., Zhang, Q.-Q., Tan, M.-S., Cao, L., et al. (2015). Ischemic Preconditioning Provides Neuroprotection by Induction of AMP-Activated Protein Kinase-dependent Autophagy in a Rat Model of Ischemic Stroke. *Mol. Neurobiol.* 51 (1), 220–229. doi:10.1007/s12035-014-8725-6

Kernan, W. N., Ovbiagele, B., Black, H. R., Bravata, D. M., Chimowitz, M. I., Ezekowitz, M. D., et al. (2014). Guidelines for the Prevention of Stroke in Patients with Stroke and Transient Ischemic Attack. *Stroke* 45 (7), 2160–2236. doi:10.1161/str.0000000000000024

Lasda, E., and Parker, R. (2014). Circular RNAs: Diversity of Form and Function. *Rna* 20 (12), 1829–1842. doi:10.1261/rna.047126.114

Lefrançais, E., Ortiz-Muñoz, G., Caudrillier, A., Mallavia, B., Liu, F., Sayah, D. M., et al. (2017). The Lung Is a Site of Platelet Biogenesis and a Reservoir for Haematopoietic Progenitors. *Nature* 544 (7648), 105–109. doi:10.1038/nature21706

Li, L., Lou, W., Li, H., Zhu, Y., and Huang, X. a. (2020a). Upregulated C-C Motif Chemokine Ligand 2 Promotes Ischemic Stroke via Chemokine Signaling Pathway. *Ann. Vasc. Surg.* 68, 476–486. doi:10.1016/j.avsg.2020.04.047

Li, P., Chen, S., Chen, H., Mo, X., Li, T., Shao, Y., et al. (2015). Using Circular RNA as a Novel Type of Biomarker in the Screening of Gastric Cancer. *Clinica Chim. Acta* 444, 132–136. doi:10.1016/j.cca.2015.02.018

Li, S., Chen, L., Xu, C., Qu, X., Qin, Z., Gao, J., et al. (2020b). Expression Profile and Bioinformatics Analysis of Circular RNAs in Acute Ischemic Stroke in a South Chinese Han Population. *Sci. Rep.* 10 (1), 10138. doi:10.1038/s41598-020-66990-y

Li, S., Hu, W., Deng, F., Chen, S., Zhu, P., Wang, M., et al. (2021). Identification of Circular RNA Hsa_circ_0001599 as a Novel Biomarker for Large-Artery Atherosclerotic Stroke. *DNA Cel Biol.* 40 (3), 457–468. doi:10.1089/dna.2020.5662

Liu, G., Wu, F., Jiang, X., Que, Y., Qin, Z., Hu, P., et al. (2020). Inactivation of Cys 674 in SERCA2 Increases BP by Inducing Endoplasmic Reticulum Stress and Soluble Epoxide Hydrolase. *Br. J. Pharmacol.* 177 (8), 1793–1805. doi:10.1111/bph.14937

Liu, P., Xiang, J.-W., and Jin, S.-X. (2015). Serum CXCL12 Levels Are Associated with Stroke Severity and Lesion Volumes in Stroke Patients. *Neurol. Res.* 37 (10), 853–858. doi:10.1179/1743132815y.0000000063

Liu, W., Zhang, J., Zou, C., Xie, X., Wang, Y., Wang, B., et al. (2017a). Microarray Expression Profile and Functional Analysis of Circular RNAs in Osteosarcoma. *Cell Physiol Biochem* 43 (3), 969–985. doi:10.1159/000481650

Liu, X. S., Fan, B. Y., Pan, W. L., Li, C., Levin, A. M., Wang, X., et al. (2017b). Identification of miRNomes Associated with Adult Neurogenesis after Stroke Using Argonaute 2-based RNA Sequencing. *RNA Biol.* 14 (5), 488–499. doi:10.1080/15476286.2016.1196320

Livak, K. J., and Schmittgen, T. D. (2001). Analysis of Relative Gene Expression Data Using Real-Time Quantitative PCR and the 2−ΔΔCT Method. *Methods* 25 (4), 402–408. doi:10.1006/meth.2001.1262

Lu, D., Ho, E. S., Mai, H., Zang, J., Liu, Y., Li, Y., et al. (2020). Identification of Blood Circular RNAs as Potential Biomarkers for Acute Ischemic Stroke. *Front. Neurosci.* 14, 81. doi:10.3389/fnins.2020.00081

Lukiw, W. J. (2013). Circular RNA (circRNA) in Alzheimer's Disease (AD). *Front. Genet.* 4, 307. doi:10.3389/fgene.2013.00307

Memczak, S., Jens, M., Elefsinioti, A., Torti, F., Krueger, J., Rybak, A., et al. (2013). Circular RNAs Are a Large Class of Animal RNAs with Regulatory Potency. *Nature* 495 (7441), 333–338. doi:10.1038/nature11928

Mousavi, S., Moallem, R., Hassanian, S. M., Sadeghzade, M., Mardani, R., Ferns, G. A., et al. (2019). Tumor-derived Exosomes: Potential Biomarkers and Therapeutic Target in the Treatment of Colorectal Cancer. *J. Cel Physiol* 234 (8), 12422–12432. doi:10.1002/jcp.28080

Murphy, J. M., Jeong, K., Rodriguez, Y. A. R., Kim, J.-H., Ahn, E.-Y. E., and Lim, S.-T. S. (2019). FAK and Pyk2 Activity Promote TNF-α and IL-1β-mediated Pro-inflammatory Gene Expression and Vascular Inflammation. *Sci. Rep.* 9 (1), 7617. doi:10.1038/s41598-019-44098-2

Naiel, S., Carlisle, R. E., Lu, C., Tat, V., and Dickhout, J. G. (2019). Endoplasmic Reticulum Stress Inhibition Blunts the Development of Essential Hypertension in the Spontaneously Hypertensive Rat. *Am. J. Physiology-Heart Circulatory Physiol.* 316 (5), H1214–h1223. doi:10.1152/ajpheart.00523.2018

O'Leary, V. B., Smida, J., Matjanovski, M., Brockhaus, C., Winkler, K., Moertl, S., et al. (2017). The circRNA Interactome-Innovative Hallmarks of the Intra- and Extracellular Radiation Response. *Oncotarget* 8 (45), 78397–78409. doi:10.18632/oncotarget.19228

Ostolaza, A., Blanco-Luquin, I., Urdánoz-Casado, A., Rubio, I., Labarga, A., Zandio, B., et al. (2020). Circular RNA Expression Profile in Blood According to Ischemic Stroke Etiology. *Cell Biosci* 10, 34. doi:10.1186/s13578-020-00394-3

Pamudurti, N. R., Bartok, O., Jens, M., Ashwal-Fluss, R., Stottmeister, C., Ruhe, L., et al. (2017). Translation of CircRNAs. *Mol. Cel* 66 (1), 9–21. doi:10.1016/j.molcel.2017.02.021

Peng, X., Jing, P., Chen, J., and Xu, L. (2019). The Role of Circular RNA HECTD1 Expression in Disease Risk, Disease Severity, Inflammation, and Recurrence of Acute Ischemic Stroke. *J. Clin. Lab. Anal.* 33 (7), e22954. doi:10.1002/jcla.22954

Powers, W. J., Rabinstein, A. A., Ackerson, T., Adeoye, O. M., Bambakidis, N. C., Becker, K., et al. (2018). 2018 Guidelines for the Early Management of Patients with Acute Ischemic Stroke: A Guideline for Healthcare Professionals from the American Heart Association/American Stroke Association. *Stroke* 49 (3), e46–e110. doi:10.1161/str.0000000000000158

Ragan, C., Goodall, G. J., Shirokikh, N. E., and Preiss, T. (2019). Insights into the Biogenesis and Potential Functions of Exonic Circular RNA. *Sci. Rep.* 9 (1), 2048. doi:10.1038/s41598-018-37037-0

Raposo, G., and Stoorvogel, W. (2013). Extracellular Vesicles: Exosomes, Microvesicles, and Friends. *J. Cel Biol* 200 (4), 373–383. doi:10.1083/jcb.201211138

Ruytinx, P., Proost, P., Van Damme, J., and Struyf, S. (2018). Chemokine-Induced Macrophage Polarization in Inflammatory Conditions. *Front. Immunol.* 9, 1930. doi:10.3389/fimmu.2018.01930

Rybak-Wolf, A., Stottmeister, C., Glažar, P., Jens, M., Pino, N., Giusti, S., et al. (2015). Circular RNAs in the Mammalian Brain Are Highly Abundant, Conserved, and Dynamically Expressed. *Mol. Cel* 58 (5), 870–885. doi:10.1016/j.molcel.2015.03.027

Schmalbach, B., Stepanow, O., Jochens, A., Riedel, C., Deuschl, G., and Kuhlenbäumer, G. (2015). Determinants of Platelet-Leukocyte Aggregation and Platelet Activation in Stroke. *Cerebrovasc. Dis.* 39 (3-4), 176–180. doi:10.1159/000375396

Sen, S., Tewari, M., Zajac, A., Barton, E., Sweeney, H. L., and Discher, D. E. (2011). Upregulation of Paxillin and Focal Adhesion Signaling Follows Dystroglycan Complex Deletions and Promotes a Hypertensive State of Differentiation. *Eur. J. Cel Biol.* 90 (2-3), 249–260. doi:10.1016/j.ejcb.2010.06.005

Sheng, R., Zhang, L.-S., Han, R., Liu, X.-Q., Gao, B., and Qin, Z.-H. (2010). Autophagy Activation Is Associated with Neuroprotection in a Rat Model of Focal Cerebral Ischemic Preconditioning. *Autophagy* 6 (4), 482–494. doi:10.4161/auto.6.4.11737

Simons, M., and Raposo, G. (2009). Exosomes - Vesicular Carriers for Intercellular Communication. *Curr. Opin. Cel Biol.* 21 (4), 575–581. doi:10.1016/j.ceb.2009.03.007

Skotland, T., Sandvig, K., and Llorente, A. (2017). Lipids in Exosomes: Current Knowledge and the Way Forward. *Prog. Lipid Res.* 66, 30–41. doi:10.1016/j.plipres.2017.03.001

Snow, S. J. (2016). Stroke and T-PA - Triggering New Paradigms of Care. *N. Engl. J. Med.* 374 (9), 809–811. doi:10.1056/NEJMp1514696

Sugimura, K., Fukumoto, Y., Nawata, J., Wang, H., Onoue, N., Tada, T., et al. (2010). Hypertension Promotes Phosphorylation of Focal Adhesion Kinase and Proline-Rich Tyrosine Kinase 2 in Rats: Implication for the Pathogenesis of Hypertensive Vascular Disease. *Tohoku J. Exp. Med.* 222 (3), 201–210. doi:10.1620/tjem.222.201

Sun, H., Zhong, D., Wang, C., Sun, Y., Zhao, J., and Li, G. (2018). MiR-298 Exacerbates Ischemia/Reperfusion Injury Following Ischemic Stroke by Targeting Act1. *Cel Physiol Biochem* 48 (2), 528–539. doi:10.1159/000491810

Sun, Y., Zhang, T., Li, L., and Wang, J. (2015). Induction of Apoptosis by Hypertension via Endoplasmic Reticulum Stress. *Kidney Blood Press. Res.* 40 (1), 41–51. doi:10.1159/000368481

Suzuki, H., Zuo, Y., Wang, J., Zhang, M. Q., Malhotra, A., and Mayeda, A. (2006). Characterization of RNase R-Digested Cellular RNA Source that Consists of Lariat and Circular RNAs from Pre-mRNA Splicing. *Nucleic Acids Res.* 34 (8), e63. doi:10.1093/nar/gkl151

Szegedi, I., Szapáry, L., Csécsei, P., Csanádi, Z., and Csiba, L. (2017). Potential Biological Markers of Atrial Fibrillation: A Chance to Prevent Cryptogenic Stroke. *Biomed. Res. Int.* 2017, 1–10. doi:10.1155/2017/8153024

Tabas, I. (2010). The Role of Endoplasmic Reticulum Stress in the Progression of Atherosclerosis. *Circ. Res.* 107 (7), 839–850. doi:10.1161/circresaha.110.224766

Tejeda, G. S., Esteban-Ortega, G. M., San Antonio, E., Vidaurre, Ó. G., and Díaz-Guerra, M. (2019). Prevention of Excitotoxicity-induced Processing of BDNF Receptor TrkB-FL Leads to Stroke Neuroprotection. *EMBO Mol. Med.* 11 (7), e9950. doi:10.15252/emmm.201809950

Troulinaki, K., and Tavernarakis, N. (2012). Endocytosis and Intracellular Trafficking Contribute to Necrotic Neurodegeneration inC. Elegans. *EMBO J.* 31 (3), 654–666. doi:10.1038/emboj.2011.447

von Essen, M., Rahikainen, R., Oksala, N., Raitoharju, E., Seppälä, I., Mennander, A., et al. (2016). Talin and Vinculin Are Downregulated in Atherosclerotic Plaque; Tampere Vascular Study. *Atherosclerosis* 255, 43–53. doi:10.1016/j.atherosclerosis.2016.10.031

Wang, M.-M., Zhang, M., Feng, Y.-S., Xing, Y., Tan, Z.-X., Li, W.-B., et al. (2020). Electroacupuncture Inhibits Neuronal Autophagy and Apoptosis via the PI3K/AKT Pathway Following Ischemic Stroke. *Front. Cel. Neurosci.* 14, 134. doi:10.3389/fncel.2020.00134

Wang, P., Guan, Y.-F., Du, H., Zhai, Q.-W., Su, D.-F., and Miao, C.-Y. (2012). Induction of Autophagy Contributes to the Neuroprotection of Nicotinamide Phosphoribosyltransferase in Cerebral Ischemia. *Autophagy* 8 (1), 77–87. doi:10.4161/auto.8.1.18274

Wang, P., Xu, T.-Y., Wei, K., Guan, Y.-F., Wang, X., Xu, H., et al. (2014). ARRB1/β-arrestin-1 Mediates Neuroprotection through Coordination of BECN1-dependent Autophagy in Cerebral Ischemia. *Autophagy* 10 (9), 1535–1548. doi:10.4161/auto.29203

Won Kim, H., Haider, H. K., Jiang, S., and Ashraf, M. (2009). Ischemic Preconditioning Augments Survival of Stem Cells via miR-210 Expression by Targeting Caspase-8-Associated Protein 2. *J. Biol. Chem.* 284 (48), 33161–33168. doi:10.1074/jbc.M109.020925

Wu, N., Jin, L., and Cai, J. (2017). Profiling and Bioinformatics Analyses Reveal Differential Circular RNA Expression in Hypertensive Patients. *Clin. Exp. Hypertens.* 39 (5), 454–459. doi:10.1080/10641963.2016.1273944

Wu, W., Xiao, H., Laguna-Fernandez, A., Villarreal, G., Jr., Wang, K.-C., Geary, G. G., et al. (2011). Flow-Dependent Regulation of Krüppel-like Factor 2 Is Mediated by MicroRNA-92a. *Circulation* 124 (5), 633–641. doi:10.1161/circulationaha.110.005108

Xiao, Q., Yin, R., Wang, Y., Yang, S., Ma, A., Pan, X., et al. (2021). Comprehensive Analysis of Peripheral Exosomal circRNAs in Large Artery Atherosclerotic Stroke. *Front. Cel Dev. Biol.* 9, 685741. doi:10.3389/fcell.2021.685741

Yan, Y., Thakur, M., van der Vorst, E. P. C., Weber, C., and Döring, Y. (2021). Targeting the Chemokine Network in Atherosclerosis. *Atherosclerosis* 330, 95–106. doi:10.1016/j.atherosclerosis.2021.06.912

Yang, C., Hawkins, K. E., Doré, S., and Candelario-Jalil, E. (2019). Neuroinflammatory Mechanisms of Blood-Brain Barrier Damage in Ischemic Stroke. *Am. J. Physiology-Cell Physiol.* 316 (2), C135–c153. doi:10.1152/ajpcell.00136.2018

Yang, Y., Fan, X., Mao, M., Song, X., Wu, P., Zhang, Y., et al. (2017). Extensive Translation of Circular RNAs Driven by N6-Methyladenosine. *Cell Res* 27 (5), 626–641. doi:10.1038/cr.2017.31

Yang, Y., Gao, X., Zhang, M., Yan, S., Sun, C., Xiao, F., et al. (2018). Novel Role of FBXW7 Circular RNA in Repressing Glioma Tumorigenesis. *J. Natl. Cancer Inst.* 110 (3), 304–315. doi:10.1093/jnci/djx166

Yao, J.-T., Zhao, S.-H., Liu, Q.-P., Lv, M.-Q., Zhou, D.-X., Liao, Z.-J., et al. (2017). Over-expression of CircRNA_100876 in Non-small Cell Lung Cancer and its Prognostic Value. *Pathol. - Res. Pract.* 213 (5), 453–456. doi:10.1016/j.prp.2017.02.011

Yoo, W., Zieba, J. K., Foegeding, N. J., Torres, T. P., Shelton, C. D., Shealy, N. G., et al. (2021). High-fat Diet-Induced Colonocyte Dysfunction Escalates Microbiota-Derived Trimethylamine N -oxide. *Science* 373 (6556), 813–818. doi:10.1126/science.aba3683

Yorimitsu, T., Nair, U., Yang, Z., and Klionsky, D. J. (2006). Endoplasmic Reticulum Stress Triggers Autophagy. *J. Biol. Chem.* 281 (40), 30299–30304. doi:10.1074/jbc.M607007200

Zhang, H., Deng, T., Liu, R., Bai, M., Zhou, L., Wang, X., et al. (2017). Exosome-delivered EGFR Regulates Liver Microenvironment to Promote Gastric Cancer Liver Metastasis. *Nat. Commun.* 8, 15016. doi:10.1038/ncomms15016

Zhang, M., Zhao, K., Xu, X., Yang, Y., Yan, S., Wei, P., et al. (2018). A Peptide Encoded by Circular Form of LINC-PINT Suppresses Oncogenic Transcriptional Elongation in Glioblastoma. *Nat. Commun.* 9 (1), 4475. doi:10.1038/s41467-018-06862-2

Zhao, W., Liang, J., Chen, Z., Diao, Y., and Miao, G. (2020). Combined Analysis of circRNA and mRNA Profiles and Interactions in Patients with Diabetic Foot and Diabetes Mellitus. *Int. Wound J.* 17 (2), 1183–1193. doi:10.1111/iwj.13420

Zheng, L., Cheng, W., Wang, X., Yang, Z., Zhou, X., and Pan, C. (2017). Overexpression of MicroRNA-145 Ameliorates Astrocyte Injury by

Targeting Aquaporin 4 in Cerebral Ischemic Stroke. *Biomed. Res. Int.* 2017, 1–9. doi:10.1155/2017/9530951

Zheng, Q., Bao, C., Guo, W., Li, S., Chen, J., Chen, B., et al. (2016). Circular RNA Profiling Reveals an Abundant circHIPK3 that Regulates Cell Growth by Sponging Multiple miRNAs. *Nat. Commun.* 7, 11215. doi:10.1038/ncomms11215

Zuo, L., Zhang, L., Zu, J., Wang, Z., Han, B., Chen, B., et al. (2020). Circulating Circular RNAs as Biomarkers for the Diagnosis and Prediction of Outcomes in Acute Ischemic Stroke. *Stroke* 51 (1), 319–323. doi:10.1161/strokeaha.119.027348

Conflict of Interest: The authors declare that the research was conducted in the absence of any commercial or financial relationships that could be construed as a potential conflict of interest.

Publisher's Note: All claims expressed in this article are solely those of the authors and do not necessarily represent those of their affiliated organizations, or those of the publisher, the editors and the reviewers. Any product that may be evaluated in this article, or claim that may be made by its manufacturer, is not guaranteed or endorsed by the publisher.

frontiers | Frontiers in Genetics

ORIGINAL RESEARCH
published: 13 April 2022
doi: 10.3389/fgene.2022.848364

RNA Sequencing of Cardiac in a Rat Model Uncovers Potential Target LncRNA of Diabetic Cardiomyopathy

Yangbo Xi[1,2†], Dongping Chen[3†], Zhihui Dong[3], Hingcheung Lam[1], Jiading He[1], Keyi Du[1], Can Chen[4], Jun Guo[1,2] and Jianmin Xiao[1,3,5]**

[1]Department of The First Clinical Medical College, Jinan University, Guangzhou, China, [2]Department of Cardiology, The First Affiliated Hospital of Jinan University, Guangzhou, China, [3]Central Laboratory, The Dongguan Affiliated Hospital of Jinan University, Binhaiwan Central Hospital of Dongguan, Dongguan, China, [4]Department of Pathology, The Dongguan Affiliated Hospital of Jinan University, Binhaiwan Central Hospital of Dongguan, Dongguan, China, [5]Department of Cardiology, The Dongguan Affiliated Hospital of Jinan University, Binhaiwan Central Hospital of Dongguan, Dongguan, China

OPEN ACCESS

Edited by:
Amanda Salviano-Silva,
University Medical Center Hamburg-Eppendorf, Germany

Reviewed by:
Tarun Pant,
Medical College of Wisconsin, United States
Gang Yuan,
Huazhong University of Science and Technology, China

***Correspondence:**
Jun Guo
dr.guojun@163.com
Jianmin Xiao
xiaokang20082008@163.com

[†]These authors have contributed equally to this work and share first authorship

Specialty section:
This article was submitted to RNA, a section of the journal Frontiers in Genetics

Received: 04 January 2022
Accepted: 18 March 2022
Published: 13 April 2022

Citation:
Xi Y, Chen D, Dong Z, Lam H, He J, Du K, Chen C, Guo J and Xiao J (2022) RNA Sequencing of Cardiac in a Rat Model Uncovers Potential Target LncRNA of Diabetic Cardiomyopathy. Front. Genet. 13:848364. doi: 10.3389/fgene.2022.848364

Background: Diabetic cardiomyopathy (DCM) is one of the major causes of heart failure in diabetic patients; however, its pathogenesis remains unclear. Long non-coding RNAs (lncRNAs) are involved in the development of various cardiovascular diseases, but little is known in DCM.

Objective: The present study was conducted to investigate the altered expression signature of lncRNAs and mRNAs by RNA-sequencing and uncovers the potential targets of DCM.

Methods: A DCM rat model was established, and the genome-wide expression profile of cardiac lncRNAs and mRNAs was investigated in the rat model with and without DCM by RNA-sequencing. Bioinformatics analysis included the co-expression, competitive endogenous RNA (ceRNA) network, and functional enrichment analysis of deregulated lncRNAs and mRNAs.

Results: A total of 355 lncRNA transcripts and 828 mRNA transcripts were aberrantly expressed. The ceRNA network showed that lncRNA XR_351927.3, ENSRNOT00000089581, XR_597359.2, XR_591602.2, and XR_001842089.1 are associated with the greatest number of differentially expressed mRNAs and AURKB, MELK, and CDK1 may be the potential regulatory targets of these lncRNAs. Functional analysis showed that these five lncRNAs are closely associated with fibration, cell proliferation, and energy metabolism of cardiac myocytes, indicating that these core lncRNAs have high significance in DCM.

Conclusions: The present study profiled the DCM-specific lncRNAs and mRNAs, constructed the lncRNA-related ceRNA regulatory network, and identified the potential prognostic biomarkers, which provided new insights into the pathogenesis of DCM.

Keywords: diabetic cardiomyopathy, long non-coding RNA, transcriptome sequencing, bioinformatic analyses, ceRNA

INTRODUCTION

Diabetic cardiomyopathy (DCM) is a diabetes mellitus (DM)–induced pathophysiological condition characterized by abnormal cardiac function and structure in the absence of hypertension, coronary artery disease, and valvular heart disease (Ritchie and Abel, 2020) and is one of the major causes of heart failure in diabetic patients. Reportedly, the prevalence of cardiac dysfunction in patients with type 1 diabetes mellitus (T1DM) and T2DM is 14.5 and 35%, respectively (Bouthoorn et al., 2018; Tan et al., 2020). Although the number of studies on DCM increased exponentially over the past decade, and the pathogenesis of this condition is yet unclear.

Accumulating evidence has shown that long non-coding RNAs (lncRNAs) play critical roles in the pathology and physiology of cardiovascular diseases (CVDs) and can be used as potential targets for the diagnosis and prevention of CVDs (Uchida and Dimmeler, 2015). LncRNAs are endogenous RNA transcripts longer than 200 nucleotides that do not have protein-coding potential. However, they are significant molecules in almost every gene function and regulation level, including cell proliferation, epigenetic regulation, and genomic imprinting (Wang and Sun, 2020). Some studies indicated that lncRNAs are potential regulators of various CVDs due to their function in cardiomyocyte proliferation, differentiation, cardiac gene expression, and cardiac remodeling (Ritchie and Abel, 2020).

LncRNAs have an mRNA-like structure with a 5′-end methylated cap and a 3′-end poly-A tail and act as competitive endogenous RNAs (ceRNAs) to regulate mRNA expression by interaction with the shared miRNAs on target genes (Salmena et al., 2011). This participates in the occurrence and development of various CVDs (Li et al., 2019), including congenital heart disease (Wang and Yuan, 2019; Zhang et al., 2021), cardiac hypertrophy (Viereck et al., 2020), heart failure (Li et al., 2019), and cardiac fibrosis (Hao et al., 2019) by epigenetic regulation of target genes. However, few studies have focused on the role of lncRNAs in DCM development, and the lncRNA-related ceRNA regulation in DCM is yet to be clarified.

DCM occurs as a result of hyperglycemia-induced impairment of myocardial function. A streptozocin (STZ)-induced rat model of T1DM has been generated to study the impact of diabetes on the heart. In the present study, we established the DCM rat model and investigated the altered expression signature of lncRNAs and mRNAs by RNA-sequencing. Furthermore, we conducted bioinformatics analysis of the deregulated lncRNA–mRNA with co-expression, ceRNA network, and functional enrichment analysis. The parallel analysis of lncRNA and mRNA expression profiles allowed us to evaluate the impact of lncRNA deregulation and their potential pathogenetic role in DCM.

METHODS

Establishment of the Animal Model and Echocardiographic Analysis

The animal study was reviewed and approved by the Medical Ethics Committee of the Dongguan Affiliated Hospital of Jinan University. After overnight fasting, the model group rats (8 weeks old, male, n = 25) were injected a single dose of streptozocin (STZ) solution (1% in citrate saline, freshly prepared, 50 mg/kg, intraperitoneal (i.p.)). The control group rats (8 weeks old, male, n = 12) were injected (i.p.) with equivalent doses of citrate saline (STZ solvent) and fed under the same conditions. Three rats were housed together in a cage and given adequate water and standard rat chow. The blood glucose level was measured 5 days after i.p. injection. The rats with blood glucose >16.7 mmol/L for two consecutive days were presumed to be diabetic.

For echocardiographic analysis, the rats were anesthetized with 2% (vol/vol), 50 mg/kg phenobarbital (H20057384), and echocardiography was performed after 20 weeks post-intraperitoneal injection. The left ventricle internal dimension at end-diastole (LVID;d), left ventricle internal dimension at end-systole (LVID;s), left ventricle posterior wall thickness at end-diastole (LVPW;d), and interventricular septum thickness at end-diastole (IVS;d) were measured by M-mode tracing using an L15-7io probe (Ultrasound Transducer Bothell, WA, United States) (n = 11 in the control group, n = 25 in the model group). The percentage of fractional shortening (FS) was calculated as follows: [(LVEDD-LVESD)/LVEDD] × 100 and ejection fraction (EF) percentage using the equation: [(EDV−ESV)/EDV)] × 100, where EDV represents end-diastolic volume and ESV represents end-systolic volume.

Estimation of Histological and Blood Parameters

After administering anesthesia with 70 mg/kg phenobarbital, thoracotomy was performed to collect blood by puncturing with a syringe needle in the left ventricle. The blood insulin, glucagon, total cholesterol (TC), triglyceride (TG), high-density lipoprotein cholesterol (HDL-c), low-density lipoprotein cholesterol (LDL-c), brain natriuretic peptide (BNP), cardiac troponin I (cTn I), and creatinine (Cr) were measured using assay kits (Nanjing Jiancheng Bio.: A111-A113-2-1, CUSABIO: CSB-E07972r, CSB-E08594r, CSB-E05070r, CSB-E12800r, China). (n = 4 in the control group, n = 5 in the model group).

After overdosing with anesthesia, the myocardium from the left ventricles of the rats was harvested (n = 5 for each group). For histological analysis, the freshly harvested myocardium samples were fixed with 4% paraformaldehyde, embedded in paraffin, sectioned into 4-μm-thick slices, and stained with hematoxylin and eosin (H&E, BBC Biochemical) and Masson's trichome staining (Abcam, ab150681). To further analyze the ultrastructural changes in the cardiomyocytes, transmission electron microscopy analysis was conducted at the Guangzhou Huiyuanyuan Pharmaceutical Technology Co., Ltd. For this, the myocardium samples were fixed with 2.5% glutaraldehyde and 1% osmium acid, rinsed with 0.1 M phosphate buffer, embedded in paraffin, sectioned into 50–70 nm thick slices, and observed under a transmission electron microscope (Japan Electron Optics Laboratory Co., Ltd., JEM-1400 PLUS).

Tissue Collection and RNA-Sequencing

For RNA-sequencing, the myocardium harvested from the left ventricle of rats was immediately snap-frozen at −80°C before

TABLE 1 | List of primer sequences for RT-qPCR.

	Forward (5′-3′)	Reverse (5′-3′)
mRNA		
Bok	5′-CCCAGCGTATATCGGAATGTGG-3′	5′-CACTACCTTGCCCCATGTGA-3′
Hmox1	5′-CTTCCCGAGCATCGACAACC-3′	5′-AATGTTGAGCAGGAAGGCGG-3′
Ckb	5′-GACGTTCCTGGTGTGGATCA-3′	5′-GAGTGAGGCCAGTGCAGAAT-3′
Pla2g7	5′-GTTCCAAGGCTCTCAGTGCAA-3′	5′-CTCACGGGAAACATCCACGG-3′
Col1a2	5′-TACAACGCAGAAGGGGTGTC-3′	5′-TCCAGGTACGCAATGCTGTT-3′
Col3a1	5′-CCCTGAACTCAAGAGCGGAGA-3′	5′-ACCAGCATCTGTCCACCAGT-3′
Eno3	5′-ATCAGTGGGGAGAAGCTCGG-3′	5′-CCCAGCCATTAGACTGTGCC-3′
Hmox1	5′-CTTCCCGAGCATCGACAACC-3′	5′-AATGTTGAGCAGGAAGGCGG-3′
GAPDH	5′-ACCACCATGGAGAAGGCTGC-3′	5′-CTCAGTGTAGCCCAGGATGC-3′
lncRNA		
XR_001842342.1	5′-TTCTTGCCCCTCCTTCCTAGT-3′	5′-GGAACATCAGCGGAGACCCT-3′
XR_590344.2	5′-TGGAAGAAGAGGGCCACCAA-3′	5′-CAGATCAGGCTGACGGCAAG-3′
XR_357664.3	5′-ACGAGATAAGCCGGATGCAAG-3′	5′-CGGGTGCAAAGTGTAGTGGT-3′
XR_350940.2	5′-AAAGTGTTCTTGCCCCTCCTT-3′	5′-AGACCGTCAACAGCTTAGCC-3′
XR_349856.3	5′-TATACACATTGCGGGGCCAAC-3′	5′-AGAAATGCCCACAGCAGTAGT-3′
XR_146366.4	5′-GCAGCCAGAAGCAAATGAGC-3′	5′-GACCAAGCACCAGCTATGGG-3′
XR_001842089.1	5′-TTGGCTGGTTTTTCTGGGCAT-3′	5′-ACCAAACCCCAGCATATCGG-3′
ENSRNOT80276	5′-GGAGCACTGCCCTGGTTAGA-3′	5′-CTCGTTTCTCGTGGGCGTTC-3′

RNA extraction. Total RNA was extracted from heart samples using the mirVana miRNA Isolation Kit (Ambion) following the manufacturer's protocol. RNA integrity was evaluated using the Agilent 2100 Bioanalyzer (Agilent Technologies, Santa Clara, CA, United States). The samples with RNA integrity number (RIN) ≥7 were subjected to subsequent analysis. The libraries were constructed using TruSeq Stranded Total RNA with Ribo-Zero Gold, according to the manufacturer's instructions, sequenced on the Illumina sequencing platform (HiSeqTM 2500), and 150-bp/125-bp paired-end reads were generated. The RNA-depleted RNA-seq was carried out at the laboratory of Shanghai OE Biotech Company.

RNA-Sequencing Data Validation by RT-qPCR

To validate the expression profile data obtained from RNA-sequencing, we selected eight lncRNAs and eight mRNAs that met the screening criteria for validation using RT-qPCR. Total RNA was isolated from five samples each from the control and model groups. An equivalent of 1 μg RNA was converted to complementary DNA (cDNA) as per the manufacturer's guidelines (Takara, RR047Q, Japan). The expression level of lncRNA and mRNA was determined by RT-qPCR using Universal SYBR qPCR Master Mix (Biosharp, BL697A, China). PCR was performed on an SLAN-96S instrument (Shanghai Hongshi Medical Technology Co., Ltd., China) using a PrimeScript™ RT reagent Kit (Takara, RR047Q, Japan) and the reaction conditions were as follows: pre-denaturation at 95°C for 3 min, 40 cycles of denaturation at 95°C for 5 s, and annealing at 60°C for 1 min. The PCR reaction consisted of 10.0 μl of SYBR Mix, 1.0 μl of PCR forward primer, 1.0 μl of PCR reverse primer, 1.0 μl of the cDNA template, and 7.0 μl of RNase-free dH_2O in a total volume of 20 μl. *GAPDH* was used as the internal reference for real-time PCR. The relative expression of the target gene was calculated using the $2^{-\Delta\Delta Ct}$ method. The primers are listed in **Table 1**.

Bioinformatic Analysis

The raw reads generated during high-throughput sequencing are in the FASTQ format. In order to obtain high-quality reads for subsequent analysis, the raw reads were subjected to a quality filter. Trimmomatic (Bolger et al., 2014) was first used for adapter removal, and then low-quality bases and N-bases or low-quality reads were filtered out. Using HISAT2 (Kim et al., 2015) to align clean reads to the reference genome of the experimental species, the sample was assessed by genomic and gene alignment. Stringtie software (Pertea et al., 2015) was utilized to assemble the reads, and the new transcript was spliced. Then, the candidate lncRNA transcripts were selected by comparing the gene annotation information of the reference sequence produced by Cuffcompare (Trapnell et al., 2012) software. Finally, transcripts with coding potential were screened out by CPC (Kong et al., 2007), Pfam (Finn et al., 2006), and PLEK (Li et al., 2014) to obtain lncRNA-predicted sequences.

Subsequently, Size Factors function of the DESeq (2012) R package was used to normalize the counts, and nbinom test function was applied to calculate the *p*-value and fold-change values for the comparison of differences. The differential transcripts with *p*-values ≤ 0.05 and fold change ≥ 2 were selected to identify the differentially expressed lncRNAs and mRNAs. Kyoto Encyclopedia of Genes and Genomes (KEGG) pathway enrichment and Gene Ontology (GO) analysis of differentially expressed mRNAs (DE-mRNAs) were conducted using the SWISS-PROT database (http://www.gpmaw.com) and online analysis tool KAAS (http://www.genome.jp/tools/kaas/).

Construction of the ceRNA Network

In order to construct the ceRNA regulatory network, the miRNA data (FASTA file) rno_miRNA.fa were obtained from the miRBase platform (www.mirbase.org).The miRNA–mRNA and lncRNA–miRNA interactions were predictive analyses by miRanda (v3.3a). The ceRNA score was calculated using the MuTaME (H. Wang et al., 2020), and the *p*-value of the ceRNA

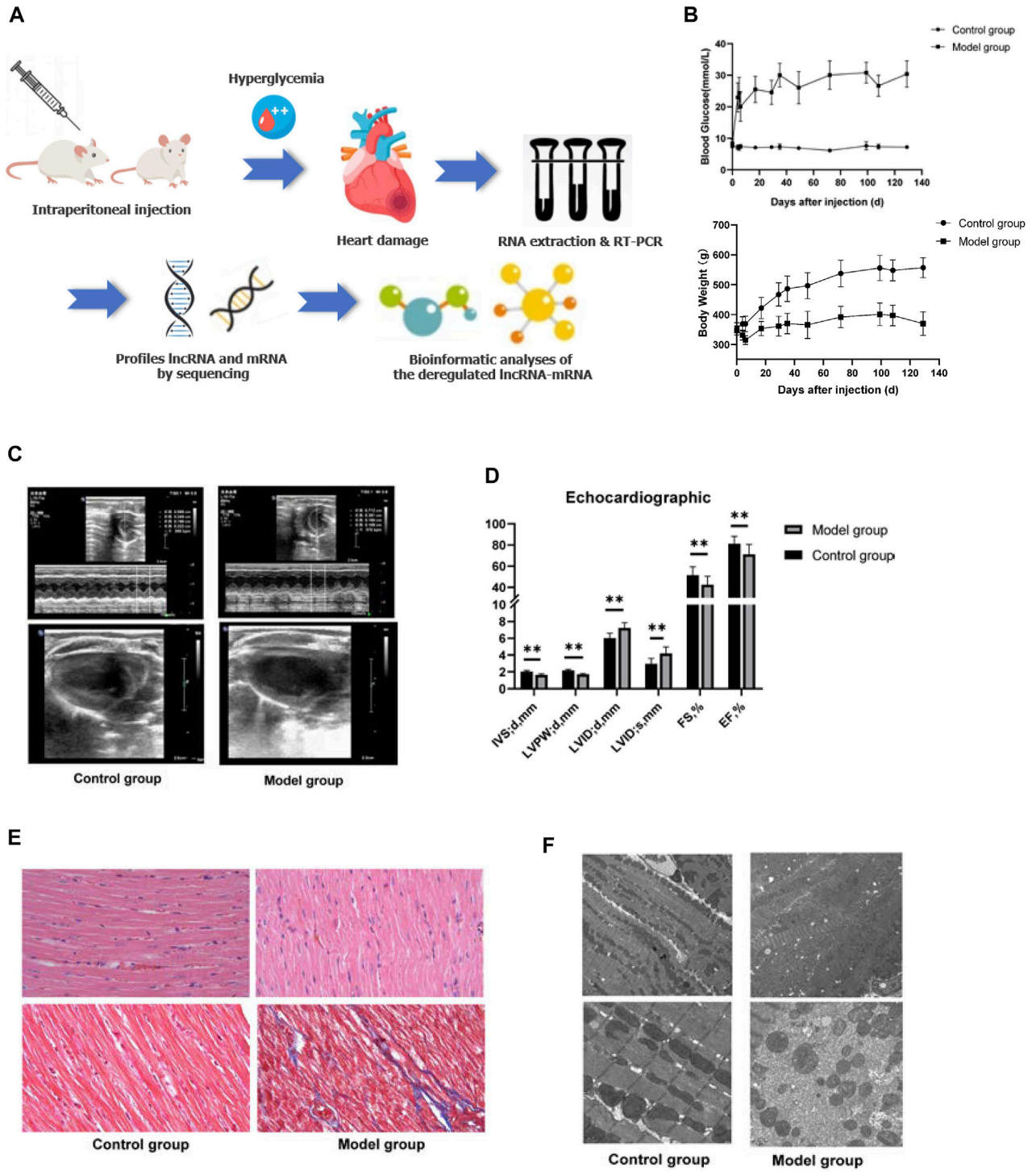

FIGURE 1 | General characteristics of the animal model. **(A)** Schematic depiction of the experimental design. **(B)** Blood glucose and body weight of the animals in the two groups after STZ injection. **(C,D)** Echocardiography of the animal model. Left ventricle internal dimension at end-diastole (LVID;d), left ventricle internal dimension at end-systole (LVID;s), ejection fraction (EF), fractional shortening (FS), left ventricle posterior wall thickness at end-diastole (LVPW;d), interventricular septum thickness at end-diastole (IVS;d). Data are represented as mean ± SEM, $^{**}p < 0.05$. **(E)** HE (upper part), and Masson's (lower part) staining. Masson's staining identified massive fibrosis in the diabetic myocardium. **(F)** Transmission electron microscopy observed that cardiomyocytes in diabetic hearts appear damaged with loss of sarcomeres and pathological changes in the mitochondrial shape involving loss or reorientation of cristae and matrix depletion.

TABLE 2 | Plasma parameters of animals.

	Control group	Model group	*p*-value
TC, mmol/L	1.70 ± 0.14	1.54 ± 0.16	0.610
TG, mmol/L	1.23 ± 0.26	0.83 ± 0.37	0.112
LDL-c, mmol/L	0.99 ± 0.26	0.79 ± 0.39	0.394
HDL-c, mmol/L	1.48 ± 0.25	1.59 ± 0.26	0.532
Cr, μmol/L	60.08 ± 31.58	32.80 ± 9.64	0.106
BNP, pg/ml	1129.65 ± 472.17	4356.79 ± 2112.40	0.021
cTn I, pg/ml	60.83 ± 12.91	54.55 ± 7.17	0.382
Insulin, nUl/ml	901.61 ± 49.80	320.66 ± 113.43	<0.001
Glucagon, pg/ml	52.86 ± 9.84	26.19 ± 18.01	0.033

TC, total cholesterol; TG, triglyceride; LDL-c, low-density lipoprotein cholesterol; HDL-c, high-density lipoprotein cholesterol; Cr, creatinine; BNP, brain natriuretic peptide; cTn I, cardiac troponin I, data are represented as mean ± SEM.

interactions was based on the hypergeometric distribution (Liu K. et al., 2013).

Pearson's correlation test was used to calculate the correlation between the expression of differential lncRNA (length <6000 nt) and differential mRNA expression data: the correlation of the pair was >0.8 or < −0.8 and $p < 0.05$. The positively related mRNA–lncRNA co-expression interactions were screened out. The ceRNA network was based on the intersection interactions between the co-expression and ceRNA score. The lncRNA–miRNA–mRNA (ceRNA) interaction regulatory network was integrated using Cytoscape software (v3.7.2).

RESULTS

General Characteristics and Echocardiography of Animals

The plasma and echocardiographic parameters of the animal are shown in **Figure 1** and **Table 2**. The rats of the control group lost weight at 1 week after the STZ injection, and the body weight was significantly lesser than that of the age-matched rats of the control group up to 20 weeks of follow-up ($p < 0.05$). The blood glucose level of the model group rats increased significantly within 1 week after the STZ injection compared to the control group and remained at a higher level (>16.7 mmol/L) for up to 20 weeks post follow-up (**Figures 1A,B**). The histological analysis revealed that the spaces between cardiomyocytes in diabetic hearts are enlarged with disorders of myocardial cell arrangement compared to control hearts, indicating altered cellular structure. Masson's staining showed massive fibrosis in the diabetic myocardium (**Figure 1E**). At the ultrastructural level, cardiomyocytes in diabetic hearts were damaged with the loss of sarcomeres, and the pathological changes in the mitochondrial shape involved loss or reorientation of cristae and matrix depletion (**Figure 1F**). Furthermore, the level of BNP was substantially elevated in blood from 20-week diabetic rats compared to that in the control hearts ($p < 0.05$), indicating hyperglycemic damage to the myocardium. Simultaneously, no significant differences were detected in HDL-c, LDL-c, TG, TC, and Cr levels among the groups (**Table 2**). The blood level of insulin and glucagon decreased significantly in the model group, indicating impaired islet function after intraperitoneal injection of STZ.

The assessment of cardiac contractile function revealed that the echocardiogram analysis of the control and model group had significantly increased LVID and left ventricular volume (LVEV) at both end-diastole and end-systole, while IVS, LVPW, FS, and EF were significantly decreased in the model group at 20 weeks compared to those of the age-mated control group ($p < 0.05$). These data suggested that hyperglycemia causes cardiac dysfunction and cardiomyopathy (**Figures 1C,D**).

LncRNA and mRNA Expression Profile in the Rat Model

In order to uncover the deregulated genes and lncRNA expression, RNA-sequencing on the myocardium from both DCM rats ($n = 5$) and normal rats ($n = 5$) was performed. The lncRNA/mRNA expression profile in the rat myocardium is shown in **Figures 2A–D**. Among 22,601 mRNAs and 15,633 lncRNAs transcripts, 339 mRNAs and 182 lncRNAs were upregulated and 489 mRNAs and 227 lncRNAs were downregulated in the model group (fold change >2.0 and $p < 0.05$) (**Supplementary Table S1**). In addition, the hierarchical clustering analysis revealed that the regulatory profiles of mRNAs and lncRNAs differed significantly between the DCM rats compared to the controls (**Figures 2C,D**).

The chromosomal distribution of deregulated lncRNAs is shown in **Figure 2E**. Chromosome 1 had the maximum number of deregulated lncRNAs and mRNAs. The classification of differently expressed lncRNAs in the rat myocardium of the two groups is shown in **Figure 2F**. Intergenic and genic lncRNAs accounted for 58 and 42% of differently expressed lncRNAs in the DCM rat myocardium, respectively.

Validation of lncRNAs and mRNAs by RT-qPCR Analysis

The RNA-sequencing data were validated by RT-qPCR. The results showed that the expression levels of the mRNAs *Bok*, *HMOX1*, *Pla2g7*, and *Hmgcs2* were upregulated, whereas those of *Ckb*, *Clo1a2*, *Clo3a1*, and *Eno* were downregulated in the rat myocardium (**Figure 3A**). Similarly, the expression levels of the lncRNAs XR_357664.3, XR_350940.2, XR_349856.3, XR_146366.4, XR_001842089, and ensrnot80276 were upregulated, while those of XR_3001842342.1 and XR_590344.2 were downregulated in the rat myocardium (**Figure 3B**). The RT-qPCR results were consistent with the RNA-sequencing data in both lncRNAs and mRNAs.

Functional Enrichment Analysis of DE-mRNAs

GO and KEGG pathway analyses were performed to determine the potential function of DE-mRNA. GO enrichment analysis consists of three levels: molecular function, biological process, and cellular component; each one explains the biological function of the genes at different levels. The results showed that the upregulated mRNAs were associated with regulation of wound

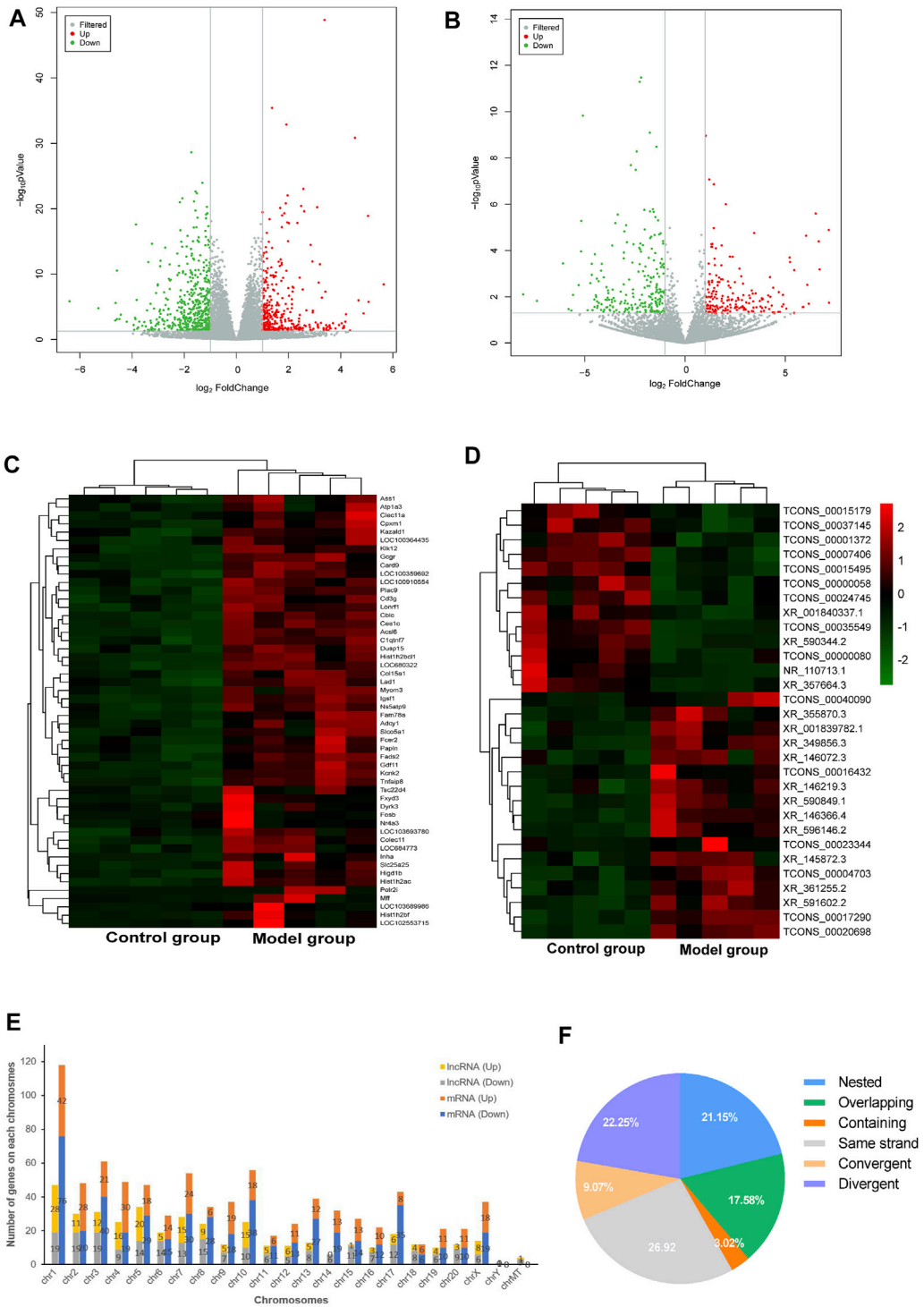

FIGURE 2 | LncRNA and mRNA expression profile of the rat myocardium. **(A**,**B)** Volcano plots show DE-mRNAs **(A)** and lncRNAs **(B)** in the two groups. The red and green points represent up- and downregulated mRNAs/lncRNAs (compare to the control group), respectively. The horizontal green line depicts $^{*}p < 0.05$, whereas the vertical green line shows a two-fold change in up and downregulation. **(C**,**D)** Hierarchical clustering analysis presents differentially expressed mRNAs **(C)** and lncRNAs **(D)** and red and green represent up- and down regulated mRNAs/lncRNAs with ≥ two-fold changed, respectively (3 < FPKM<50). **(E)** Chromosomal distribution of deregulated mRNAs and lncRNAs. **(F)** Intergenic lncRNAs included convergent, divergent, and same strand accounting for 58% and genic lncRNAs included containing, nested, and overlapping were accounted for 42%.

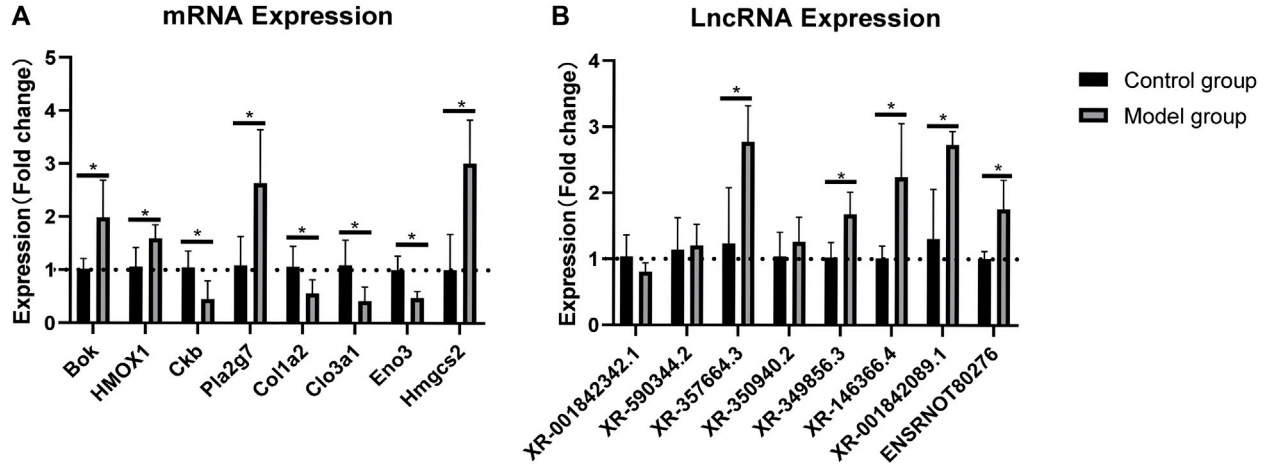

FIGURE 3 | Validation of lncRNAs and mRNAs by RT-qPCR analysis. Relative expression of each lncRNA and mRNA was normalized to that of *GAPDH*. Data are represented as mean ± SEM, $^*p < 0.05$.

healing (GO:0042060), oxidation–reduction process (GO: 0055114), angiogenesis (GO:0001525), response to hypoxia (GO:0001666), and regulation of apoptotic process (GO: 0008284 and GO:0008285) (**Figure 4A**), while the downregulated mRNAs were associated with cell division processes such as chromosome segregation (GO:0007059), mitotic cytokinesis (GO:0000281 and GO:0000278), and cell division (GO:0051301) (**Figure 4B**) at the biological process level. In the category of cellular component, the upregulated mRNAs were enriched in the extracellular matrix (GO:0031012 and GO:0005615) and membrane (GO:0016020) (**Figure 4A**), while the down deregulated mRNAs were associated with the nucleus (GO:0005634) and nucleoplasm (GO:0005654) (**Figure 4B**). For molecular function, the deregulated mRNAs were related to protein homodimerization activity (GO:0042803), iron ion binding (GO:0005506), DNA binding (GO:0003677), and ATP binding (GO:0005524) (**Figures 4A,B**) (**Supplementary Table S2**).

KEGG pathway enrichment analysis is used for functional annotation in order to elucidate the related functions and pathways of the differentially expressed genes. Our KEGG pathway analysis results showed that the DE-mRNAs were associated with the PI3K-Akt signaling pathway (rno05166), viral carcinogenesis (rno05203), cell cycle (rno04110), and alcoholism (rno05034) (**Figure 4D**). The upregulated mRNA enrichment pathways included cancer (rno05200), Wnt signaling pathway (rno04310), fatty acid elongation (rno00062), and ferroptosis (rno04216) (**Figure 4C** and **Supplementary Table S2**). The results suggested a major role of those pathways in the occurrence and development of DCM.

LncRNA–mRNA Co-expression and ceRNA Regulatory Network

The co-expression networks (CENs) are constructed based on the evaluation of the co-expression correlation between genes and lncRNAs according to the normalized intensity of the signal values. The CENs are commonly used to reveal the core regulatory lncRNAs. The significantly co-expressed lncRNAs–mRNAs (Pearson's correlation >0.8 and $p < 0.05$) were integrated into CENs. Finally, 29,289 connections were identified between 385 lncRNAs and 827 mRNAs in the DCM rat myocardium (**Supplementary Table S3**). The top 10 KEGG level 1 enriched genes in the CENs are shown in **Figure 5**. KEGG level 1 category included cellular processes (CP), environmental information processing (EIP), genetic information processing (GIP), human diseases (HD), metabolism (Meta.), and organismal systems (OS).

Next, we constructed the ceRNA regulatory networks based on the lncRNA–mRNA CENs. A total of 206,942 pairs of miRNA–mRNA interactions and 66,471 pairs of lncRNA–miRNA interactions were obtained. Then, the ceRNA network was constructed by integrating these interactions using Cytoscape software v3.7.2 (**Figure 6**). The top 200 miRNA–mRNA and lncRNA–miRNA and top 100 lncRNA–mRNA of the ceRNA interaction network are shown in **Figures 6A–C** and **Supplementary Table S3**.

Among them, the lncRNA, XR_351927.3, ENSRNOT00000089581, XR_597359.2, XR_591602.2, and XR_001842089.1 have maximum connections with DE-mRNAs in the ceRNA network, indicating that these lncRNAs might comprise a significant core (**Figure 6D** and **Supplementary Table S3**). Bioinformatics analysis revealed that these mRNAs related to the five lncRNAs are closely associated with fibration and energy failure. Some of these molecules were ARG1 and SERPINH1 related to collagen biosynthetic process (GO: 0032964); GREM1, COL1A2, LUM, SERPINH1, and SCX related to collagen fibril organization (GO:0030199); MELK, UHRF1, CKS2, CDK1, MKI67, FAM83D, CD34, AURKB, E2F8, and BOK related to cell proliferation (GO:0008283); TOP2A, KIF14, ATP1A3, BUB1B, TTK, KIF11, AURKB, P2RY1, PBK, NEK2, CKB, EPHB1, POLQ, UBE2C, PLK1, ACSL6, KIF24, KIF23, NEK2L1,

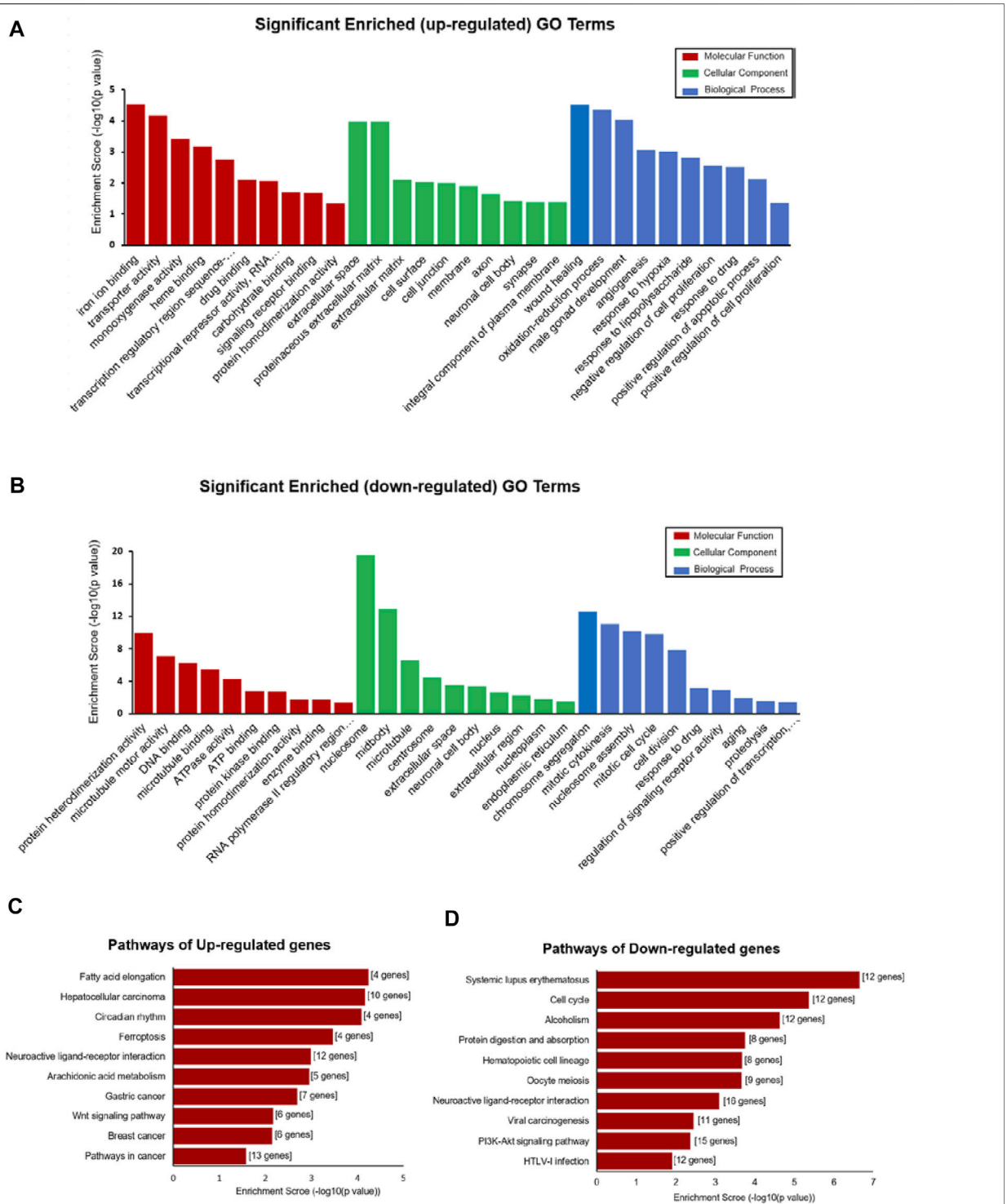

FIGURE 4 | Functional enrichment analysis of DE-mRNAs. **(A**,**B)** Top 30 GO terms (comprises cellular component (CC), molecular function (MF), and biological process (BP)) consisting of significantly enriched upregulated GO terms **(A)** and downregulated GO terms **(B)**. **(C**,**D)** Pathways depict the significant difference among the control and DCM groups, significantly upregulated pathway terms, **(C)** and downregulated pathway terms **(D)**.

KIF22, MASTL, ASS1, MYO16, CIT, SBK2, CENPE, MELK, KIF18B, KIFC1, KIF4A, CDK1, TUT1, KIF20A, KIF20B, FKBP4, MYH6, and TTLL9 related to ATP binding (GO:0005524). The deregulated mRNAs, *AURKB*, *MELK*, and *CDK1*, repeated multiple enrichment in related items might be associated with the pathogenesis of DCM.

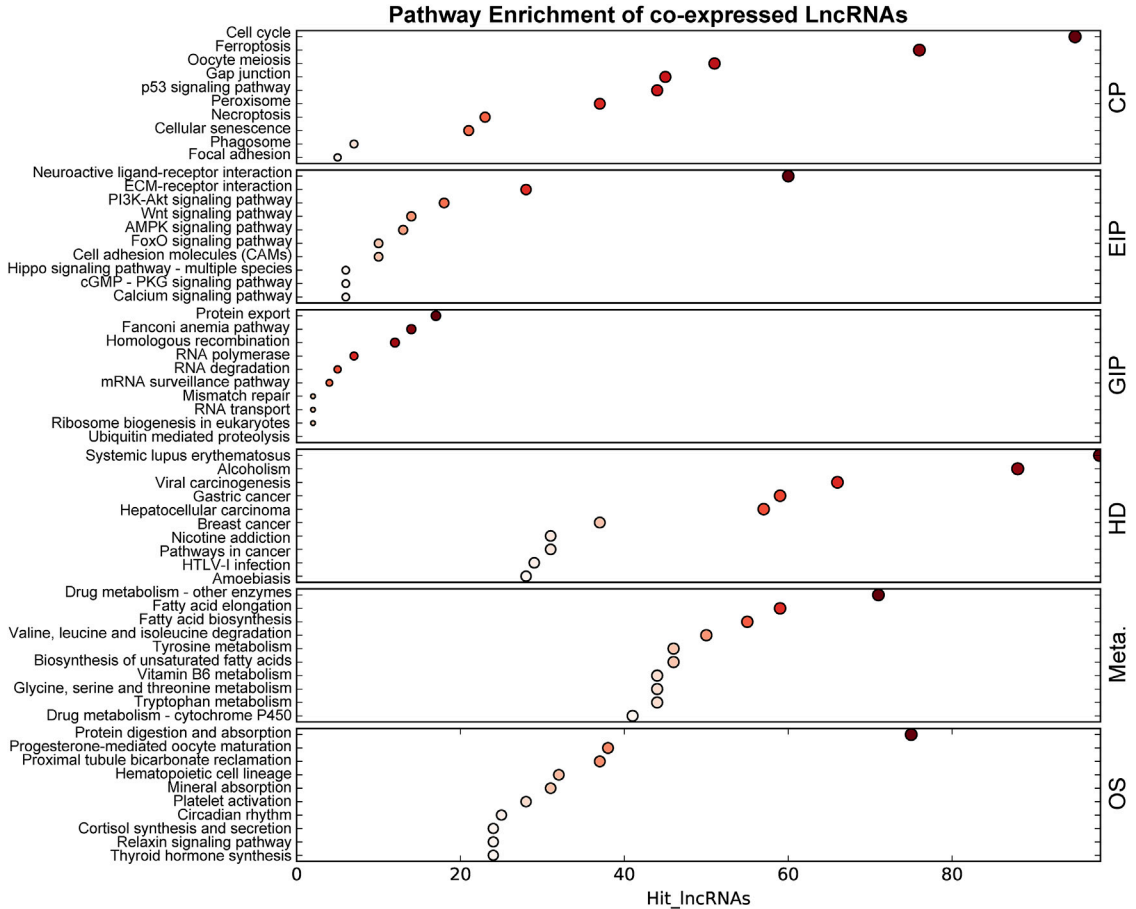

FIGURE 5 | KEGG enrichment of genes in the co-expressed network. The size of the bubble represents the number of differential genes, and the bubble's color represents enriched *p*-value. Hit_lncRNAs indicate the number of lncRNAs with co-expressed mRNAs. KEGG level 1 category included cellular processes (CP), environmental information processing (EIP), genetic information processing (GIP), human diseases (HD), metabolism (Meta.), and organismal systems (OS).

DISCUSSION

Previous studies indicated that diabetes has adverse effects on the different cell types of the heart, including endothelial cells, fibroblasts, and cardiomyocytes. DCM is attributed to hyperglycemia-induced impairment of myocardial function, and heart failure is the endpoint of DCM. In the present study, we used STZ to induce diabetes and established a DCM animal model (Liu Z.-W. et al., 2013; Riehle and Bauersachs, 2018). STZ is a glucosamine-nitrosourea similar to the glucose molecule that needs to be transported into the cells alone by the low-affinity glucose transporter (GLUT2) on islet β-cells, destroying the islet β-cells, resulting in insulin synthesis, decreased secretion, and disrupted glucose metabolism; currently, it is the most widely used chemical inducer in diabetic animal models (Bonnevie-Nielsen et al., 1981). The present study confirmed that STZ-induced rats exhibit decreased body weight and plasma insulin levels. Furthermore, our rat model also confirmed that STZ-induced diabetes leads to a pronounced DCM characterized by myocardial fibrosis, mitochondrial dysfunction, and associated diastolic and systolic dysfunction, which is similar to that observed previously (Joffe et al., 1999; Xie et al., 2020; Yu et al., 2021). In addition, RNA-sequencing of cardiac tissue uncovers a large number of DE-lncRNAs and mRNAs, indicating that lncRNA epigenetic regulation plays a major role in heart damage during the diabetic state. Several studies have demonstrated the regulatory role of lncRNAs in various CVDs (Liu et al., 2018; Lv et al., 2018). The lncRNA can target and modulate the physiological functions of cardiomyocytes (Uchida and Dimmeler, 2015; Y.; Wang et al., 2020) and regulate them in a cell-type/tissue-specific manner (Ritchie and Abel, 2020). The role of lncRNAs in CVDs has gained increasing attention. Thus, it is essential to focus on the role of lncRNAs in DCM. Whole-transcriptome profiling of lncRNAs and mRNAs was conducted in the DCM animal model, which opened up new possibilities to explore the lncRNA dysregulation in the pathogenesis of DCM.

The RNA-sequencing results revealed significant differences in lncRNA/mRNA expression between the DCM and control groups. Next, we identified 409 lncRNAs aberrantly expressed in the myocardium of DCM rats. However, further investigation is required to identify the potential lncRNA targets for DCM

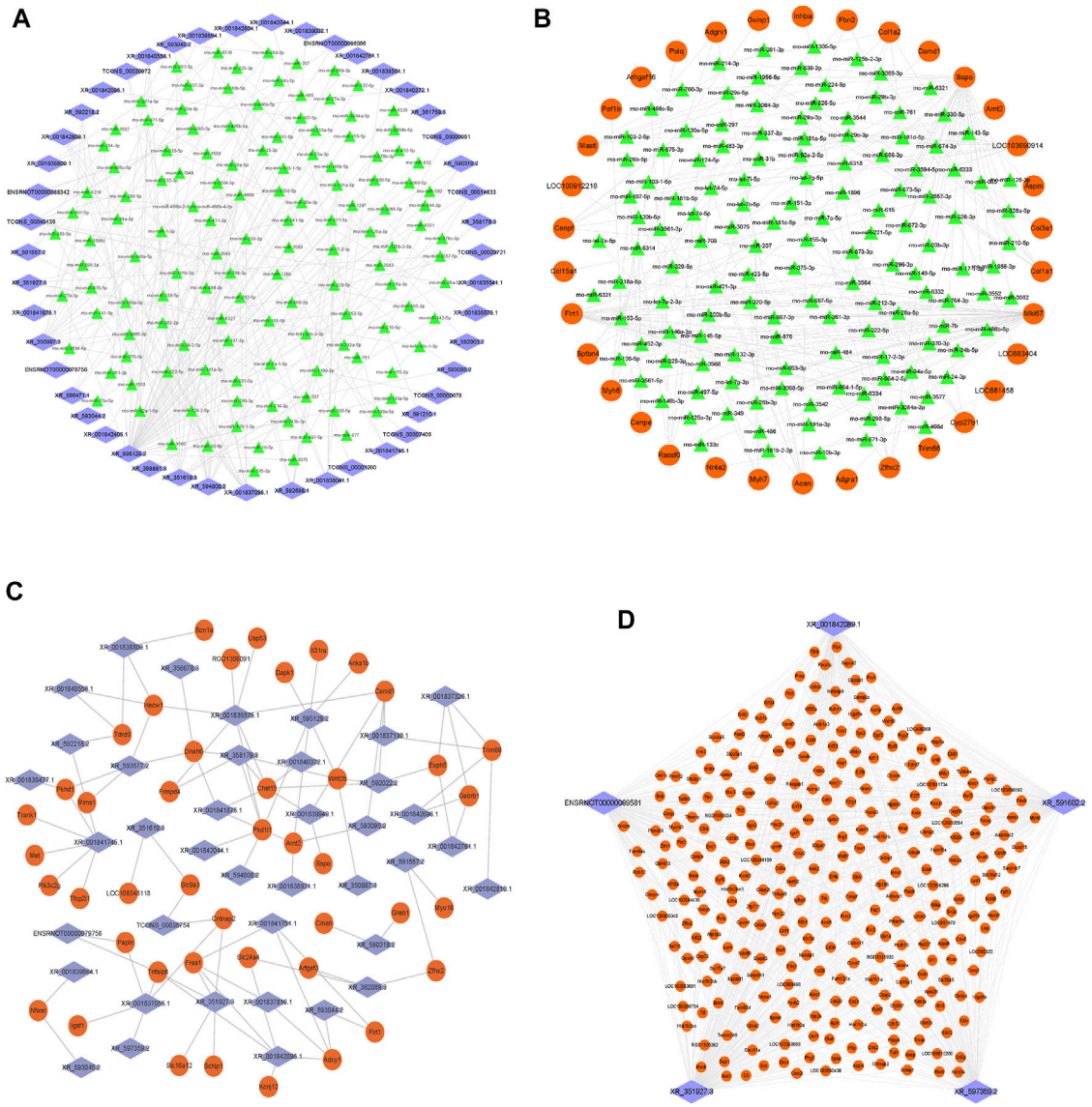

FIGURE 6 | Construction of the lncRNA–miRNA–mRNA network. **(A)** Network of the top 200 miRNA–lncRNA interactions. **(B)** Network of the top 200 miRNA–mRNA interactions. **(C)** Network of the top 100 lncRNA–mRNA of ceRNA interactions. **(D)** Top five lncRNA XR_351927.3, ENSRNOT00000089581, XR_597359.2, XR_591602.2, and XR_001842089.1 connections with DE-mRNAs in the ceRNA network. The blue diamond represents lncRNAs, the green triangle represents miRNAs, and the orange circle represents mRNAs.

progression and pathogenesis. Diabetes and CVDs are associated with genetic predisposition (Dahlstrom and Sandholm, 2017; Sandholm and Groop, 2018). These deregulated lncRNAs in this study were not evenly distributed on 21 chromosomes. As shown in **Figure 2E**, chromosome 1 has the maximal number of deregulated lncRNAs compared to other chromosomes, indicating that chromosome 1 may be susceptible to DCM pathology. Based on the correlation between lncRNAs and their affiliated protein-coding genes, lncRNAs are subdivided into the following types: genic lncRNA (lncRNA overlapping a protein-coding transcript at one or more nucleotides, including containing, nested, and overlapping) and intergenic lncRNA (lincRNA, lncRNA not overlapping a protein-coding transcript, including convergent, divergent, and same strand) (Ransohoff et al., 2018). The CEN results showed that 80% of lincRNAs were co-expressed with their neighboring genes, indicating that lincRNA should be studied with respect to the underlying regulatory mechanisms. The CENs indicated that 80% of lincRNAs and their adjacent genes were co-expressed in a similar direction, which could be useful to decipher the underlying regulatory mechanisms. Many aberrantly expressed lincRNAs in DCM suggest that lncRNAs may regulate the development of DCM *via* protein-coding genes.

Moreover, our results showed that the expression of several mRNAs was dysregulated in DCM. Taken together, 827 mRNAs were found to be differentially expressed in DCM.

Consistent with the distribution of deregulated lncRNAs, chromosome 1 had the maximum number of DE-mRNAs. Based on the GO and KEGG analyses, upregulated genes were significantly enriched for pathways in cancer (rno05200), neuroactive ligand–receptor interaction (rno04080), fatty acid elongation (rno00062), oxidation–reduction process (GO:0055114), and cell proliferation (GO:0008285 and GO: 0008284), whereas downregulated mRNAs were significantly enriched with neuroactive ligand–receptor interaction (rno04080), PI3K-Akt (rno04151), protein homodimerization activity (GO:0042803), microtubule motor activity (GO:0003777), and ATPase activity (GO: 0016887). Previous studies depicted that the signaling pathways, such as fatty acid elongation, cell proliferation, and oxidation–reduction processes, are associated with DCM pathogenesis. Some studies confirmed that diabetes patients have a high prevalence of cancer, viral infections, and tuberculosis (Blumenthal et al., 2017; Desbois and Cacoub, 2017). Therefore, we speculated that these regulated mRNAs in diabetes might be associated with increased cancer and infection. Moreover, the KEGG pathway analysis revealed that the pathways, such as neuroactive ligand–receptor interaction, protein homodimerization activity, and cell proliferation, were involved in the pathogenesis of DCM. Previous studies have shown that protein homodimerization is associated with the complications of diabetes, including neuropathy (Iyer et al., 2019), diabetic foot ulcers (Embil and Nagai, 2002) and diabetic nephropathy (Erol et al., 2019). These pathway analysis results demonstrated that the phenotype of the STZ-induced DCM model is similar to that observed in diabetic progressive DCM patients, providing a new rationale for further study on DCM. In addition, the results of the ceRNA regulatory network revealed that lncRNA, XR_351927.3, ENSRNOT-00000089581, XR_597359.2, XR_ 591602.2, and XR_001842089.1 have maximum connections with DE-mRNAs, and AURKB, MELK, and CDK1 are potential regulatory targets of these lncRNAs throughout the development of DCM. Given that these five lncRNAs are associated with fibration, cell proliferation, and energy metabolism of cardiac myocytes, they may serve as potential therapeutic and diagnostic targets for DCM.

In conclusion, heart damage in the diabetic state is a major cause of cardiovascular complications in diabetic patients. The present study showed that many lncRNAs and mRNAs are deregulated in the DCM myocardium. In this study, an lncRNA-related ceRNA regulatory network was constructed to uncover the potential target lncRNAs, which provided therapeutic targets or diagnostic biomarkers of DCM.

DATA AVAILABILITY STATEMENT

The datasets presented in this study can be found in online repositories. The names of the repository/repositories and accession number(s) can be found below: Gene Expression Omnibus, accession number GSE197999.

ETHICS STATEMENT

The animal study was reviewed and approved by the Medical Ethics Committee of the Dongguan Affiliated Hospital of Jinan University.

AUTHOR CONTRIBUTIONS

YX, DC, JX and JG conceived and designed the experiments. YX and DC wrote the main manuscript text. ZD, HL, JH and KD performed the experiments. YX and CC analyzed the data. All authors have reviewed the manuscript.

FUNDING

This study was supported by the Guangdong Basic and Applied Basic Research Foundation (No. 2021B1515140036) and Scientific Research Project of the Binhaiwan Central Hospital of Dongguan (No.2021010).

ACKNOWLEDGMENTS

We appreciated Junhua Zhou, Xiaoying Lu, Aochu Yang, and Pan Zhang at Shanghai OE Biotech Co. for their support on RNA sequencing.

SUPPLEMENTARY MATERIAL

The Supplementary Material for this article can be found online at: https://www.frontiersin.org/articles/10.3389/fgene.2022.848364/full#supplementary-material

REFERENCES

Blumenthal, M. J., Ujma, S., Katz, A. A., and Schäfer, G. (2017). The Role of Type 2 Diabetes for the Development of Pathogen-Associated Cancers in the Face of the HIV/AIDS Epidemic. *Front. Microbiol.* 8, 2368. doi:10.3389/fmicb.2017.02368

Bolger, A. M., Lohse, M., and Usadel, B. (2014). Trimmomatic: a Flexible Trimmer for Illumina Sequence Data. *Bioinformatics* 30 (15), 2114–2120. doi:10.1093/bioinformatics/btu170

Bonnevie-Nielsen, V., Steffes, M. W., and Lernmark, Å. (1981). A Major Loss in Islet Mass and B-Cell Function Precedes Hyperglycemia in Mice Given Multiple Low Doses of Streptozotocin. *Diabetes* 30 (5), 424–429. doi:10.2337/diab.30.5.424

Bouthoorn, S., Valstar, G. B., Gohar, A., den Ruijter, H. M., Reitsma, H. B., Hoes, A. W., et al. (2018). The Prevalence of Left Ventricular Diastolic Dysfunction and Heart Failure with Preserved Ejection Fraction in Men and Women with Type 2 Diabetes: A Systematic Review and Meta-Analysis. *Diabetes Vasc. Dis. Res.* 15 (6), 477–493. doi:10.1177/1479164118787415

Dahlström, E., and Sandholm, N. (2017). Progress in Defining the Genetic Basis of Diabetic Complications. *Curr. Diab Rep.* 17 (9), 80. doi:10.1007/s11892-017-0906-z

Desbois, A.-C., and Cacoub, P. (2017). Diabetes Mellitus, Insulin Resistance and Hepatitis C Virus Infection: A Contemporary Review. *World J. Gastroenterol.* 23 (9), 1697–1711. doi:10.3748/wjg.v23.i9.1697

Embil, J. M., and Nagai, M. K. (2002). Becaplermin: Recombinant Platelet Derived Growth Factor, a New Treatment for Healing Diabetic Foot Ulcers. *Expert Opin. Biol. Ther.* 2 (2), 211–218. doi:10.1517/14712598.2.2.211

Erol, I., Cosut, B., and Durdagi, S. (2019). Toward Understanding the Impact of Dimerization Interfaces in Angiotensin II Type 1 Receptor. *J. Chem. Inf. Model.* 59 (10), 4314–4327. doi:10.1021/acs.jcim.9b00294

Finn, R. D., Mistry, J., Schuster-Bockler, B., Griffiths-Jones, S., Hollich, V., Lassmann, T., et al. (2006). Pfam: Clans, Web Tools and Services. *Nucleic Acids Res.* 34, D247–D251. doi:10.1093/nar/gkj149

Hao, K., Lei, W., Wu, H., Wu, J., Yang, Z., Yan, S., et al. (2019). LncRNA-Safe Contributes to Cardiac Fibrosis through Safe-Sfrp2-HuR Complex in Mouse Myocardial Infarction. *Theranostics* 9 (24), 7282–7297. doi:10.7150/thno.33920

Iyer, S., Sam, F. S., DiPrimio, N., Preston, G., Verheijen, J., Murthy, K., et al. (2019). Repurposing the Aldose Reductase Inhibitor and Diabetic Neuropathy Drug Epalrestat for the Congenital Disorder of Glycosylation PMM2-CDG. *Dis. Model. Mech.* 12 (11), dmm040584. doi:10.1242/dmm.040584

Joffe, I. I., Travers, K. E., Perreault-Micale, C. L., Hampton, T., Katz, S. E., Morgan, J. P., et al. (1999). Abnormal Cardiac Function in the Streptozotocin-Induced, Non-insulin-dependent Diabetic ratJournal Article; Research Support. *Coll. Cardiol.* 34 (7), 2111–2119. doi:10.1016/s0735-1097(99)00436-2

Kim, D., Langmead, B., and Salzberg, S. L. (2015). HISAT: a Fast Spliced Aligner with Low Memory Requirements. *Nat. Methods* 12 (4), 357–360. doi:10.1038/nmeth.3317

Kong, L., Zhang, Y., Ye, Z.-Q., Liu, X.-Q., Zhao, S.-Q., Wei, L., et al. (2007). CPC: Assess the Protein-Coding Potential of Transcripts Using Sequence Features and Support Vector machineResearch Support, Non-U.S. Gov't]. *[Journal Articlenucleic Acids Res.* 35, W345–W349. doi:10.1093/nar/gkm391

Li, A., Zhang, J., and Zhou, Z. (2014). PLEK: A Tool for Predicting Long Non-coding RNAs and Messenger RNAs Based on an Improved K-Mer Scheme. *BMC Bioinformatics* 15, 311. doi:10.1186/1471-2105-15-311

Li, M., Duan, L., Li, Y., and Liu, B. (2019). Long Noncoding RNA/circular Noncoding RNA-miRNA-mRNA Axes in Cardiovascular Diseases. *Life Sci.* 233, 116440. doi:10.1016/j.lfs.2019.04.066

Liu, C.-Y., Zhang, Y.-H., Li, R.-B., Zhou, L.-Y., An, T., Zhang, R.-C., et al. (2018). LncRNA CAIF Inhibits Autophagy and Attenuates Myocardial Infarction by Blocking P53-Mediated Myocardin Transcription. *Nat. Commun.* 9 (1), 29. doi:10.1038/s41467-017-02280-y

Liu, K., Yan, Z., Li, Y., and Sun, Z. (2013a). Linc2GO: a Human LincRNA Function Annotation Resource Based on ceRNA Hypothesis. *Bioinformatics* 29 (17), 2221–2222. doi:10.1093/bioinformatics/btt361

Liu, Z.-W., Zhu, H.-T., Chen, K.-L., Dong, X., Wei, J., Qiu, C., et al. (2013b). Protein Kinase RNA- like Endoplasmic Reticulum Kinase (PERK) Signaling Pathway Plays a Major Role in Reactive Oxygen Species (ROS)- Mediated Endoplasmic Reticulum Stress- Induced Apoptosis in Diabetic Cardiomyopathy. *Cardiovasc. Diabetol.* 12, 158. doi:10.1186/1475-2840-12-158

Lv, L., Li, T., Li, X., Xu, C., Liu, Q., Jiang, H., et al. (2018). The lncRNA Plscr4 Controls Cardiac Hypertrophy by Regulating miR-214. *Mol. Ther. - Nucleic Acids* 10, 387–397. doi:10.1016/j.omtn.2017.12.018

Pertea, M., Pertea, G. M., Antonescu, C. M., Chang, T.-C., Mendell, J. T., and Salzberg, S. L. (2015). StringTie Enables Improved Reconstruction of a Transcriptome from RNA-Seq Reads. *Nat. Biotechnol.* 33 (3), 290–295. doi:10.1038/nbt.3122

Ransohoff, J. D., Wei, Y., and Khavari, P. A. (2018). The Functions and Unique Features of Long Intergenic Non-coding RNA. *Nat. Rev. Mol. Cel Biol* 19 (3), 143–157. doi:10.1038/nrm.2017.104

Riehle, C., and Bauersachs, J. (2018). Of Mice and Men: Models and Mechanisms of Diabetic Cardiomyopathy. *Basic Res. Cardiol.* 114 (1), 2. doi:10.1007/s00395-018-0711-0

Ritchie, R. H., and Abel, E. D. (2020). Basic Mechanisms of Diabetic Heart Disease. *Circ. Res.* 126 (11), 1501–1525. doi:10.1161/CIRCRESAHA.120.315913

Salmena, L., Poliseno, L., Tay, Y., Kats, L., and Pandolfi, P. P. (2011). A ceRNA Hypothesis: The Rosetta Stone of a Hidden RNA Language? *Cell* 146 (3), 353–358. doi:10.1016/j.cell.2011.07.014

Sandholm, N., and Groop, P.-H. (2018). Genetic Basis of Diabetic Kidney Disease and Other Diabetic Complications. *Curr. Opin. Genet. Develop.* 50, 17–24. doi:10.1016/j.gde.2018.01.002

Tan, Y., Zhang, Z., Zheng, C., Wintergerst, K. A., Keller, B. B., and Cai, L. (2020). Mechanisms of Diabetic Cardiomyopathy and Potential Therapeutic Strategies: Preclinical and Clinical Evidence. *Nat. Rev. Cardiol.* 17, 585–607. doi:10.1038/s41569-020-0339-2

Trapnell, C., Roberts, A., Goff, L., Pertea, G., Kim, D., and Kelley, D. R. (2012). Differential Gene and Transcript Expression Analysis of RNA-Seq Experiments with TopHat and Cufflinks. *Nat. Protoc.* 7 (3), 562–578. doi:10.1038/nprot.2012.016

Uchida, S., and Dimmeler, S. (2015). Long Noncoding RNAs in Cardiovascular Diseases. *Circ. Res.* 116 (4), 737–750. doi:10.1161/CIRCRESAHA.116.302521

Viereck, J., Bührke, A., Foinquinos, A., Chatterjee, S., Kleeberger, J. A., Xiao, K., et al. (2020). Targeting Muscle-Enriched Long Non-coding RNA H19 Reverses Pathological Cardiac Hypertrophy. *Eur. Heart J.* 41 (36), 3462–3474. doi:10.1093/eurheartj/ehaa519

Wang, H., Radomska, H. S., and Phelps, M. A. (2020). Replication Study: Coding-independent Regulation of the Tumor Suppressor PTEN by Competing Endogenous mRNAs. *eLife* 9, e56651. doi:10.7554/eLife.56651

Wang, P., and Yuan, Y. (2019). Retracted : LncRNA-ROR Alleviates Hypoxia-triggered Damages by Downregulating miR-145 in Rat Cardiomyocytes H9c2 Cells. *J. Cell Physiol.* 234 (12), 23695–23704. doi:10.1002/jcp.28938

Wang, Y., and Sun, X. (2020). The Functions of LncRNA in the Heart. *Diabetes Res. Clin. Pract.* 168, 108249. doi:10.1016/j.diabres.2020.108249

Xie, Y., Huang, Y., Ling, X., Qin, H., Wang, M., and Luo, B. (2020). Chemerin/CMKLR1 Axis Promotes Inflammation and Pyroptosis by Activating NLRP3 Inflammasome in Diabetic Cardiomyopathy Rat. *Front. Physiol.* 11, 381. doi:10.3389/fphys.2020.00381

Yu, L. M., Dong, X., Xue, X. D., Xu, S., Zhang, X., Xu, Y. L., et al. (2021). Melatonin Attenuates Diabetic Cardiomyopathy and Reduces Myocardial Vulnerability to Ischemia-reperfusion Injury by Improving Mitochondrial Quality Control: Role of SIRT6. *J. Pineal Res.* 70 (1), e12698. doi:10.1111/jpi.12698

Zhang, X., Gao, Y., Zhang, X., Wang, B., Xu, Z., Fu, Q., et al. (2021). FGD5-AS1 Is a Hub lncRNA ceRNA in Hearts with Tetralogy of Fallot Which Regulates Congenital Heart Disease Genes Transcriptionally and Epigenetically]. *Front. Cel Dev. Biol.* 9, 630634. doi:10.3389/fcell.2021.630634

Conflict of Interest: The authors declare that the research was conducted in the absence of any commercial or financial relationships that could be construed as a potential conflict of interest.

Publisher's Note: All claims expressed in this article are solely those of the authors and do not necessarily represent those of their affiliated organizations, or those of the publisher, the editors, and the reviewers. Any product that may be evaluated in this article, or claim that may be made by its manufacturer, is not guaranteed or endorsed by the publisher.

frontiers | Frontiers in Genetics

REVIEW
published: 04 May 2022
doi: 10.3389/fgene.2022.862642

The Effect of miRNA Gene Regulation on HIV Disease

Romona Chinniah[1,2†], *Theolan Adimulam*[2†], *Louansha Nandlal*[1], *Thilona Arumugam*[2] and *Veron Ramsuran*[1,2*]

[1]Centre for the AIDS Programme of Research in South Africa (CAPRISA), University of KwaZulu-Natal, Durban, South Africa, [2]School of Laboratory Medicine and Medical Sciences, University of KwaZulu-Natal, Durban, South Africa

Over many years, research on HIV/AIDS has advanced with the introduction of HAART. Despite these advancements, significant gaps remain with respect to aspects in HIV life cycle, with specific attention to virus-host interactions. Investigating virus-host interactions may lead to the implementation of novel therapeutic strategies against HIV/AIDS. Notably, host gene silencing can be facilitated by cellular small non-coding RNAs such as microRNAs paving the way for epigenetic anti-viral therapies. Numerous studies have elucidated the importance of microRNAs in HIV pathogenesis. Some microRNAs can either promote viral infection, while others can be detrimental to viral replication. This is accomplished by targeting the HIV-proviral genome or by regulating host genes required for viral replication and immune responses. In this review, we report on 1) the direct association of microRNAs with HIV infection; 2) the indirect association of known human genetic factors with HIV infection; 3) the regulation of human genes by microRNAs in other diseases that can be explored experimentally to determine their effect on HIV-1 infection; and 4) therapeutic interactions of microRNA against HIV infection.

Keywords: microRNA, HIV, host-genetics, epigenetics, miRNA

Edited by:
Gabriel Adelman Cipolla,
Federal University of Paraná, Brazil

Reviewed by:
Weizhong Chang,
National Cancer Institute at Frederick (NIH), United States
Shokrollah Elahi,
University of Alberta, Canada
Shaheen Mowla,
University of Cape Town, South Africa

***Correspondence:**
Veron Ramsuran
ramsuranv@ukzn.ac.za

†These authors have contributed equally to this work

Specialty section:
This article was submitted to RNA, a section of the journal Frontiers in Genetics

Received: *26 January 2022*
Accepted: *13 April 2022*
Published: *04 May 2022*

Citation:
Chinniah R, Adimulam T, Nandlal L, Arumugam T and Ramsuran V (2022) The Effect of miRNA Gene Regulation on HIV Disease. Front. Genet. 13:862642. doi: 10.3389/fgene.2022.862642

1 INTRODUCTION

The Human Immunodeficiency Virus (HIV) is a member of the lentivirus family of retroviruses that infects humans and increases susceptibility to Acquired Immunodeficiency Syndrome (AIDS). At the end of 2020, more than 38 million people were living with HIV globally (Global, 2020). While an effective vaccine remains elusive, extensive research on the inhibition of various stages of the HIV life cycle has paved the way for the development of many antiretroviral drugs (Cohen et al., 2016). Despite the progress with lifesaving, highly active antiretroviral therapy (HAART), treatment may lead to the development of drug toxicities and resistance (Pomerantz and Horn, 2003). HAART has also been implicated in the onset of adverse metabolic effects such as dyslipidaemia, elevated blood pressure, and insulin resistance (Palios et al., 2011). These compounding factors emphasise the necessity for new less toxic, more effective and additional, complementary therapeutic approaches.

Advancements in discovering and determining the function of host factors in viral biogenesis and transmission highlight the possibility of developing new therapeutic tools for preventative measures and treatment of HIV/AIDS (Hoxie and June, 2012). As such, modulating gene expression post-transcriptionally using small non-coding RNAs (sncRNAs) mediates cellular gene silencing through RNA interference (RNAi). This mode of regulation has become increasingly utilized in the development and delivery of the therapeutic anti-viral strategy (Balasubramaniam et al., 2018). Eukaryotic cells possess endogenous RNAi mechanisms, of which microRNAs (miRNAs) are the most significant family of sncRNAs (Ghildiyal and Zamore, 2009). MiRNAs are a class of small non-

coding RNA molecules (21–25 nucleotides in length) that are instrumental in regulating gene expression of multiple cellular processes, including differentiation, development, apoptosis, and stress response (Felekkis et al., 2010). These molecules exert their regulatory mechanisms by mRNA degradation or translational repression (prevention of translation of target mRNAs) (Cai et al., 2009; Fabian et al., 2010; Inui et al., 2010; Subramanian and Steer, 2010). The biogenesis of miRNAs is detailed profoundly in several manuscripts, which describe the two principal pathways (canonical and non-canonical) (O'Brien et al., 2018; Ha and Kim, 2014; Macfarlane and R. Murphy, 2010; Zhao et al., 2019).

Briefly, the canonical pathway begins in the nucleus where a primary RNA (pri-miRNA), usually ~80 nucleotides long, is transcribed from its specific gene by RNA polymerase II. The pri-miRNA is then cleaved to form a precursor miRNA (pre-miRNA), generally ~60 nucleotides long, by the Microprocessor complex (Zhao et al., 2019). The Multiprocessor complex consists of two multiprotein units. The first is a large multiprotein unit. The second is a small multiprotein which constitutes of Drosha (RNase III enzyme) and the RNA binding protein DiGeorge Syndrome Critical Region 8 (DGCR8) (Gregory et al., 2004). Once the pre-miRNA is generated, it is transported to the cytoplasm by exportin-5 and Ran-GTP, where it undergoes cleavage by Dicer (O'Brien et al., 2018). The Dicer enzyme removes the terminal loop, thus resulting in a double-stranded product that consists of the mature miRNA guide strand and a passenger strand. The mature miRNA product will be transferred onto Argonaute (AGO) protein (Macfarlane and R. Murphy, 2010). The remaining passenger strands are usually directed toward degradation. However, the guide strand is further integrated into the RNA-induced silencing complex (RISC) (O'Brien et al., 2018; Macfarlane and R. Murphy, 2010). Finally, the RISC-miRNA complex principally binds to the 3′UTR of the target mRNA. The complementarity of this binding predicts the fate of the mRNA, such that, in the event of perfect complementarity, the target mRNA is degraded. However, when this binding is incomplete, the mRNA is translationally repressed (Cai et al., 2009).

Several non-canonical pathways have been described (Annese et al., 2020). In summary, non-canonical pathways are classified into Drosha/DGCR8-independent and Dicer-independent pathways. The class of Drosha/DGCR8-independent miRNAs which originate from spliced introns are commonly known as mirtrons. These miRNAs are instantly transported to the cytoplasm via Dicer processing (Treiber et al., 2019). On the contrary, Dicer-independent miRNAs are uncommon. Drosha processes Dicer-independent miRNAs from endogenous short hairpin RNA (shRNA) transcripts, directly recognised by Ago proteins, thus making them Dicer-independent (Dai et al., 2019).

Multiple studies have linked aberrant miRNA profiles to diseases such as cancer (Croce and Calin, 2005; Calin and Croce, 2006), neurodegenerative disease (Kim et al., 2007; Wang et al., 2008), autoimmune disease (Dai et al., 2007; Stanczyk et al., 2008; Zhao et al., 2010), inflammatory diseases (Sonkoly et al., 2007), muscular disorders (Eisenberg et al., 2007), cardiovascular disorders (Carè et al., 2007; Ikeda et al., 2007), in addition to developmental abnormalities and psychiatric disorders (Lewis et al., 2003). Moreover, the five biggest infectious killers globally, including HIV/AIDS, are responsible for approximately 80% of the total contagious disease burden. About 12 million people per year succumb to these diseases, primarily in developing countries (Organization, 2020). Comparable to non-infectious conditions, miRNAs affect host and virus interactions in various ways. They are characterised as direct alteration of viral replication by influencing viral susceptibility or as indirect alteration of host genes that influence viral replication (Scaria et al., 2007; Kumar and Jeang, 2008).

MiRNAs have previously been implicated in HIV infection (Sun et al., 2016; Balasubramaniam et al., 2018; Su et al., 2018). As a field in its infancy, there is a substantial benefit in determining the impact of miRNAs on HIV infection.

This review discusses the direct alterations of miRNAs in HIV infection and the indirect alterations of known human genetic factors in HIV infection. Thereafter, we describe miRNA associations of known human genetic factors with other diseases that can be exploited to determine their specific effect on HIV infection, and the potential use of miRNAs as therapeutic interactions against HIV infection.

2 EFFECT OF MIRNAS ON HIV INFECTION

MiRNAs can aid or obstruct HIV infection at various stages of the viral life cycle, affecting viral replication, host immune response, and ultimately disease management (**Figure 1**). HIV exploits and uses cellular miRNAs to modulate its replication by directly targeting its RNA or host mRNAs that would negatively impact HIV replication. In addition, miRNAs are linked with a possible susceptibility to HIV infection in monocytes and macrophages (Wang et al., 2009; Qiuling et al., 2018). Furthermore, the viral genome may produce viral encoded miRNAs that modulate viral RNAs as well as cellular mRNAs (Cullen, 2006; Skalsky and Cullen, 2010). This suggests that HIV could potentially regulate its replication cycle and possibly program its own latency (Omoto et al., 2004; Bennasser et al., 2006; Ouellet et al., 2013; Zhang et al., 2014). Several cellular miRNAs have demonstrated the ability to modulate HIV infection, either directly or indirectly (**Table 1**).

2.1 Regulation of HIV Replication Through Viral Genome

Host derived miRNAs can bind to HIV RNA, directly regulating pathogenesis (Trobaugh and Klimstra, 2017). For instance, recent data has shown that miR-139-5p plays a role in activating latent HIV infected cells, by regulating *FOX01*, as well as FOS and JUN transcription factors (Okoye et al., 2021). The expression of miR-28, miR-125b, miR-150, miR-223, and miR-382 were significantly lower in activated CD4+ T cells in comparison to its resting counterpart. The same group of miRNAs may play a role in establishing viral latency by interacting with a conserved 1.2 kb fragment found in the 3′UTR of all HIV transcripts. These miRNAs

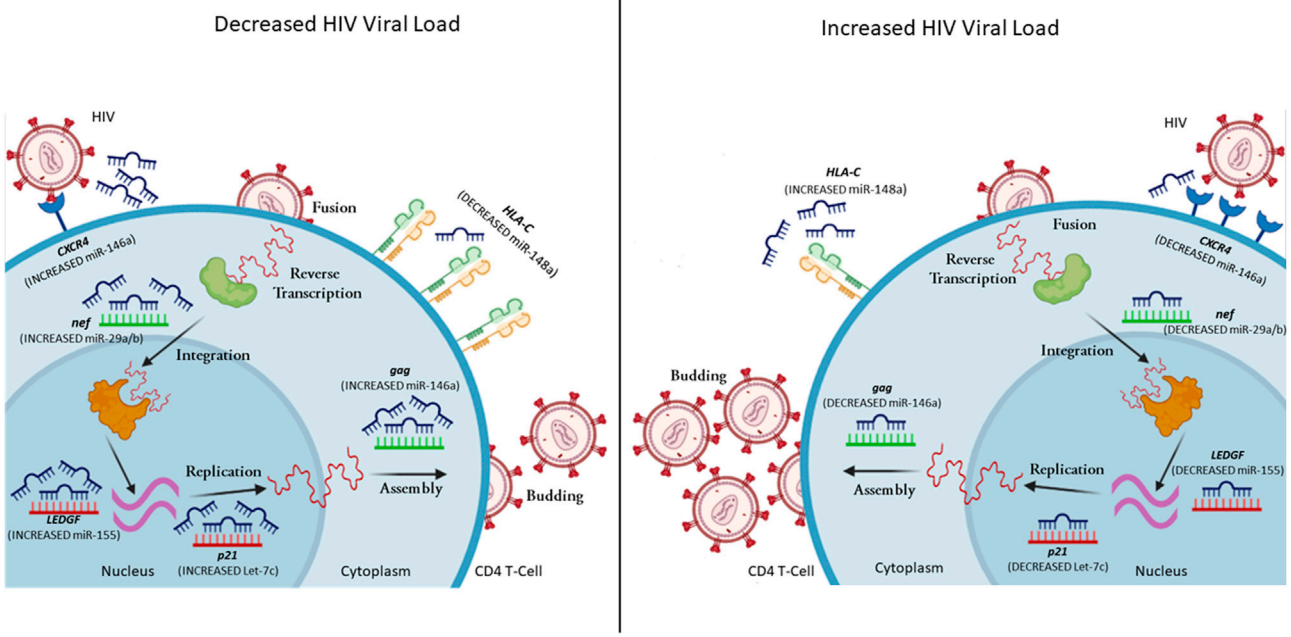

FIGURE 1 | A representation of selected miRNAs that control gene expression levels, leading to variability in HIV viral load. MiRNA can regulate both host (red mRNA) and viral (green mRNA) mRNA. In the case of decreased viral load, the CD4+ T cell has increased expression of miR-146a (reduces *CXCR4* and *gag* expression), miR-29a/b (reduces *nef* expression), miR-155 (reduces *LEDGF* expression), Let-7c (reduces *p21* expression), while decreased expression of miR-148a upregulates HLA-C expression. In the case of increased viral load, the CD4+ T cell has decreased expression of miR-146a (increases *CXCR4* and *gag* expression), miR-29a/b (increases *nef* expression), miR-155 (increases *LEDGF* expression), Let-7c (increases *p21* expression), while increased expression of miR-148a down-regulates *HLA-C* expression (complied using BioRender).

can inhibit the translation of all viral proteins with the exception of *nef* (Huang et al., 2007). Moreover, the study showed that infected cells with established latency could be reactivated by treatment with miRNA inhibitors, suggesting that cellular miRNAs may provide a mechanistic effect towards HIV latency (Huang et al., 2007). Besides their role in promoting HIV latency, these five miRNAs play a crucial role in preventing HIV infection of monocytes and monocyte-derived macrophages (MDM). MiR-28, miR-125b, miR-150, miR-223, and miR-382 were observed at significantly higher levels in monocytes compared to MDM. These miRNAs were found to impede HIV reverse transcriptase activity in both cell types. However, the activity of HIV reverse transcriptase was dependant on the level of these miRNAs. This may explain why monocyte differentiation into macrophages is required for effective HIV infection (Wang et al., 2009).

Nef expression can also be influenced by cellular miRNAs (Ahluwalia et al., 2008; Sun et al., 2012). Ahluwalia *et al.* found that miR-29a and miR-29b may target HIV *nef* expression, which resulted in repression of *nef* translation and subsequent decrease in viral load (**Figure 1**) (Ahluwalia et al., 2008).

Moreover, in a series of refined experiments, Sun *et al.* demonstrated a new regulatory circuit during HIV infection (Sun et al., 2012). The downregulation of the miR-29 family could be associated with *nef* up-regulation and apoptosis of CD4+ cells (Sun et al., 2012). In addition, previous studies showed that miR-29 inhibited HIV replication by approximately 60%, while miR-133b, miR-138, miR-326, miR-149, and miR-92a reduced HIV viral replication by 40% (Houzet et al., 2012). In silico screening showed that these miRNAs may possibly target the *5′LTR* (miR-326), *env* (miR-133b, miR-138), *gag* (miR-149), and *pol* (miR-92a) leading to the repression of viral replication.

Recent work by Chen *et al.* showed another form of miRNA regulation of HIV viruses through the interaction of miR-146a with the viral protein *gag* (**Figure 1**) (Chen et al., 2014). This interaction resulted in a viral-RNA-mediated gag assembly blockage, thereby interfering with viral budding and infectivity (Chen et al., 2014). These findings illustrate that miRNAs can alter viral gene expression via direct targeting of HIV mRNAs, with variable mechanisms of action dictated by the cell types.

2.2 Host Factors That Regulate HIV Replication

MiRNAs regulate HIV infection through indirect modulation of host factor expression. One viral-dependent factor in cells is Cyclin T1, characterised as an essential part of the PTEFb complex, responsible for facilitating viral transcription (Hoque et al., 2011). The direct modulation is facilitated through the interaction with *tat,* which recruits the complex to HIV TAR, thereby impacting viral latency (Hoque et al., 2011). Recent work by Sung *et al.* described that miR-198targets and down-regulates Cyclin T1 mRNA and protein expression, which subsequently

TABLE 1 | Studies showing microRNAs affecting host cell genes in the context of HIV infection.

microRNA	Target	Action	Experimental approach/observation	References number
miR-148a	*HLA-C*	Impaired control of HIV viral load	*In vitro* studies Genetic association with HIV $P = 2 \times 10^{-14,}$ R = 0.33·N = 2.527 (European cohort)	Kulkarni et al. (2011)
miR-146a	*CXCR4*	Prevents HIV entry	*In vitro*	Quaranta et al. (2015)
miR-132	*MeCP2*	Enhances HIV infection	*In vitro*	Chiang et al. (2013)
miR-182	*NAMPT*	Enhance HIV tat-mediated trans-activation	*In vitro*	Chen et al. (2013)
miR-34a miR-217	*SIRT1*	Enhances HIV tat mediated trans-activation	*In vitro In vitro*	Zhang et al. (2012a), Zhang et al. (2012b)
miR-34a	*PNUTS*	Promotes HIV -1 transcription	*In vitro*	Kapoor et al. (2015)
miR- 155	*TRIM32*	Promotes reactivation of latent HIV via NF-kB signalling	*In vitro*	Ruelas et al. (2015)
miR-17-5p miR-20a	*PCAF*	Reduction of HIV infection	*In vitro*	Triboulet et al. (2007)
miR-198 miR-27b	*Cyclin T1*	Impaired replication in monocytes	*In vitro In vitro*	Sung and Rice. (2009),
miR-29b miR-150 miR-223		Impaired HIV replication in resting CD4+ T cells		Chiang et al. (2012)
miR-15a miR-15b miR-16 miR-20a miR-93 miR-106b	*Pur-Alpha*	Impaired HIV replication in monocytes	*In vitro*	Shen et al. (2012)
miR-155	*ADAM 10*	Reduction of HIV late RT products and viral DNA integration in MDM	*In vitro*	Swaminathan et al. (2012c)
miR-155	*NUP153*	Reduction of HIV late RT products and viral DNA integration in MDM	*In vitro*	Swaminathan et al. (2012c)
miR-155	*LEDGF/p75*	Reduction of HIV late RT products and viral DNA integration in MDM	*In vitro*	Swaminathan et al. (2012c)
miR-155 miR-181	*SAMHD1*	Overexpression of miR-155/181a enhanced HIV replication in astrocytes	*In vitro*	Pilakka-Kanthikeel et al. (2015)
miR1236	*VprBP*	Impaired HIV replication in monocytes	*In vitro*	Ma et al. (2014)
let-7c	*p21*	Increased HIV replication	*In vitro*	Farberov et al. (2015)
miR-124a miR34a-5p	*TASK1*	Increased HIV replication	*In vitro*	Farberov et al. (2015)
miR-146a	*CCL5*	Enhance HIV infection	*In vitro*	Qiuling et al. (2018)
miR-21	*IP-10*	miR-21 expression downregulates IP-10 controlling the loss of CD4+ T cells which is closely related to disease progression	Genetic association in HIV disease $p <$ 0.0001, R = 0.706, N = 32 (Chinese cohort)	Wu et al. (2017)
miR-155	*PU.1 (DC-SIGN)*	Reduces HIV entry into T lymphocytes	*In vitro*	Martinez-Nunez et al. (2009)
miR-9	*BLIMP-1*	Reduced HIV infection	*Ex vivo and in vitro*	Seddiki et al. (2013)
let-7	*IL-10*	Reduced HIV infection	*Ex vivo and in vitro*	Swaminathan et al. (2012c)
miR-221 miR-222	*CD4*	Inhibition of HIV entry in macrophages	*In vitro*	Lodge et al. (2017)
miR-34c-5p	Several genes are involved in TCR signaling and activation of naïve $CD4^+$ T cells	Increased HIV replication	*In vitro*	Amaral et al. (2017)
miR-29a miR-29b miR-29c	*IL-32*	Proviral load and disease progression	Genetic association in HIV disease p = 0.079, R = 0.232, N = 58 p = 0.102, R = 0.445, N = 58 p = 0.103, R = 0.216, N = 58	Monteleone et al. (2015)

Notes: P represents the p value for the specific result. R represents the value of the statistical Pearson R. N is representative of the number of samples. The italic values under the "Target" column is indicative of gene names. While the italic values under the "Experimental approach/observation" is the Latin caption used to define how the experiment was performed.

impairs the *tat*-mediated transcriptional activation of HIV in infected monocytes and macrophages (Sung and Rice, 2009). Over-expression of miR-198 inhibited HIV replication in macrophages, suggesting that cell type-specific mechanisms may be an effect executed by miRNAs (Sung and Rice, 2009). Additional studies identified that Cyclin T1 inhibition is exerted by cellular miRNAs (miR-27b, miR-29b, miR-150, and miR-223) in resting CD4+ T cells (Chiang et al., 2012). However, CD4+ T cell activation followed the downregulation of the miRNAs. This result was correlated with enhanced HIV susceptibility and productive replication (Chiang et al., 2012).

The viral protein *tat* is an essential transcriptional activator that interacts with several cellular proteins. For efficient HIV transcriptional activation, *tat* must be acetylated by p300-CREB binding protein associated factor (PCAF) (D'Orso and Frankel, 2009). Remarkably, miR-17/92 family of host miRNAs impedes HIV infection by downregulating PCAF (Triboulet et al., 2007). Triboulet *et al.* also showed that miR-17 as well as miR-20a inhibited PCAF expression at the mRNA and protein levels. In addition, HIV can actively repress miR-17-5p and miR-20a to enhance viral translation through p300/PCAF-dependant *tat* activation (Triboulet et al., 2007).

Another well characterised cellular factor that interacts with HIV *tat* to up-regulate viral transcription is the purine-rich element binding protein α (Pur-α) (Wortman et al., 2000). A collection of six cellular miRNAs (miR-15a, miR-15b, miR-16, miR-20a, miR-93, and miR-106b) enriched in monocytes were linked with the repression of Pur-α (Shen et al., 2012). Consequently, inhibition of these miRNAs in monocytes increased the expression of Pur-α, resulting in an increase in HIV infection (Shen et al., 2012).

MiR-155 has demonstrated significant effects on HIV infection through a Toll-Like receptor (TLR)-dependant mechanism (Swaminathan et al., 2012a). Swaminathan *et al.* showed that miR-155 is significantly up-regulated in MDMs, stimulated by TLR3 and TLR4 (Swaminathan et al., 2012a). Furthermore, up-regulation of miR-155 through TLR stimulation leads to decreased mRNA and protein expression of ADAM10, TNPO3, NUP153, and LEDGF/p75, in MDMs (Swaminathan et al., 2012a). Gene silencing of *LEDGF* had the most significant effect on HIV infection (**Figure 1**) (Swaminathan et al., 2012a). However, co-silencing of both *LEDGF* and *ADAM10* had a more substantial impact, impairing the transport of viral pre-integration complexes (Swaminathan et al., 2012a).

The inhibition of *TRIM32* by miR-155 results in post-integration latency of HIV (Ruelas et al., 2015). TRIM32 directs NF-κB to the nucleus via a *tat*-independent mechanism, as described by Ruelas et al. (2015). The study characterises a novel mechanism by which TRIM32 activates NF-κB. Collectively, the inhibitory effect of miR-155 on *TRIM32* highlights a new tool for HIV remaining in infected reservoirs (Ruelas et al., 2015). Despite this significant study, recent studies have identified miR-155 as a potent biomarker of activated T cells and immune dysfunction in HIV-infected individuals (Jin et al., 2017a; Jin et al., 2017b; Zhang et al., 2021a).

MiRNAs can also restrict viral entry by targeting the receptors and co-receptors exploited for HIV entry. Orecchini *et al.* report a *tat*-dependant mechanism that controls CD4 receptor by up-regulating miR-222 (Orecchini et al., 2014). In addition, Lodge *et al.* demonstrated that miR-221 and miR-222 are up-regulated in MDMs, targeting the 3′ UTR of CD4 (Orecchini et al., 2014). The mRNA and subsequent protein expression are reduced, ultimately impairing HIV entry into MDM (Lodge et al., 2017). Labbaye *et al.* showed that promyelocytic leukaemia zinc finger (PLZF) could regulate miR-146a, subsequently controlling the expression of *CXCR4 in vitro* (Labbaye et al., 2008). Activation of resting CD4+ T cells by phytohemagglutinin results in the downregulation of miR-146a (Quaranta et al., 2015). Downregulation of miR-146a results in the overexpression of CXCR4 co-receptor promoting viral entry in CD4+ T cells (Quaranta et al., 2015).

Vpr HIV-binding protein (vprBP) is a cellular cofactor that forms part of a ubiquitin protein ligase complex. VprBP promotes HIV infection (Ma et al., 2014). Ma *et al.* demonstrated that miR-1236 inhibitors increased translation of vprBP in monocytes, thus facilitating HIV infection. Contrary to monocytes, miR-1236 mimics in monocyte-derived dendritic cells had supressed vprBP, which was complemented by decreased infection (Ma et al., 2014).

High surface expression of human leukocyte antigen C (HLA-C) greatly corresponded with slower disease progression via superior control of HIV viremia. Several genetic variants have been shown to disrupt miR-148a regulation of HLA-C (Kulkarni et al., 2011; Blais et al., 2012; Kulkarni et al., 2013). Disruption of miRNA binding site allows high expressing HLA-C alleles to escape miR-148a regulation (Kulkarni et al., 2011). HLA-C alleles that do not have a disrupted miR-148a binding site are tightly regulated by miR-148a and are expressed at low levels. The polymorphisms affecting HLA-C expression through disrupted miR-148a binding are rs9264942, rs67384697, and rs735316, with the variants of rs9264942 and rs67384697 being in linkage disequilibrium (Kulkarni et al., 2011; Blais et al., 2012; Kulkarni et al., 2013). All three variants are associated with control and progression of HIV infection by miR-148a-mediated post-transcriptional regulation of HLA-C.

IL-10 is a multifunctional anti-inflammatory cytokine produced by various immune cells. With regards to miRNA regulation of IL-10, the let-7 family can directly target *IL10*. *In vitro* infection with HIV elevated *IL10* levels through the reduction of let-7. In addition, CD4+ T cells of chronically infected HIV-positive individuals had significantly lower let-7 levels than uninfected individuals and long-term non-progressors. (Swaminathan et al., 2012b). A single miRNA is able to regulate multiple target genes. In addition to *IL10*, let-7c is involved in the regulation of *p21*. let-7c overexpression in Jurkat cells resulted in a 1.38-fold change in p21 expression (**Figure 1**) (Farberov et al., 2015).

B lymphocyte-induced maturation protein-1 (Blimp-1) is a transcriptional repressor of IL-2 (an important cytokine required for T cell growth and survival). In HIV-infected individuals, BLIMP-1 may contribute to T cell dysregulation through alterations in IL-2 levels. MiR-9 inhibited *BLIMP1* expression in CD4+ T cells. Chronically infected HIV-positive patients had lower miR-9 and higher *BLIMP1* expression in comparison to uninfected healthy individuals and long-term non-progressors (Seddiki et al., 2013).

2.3 Predicted miRNA Targets for HIV

It is estimated that 1,254 human genes are involved in viral replication. Genome-wide RNA interference has enabled researchers to identify multiple host factors that are involved in HIV life cycle. This large array of host gene targets may be essential in the development of new therapeutic strategies against HIV. By identifying and understanding the mechanisms behind the associations of specific miRNAs and their targets, we can exploit these factors for HIV viral control. Several HIV-associated genes are shown to be under the regulation of miRNAs in other diseases.

Blocking the access of HIV into host cells is the first step in preventing the HIV proviral genome from integrating into the host's genome. The human chemokine receptor 5 (CCR5) plays an important role in the internalization of HIV into the host cell (Lederman et al., 2006). Individuals with the 32 base pair deletion in their *CCR5* gene are known to be resistant to HIV as they have lower levels of CCR5 on the surface of their CD4+ T cells. Thus, the regulation of CCR5 expression

may be essential in inhibiting HIV replication. Che *et al.* found that miR-107 binds to the 3′UTR of *CCR5* (Che et al., 2016). CCR5 proteins and gene expression were found to be significantly lower in the presence of miR-107 (Che et al., 2016). Since CCR5 is important in the HIV context, miR-107 may be of potential therapeutic value in preventing HIV infection.

Intercellular adhesion molecule 1 (ICAM-1) also plays a significant role in HIV entry. The binding of ICAM-1 with LFA-1 on the cell surface facilitates viral infectivity. ICAM-1 increases viral infectivity by directly inserting into mature HIV virions (Fortin et al., 1997; Bounou et al., 2002). Lui et al. demonstrated that *ICAM1* is negatively regulated by miR-296-3p in the malignant highly metastatic M12 cell line (Liu et al., 2013). Furthermore, in prostate cancer cells there is a negative correlation between miR-296-3p and *ICAM1* (Liu et al., 2013). In the context of HIV, the downregulation of *ICAM1* by miR-296-3p would reduce the rate of infectivity (Liu et al., 2013).

The tripartite motif (TRIM) proteins are a family of E3 ubiquitin ligases with diverse anti-viral functions (van Gent et al., 2018). TRIM22, TRIM11, and KAP1 (TRIM28) were previously shown to have anti-HIV activity (Barr et al., 2008; Allouch et al., 2009; Yuan et al., 2016). TRIM22 inhibits the processing of viral particles and viral budding through the ubiquitylation in HIV. TRIM22 also has anti-Hepatitis C virus (HCV) activity. Tian *et al.* confirmed that *TRIM22* was regulated by miR-215 (Tian and He, 2018). In Con1b cells, the overexpression of miR-215 facilitated HCV replication by downregulating *TRIM22.* Knockdown of miR-215 suppressed HCV replication through the increased expression of *TRIM22* in Huh7.5.1 cells (Tian and He, 2018). In colon cancer, *TRIM11* is negatively regulated by miR-24-3p, promoting cellular proliferation and inhibiting apoptosis (Yin et al., 2016). Likewise, Qi *et al.* demonstrated that miR-491 levels inversely corresponded with *TRIM28* expression in glioblastoma multiforme (GBM) (Qi et al., 2016). Their data showed that miR-491 was reduced in GBM and indicated that the low levels of miR-491 are associated with poor prognosis (Qi et al., 2016). miR-491 inhibited TRIM28 translation in GBM cells (Qi et al., 2016).

Studies have also demonstrated a link between *RAD51* expression and HIV disease (Chipitsyna et al., 2004; Cosnefroy et al., 2012; Kaminski et al., 2014; Thierry et al., 2015). Elevated expression of *RAD51* promotes HIV-1 transcription (Kaminski et al., 2014). Evidence demonstrates that *RAD51* may have stimulatory or inhibitory effects on specific steps of retroviral replication cycles (Thierry et al., 2015). These effects depend on RAD51 being able to recruit both transcription machinery and proteins implicated in chromatin remodelling and formulation of RAD51 stimulatory compound (Thierry et al., 2015). Findings from Gasparini *et al.* indicate that DNA repair is indirectly regulated by miR-155 through its interaction with RAD51 in breast cancer (Gasparini et al., 2014).

The regulation of several other HIV-associated host factors such as TRAF6, CCL4, CCL3, IRF7, RSAD2, ISG15, TLR3, SETDB1, and Rab27a by miRNAs could potentially play a role in HIV infection. **Table 2** provides a list of HIV-associated host genes which should be investigated in future miRNA studies. The host's genes and associated miRNAs described in **Table 2** may provide novel therapeutic targets against HIV.

2.4 Therapeutic miRNA Targets for HIV

Extensive research has paved the way for developing multiple antiretroviral drugs targeting specific phases of the viral life cycle, leading to a combination of antiretroviral therapy (cART). Currently, this treatment results in controlled viral replication in many treated individuals (Cohen et al., 2016). Despite the progress with lifesaving HAART, infection with HIV remains pathogenic and incurable. In addition, these drugs lead to the development of toxicities and adverse side effects which may only be combated by changing the drug regimen. Furthermore, the increasing emergence of HIV drug resistance poses a threat to the success of the current regimens (Bertagnolio et al., 2012; Le Douce et al., 2012; Stadeli and Richman, 2013). These compounding factors highlight the importance of identifying novel and complementary treatment regimens.

RNA-based therapeutics appear ready to deliver on their promise. Significant success has been observed in several clinical trials using potential miRNA drugs in multiple infectious and non-infectious diseases, including cancer (Hatley et al., 2010; Li et al., 2010; Steele et al., 2011; Wong et al., 2012; Yamanaka et al., 2012), hepatitis C (Jopling et al., 2005; Sarasin-Filipowicz et al., 2009; Lanford et al., 2010), heart abnormalities (Thum et al., 2008; Liu et al., 2010), kidney disease, pathologic fibrosis, and even keloid formation. Interestingly, studies have also shown that dysregulated miRNA profiles play a role in HIV replication (Barr et al., 2008; Pincetic et al., 2010; Liu et al., 2011; Sirois et al., 2011; Tyagi and Kashanchi, 2012; Raposo et al., 2013; Doyle et al., 2015). The vaccine, iHIVARNA is a combination of mRNA sequences that serve as an HIV immunogen. In the first round of clinical trials, iHIVARNA is tolerated in HIV-infected patients on chronic cART (De Jong et al., 2019). Despite this progress, the application of miRNAs as diagnostic and interventional medicine remains an underexplored area of research. The clinical trial was merely a proof-of-concept trial; the stability and delivery of the mRNA are still being tested (De Jong et al., 2019).

The Achilles heel of miRNA-based viral therapy is the lack of targeted miRNA delivery systems, off-target effects, and unidentified targets of miRNAs. In addition, miRNAs are relatively unstable, which may result in insufficient circulation and poor half-life of the miRNA-based therapy. Future research should be directed towards constructing optimal miRNA delivery systems and identifying methods to prevent off-target effects. As the use of miRNAs as treatment strategies is a growing field, only a few drugs have been FDA approved (Nature Biotechnology, 2020; Zhang et al., 2021b), which highlights the potential of RNAs for therapeutic intervention. MiRNAs provide a unique, reversible approach to treating human diseases and may be our secret weapon in our fight against HIV.

TABLE 2 | Genes associated with HIV infection shown to be regulated by miRNAs in other diseases.

HIV infection			Other disease		
Gene	**Effect**	**References number**	**microRNA**	**Disease or infection**	**References number**
Viral receptors					
CCR5	responsible for HIV infection and entry	Blanpain et al. (2002); Lederman et al. (2006)	miR-107	Cancer	Che et al. (2016)
ICAM-1	assists with HIV entry increasing virus infectivity	Fortin et al., (1997); Bounou et al. (2002)	miR-296-3p	Prostate cancer	Liu et al. (2013)
Innate immune regulators					
TRIM22	blocks HIV replication in cell by preventing the assembly of the virus	Barr et al. (2008)	miR-215	HCV	Tian and He, (2018)
TRIM28 (KAP1)	inhibits HIV-1 through by targeting the integration step	Allouch et al. (2009)	miR-149	Cancer	Qi et al. (2016)
TRIM11	restricts HIV-1 reverse transcription by accelerating viral un-coating	Yuan et al. (2016)	miR-24-3p	Colon cancer	Yin et al. (2016)
TRAF6	induced as part of the normal innate immune response against HIV virus	Sirois et al. (2011)	miR-146a miR-144	Dengue virus influenza virus, EMCV, and VSV	Wu et al. (2013) Rosenberger et al. (2017)
T cell exhaustion markers					
CCL4	CCR5 ligand involved in blocking HIV entry	Carrol et al. (1999)	miR-125b	Aging	Cheng et al. (2015)
CCL3	CCR5 ligand involved in blocking HIV entry	Modi et al., (2006); Levine et al., (2009)	miR-223	Tuberculosis	Dorhoi et al. (2013)
IRF7	contributes to enhanced HIV-1 replication	Sirois et al. (2011)	miR-541	Vascular smooth muscle cells	Yang et al. (2016)
RSAD2 (viperin)	Inhibits viral production	Raposo et al. (2013)	miR-200a miR-200b miR-429	Cell differentiation studies	Li et al. (2016)
ISG15	Suppresses HIV replication at various parts of the HIV life cycle	Pincetic et al. (2010); Doyle et al., (2015)	miR-138 miR-370	Oral cancer	Zhang et al. (2017)
Toll-like receptors					
TLR3	Innate immune response. Reduces HIV infection	Akira et al., (2006); Swaminathan et al. (2012c)	miR-26a	Arthritis	Jiang et al. (2014)
Other					
RAD51	stimulatory or inhibitory effects on specific steps on retroviral replication cycles	(Kaminski et al., 2014; Thierry et al., 2015)	miR-155	Cancer	Gasparini et al. (2014)
SETDB1	Inhibits HIV-1 replication at a step prior to integration	(Liu et al., 2011; Tyagi and Kashanchi, 2012)	miR-381-3p	Breast cancer	Wu et al. (2018)
Rab27a	Favours HIV assembly	Gerber et al. (2015)	miR-134-3p	Ovarian cancer	Chang et al. (2017)

Notes: HCV, abbreviates Hepatitis C. EMCV, abbreviates encephalomyocarditis virus; VSV, abbreviates vesicular stomatitis virus.

3 CONCLUSION

MiRNAs play a significant role in regulating gene expression. While the role of miRNAs in diseases such as cancer has been thoroughly investigated, the interplay between miRNAs and HIV infection has only begun to emerge. MiRNAs have emerged as key contributors to immune dysfunction observed in HIV disease. As research develops in specific subsets and more targeted populations, the understanding of this field matures as more can be uncovered. Considering that key genes involved in the HIV life cycle are affected by differentially expressed miRNAs, there is a link between the host's RNA interference machinery and HIV pathogenicity. Future research should focus on identifying differentially expressed miRNAs in HIV-infected donors from different population groups., which may be exploited for therapeutic benefit.

In addition, the application of specific miRNA mimics and inhibitors (Andorfer et al., 2011; He et al., 2012; De Santa et al., 2013) is an appealing avenue for future investigations. Noting that one miRNA alone may be able to target several host genetic factors, the combined effect of several miRNAs together offers the potential for a multi-targeted effect. This treatment strategy can complement current cART regimen. Furthermore, inhibition of selected miRNAs is advantageous. For instance, selectively blocking miRNAs that target anti-viral proteins or pathways could potentially enhance anti-viral responses. This approach is efficient during the onset of infection, as the anti-viral response to HIV can be improved.

AUTHOR CONTRIBUTIONS

Conceptualization and conceiving of idea, VR. Additional input with regards to conceptualization, RC. Writing, RC, TA, TAR, and LN. Research, RC, TA, TAR, and LN. Figure design, TA and VR. Editing of manuscript, VR. All authors contributed to the article and approved the submitted version.

FUNDING

VR was funded as a FLAIR Research Fellow (the Future Leader in African Independent Research (FLAIR) Fellowship Programme was a partnership between the African Academy of Sciences (AAS) and the Royal Society that was funded by the UK Government as part of the Global Challenge Research Fund (GCRF) Grant # FLAIR-FLR\R1\190204); supported by the South African Medical Research Council (SAMRC) with funds from the Department of Science and Technology (DST); and VR was also supported in part through the Sub-Saharan African Network for TB/HIV Research Excellence (SANTHE), a DELTAS Africa Initiative (Grant # DEL-15-006) by the AAS. TA is funded by the Poliomyelitis Research Foundation (PRF) Grant # 21/49.

ACKNOWLEDGMENTS

In Memoriam of the late author Romona Chinniah.

REFERENCES

Ahluwalia, J. K., Khan, S. Z., Soni, K., Rawat, P., Gupta, A., Hariharan, M., et al. (2008). Human Cellular microRNA Hsa-miR-29a Interferes with Viral Nef Protein Expression and HIV-1 Replication. *Retrovirology* 5, 117. doi:10.1186/1742-4690-5-117

Akira, S., Uematsu, S., and Takeuchi, O. (2006). Pathogen Recognition and Innate Immunity. *Cell* 124 (4), 783–801. doi:10.1016/j.cell.2006.02.015

Allouch, A., et al. (2009). HIV-1 Acetylated Integrase Is Targeted by KAP1 (TRIM28) to Inhibit Viral Integration. *Retrovirology* 6 (Suppl. 2), P2. doi:10.1186/1742-4690-6-s2-p2

Amaral, A. J., Andrade, J., Foxall, R. B., Matoso, P., Matos, A. M., Soares, R. S., et al. (2017). Mi RNA Profiling of Human Naive CD 4 T Cells Links miR-34c-5p to Cell Activation and HIV Replication. *Embo j* 36 (3), 346–360. doi:10.15252/embj.201694335

Andorfer, C. A., Necela, B. M., Thompson, E. A., and Perez, E. A. (2011). MicroRNA Signatures: Clinical Biomarkers for the Diagnosis and Treatment of Breast Cancer. *Trends Mol. Med.* 17 (6), 313–319. doi:10.1016/j.molmed.2011.01.006

Annese, T., Tamma, R., De Giorgis, M., and Ribatti, D. (2020). microRNAs Biogenesis, Functions and Role in Tumor Angiogenesis. *Front. Oncol.* 10, 581007. doi:10.3389/fonc.2020.581007

Balasubramaniam, M., Pandhare, J., and Dash, C. (2018). Are microRNAs Important Players in HIV-1 Infection? an Update. *Viruses* 10 (3), 110. doi:10.3390/v10030110

Barr, S. D., Smiley, J. R., and Bushman, F. D. (2008). The Interferon Response Inhibits HIV Particle Production by Induction of TRIM22. *Plos Pathog.* 4 (2), e1000007-e1000007. doi:10.1371/journal.ppat.1000007

Bennasser, Y., Bennasser, Y., Le, S. Y., Yeung, M. L., and Jeang, K. T. (2006). MicroRNAs in Human Immunodeficiency Virus-1 Infection. *Methods Mol Biol*342, 241–253. doi:10.1385/1-59745-123-1:241

Bertagnolio, S., De Luca, A., Vitoria, M., Essajee, S., Penazzato, M., Hong, S. Y., et al. (2012). Determinants of HIV Drug Resistance and Public Health Implications in Low- and Middle-Income Countries. *Antivir. Ther.* 17 (6), 941–953. doi:10.3851/imp2320

Blais, M.-E., Zhang, Y., Rostron, T., Griffin, H., Taylor, S., Xu, K., et al. (2012). High Frequency of HIV Mutations Associated with HLA-C Suggests Enhanced HLA-C-Restricted CTL Selective Pressure Associated with an AIDS-Protective Polymorphism. *J.I.* 188 (9), 4663–4670. doi:10.4049/jimmunol.1103472

Blanpain, C., Libert, F., Vassart, G., and Parmentier, M. (2002). CCR5 and HIV Infection. *Receptors and Channels* 8 (1), 19–31. doi:10.3109/10606820212135

Bounou, S., Leclerc, J. E., and Tremblay, M. J. (2002). Presence of Host ICAM-1 in Laboratory and Clinical Strains of Human Immunodeficiency Virus Type 1 Increases Virus Infectivity and CD4 + -T-Cell Depletion in Human Lymphoid Tissue, a Major Site of Replication *In Vivo*. *J. Virol.* 76 (3), 1004–1014. doi:10.1128/jvi.76.3.1004-1014.2002

Cai, Y., Yu, X., Hu, S., and Yu, J. (2009). A Brief Review on the Mechanisms of miRNA Regulation. *Genomics, proteomics & bioinformatics* 7 (4), 147–154. doi:10.1016/s1672-0229(08)60044-3

Calin, G. A., and Croce, C. M. (2006). MicroRNA Signatures in Human Cancers. *Nat. Rev. Cancer* 6 (11), 857–866. doi:10.1038/nrc1997

Carè, A., Catalucci, D., Felicetti, F., Bonci, D., Addario, A., Gallo, P., et al. (2007). MicroRNA-133 Controls Cardiac Hypertrophy. *Nat. Med.* 13 (5), 613–618. doi:10.1038/nm1582

Carrol, E. D., Mankhambo, L. A., Balmer, P., Nkhoma, S., Banda, D. L., Guiver, M., et al. (1999). Chemokine Responses Are Increased in HIV-Infected Malawian Children with Invasive Pneumococcal Disease. *J. Acquir Immune Defic Syndr.* 44 (4), 443–450. doi:10.1097/QAI.0b013e31802f8390

Chang, C., Liu, T., Huang, Y., Qin, W., Yang, H., and Chen, J. (2017). MicroRNA-134-3p Is a Novel Potential Inhibitor of Human Ovarian Cancer Stem Cells by Targeting RAB27A. *Gene* 605, 99–107. doi:10.1016/j.gene.2016.12.030

Che, L.-F., Shao, S.-F., and Wang, L.-X. (2016). Downregulation of CCR5 Inhibits the Proliferation and Invasion of Cervical Cancer Cells and Is Regulated by microRNA-107. *Exp. Ther. Med.* 11 (2), 503–509. doi:10.3892/etm.2015.2911

Chen, A. K., Sengupta, P., Waki, K., Van Engelenburg, S. B., Ochiya, T., Ablan, S. D., et al. (2014). MicroRNA Binding to the HIV-1 Gag Protein Inhibits Gag Assembly and Virus Production. *Proc. Natl. Acad. Sci. U S A.* 111 (26), E2676–E2683. doi:10.1073/pnas.1408037111

Chen, X.-Y., Zhang, H.-S., Wu, T.-C., Sang, W.-W., and Ruan, Z. (2013). Down-regulation of NAMPT Expression by miR-182 Is Involved in Tat-Induced HIV-1 Long Terminal Repeat (LTR) Transactivation. *Int. J. Biochem. Cel Biol.* 45 (2), 292–298. doi:10.1016/j.biocel.2012.11.002

Cheng, N. L., Chen, X., Kim, J., Shi, A. H., Nguyen, C., Wersto, R., et al. (2015). MicroRNA-125b Modulates Inflammatory Chemokine CCL4 Expression in Immune Cells and its Reduction Causes CCL4 Increase with Age. *Aging cell* 14 (2), 200–208. doi:10.1111/acel.12294

Chiang, K., Liu, H., and Rice, A. P. (2013). miR-132 Enhances HIV-1 Replication. *Virology* 438 (1), 1–4. doi:10.1016/j.virol.2012.12.016

Chiang, K., Sung, T.-L., and Rice, A. P. (2012). Regulation of Cyclin T1 and HIV-1 Replication by MicroRNAs in Resting CD4 + T Lymphocytes. *J. Virol.* 86 (6), 3244–3252. doi:10.1128/jvi.05065-11

Chipitsyna, G., Slonina, D., Siddiqui, K., Peruzzi, F., Skorski, T., Reiss, K., et al. (2004). HIV-1 Tat Increases Cell Survival in Response to Cisplatin by Stimulating Rad51 Gene Expression. *Oncogene* 23 (15), 2664–2671. doi:10.1038/sj.onc.1207417

Cohen, M. S., Chen, Y. Q., McCauley, M., Gamble, T., Hosseinipour, M. C., Kumarasamy, N., et al. (2016). Antiretroviral Therapy for the Prevention of HIV-1 Transmission. *N. Engl. J. Med.* 375 (9), 830–839. doi:10.1056/NEJMoa1600693

Cosnefroy, O., Tocco, A., Lesbats, P., Thierry, S., Calmels, C., Wiktorowicz, T., et al. (2012). Stimulation of the Human RAD51 Nucleofilament Restricts HIV-1 Integration *In Vitro* and in Infected Cells. *J. Virol.* 86 (1), 513–526. doi:10.1128/jvi.05425-11

Croce, C. M., and Calin, G. A. (2005). miRNAs, Cancer, and Stem Cell Division. *Cell* 122 (1), 6–7. doi:10.1016/j.cell.2005.06.036

Cullen, B. R. (2006). Viruses and microRNAs. *Nat. Genet.* 38 Suppl (6), S25–S30. doi:10.1038/ng1793

D'Orso, I., and Frankel, A. D. (2009). Tat Acetylation Modulates Assembly of a Viral-Host RNA-Protein Transcription Complex. *Proc. Natl. Acad. Sci. U.S.A.* 106 (9), 3101–3106. doi:10.1073/pnas.0900012106

Dai, X., Kaushik, A. C., and Zhang, J. (2019). The Emerging Role of Major Regulatory RNAs in Cancer Control. *Front. Oncol.* 9, 920. doi:10.3389/fonc.2019.00920

Dai, Y., Huang, Y.-S., Tang, M., Lv, T.-Y., Hu, C.-X., Tan, Y.-H., et al. (2007). Microarray Analysis of microRNA Expression in Peripheral Blood Cells of Systemic Lupus Erythematosus Patients. *Lupus* 16 (12), 939–946. doi:10.1177/0961203307084158

De Jong, W., Aerts, J., Allard, S., Brander, C., Buyze, J., Florence, E., et al. (2019). iHIVARNA Phase IIa, a Randomized, Placebo-Controlled, Double-Blinded Trial to Evaluate the Safety and Immunogenicity of iHIVARNA-01 in Chronically HIV-Infected Patients under Stable Combined Antiretroviral Therapy. *Trials* 20 (1), 361–410. doi:10.1186/s13063-019-3409-1

De Santa, F., Iosue, I., and Fazi, F. (2013). microRNA Biogenesis Pathway as a Therapeutic Target for Human Disease and Cancer. *Curr. Pharm. Des.* 19, 745–764. doi:10.2174/138161213804581846

Dorhoi, A., Iannaccone, M., Farinacci, M., Faé, K. C., Schreiber, J., Moura-Alves, P., et al. (2013). MicroRNA-223 Controls Susceptibility to Tuberculosis by Regulating Lung Neutrophil Recruitment. *J. Clin. Invest.* 123 (11), 4836–4848. doi:10.1172/jci67604

Doyle, T., Goujon, C., and Malim, M. H. (2015). HIV-1 and Interferons: Who's Interfering with Whom? *Nat. Rev. Microbiol.* 13 (7), 403–413. doi:10.1038/nrmicro3449

Eisenberg, I., Eran, A., Nishino, I., Moggio, M., Lamperti, C., Amato, A. A., et al. (2007). Distinctive Patterns of microRNA Expression in Primary Muscular Disorders. *Proc. Natl. Acad. Sci. U.S.A.* 104 (43), 17016–17021. doi:10.1073/pnas.0708115104

Fabian, M. R., Sonenberg, N., and Filipowicz, W. (2010). Regulation of mRNA Translation and Stability by microRNAs. *Annu. Rev. Biochem.* 79, 351–379. doi:10.1146/annurev-biochem-060308-103103

Farberov, L., Herzig, E., Modai, S., Isakov, O., Hizi, A., and Shomron, N. (2015). MicroRNA-mediated Regulation of P21 and TASK1 Cellular Restriction Factors Enhances HIV-1 Infection. *J. Cel Sci* 128 (8), 1607–1616. doi:10.1242/jcs.167817

Felekkis, K., Touvana, E., Stefanou, C. h., and Deltas, C. (2010). microRNAs: a Newly Described Class of Encoded Molecules that Play a Role in Health and Disease. *Hippokratia* 14 (4), 236–240.

Fortin, J. F., Cantin, R., Lamontagne, G., and Tremblay, M. (1997). Host-derived ICAM-1 Glycoproteins Incorporated on Human Immunodeficiency Virus Type 1 Are Biologically Active and Enhance Viral Infectivity. *J. Virol.* 71 (5), 3588–3596. doi:10.1128/jvi.71.5.3588-3596.1997

Gasparini, P., Lovat, F., Fassan, M., Casadei, L., Cascione, L., Jacob, N. K., et al. (2014). Protective Role of miR-155 in Breast Cancer through RAD51 Targeting Impairs Homologous Recombination after Irradiation. *Proc. Natl. Acad. Sci. U.S.A.* 111 (12), 4536–4541. doi:10.1073/pnas.1402604111

Gerber, P. P., Cabrini, M., Jancic, C., Paoletti, L., Banchio, C., von Bilderling, C., et al. (2015). Rab27a Controls HIV-1 Assembly by Regulating Plasma Membrane Levels of Phosphatidylinositol 4,5-bisphosphate. *J. Cel. Biol.* 209 (3), 435–452. doi:10.1083/jcb.201409082

Ghildiyal, M., and Zamore, P. D. (2009). Small Silencing RNAs: an Expanding Universe. *Nat. Rev. Genet.* 10 (2), 94–108. doi:10.1038/nrg2504

Global, U. N. A. I. D. S. (2020). HIV & AIDS Statistics — Fact Sheet. Available at: https://www.unaids.org/en/resources/fact-sheet.

Gregory, R. I., Yan, K.-p., Amuthan, G., Chendrimada, T., Doratotaj, B., Cooch, N., et al. (2004). The Microprocessor Complex Mediates the Genesis of microRNAs. *Nature* 432 (7014), 235–240. doi:10.1038/nature03120

Ha, M., and Kim, V. N. (2014). Regulation of microRNA Biogenesis. *Nat. Rev. Mol. Cel Biol* 15 (8), 509–524. doi:10.1038/nrm3838

Hatley, M. E., Patrick, D. M., Garcia, M. R., Richardson, J. A., Bassel-Duby, R., van Rooij, E., et al. (2010). Modulation of K-ras-dependent Lung Tumorigenesis by MicroRNA-21. *Cancer cell* 18 (3), 282–293. doi:10.1016/j.ccr.2010.08.013

He, M.-L., Luo, M. X.-M., Lin, M. C., and Kung, H.-f. (2012). MicroRNAs: Potential Diagnostic Markers and Therapeutic Targets for EBV-Associated Nasopharyngeal Carcinoma. *Biochim. Biophys. Acta (Bba) - Rev. Cancer* 1825 (1), 1–10. doi:10.1016/j.bbcan.2011.09.001

Hoque, M., Shamanna, R. A., Guan, D., Pe'ery, T., and Mathews, M. B. (2011). HIV-1 Replication and Latency Are Regulated by Translational Control of Cyclin T1. *J. Mol. Biol.* 410 (5), 917–932. doi:10.1016/j.jmb.2011.03.060

Houzet, L., Klase, Z., Yeung, M. L., Wu, A., Le, S.-Y., Quiñones, M., et al. (2012). The Extent of Sequence Complementarity Correlates with the Potency of Cellular miRNA-Mediated Restriction of HIV-1. *Nucleic Acids Res.* 40 (22), 11684–11696. doi:10.1093/nar/gks912

Hoxie, J. A., and June, C. H. (2012). Novel Cell and Gene Therapies for HIV. *Cold Spring Harbor Perspect. Med.* 2 (10), a007179. doi:10.1101/cshperspect.a007179

Huang, J., Wang, F., Argyris, E., Chen, K., Liang, Z., Tian, H., et al. (2007). Cellular microRNAs Contribute to HIV-1 Latency in Resting Primary CD4+ T Lymphocytes. *Nat. Med.* 13 (10), 1241–1247. doi:10.1038/nm1639

Ikeda, S., Kong, S. W., Lu, J., Bisping, E., Zhang, H., Allen, P. D., et al. (2007). Altered microRNA Expression in Human Heart Disease. *Physiol. genomics* 31 (3), 367–373. doi:10.1152/physiolgenomics.00144.2007

Inui, M., Martello, G., and Piccolo, S. (2010). MicroRNA Control of Signal Transduction. *Nat. Rev. Mol. Cel Biol* 11 (4), 252–263. doi:10.1038/nrm2868

Jiang, C., Zhu, W., Xu, J., Wang, B., Hou, W., Zhang, R., et al. (2014). MicroRNA-26a Negatively Regulates Toll-like Receptor 3 Expression of Rat Macrophages and Ameliorates Pristane Induced Arthritis in Rats. *Arthritis Res. Ther.* 16 (1), R9. doi:10.1186/ar4435

Jin, C., Cheng, L., Höxtermann, S., Xie, T., Lu, X., Wu, H., et al. (2017). MicroRNA-155 Is a Biomarker of T-Cell Activation and Immune Dysfunction in HIV-1-Infected Patients. *HIV Med.* 18 (5), 354–362. doi:10.1111/hiv.12470

Jin, C., Cheng, L., Lu, X., Xie, T., Wu, H., and Wu, N. (2017). Elevated Expression of miR-155 Is Associated with the Differentiation of CD8+ T Cells in Patients with HIV-1. *Mol. Med. Rep.* 16 (2), 1584–1589. doi:10.3892/mmr.2017.6755

Jopling, C. L., Yi, M., Lancaster, A. M., Lemon, S. M., and Sarnow, P. (2005). Modulation of Hepatitis C Virus RNA Abundance by a Liver-specific MicroRNA. *science* 309 (5740), 1577–1581. doi:10.1126/science.1113329

Kaminski, R., Wollebo, H. S., Datta, P. K., White, M. K., Amini, S., and Khalili, K. (2014). Interplay of Rad51 with NF-Kb Pathway Stimulates Expression of HIV-1. *PLoS ONE* 9, e98304. doi:10.1371/journal.pone.0098304

Kapoor, R., Arora, S., Ponia, S. S., Kumar, B., Maddika, S., and Banerjea, A. C. (2015). The miRNA miR-34a Enhances HIV-1 Replication by Targeting PNUTS/PPP1R10, Which Negatively Regulates HIV-1 Transcriptional Complex Formation. *Biochem. J.* 470 (3), 293–302. doi:10.1042/bj20150700

Kim, J., Inoue, K., Ishii, J., Vanti, W. B., Voronov, S. V., Murchison, E., et al. (2007). A MicroRNA Feedback Circuit in Midbrain Dopamine Neurons. *Science* 317 (5842), 1220–1224. doi:10.1126/science.1140481

Kulkarni, S., Qi, Y., O'hUigin, C., Pereyra, F., Ramsuran, V., McLaren, P., et al. (2013). Genetic Interplay between HLA-C and MIR148A in HIV Control and Crohn Disease. *Proc. Natl. Acad. Sci. U.S.A.* 110 (51), 20705–20710. doi:10.1073/pnas.1312237110

Kulkarni, S., Savan, R., Qi, Y., Gao, X., Yuki, Y., Bass, S. E., et al. (2011). Differential microRNA Regulation of HLA-C Expression and its Association with HIV Control. *Nature* 472 (7344), 495–498. doi:10.1038/nature09914

Kumar, A., and Jeang, K.-T. (2008). Insights into Cellular microRNAs and Human Immunodeficiency Virus Type 1 (HIV-1). *J. Cel. Physiol.* 216 (2), 327–331. doi:10.1002/jcp.21488

Labbaye, C., Spinello, I., Quaranta, M. T., Pelosi, E., Pasquini, L., Petrucci, E., et al. (2008). A Three-step Pathway Comprising PLZF/miR-146a/CXCR4 Controls Megakaryopoiesis. *Nat. Cel Biol* 10 (7), 788–801. doi:10.1038/ncb1741

Lanford, R. E., Hildebrandt-Eriksen, E. S., Petri, A., Persson, R., Lindow, M., Munk, M. E., et al. (2010). Therapeutic Silencing of microRNA-122 in Primates with Chronic Hepatitis C Virus Infection. *Science* 327 (5962), 198–201. doi:10.1126/science.1178178

Le Douce, V., Janossy, A., Hallay, H., Ali, S., Riclet, R., Rohr, O., et al. (2012). Achieving a Cure for HIV Infection: Do We Have Reasons to Be Optimistic? *J. Antimicrob. Chemother.* 67 (5), 1063–1074. doi:10.1093/jac/dkr599

Lederman, M. M., Penn-Nicholson, A., Cho, M., and Mosier, D. (2006). Biology of CCR5 and its Role in HIV Infection and Treatment. *Jama* 296 (7), 815–826. doi:10.1001/jama.296.7.815

Levine, A., et al. (2009). CCL3 Genotype and Current Depression Increase Risk of HIV-Associated Dementia. *Neurobehav HIV Med.* Vol. 1, 1–7. doi:10.2147/nbhiv.s6820

Lewis, B. P., Shih, I.-h., Jones-Rhoades, M. W., Bartel, D. P., and Burge, C. B. (2003). Prediction of Mammalian microRNA Targets. *Cell* 115 (7), 787–798. doi:10.1016/s0092-8674(03)01018-3

Li, Y., Zhu, X., Gu, J., Hu, H., Dong, D., Yao, J., et al. (2010). Anti-miR-21 Oligonucleotide Enhances Chemosensitivity of Leukemic HL60 Cells to

Arabinosylcytosine by Inducing Apoptosis. *Hematology* 15 (4), 215–221. doi:10.1179/102453310x12647083620840

Li, Z., Yin, H., Hao, S., Wang, L., Gao, J., Tan, X., et al. (2016). miR-200 Family Promotes Podocyte Differentiation through Repression of RSAD2. *Sci. Rep.* 6, 27105. doi:10.1038/srep27105

Liu, G., Friggeri, A., Yang, Y., Milosevic, J., Ding, Q., Thannickal, V. J., et al. (2010). miR-21 Mediates Fibrogenic Activation of Pulmonary Fibroblasts and Lung Fibrosis. *J. Exp. Med.* 207 (8), 1589–1597. doi:10.1084/jem.20100035

Liu, L., Oliveira, N. M., Cheney, K. M., Pade, C., Dreja, H., Bergin, A.-M. H., et al. (2011). A Whole Genome Screen for HIV Restriction Factors. *Retrovirology* 8, 94. doi:10.1186/1742-4690-8-94

Liu, X., Chen, Q., Yan, J., Wang, Y., Zhu, C., Chen, C., et al. (2013). MiRNA-296-3p-ICAM-1 axis Promotes Metastasis of Prostate Cancer by Possible Enhancing Survival of Natural Killer Cell-Resistant Circulating Tumour Cells. *Cell Death Dis* 4, e928. doi:10.1038/cddis.2013.458

Lodge, R., Ferreira Barbosa, J. A., Lombard-Vadnais, F., Gilmore, J. C., Deshiere, A., Gosselin, A., et al. (2017). Host MicroRNAs-221 and -222 Inhibit HIV-1 Entry in Macrophages by Targeting the CD4 Viral Receptor. *Cel Rep.* 21 (1), 141–153. doi:10.1016/j.celrep.2017.09.030

Ma, L., Shen, C.-J., Cohen, É. A., Xiong, S.-D., and Wang, J.-H. (2014). miRNA-1236 Inhibits HIV-1 Infection of Monocytes by Repressing Translation of Cellular Factor VprBP. *PloS one* 9 (6), e99535. doi:10.1371/journal.pone.0099535

Macfarlane, L.-A., and R. Murphy, P. (2010). MicroRNA: Biogenesis, Function and Role in Cancer. *Curr. Genomics* 11 (7), 537–561. doi:10.2174/138920210793175895

Martinez-Nunez, R. T., Louafi, F., Friedmann, P. S., and Sanchez-Elsner, T. (2009). MicroRNA-155 Modulates the Pathogen Binding Ability of Dendritic Cells (DCs) by Down-Regulation of DC-specific Intercellular Adhesion Molecule-3 Grabbing Non-integrin (DC-SIGN). *J. Biol. Chem.* 284 (24), 16334–16342. doi:10.1074/jbc.m109.011601

Modi, W. S., Lautenberger, J., An, P., Scott, K., Goedert, J. J., Kirk, G. D., et al. (2006). Genetic Variation in the CCL18-CCL3-CCL4 Chemokine Gene Cluster Influences HIV Type 1 Transmission and AIDS Disease Progression. *Am. J. Hum. Genet.* 79 (1), 120–128. doi:10.1086/505331

Monteleone, K., Selvaggi, C., Cacciotti, G., Falasca, F., Mezzaroma, I., D'Ettorre, G., et al. (2015). MicroRNA-29 Family Expression and its Relation to Antiviral Immune Response and Viro-Immunological Markers in HIV-1-Infected Patients. *BMC Infect. Dis.* 15, 51. doi:10.1186/s12879-015-0768-4

Nature Biotechnology (2020). Second RNAi Drug Approved. *Nat. Biotechnol.* 38, 385.doi:10.1038/s41587-020-0494-3

O'Brien, J., Hayder, H., Zayed, Y., and Peng, C. (2018). Overview of microRNA Biogenesis, Mechanisms of Actions, and Circulation. *Front. Endocrinol.* 9, 402. doi:10.3389/fendo.2018.00402

Okoye, I., Xu, L., Oyegbami, O., Shahbaz, S., Pink, D., Gao, P., et al. (2021). Plasma Extracellular Vesicles Enhance HIV-1 Infection of Activated CD_4+ T Cells and Promote the Activation of Latently Infected J-Lat10.6 Cells via miR-139-5p Transfer. *Front. Immunol.* 12, 697604. doi:10.3389/fimmu.2021.697604

Omoto, S., Ito, M., Tsutsumi, Y., Ichikawa, Y., Okuyama, H., Brisibe, E. A., et al. (2004). HIV-1 Nef Suppression by Virally Encoded microRNA. *Retrovirology* 1 (1), 44–12. doi:10.1186/1742-4690-1-44

Orecchini, E., Doria, M., Michienzi, A., Giuliani, E., Vassena, L., Ciafrè, S. A., et al. (2014). The HIV-1 Tat Protein Modulates CD4 Expression in Human T Cells through the Induction of miR-222. *RNA Biol.* 11 (4), 334–338. doi:10.4161/rna.28372

Organization, W. H. (2020). Global Health Estimates 2016: Disease burden by Cause, Age, Sex, by Country and by Region, 2000–2016, 2018. *Geneva. Recuperado de* 390, 10100.

Ouellet, D. L., Vigneault-Edwards, J., Létourneau, K., Gobeil, L. A., Plante, I., Burnett, J. C., et al. (2013). Regulation of Host Gene Expression by HIV-1 TAR microRNAs. *Retrovirology* 10 (1), 86–15. doi:10.1186/1742-4690-10-86

Palios, J., Kadoglou, N. P., and Lampropoulos, S. (2011). *The Pathophysiology of HIV-/HAART-Related Metabolic Syndrome Leading to Cardiovascular Disorders: The Emerging Role of Adipokines*. Experimental Diabetes Research.

Pilakka-Kanthikeel, S., Raymond, A., Atluri, V. S. R., Sagar, V., Saxena, S. K., Diaz, P., et al. (2015). Sterile Alpha Motif and Histidine/aspartic Acid Domain-Containing Protein 1 (SAMHD1)-Facilitated HIV Restriction in Astrocytes Is Regulated by miRNA-181a. *J. Neuroinflammation* 12, 66. doi:10.1186/s12974-015-0285-9

Pincetic, A., Kuang, Z., Seo, E. J., and Leis, J. (2010). The Interferon-Induced Gene ISG15 Blocks Retrovirus Release from Cells Late in the Budding Process. *J. Virol.* 84 (9), 4725–4736. doi:10.1128/jvi.02478-09

Pomerantz, R. J., and Horn, D. L. (2003). Twenty Years of Therapy for HIV-1 Infection. *Nat. Med.* 9 (7), 867–873. doi:10.1038/nm0703-867

Qi, Z., Cai, S., Cai, J., Chen, L., Yao, Y., Chen, L., et al. (2016). miR-491 Regulates Glioma Cells Proliferation by Targeting TRIM28 *In Vitro*. *BMC Neurol.* 16 (1), 248. doi:10.1186/s12883-016-0769-y

Qiuling, H., Chen, L., Luo, M., Lv, H., Luo, D., Li, T., et al. (2018). HIV-1-Induced miR-146a Attenuates Monocyte Migration by Targeting CCL5 in Human Primary Macrophages. *AIDS Res. Hum. Retroviruses* 34 (7), 580–589. doi:10.1089/AID.2017.0217

Quaranta, M. T., Olivetta, E., Sanchez, M., Spinello, I., Paolillo, R., Arenaccio, C., et al. (2015). miR-146a Controls CXCR4 Expression in a Pathway that Involves PLZF and Can Be Used to Inhibit HIV-1 Infection of CD_4+ T Lymphocytes. *Virology* 478, 27–38. doi:10.1016/j.virol.2015.01.016

Raposo, R. A. S., Abdel-Mohsen, M., Bilska, M., Montefiori, D. C., Nixon, D. F., and Pillai, S. K. (2013). Effects of Cellular Activation on Anti-HIV-1 Restriction Factor Expression Profile in Primary Cells. *J. Virol.* 87 (21), 11924–11929. doi:10.1128/jvi.02128-13

Rosenberger, C. M., Podyminogin, R. L., Diercks, A. H., Treuting, P. M., Peschon, J. J., Rodriguez, D., et al. (2017). miR-144 Attenuates the Host Response to Influenza Virus by Targeting the TRAF6-IRF7 Signaling axis. *Plos Pathog.* 13 (4), e1006305. doi:10.1371/journal.ppat.1006305

Ruelas, D. S., Chan, J. K., Oh, E., Heidersbach, A. J., Hebbeler, A. M., Chavez, L., et al. (2015). MicroRNA-155 Reinforces HIV Latency. *J. Biol. Chem.* 290 (22), 13736–13748. doi:10.1074/jbc.m115.641837

Sarasin-Filipowicz, M., Krol, J., Markiewicz, I., Heim, M. H., and Filipowicz, W. (2009). Decreased Levels of microRNA miR-122 in Individuals with Hepatitis C Responding Poorly to Interferon Therapy. *Nat. Med.* 15 (1), 31–33. doi:10.1038/nm.1902

Scaria, V., Hariharan, M., Pillai, B., Maiti, S., and Brahmachari, S. K. (2007). Host-virus Genome Interactions: Macro Roles for microRNAs. *Cell Microbiol.* 9 (12), 2784–2794. doi:10.1111/j.1462-5822.2007.01050.x

Seddiki, N., Phetsouphanh, C., Swaminathan, S., Xu, Y., Rao, S., Li, J., et al. (2013). The microRNA-9/b-Lymphocyte-Induced Maturation protein-1/IL-2 axis Is Differentially Regulated in Progressive HIV Infection. *Eur. J. Immunol.* 43 (2), 510–520. doi:10.1002/eji.201242695

Shen, C. J., Jia, Y. H., Tian, R. R., Ding, M., Zhang, C., and Wang, J. H. (2012). Translation of Pur-α Is Targeted by Cellular miRNAs to Modulate the Differentiation-dependent Susceptibility of Monocytes to HIV-1 Infection. *FASEB J.* 26 (11), 4755–4764. doi:10.1096/fj.12-209023

Sirois, M., Robitaille, L., Allary, R., Shah, M., Woelk, C. H., Estaquier, J., et al. (2011). TRAF6 and IRF7 Control HIV Replication in Macrophages. *PLOS ONE* 6 (11), e28125. doi:10.1371/journal.pone.0028125

Skalsky, R. L., and Cullen, B. R. (2010). Viruses, microRNAs, and Host Interactions. *Annu. Rev. Microbiol.* 64, 123–141. doi:10.1146/annurev.micro.112408.134243

Sonkoly, E., Wei, T., Janson, P. C. J., Sääf, A., Lundeberg, L., Tengvall-Linder, M., et al. (2007). MicroRNAs: Novel Regulators Involved in the Pathogenesis of Psoriasis? *PloS one* 2 (7), e610. doi:10.1371/journal.pone.0000610

Stadeli, K. M., and Richman, D. D. (2013). Rates of Emergence of HIV Drug Resistance in Resource-Limited Settings: a Systematic Review. *Antivir. Ther.* 18 (1), 115–123. doi:10.3851/IMP2437

Stanczyk, J., Pedrioli, D. M. L., Brentano, F., Sanchez-Pernaute, O., Kolling, C., Gay, R. E., et al. (2008). Altered Expression of MicroRNA in Synovial Fibroblasts and Synovial Tissue in Rheumatoid Arthritis. *Arthritis Rheum.* 58 (4), 1001–1009. doi:10.1002/art.23386

Steele, C. W., Oien, K. A., McKay, C. J., and Jamieson, N. B. (2011). Clinical Potential of microRNAs in Pancreatic Ductal Adenocarcinoma. *Pancreas* 40 (8), 1165–1171. doi:10.1097/mpa.0b013e3182218ffb

Su, B., Fu, Y., Liu, Y., Wu, H., Ma, P., Zeng, W., et al. (2018). Potential Application of microRNA Profiling to the Diagnosis and Prognosis of HIV-1 Infection. *Front. Microbiol.* 9, 3185. doi:10.3389/fmicb.2018.03185

Subramanian, S., and Steer, C. J. (2010). MicroRNAs as Gatekeepers of Apoptosis. *J. Cel Physiol* 223 (2), 289–298. doi:10.1002/jcp.22066

Sun, B., Yang, R., and Mallardo, M. (2016). Roles of microRNAs in HIV-1 Replication and Latency. *Mirna* 5 (2), 120–123. doi:10.2174/2211536605666160829123118

Sun, G., Li, H., Wu, X., Covarrubias, M., Scherer, L., Meinking, K., et al. (2012). Interplay between HIV-1 Infection and Host microRNAs. *Nucleic Acids Res.* 40 (5), 2181–2196. doi:10.1093/nar/gkr961

Sung, T.-L., and Rice, A. P. (2009). miR-198 Inhibits HIV-1 Gene Expression and Replication in Monocytes and its Mechanism of Action Appears to Involve Repression of Cyclin T1. *Plos Pathog.* 5 (1), e1000263. doi:10.1371/journal.ppat.1000263

Swaminathan, G., Rossi, F., Sierra, L. J., Gupta, A., Navas-Martín, S., and Martín-García, J. (2012). A Role for microRNA-155 Modulation in the Anti-HIV-1 Effects of Toll-like Receptor 3 Stimulation in Macrophages. *PLoS Pathogens* 8 (9), e1002937. doi:10.1371/journal.ppat.1002937

Swaminathan, G., Rossi, F., Sierra, L.-J., Gupta, A., Navas-Martín, S., and Martín-García, J. (2012). A Role for microRNA-155 Modulation in the Anti-HIV-1 Effects of Toll-like Receptor 3 Stimulation in Macrophages. *Plos Pathog.* 8 (9), e1002937. doi:10.1371/journal.ppat.1002937

Swaminathan, S., Suzuki, K., Seddiki, N., Kaplan, W., Cowley, M. J., Hood, C. L., et al. (2012). Differential Regulation of the Let-7 Family of microRNAs in CD4+ T Cells Alters IL-10 Expression. *J. Immunol.* 188 (12), 6238–6246. doi:10.4049/jimmunol.1101196

Thierry, S., Benleulmi, M. S., Sinzelle, L., Thierry, E., Calmels, C., Chaignepain, S., et al. (2015). Dual and Opposite Effects of hRAD51 Chemical Modulation on HIV-1 Integration. *Chem. Biol.* 22 (6), 712–723. doi:10.1016/j.chembiol.2015.04.020

Thum, T., Gross, C., Fiedler, J., Fischer, T., Kissler, S., Bussen, M., et al. (2008). MicroRNA-21 Contributes to Myocardial Disease by Stimulating MAP Kinase Signalling in Fibroblasts. *Nature* 456 (7224), 980–984. doi:10.1038/nature07511

Tian, H., and He, Z. (2018). miR-215 Enhances HCV Replication by Targeting TRIM22 and Inactivating NF-Kb Signaling. *Yonsei Med. J.* 59 (4), 511–518. doi:10.3349/ymj.2018.59.4.511

Treiber, T., Treiber, N., and Meister, G. (2019). Regulation of microRNA Biogenesis and its Crosstalk with Other Cellular Pathways. *Nat. Rev. Mol. Cel Biol* 20 (1), 5–20. doi:10.1038/s41580-018-0059-1

Triboulet, R., Mari, B., Lin, Y.-L., Chable-Bessia, C., Bennasser, Y., Lebrigand, K., et al. (2007). Suppression of microRNA-Silencing Pathway by HIV-1 during Virus Replication. *Science* 315 (5818), 1579–1582. doi:10.1126/science.1136319

Trobaugh, D. W., and Klimstra, W. B. (2017). MicroRNA Regulation of RNA Virus Replication and Pathogenesis. *Trends Molecular Medicine* 23 (1), 80–93. doi:10.1016/j.molmed.2016.11.003

Tyagi, M., and Kashanchi, F. (2012). New and Novel Intrinsic Host Repressive Factors against HIV-1: PAF1 Complex, HERC5 and Others. *Retrovirology* 9, 19. doi:10.1186/1742-4690-9-19

van Gent, M., Sparrer, K. M. J., and Gack, M. U. (2018). TRIM Proteins and Their Roles in Antiviral Host Defenses. *Annu. Rev. Virol.* 5, 385–405. doi:10.1146/annurev-virology-092917-043323

Wang, W.-X., Rajeev, B. W., Stromberg, A. J., Ren, N., Tang, G., Huang, Q., et al. (2008). The Expression of MicroRNA miR-107 Decreases Early in Alzheimer's Disease and May Accelerate Disease Progression through Regulation of -Site Amyloid Precursor Protein-Cleaving Enzyme 1. *J. Neurosci.* 28 (5), 1213–1223. doi:10.1523/jneurosci.5065-07.2008

Wang, X., Ye, L., Hou, W., Zhou, Y., Wang, Y.-J., Metzger, D. S., et al. (2009). Cellular microRNA Expression Correlates with Susceptibility of Monocytes/macrophages to HIV-1 Infection. *Blood* 113 (3), 671–674. doi:10.1182/blood-2008-09-175000

Wong, S. T., Zhang, X. Q., Zhuang, J. T., Chan, H. L., Li, C. H., and Leung, G. K. (2012). MicroRNA-21 Inhibition Enhances *In Vitro* Chemosensitivity of Temozolomide-Resistant Glioblastoma Cells. *Anticancer Res.* 32 (7), 2835–2841.

Wortman, M. J., Krachmarov, C. P., Kim, J. H., Gordon, R. G., Chepenik, L. G., Brady, J. N., et al. (2000). Interaction of HIV-1 Tat with Pur? in Nuclei of Human Glial Cells: Characterization of RNA-Mediated Protein-Protein Binding. *J. Cel. Biochem.* 77 (1), 65–74. doi:10.1002/(sici)1097-4644(20000401)77:1<65:aid-jcb7>3.0.co;2-u

Wu, M., Fan, B., Guo, Q., Li, Y., Chen, R., Lv, N., et al. (2018). Knockdown of SETDB1 Inhibits Breast Cancer Progression by miR-381-3p-Related Regulation. *Biol. Res.* 51 (1), 39. doi:10.1186/s40659-018-0189-0

Wu, S., He, L., Li, Y., Wang, T., Feng, L., Jiang, L., et al. (2013). miR-146a Facilitates Replication of Dengue Virus by Dampening Interferon Induction by Targeting TRAF6. *J. Infect.* 67 (4), 329–341. doi:10.1016/j.jinf.2013.05.003

Wu, X., Zhang, L.-L., Yin, L.-B., Fu, Y.-J., Jiang, Y.-J., Ding, H.-B., et al. (2017). Deregulated MicroRNA-21 Expression in Monocytes from HIV-Infected Patients Contributes to Elevated IP-10 Secretion in HIV Infection. *Front. Immunol.* 8, 1122. doi:10.3389/fimmu.2017.01122

Yamanaka, S., Olaru, A. V., An, F., Luvsanjav, D., Jin, Z., Agarwal, R., et al. (2012). MicroRNA-21 Inhibits Serpini1, a Gene with Novel Tumour Suppressive Effects in Gastric Cancer. *Dig. Liver Dis.* 44 (7), 589–596. doi:10.1016/j.dld.2012.02.016

Yang, F., Xu, Z., Duan, S., and Luo, M. (2016). MicroRNA-541 Promotes the Proliferation of Vascular Smooth Muscle Cells by Targeting IRF7. *Am. J. Transl Res.* 8 (2), 506–515.

Yin, Y., Zhong, J., Li, S.-W., Li, J.-Z., Zhou, M., Chen, Y., et al. (2016). TRIM11, a Direct Target of miR-24-3p, Promotes Cell Proliferation and Inhibits Apoptosis in colon Cancer. *Oncotarget* 7 (52), 86755–86765. doi:10.18632/oncotarget.13550

Yuan, T., Yao, W., Tokunaga, K., Yang, R., and Sun, B. (2016). An HIV-1 Capsid Binding Protein TRIM11 Accelerates Viral Uncoating. *Retrovirology* 13 (1), 72. doi:10.1186/s12977-016-0306-5

Zhang, H.-S., Chen, X.-Y., Wu, T.-C., Sang, W.-W., and Ruan, Z. (2012). MiR-34a Is Involved in Tat-Induced HIV-1 Long Terminal Repeat (LTR) Transactivation through the SIRT1/NFκB Pathway. *FEBS Lett.* 586 (23), 4203–4207. doi:10.1016/j.febslet.2012.10.023

Zhang, H.-S., Wu, T.-C., Sang, W.-W., and Ruan, Z. (2012). MiR-217 Is Involved in Tat-Induced HIV-1 Long Terminal Repeat (LTR) Transactivation by Down-Regulation of SIRT1. *Biochim. Biophys. Acta.* 1823 (5), 1017–1023. doi:10.1016/j.bbamcr.2012.02.014

Zhang, M. M., Bahal, R., Rasmussen, T. P., Manautou, J. E., and Zhong, X.-b. (2021). The Growth of siRNA-Based Therapeutics: Updated Clinical Studies. *Biochem. Pharmacol.* 189, 114432. doi:10.1016/j.bcp.2021.114432

Zhang, Q., He, Y., Nie, M., and Cai, W. (2017). Roles of miR-138 and ISG15 in Oral Squamous Cell Carcinoma. *Exp. Ther. Med.* 14 (3), 2329–2334. doi:10.3892/etm.2017.4720

Zhang, Y., Fan, M., Geng, G., Liu, B., Huang, Z., Luo, H., et al. (2014). A Novel HIV-1-Encoded microRNA Enhances its Viral Replication by Targeting the TATA Box Region. *Retrovirology* 11 (1), 23–15. doi:10.1186/1742-4690-11-23

Zhang, Z., Wu, Y., Chen, J., Hu, F., Chen, X., and Xu, W. (2021). Expression of microRNA-155 in Circulating T Cells is an Indicator of Immune Activation Levels in HIV-1 Infected Patients. *HIV Res. Clin. Pract.* 22 (3), 71–77.

Zhao, C., Sun, X., and Li, L. (2019). Biogenesis and Function of Extracellular miRNAs. *ExRNA* 1 (1), 1–9. doi:10.1186/s41544-019-0039-4

Zhao, J.-J., Lin, J., Lwin, T., Yang, H., Guo, J., Kong, W., et al. (2010). microRNA Expression Profile and Identification of miR-29 as a Prognostic Marker and Pathogenetic Factor by Targeting CDK6 in Mantle Cell Lymphoma. *J. Am. Soc. Hematol.* 115 (13), 2630–2639. doi:10.1182/blood-2009-09-243147

Conflict of Interest: The authors declare that the research was conducted in the absence of any commercial or financial relationships that could be construed as a potential conflict of interest.

frontiers | Frontiers in Genetics

ORIGINAL RESEARCH
published: 01 June 2022
doi: 10.3389/fgene.2022.857728

A Major Downregulation of Circulating microRNAs in Zika Acutely Infected Patients: Potential Implications in Innate and Adaptive Immune Response Signaling Pathways

Ana Carolina Carvalho-Silva[1,2†], *Almir Ribeiro Da Silva Junior*[3,4,5†], *Vagner Oliveira-Carvalho Rigaud*[3], *Waleska Kerllen Martins*[6,7], *Verônica Coelho*[3,4,5], *Irmtraut Araci Hoffmann Pfrimer*[8], *Jorge Kalil*[3,4,5], *Simone Gonçalves Fonseca*[4], *Edecio Cunha-Neto*[3,4,5‡] *and Ludmila Rodrigues Pinto Ferreira*[10,11*‡]

[1]*RNA Systems Biology Laboratory (RSBL), Departmento de Morfologia, Instituto de Ciências Biológicas, Universidade Federal de Minas Gerais, Belo Horizonte, Brazil,* [2]*Programa de Pós-Graduação em Biologia Celular, Universidade Federal de Minas Gerais (UFMG), Belo Horizonte, Brazil,* [3]*Laboratory of Immunology, Heart Institute (InCor) School of Medicine, University of São Paulo, São Paulo, Brazil,* [4]*Institute for Investigation in Immunology, iii-INCT (National Institute of Science and Technology), São Paulo, Brazil,* [5]*Division of Clinical Immunology and Allergy, School of Medicine, University of São Paulo, São Paulo, Brazil,* [6]*Instituto de Química, Universidade de São Paulo, São Paulo, Brazil,* [7]*Universidade Anhanguera, São Paulo, Brazil,* [8]*Pontifícia Universidade Católica de Goiás, Goiânia, Brazil,* [9]*Instituto de Patologia Tropical e Saúde Pública, Universidade Federal de Goiás, Goiânia, Brazil,* [10]*National Institute of Science and Technology for Vaccines (INCTV), Belo Horizonte, Brazil,* [11]*Centro de Tecnologia de Vacinas, Universidade Federal de Minas Gerais, Belo Horizonte, Brazil*

Zika virus (ZIKV) is an arbovirus mainly transmitted by mosquitos of the genus *Aedes*. The first cases of ZIKV infection in South America occurred in Brazil in 2015. The infection in humans causes diverse symptoms from asymptomatic to a syndrome-like dengue infection with fever, arthralgia, and myalgia. Furthermore, ZIKV infection during pregnancy is associated with fetal microcephaly and neurological disorders. The identification of host molecular mechanisms responsible for the modulation of different signaling pathways in response to ZIKV is the first step to finding potential biomarkers and therapeutic targets and understanding disease outcomes. In the last decade, it has been shown that microRNAs (miRNAs) are important post-transcriptional regulators involved in virtually all cellular processes. miRNAs present in body fluids can not only serve as key biomarkers for diagnostics and prognosis of human disorders but also contribute to cellular signaling offering new insights into pathological mechanisms. Here, we describe for the first time ZIKV-induced changes in miRNA plasma levels in patients during the acute and recovery phases of infection. We observed that during ZIKV acute infection, among the dysregulated miRNAs (DMs), the majority is with decreased levels when compared to convalescent and control patients. We used systems biology tools to build and highlight biological interactions between miRNAs and their multiple direct and indirect target molecules. Among the 24 DMs identified in ZIKV + patients, miR-146, miR-125a-5p, miR-30-5p, and miR-142-3p were related to signaling pathways modulated during infection and immune response. The results presented here are an effort to open new vistas for the key roles of miRNAs during ZIKV infection.

Keywords: Zika infection, systems biology, microRNA profiling, target prediction, viruses

OPEN ACCESS

Edited by:
Gabriel Adelman Cipolla, Federal University of Paraná, Brazil

Reviewed by:
Pryscilla Fanini Wowk, Carlos Chagas Institute (ICC), Brazil
Jose Artur Chies, Federal University of Rio Grande do Sul, Brazil

****Correspondence:***
Ludmila Rodrigues Pinto Ferreira
ludmila@icb.ufmg.br

†These authors have contributed equally to this work

‡These authors share senior authorship

Specialty section:
This article was submitted to RNA, a section of the journal Frontiers in Genetics

Received: *19 January 2022*
Accepted: *18 April 2022*
Published: *01 June 2022*

Citation:
Carvalho-Silva AC, Da Silva Junior AR, Rigaud VO-C, Martins WK, Coelho V, Pfrimer IAH, Kalil J, Fonseca SG, Cunha-Neto E and Ferreira LRP (2022) A Major Downregulation of Circulating microRNAs in Zika Acutely Infected Patients: Potential Implications in Innate and Adaptive Immune Response Signaling Pathways. Front. Genet. 13:857728. doi: 10.3389/fgene.2022.857728

INTRODUCTION

The Zika virus (ZIKV) is an arbovirus member of the Flaviviridae family that can be carried and spread by mosquitoes belonging to the genus *Aedes*. The first Zika epidemic in South America occurred in 2015 in the northeastern states of Brazil (Campos et al., 2015; Hamel et al., 2015; Zanluca et al., 2015). About one in five people infected with the Zika virus become symptomatic with characteristic clinical symptoms such as acute onset fever with rash, arthralgia, and conjunctivitis. Other commonly reported symptoms include myalgia, headache, retroorbital pain, and vomiting (Oehler et al., 2014; Musso et al., 2015). Previous studies have shown that ZIKV has a neuronal and glia tropism and can be also associated with neurological disorders (for example, Guillain–Barré syndrome and myelitis) (Oehler et al., 2014). Identification of viral RNA in amniotic fluid and maternal milk demonstrated that transmission may also occur from mother to fetus during pregnancy causing dysfunction and microcephaly of the developing fetal brain (De Carvalho et al., 2016). Knowledge about the pathogenesis of ZIKV infection is still limited, and an urgent scientific effort is needed to understand, develop, and identify factors associated with clinical outcomes. microRNAs (miRNAs or miRs) are single-stranded non-coding RNA molecules of ~22 nucleotides in length capable of controlling gene expression at the transcriptional and translational levels by repressing target mRNAs (Alvarezbuylla et al., 2007; van Rooij, 2011). miRNAs have been detected stably circulating in various body fluids, such as saliva, urine, serum, and plasma of control or diseased individuals being extensively reported as non-invasive diagnostic and prognostic biomarkers (Mitchell et al., 2008; Ouyang et al., 2016). Here, we describe for the first time the circulating miRNA profiling in plasma samples from ZIKV-infected individuals during acute (ZIKV+) and the recovery phase (RECZIKV+) compared to control donors (CONTROL). We have found that ZIKV + patients had a significant number of had a significant number of dysregulated miRNAs (DMs) in plasma, with most of them with decreased levels than RECZIKV+ and CONTROL individuals. To better understand and predict the potential impact of this miRNA dysregulation during Zika infection we used computational analysis to identify the potential targets of the DMs (DM Targets). Further pathway enrichment and functional analyses were performed to identify potential upstream regulators of DMs during Zika infection. Finally, DM-target networks were built, and central node molecules were found at ZIKV+ and RECZIKV + networks around the main enriched canonical pathways observed for each group. We present here a holistic view and highlight the potential role of circulating miRNAs during the response to acute infection and the disease recovery phase of ZIKV infection.

MATERIALS AND METHODS

Ethics Statement

This study was approved by the Institutional Review Board from Pontifical Catholic University of Goiás (CEP—Research Ethics Committee), under protocol number 46073815.9.0000.00370. All subjects were invited to participate in the study after being explained about the research and were at least 18 years old. All study subjects signed a written informed consent form before the interview and blood collection in accordance with the Declaration of Helsinki. The patients with Zika fever-like symptoms were also interviewed in a private room and answered a written questionnaire informing them about the day of symptom onset, types of symptoms, and demographic information.

Study Groups and Sample Collection

Our study included a total of 52 individuals aged 18–68 (mean 36 years) from Goiânia city, state of Goiás (GO), Brazil. All individuals tested negative for dengue and chikungunya. Of these 52 participants (**Supplementary Table S1**) 25 were potential blood donors recruited from the Center of Serology and Immunohematology of Goiânia-GO–Brazil, aged 27–53 (mean 36.4 years) and displaying negative blood tests for several infectious diseases (CONTROL). The remaining 27 participants showed Zika fever-like acute symptoms during the outbreak of ZIKV infection in Brazil between January and May 2016. All 27 patients were positive for ZIKV at real-time RT-PCR test (ZIKV+). A first plasma collection of ZIKV-infected subjects was done at enrollment, 2–9 days after symptom onset. A second collection was done from 6 ZIKV-infected subjects 2–3 weeks after the first sample, for evaluating the recovery phase (RECZIKV+) (**Table 1**). From these, 18 samples, we randomly selected a total for miRNA profiling: 6 control individuals (CONTROL), 7 ZIKV+ and 5 RECZIKV+. Plasma was isolated from blood samples collected into EDTA-coated Vacutainer tubes (Becton & Dickinson, United States), centrifuged at 1,200x g for 10 min, and stored at −80°C freezer until the analysis.

Detection of ZIKV Infection by Real-Time RT-PCR

Viral RNA detection and quantification were performed by extracting RNA from whole blood using the QIAamp Viral RNA Mini Kit (Qiagen, Hilden, Germany), according to the manufacturer's instructions. Real-time RT-PCR for Zika virus was performed using a kit (Bioclin®, Bio gene Zika virus PCR-K-203–6). The following primers and probes were used: ZIKV-F, 5'-CCGCTGCCCAACACAAG-3'; ZIKV-R, 5'-CCACTAACGTTCTTTTGCAGACAT-3'; ZIKV-P, 5'FAM-AGCCTACCTTGACAAGCAGTCAGACACTCAA-BHQ1-3, developed according to Lanciotti et al. (2007) with modifications (Lanciotti et al., 2008). The RT-PCR was performed following the manufacturer's instructions as published before. Also, real-time RT-PCR for chikungunya and dengue was performed using probe sequences described before (Barros et al., 2018).

Assessment of Hemolysis

Before miRNA profiling, we checked plasma for hemolysis by measuring absorbance at 350–650 nm by spectrophotometry (Nanodrop 2000 spectrophotometer, Thermo Scientific, Waltham, Massachusetts, United States). Samples were classified as hemolyzed if the OD414 exceeded a value of 0.2

TABLE 1 | Characteristics of individuals/patients from the miRNA profiling groups.

Patient code	Group	Gender	Age (years)	Days (symptom onset to sampling)	qPCR ZIKV (C.T.)**
C1	CONTROL	F	34	None	N.A
C2	CONTROL	F	36	None	N.A
C3	CONTROL	F	39	None	N.A
C4	CONTROL	F	36	None	N.A
C5	CONTROL	F	53	None	N.A
C6	CONTROL	F	37	None	N.A
ZIKV+1	ZIKV+	F	36	4	38.92
ZIKV+2	ZIKV+	F	34	3	31.25
ZIKV+3	ZIKV+	F	49	4	35.82
ZIKV+4	ZIKV+	F	36	2	35.85
ZIKV+5	ZIKV+	M	33	9	29.28
ZIKV+6	ZIKV+	M	28	2	27.21
ZIKV+7	ZIKV+	M	24	3	37.88
RECZIKV+1	ZIKV+	F	39	>15	N.A
RECZIKV+2	ZIKV+	F	36	>15	N.A
RECZIKV+3	ZIKV+	F	36	>15	N.A
RECZIKV+4	ZIKV+	F	34	>15	N.A
RECZIKV+5	ZIKV+	F	49	>15	N.A

Gender: F = female M = male; C.T, cycle threshold; none = no symptoms; N.A, not amplified. Samples used for miRNA, profiling: six control individuals (CONTROL); seven ZIKV+ and five RECZIKV + patient samples.

(Kirschner et al., 2011). Previously hemolyzed samples were not used in the study.

Purification of Plasma RNA Enriched in miRNAs

Total RNA was purified from plasma using the Qiagen miRNeasy® Mini Kit. An aliquot of 200 µl of plasma per sample was thawed on ice and centrifuged at 3,000 x g for 5 min at 4°C. The aliquot was transferred to a new tube and 750 µl of a Qiazol mixture containing 3 µl of a spike-in, a synthetic miRNA from *Caenorhabditis elegans* (cel-miR-39) at 1.6 × 108 copies/µl was added to each plasma sample (used as normalization in individual assay analyses). The tube was mixed and incubated for 5 min followed by the addition of 200 µl chloroform. The tube was mixed, incubated for 2 min, and centrifuged at 12,000 x g for 15 min at 4°C. The upper aqueous phase was transferred to a new microcentrifuge tube and 1.5 volume of 100% ethanol was added. The contents were mixed thoroughly and 750 µl of the sample was transferred to a Qiagen RNeasy® Mini spin column in a collection tube followed by centrifugation at 15,000 x g for 30 s at room temperature. The process was repeated until all remaining samples had been loaded. The Qiagen RNeasy® Mini spin column was rinsed with 700 µl of Qiagen RWT buffer and centrifuged at 15,000 x g for 1 min at room temperature followed by another rinse with 500 µl of Qiagen RPE buffer and centrifuged at 15,000 x g for 1 min at room temperature. A rinsing step (500 µl of Qiagen RPE buffer) was repeated 2X. The Qiagen RNeasy® Mini spin column was transferred to a new collection tube and centrifuged at 15,000 x g for 2 min at room temperature. The Qiagen RNeasy® Mini spin column was transferred to a new microcentrifuge tube and the lid was left uncapped for 1 min to allow the column to dry. Total RNA was eluted by adding 14 µl of RNase-free water to the membrane of the Qiagen RNeasy® mini spin column and incubating for 1 min before centrifugation at 15,000 x g for 1 min at room temperature. The concentration of the final material was determined by measuring the A260/A280 ratio using a NanoDrop ND-2000 apparatus (Thermo Scientific, Waltham, Massachusetts, United States). The RNA was stored in a −80°C freezer.

miRNA Profiling

miRNA profiling of 377 miRNAs was carried out following the manufacturer's protocol (Thermofisher). Briefly, a multiplexed RT reaction was performed followed by a pre-amplification using 2.5 µl of the cDNA and 22.5 µl of the pre-amplification master mix with cycling conditions that included 10 min at 95°C, 2 min at 55°C, and 2 min at 72°C, 12 cycles of 15 s at 95°C and 4 min at 60°C, and 10 min at 99.9°C. Quantitative real-time RT-PCR was done utilizing pre-printed TLDA microfluidic cards (Human Card A v3, format 384). The sample/master containing the Megaplex pool was loaded into the cards, centrifuged, and mechanically sealed with the Applied Biosystems sealer device. The real-time PCR reaction was carried out on a QuantStudio™ 12K Flex (Applied Biosystems) real-time machine, using the cycling conditions recommended by the manufacturer.

miRNA Statistical and Unsupervised Analyses

To analyze the miRNA levels we uploaded the real-time generated raw data files (file extension. EDS) in a Thermofisher Cloud software v1.0 (Connect, https://www.thermofisher.com/br/en/home/cloud.html). This software exploits an independent samples *t*-test to compare Ct data to one randomly selected representative reference control sample using a two-tailed *p*-value value of 0.05 and relative miRNA levels are presented as fold change. The data files were first pre-processed by using automatic baseline corrections and manually checked for each assay if the threshold cycle (Ct) value corresponded to the midpoint of the logarithmic amplification curve. miRNAs with a mean Ct > 38 and detected in <80% of all samples were considered below the detection level and excluded from further analysis. The comparative threshold cycle method was used to calculate the relative miRNA levels after global mean normalization (ΔCt) (Mestdagh et al., 2009). The sample unsupervised analysis was performed by hierarchical clustering using Manhattan distance and average linkage for column, and correlation distance and average linkage for row, and represented as a heatmap with ΔCt values for 113 miRNAs (rows), and 18 columns (samples). The PCA of miRNA levels was performed for all samples and the same set of miRNAs was used in the hierarchical clustering. PCA was performed by using a median centering of the data set. The *x*-axis corresponds to principal component 1 (PC1) and the *y*-axis to principal component 2 (PC2) and the percentages of variance in both. Both hierarchical clustering and PCA were built using the ClustVis web tool.

Quantitative Real-Time PCR Analysis of miR-142-3p Plasma Levels

After total RNA isolation, using the miRNeasy Serum/Plasma kit (Qiagen), cDNA was synthesized by reverse transcription using a fixed volume of RNA (2 µl) and the TaqMan microRNA Reverse Transcription kit (Life Technologies), according to the manufacturer's instructions. The circulating levels of miR-142-3p and a synthetic RNA (cel-miR-39) (added during RNA purification) were measured by RT-qPCR using 1.33 µl of the cDNA and miRNA-specific stem-loop primers provided by TaqMan microRNA Assays kit (Life Technologies). Quantitative PCR reactions were performed in triplicate on a QuantStudio 12K Flex (Life Technologies), according to the following program: 10 min at 95°C, 40 cycles of 15 s at 95°C and 60 s at 60°C. Values were normalized to the cel-miR-39 spike and analyzed by the comparative method of Ct (2-ΔΔCt). A threshold cycle (Ct) was observed in the exponential phase of amplification, and quantification of relative levels was performed using standard curves for miR-142-3p and cel-miR-39. Reactions were performed in triplicate and Ct values were averaged for the replicates. The levels were calculated as the mean ± s.d. for each group as individual data points and the following formula was used: relative expression (fold change over CONTROL group samples) = $2^{-(\Delta CtA - \Delta CtB)}$, where Ct is the cycle threshold as previously described (Livak and Schmittgen, 2001). The same was calculated for the CONTROL group, subtracting its mean by each individual data point, so we could plot small variations close to 1 of fold change. Groups were compared by a non-parametrical Kruskal Wallis test. The miRNAs were considered dysregulated if $p < 0.05$ and absolute fold change (FC)≥1.5.

Target Prediction, Canonical Pathway Enrichment, Function, and Network Analysis

The software Ingenuity Pathways Analysis (IPA) (Qiagen, United States) was used in all computational analyses. The target prediction was performed using an IPA tool called "target filter" which relies on four different database algorithms: TargetScan, TarBase, miRecords, and Ingenuity Expert Findings. In our target prediction analysis, we only considered the DM targets that were experimentally validated and highly predicted as targets, based on the content of date 2019–12. The canonical pathway enrichment, function, and network analysis were performed by uploading these target lists identified for each group on IPA software. The significance of the association between each list and the canonical pathway and the relationship between two node molecules in the built networks was measured by Fisher's exact test. As a result, Benjamini–Hochberg method adjusted *p*-values (<0.05) were obtained, determining the probability that the association between the targets in our data set and the canonical pathways identified and networks generated can be explained by chance alone.

Bioinformatics and Statistical Analysis

MicroRNA profiling statistical analysis was carried out by using the Thermo Fisher Cloud software (Connect) which exploits an independent samples t-test to compare ΔΔCt data to one randomly selected representative reference control sample using a two-tailed *p*-value threshold of 0.05 with adjustment for false discovery rate with the Benjamini–Hochberg method. The comparative threshold cycle method was used to calculate the relative miRNA levels after global normalization. The statistical significance threshold was defined as $p < 0.05$ and FC ≥ 1.5. Unsupervised hierarchical clustering was performed using squared Euclidean as distance measure and Ward's method for linkage analysis and Z score normalization. The PCA plot was performed using all probe sets, by using a median centering of the data set.

RESULTS

Unsupervised Analyses and Identification of DMs in Plasma of Patients Infected With ZIKV

We performed profiling of 377 miRNAs from plasma of Zika-infected patients at acute (ZIKV+) and the recovery phase

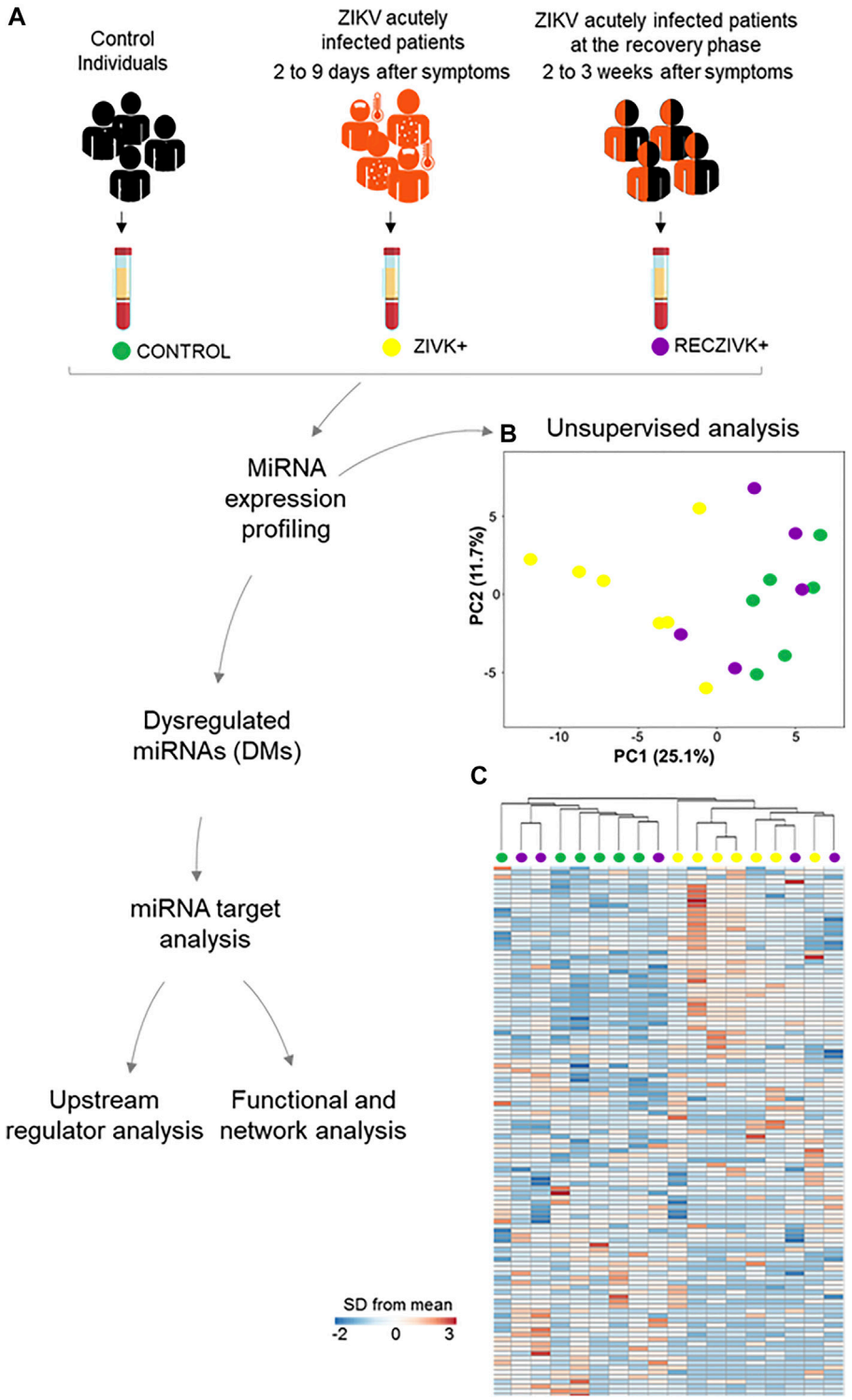

FIGURE 1 | (A–C) Workflow and unsupervised analysis of miRNAs. **(A)** Sample collection, distribution of the studied groups, data processing, and analysis of miRNA profiles in Zika acutely infected patients (ZIKV+; yellow dots) and at the recovery phase of infection (RECZIKV+; magenta dots) compared to control individuals (CONTROL; green dots). **(B)** Principal component analysis (PCA) of miRNA based on all samples and 113 miRNAs by using a median centering of the data set. **(C)** Heatmap and hierarchical clustering were performed with all samples using Manhattan distance and average linkage for columns, and correlation distance and average linkage for rows, and represented as a heatmap with ΔCt values for 113 miRNAs (rows) and 18 samples (columns). The color scale illustrates the fold change in microRNA levels relative to all groups; red and blue represents increased and decreased levels respectively.

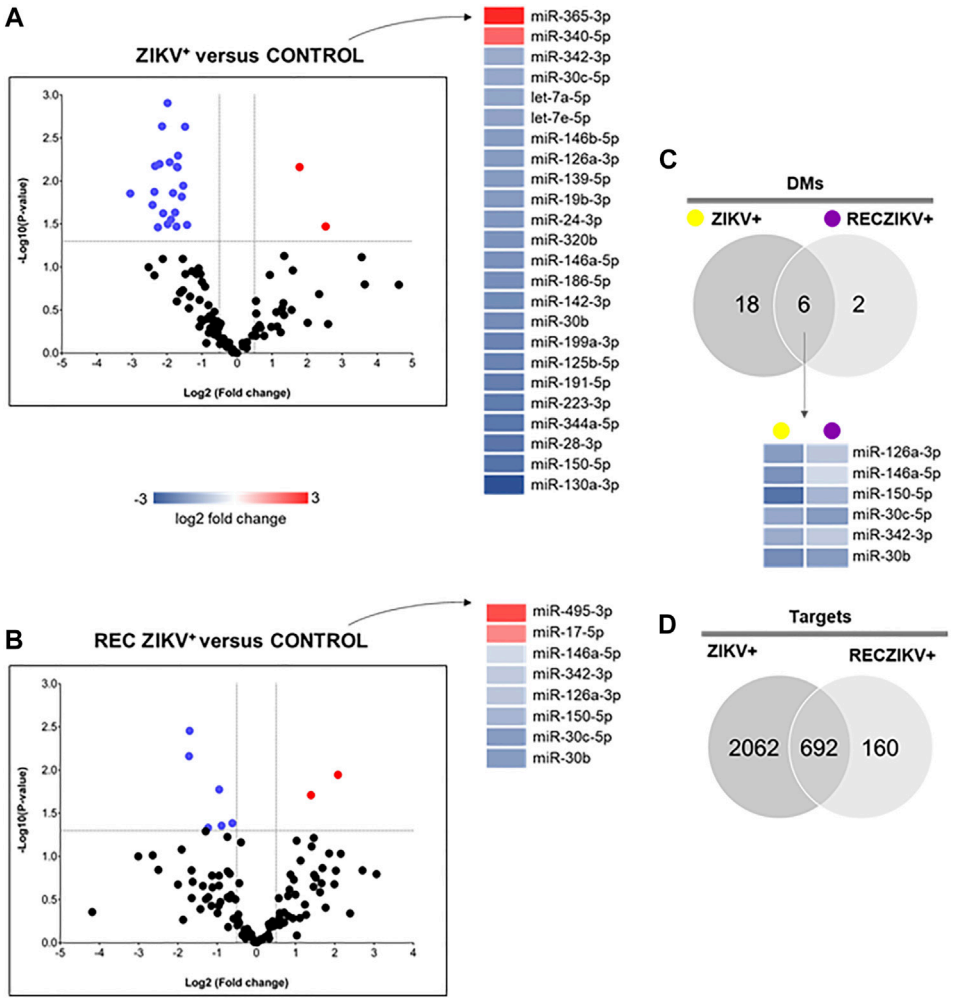

FIGURE 2 | (A–D) Profiling of dysregulated miRNA in ZIKV+, RECZIKV+, CONTROL, and their total targets. **(A,B)** Volcano plot of altered microRNAs from the samples of ZIKV + versus CONTROL group and RECZIKV + versus CONTROL group. The color scale illustrates the log2 fold change in microRNA levels relative to all groups; red and blue represents increased and decreased levels, respectively. **(C)** Venn diagram demonstrated the number of DMs from each group and six miRNAs are common between the ZIKV+ and RECZIKV+, all of them are decreased. **(D)** Venn diagram of the putative targets predicted for increased- and decreased miRNAs in ZIKV+ and RECZIKV+.

(RECZIKV+) of the disease compared to control individuals (CONTROL) from the same endemic area. **Figure 1A** summarizes the experiment workflow showing the steps from blood collection to computational analyses. Briefly, we performed miRNA profiling and identified the list of DMs using cloud-based software, as described in detail in the material and methods section. The miRNA profiles from each comparison were used to find their predicted targets. The lists of predicted targets were used in the functional, upstream regulator, and network analyses. Unsupervised analysis: PCA (**Figure 1B**) and hierarchical clustering (**Figure 1C**) were performed based on the detection of 113 miRNAs with a higher level variance (rows) from each one of the 18 samples (columns) (**Figure 1C**). miRNA profiles from ZIKV+ (yellow dots) and CONTROL (green dots) were segregated in inter-group clusters, while the RECZIKV + group (magenta dots) did not segregate from the other two. One sample clustered within the CONTROL group and the other two within the ZIKV + group. Both PCA and hierarchical clustering indicated that miRNA profiles were specific only to ZIKV+ and CONTROL groups with RECZIV + group sharing miRnome profile similarities with these other two groups.

Identification of DMs and DM Putative Target Prediction

miRNA profiling revealed the highest number of DMs in the ZIKV + compared to the CONTROL group (**Figures 2A–C**). The Volcano plot representations show 24 DMs for ZIKV + versus

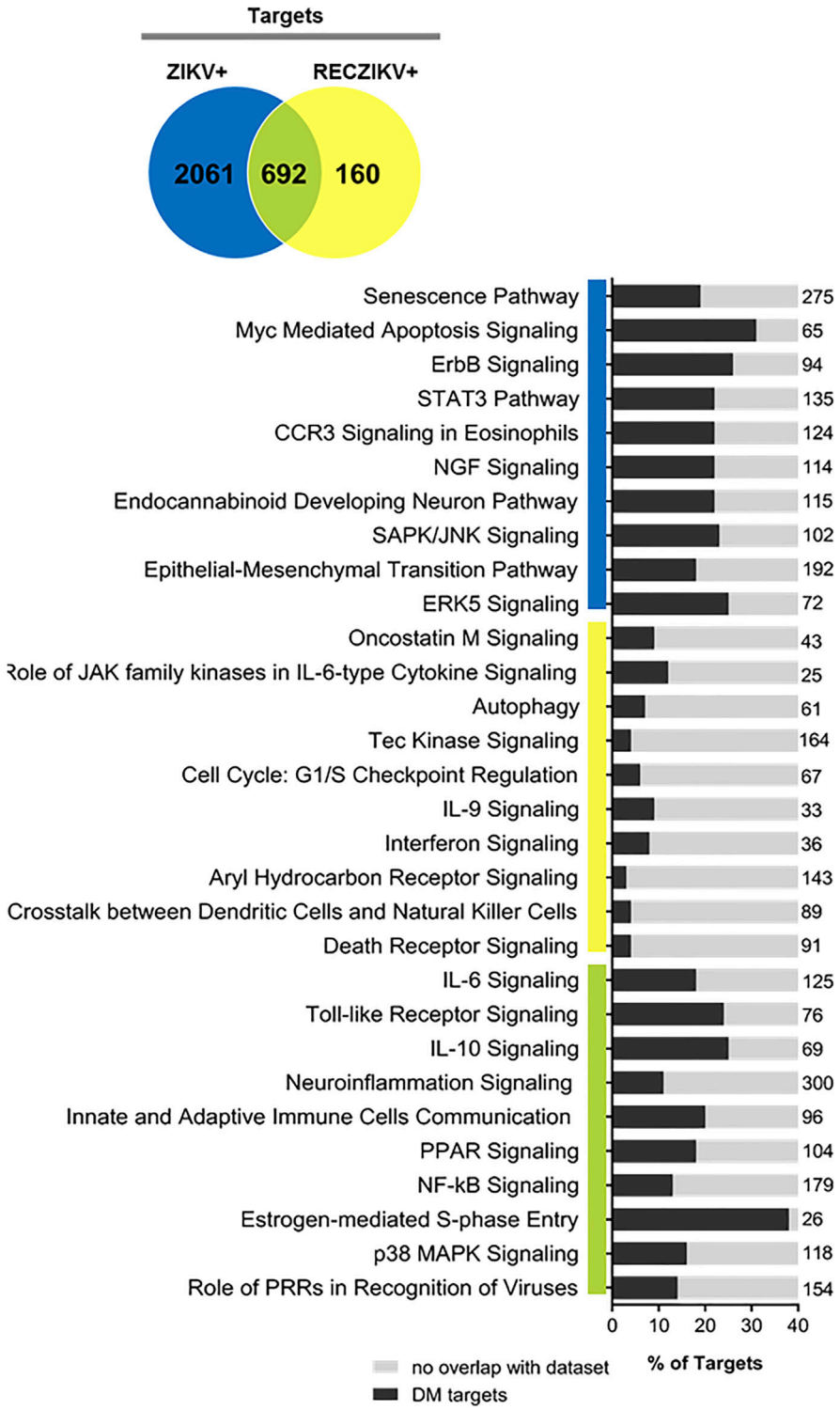

FIGURE 3 | Ingenuity Pathway Analysis (IPA) canonical pathways most significantly enriched in ZIKV+ (blue color), RECZIKV+ (yellow color), and both groups (green color). The stacked bar chart displays the percentage of DM-target molecules present in each pathway. The numerical value to the right of each bar name represents the total number of molecules in that canonical pathway. The Benjamini–Hochberg method was used to adjust the right-tailed Fisher's exact test *p*-value, which was always ($p < 0.05$).

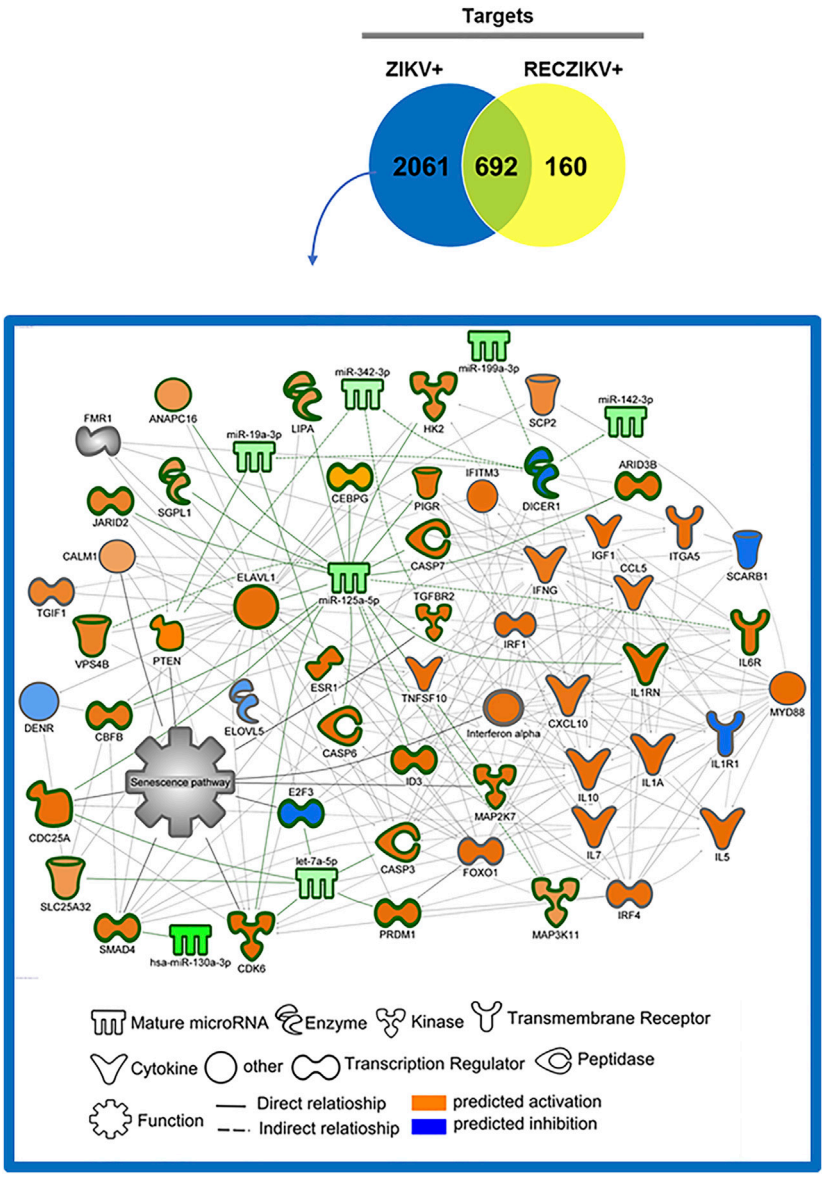

FIGURE 4 | DM and molecule network related to senescence pathway regulation in ZIKV+. The network was built using IPA software. Each molecule was represented as a node, and the biological relationship between two nodes is represented as an edge (line). All edges are supported by at least one reference from the literature or canonical information stored in the Ingenuity Knowledge Base (*IKB*). The central nodes are connected to multiple other molecules. The ZIKV + network showed some molecules as central nodes: interferon-alpha, CXCL10, interferon-gamma (IFNG), interferon regulatory factor 1 (IRF1), miR-125a-5p and its experimentally validated target *ELAV* like RNA-binding protein 1 (ELAV1). The molecules are represented in a gradient of orange or blue based on the prediction status, activated or inhibited, respectively.

CONTROL, with most miRNAs (22) levels decreased and only 2 increased (**Figure 2A**). We identified 8 DMs in RECZIKV+ compared to CONTROL groups. From these 8 DMs, 2 were with higher levels and 6 wih lower levels in patients in the recovery phase of ZIKV infection (**Figure 2B**). The **Supplementary Table S2, S3** depict the list of all DMs in each comparison. **Figure 2C** shows a Venn diagram with the number of DMs from each group, ZIKV+, and RECZIKV + compared to CONTROL, and the 6 DMs shared between the two groups (**Supplementary Table S4**). All shared miRNAs were decreased in both groups. Next, we used a miRNA target prediction tool from Ingenuity Pathway Analysis software (IPA) to screen the putative targets on each list of DMs. The target prediction analysis finds targets (RNAs) with complementary sequences to the miRNA seed region (nucleotides 2-8 from the 5' end of the mature sequence) in their 3′UTR. As miRNAs with the same

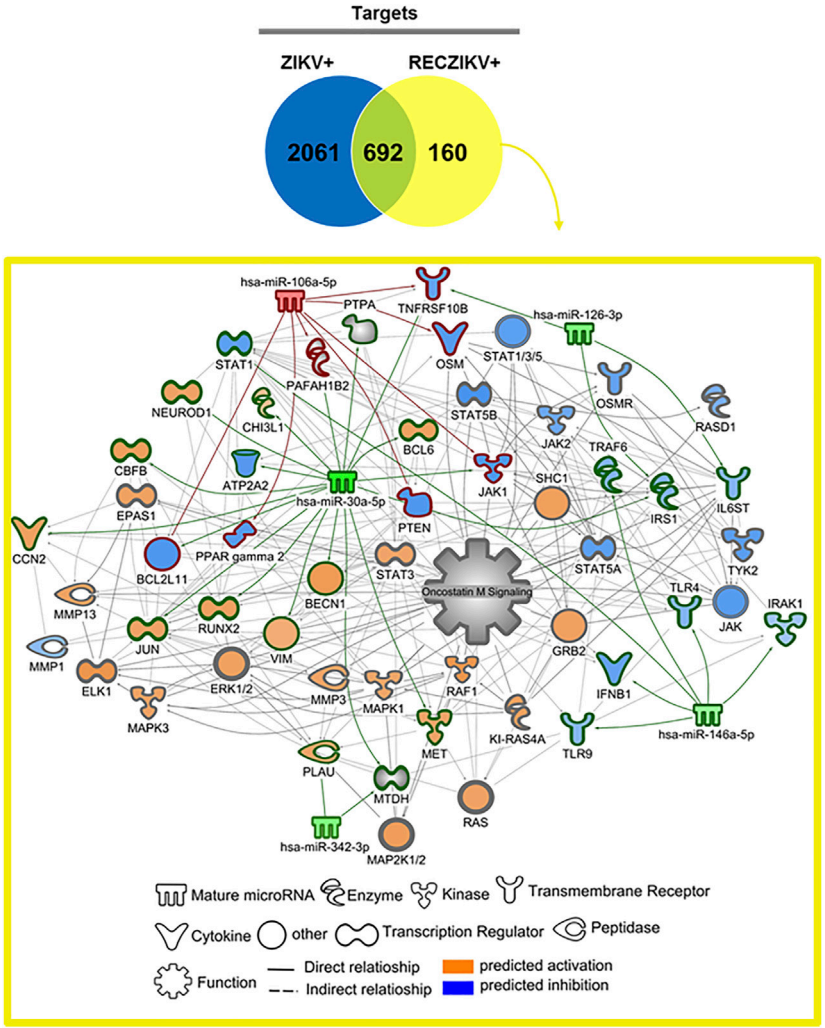

FIGURE 5 | DM and molecule network related to oncostatin M pathway regulation in RECZIKV+. The network was built using IPA software. Each molecule was represented as a node, and the biological relationship between two nodes is represented as an edge (line). All edges are supported by at least one reference from the literature or canonical information stored in the Ingenuity Knowledge Base (IKB). The molecule network is directly or indirectly related to the oncostatin M signaling canonical pathway. MiR-30a-5p is a central node targeting some other node molecules like signal transducer and activator of transcription 1 (STAT1) and 3 (STAT3), activator protein 1 (JUN), and neuronal differentiation 1 (NEUROD1).

seed sequence usually target the same RNAs, IPA software clusters together with the mature miRNAs that share the same 7-nucleotide seed sequence into one entity or "node" to increase the specificity of targeting information. Three pairs out of the 24 DMs from the ZIKV + group share the same seed sequence: let-7a-5p and let-7e-5p (seed sequence GAGGUAG), miR-146a-5p and miR-146b-5p (seed sequence GAGAACU) and miR-30b and miR-30c-5p (seed sequence GUAAACA). The set of miR-30b and miR-30c-5p is also dysregulated in the RECZIKV + group. The target prediction analysis also considers as targets only those that have been highly predicted as targets (from TargetScan database) and/or experimentally validated as targets (from miRecords, TarBase, and direct acquisition from the literature by Ingenuity knowledge Base -IKB). From the list of 24 DMs identified in ZIKV + patients, we found targeting information for 21 of them. We thus obtained a list of 2,754 targets (**Supplementary Table S5**) of the 21 DMs in ZIKV+. For the RECZIKV+, from the list of 8 DMs after filtering, we obtained a list of 7 DMs targeting a total number of 852 targets (**Supplementary Table S6**). A Venn diagram in **Figure 2D** shows that ZIKV+ and RECZIKV + have 692 targets in common (**Supplementary Table S7**).

Target Set Enrichment Analysis Reveals Potential Pathways Regulated by miRNAs During Acute and Recovery Phase of Zika Infection

To predict the canonical pathways enriched and potentially regulated by the DMs from each group we carried out a

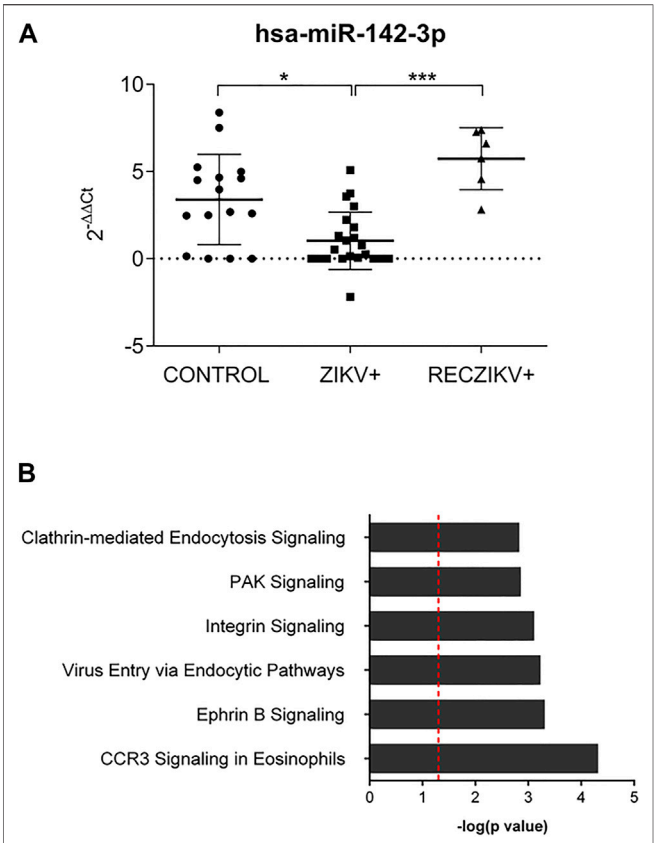

FIGURE 6 | (A,B) Evaluation of miR-142-3p in the ZIKV +, RECZIKV + and CONTROL groups. **(A)** The qPCR validation was performed with 22 ZIKV+, 16 CONTROL and 6 previously analyzed RECZIKV + plasma samples. MiR-142-3p is significantly reduced in ZIKV + compared to CONTROL (*$p < 0.05$) and RECZIKV+ (***$p < 0.005$). The levels were calculated as the mean ± s.d. for each group as individual data points using relative expression (fold change over CONTROL) by the $2^{-\Delta\Delta ct}$ method followed by a non-parametrical Kruskal–Wallis test. **(B)** Enriched canonical pathways were identified for miR-142-3p targets using IPA software.

functional analysis using IPA software. In **Figure 3**, we show the top 10 most enriched canonical pathways (Benjamini–Hochberg adjusted p values <0.05) for a specific list of targets from each group (ZIKV+ in blue, RECZIV+ in yellow, and the shared targets in green). The stacked bar charts show the percentage of targets in each one of the enriched pathways for each group and the number at the right of each bar represents the number of molecules in that given pathway. The analysis of the 692 shared targets between ZIKV+ and RECZIKV+ (in green) showed an overrepresentation of canonical pathways related to immune response such as *pattern recognition of pathogens by the innate immune response*, *toll-like receptor signaling*, and the *role of PRRs in recognition of viruses*. Also, there is an enrichment of pathways related to inflammation, for example, *IL6*, *IL10 signaling,* and most importantly neuroinflammation. Furthermore, we found pathways related to response to cell stress such as *apoptosis and senescence pathways* for the ZIKV + exclusive targets (in blue), and canonical pathways such as *oncostatin M*, *autophagy, and interferon signaling* among others for the RECZIKV+ (yellow).

DM-Target Networks Revealed Key Molecules During ZIKV + Infection

To investigate the possible role of miRNAs in regulating key targets during the acute and recovery phases of Zika infection, we built DM-target networks for both groups (ZIKV+ and RECZIKV+). IPA has a graphical database of networks of interacting molecules (Ingenuity Knowledge Base, IKB). Molecules (genes, proteins) are represented as nodes, and biological relationships between nodes are represented as edges (lines). All connections are supported by at least one reference from the literature or canonical information stored in the IKB. The built networks and prediction analysis revealed the potential role/connection of DMs and their targets in regulating the top predicted canonical pathways in each group: *senescence pathway* in the ZIKV + group (**Figure 4**) and *oncostatin M signaling* in the RECZIKV + group (**Figure 5**). The molecules are represented in a gradient of red or green based on their fold change (increased or decreased, respectively) and orange or blue (predicted to be activated or inhibited). Each node shape represents one type of molecule. The combined biological interaction in both built networks revealed genes that are central nodes connected to multiple other molecules. The ZIKV + network showed some molecules as central nodes: for example, interferon-alpha, CXCL10, interferon-gamma (IFNG), interferon regulatory factor 1 (IRF1), miR-125a-5p and its experimentally validated target ELAV like RNA-binding protein 1 (ELAV1). For the RECZIKV + network, miR-30a-5p is a central node targeting some other node molecules such as signal transducer and activator of transcription 1 (STAT1) and 3 (STAT3), activator protein 1 (JUN), and neuronal differentiation 1 (NEUROD1), molecules directly or indirectly related to *oncostatin M signaling*.

The Hematopoietic Cell-Specific miR-142-3p Downregulated During Acute Zika Infection Potentially Regulates Viral Entry Endocytic Pathways

We further investigated the levels of miR-142-3p, specifically expressed in hematopoietic cells and with decreased levels in the plasma of ZIKV + patients. We first performed qPCR validation of miR-142-3p in a greater number of plasma samples, as shown in **Figure 6A** confirming its significant decreased levels in ZIKV + infected patients compared to CONTROL and RECZIKV + groups. **Figure 6B** shows the enriched canonical pathways for miR-142-3p targets. Among them, pathways related to endocytosis mechanisms: *clathrin-mediated endocytosis signaling,* and *virus entry via endocytic pathways* may indicate that miR-142-3p can potentially regulate intracellular trafficking and ZIKV + entry pathways. **Figure 7** shows experimentally validated targets of miR-142-3p within the *virus entry via endocytic pathway*: clathrin, Rac family small GTPase 1 (RAC1), integrin beta 1, *CXADR* Ig-like cell adhesion

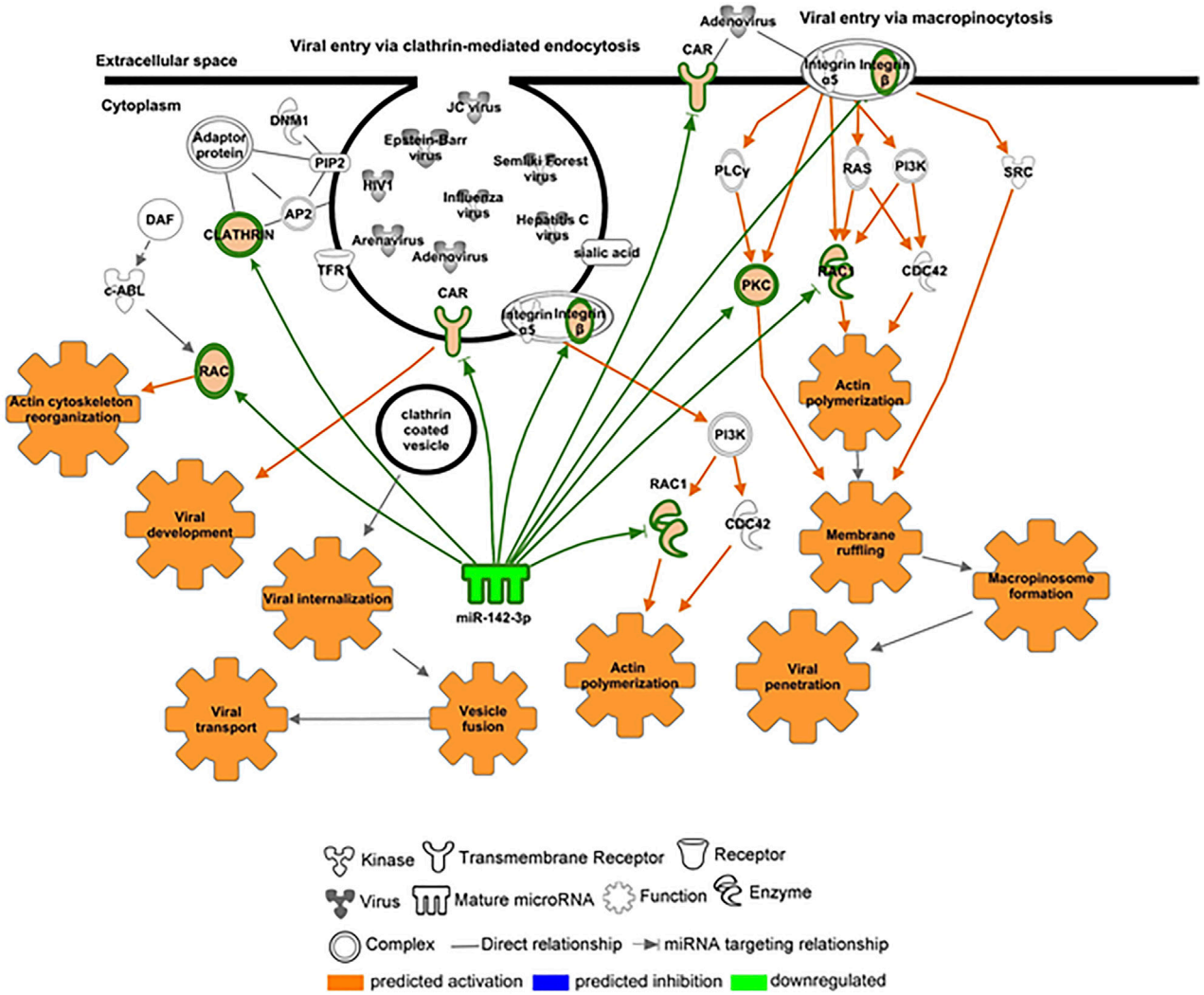

FIGURE 7 | – Targets potentially regulated by miR-142-3p within the virus entry via an endocytic canonical pathway. Molecules highly predicted and experimentally validated as targets of miR-142-3p within the *virus entry via endocytic pathway* are shown as nodes with each node shape representing one type of molecule as indicated in the figure: clathrin, Rac family small GTPase 1 (RAC1), integrin beta 1, CXADR Ig-like cell adhesion molecule (CAR) and protein kinase C (PKC). Molecules and functions are colored based on their predicted activation status: activated (orange) or inhibited (blue) or decreased (gradient of green) or increased (gradient of red).

molecule (CAR) and Protein kinase C (PKC). The prediction analysis showed that miR-142-3p could be potentially decreased by ZIKV infection and may interfere with the endocytic network activating process related to the virus intracellular trafficking incoming mechanism (in orange).

DISCUSSION

miRNAs are crucial post-transcriptional regulators which promote target messenger RNA decay or translational inhibition. In the past years, different studies have shown their biological importance in health and disease. It is also known that these small RNAs can be actively or passively present in different biofluids, including serum and plasma due to cell secretion or upon tissue damage, respectively. They can act as hormones mediating tissue crosstalk during physiological and pathogenic conditions and the study of circulating miRNA profiles can potentially reveal new biological mechanisms and disease biomarkers. Although miRNAs have been studied during Zika *in vitro* and *in vivo* infection, to the best of our knowledge, there is no study providing circulating miRNA profiling during Zika infection. In this study, we compared plasma miRNA profiles from Zika-infected patients during the acute (ZIKV+) and recovery phases of infection (RECZIKV+) compared to control individuals (CONTROL). Our results demonstrated that Zika-infected patients have a differential plasma miRNA profile compared to control individuals, characterized as a great number of DMs, most of them with decreased levels.

Some recent studies have also shown a global miRNA downregulation in ZIKV-infected neurons *in vitro*, with few upregulated (Azouz et al., 2019). Here, we found that ZIKV + patients showed a decreased level of 22 and only two (miR-340 and miR-365-3p) with increased levels in their plasma. Dysregulation in miRNA expression has been previously shown to play critical roles during viral infections, controlling virus replication and modulating antiviral immunity (Louten et al., 2015; Xiong et al., 2017). ZIKV *in vitro* infection of human astrocytes was able to downregulate a great number of miRNAs, including the miR-30 family and miR-17-5p leading to deregulation of biological processes related to *unfolded protein response pathway* and interferon (IFNβ) production (Kozak et al., 2017). MiR-340-5p was previously described to be downregulated during *in vitro* infection with influenza A virus and mediates a regulatory feedback loop during host-virus interactions to control both antiviral responses and infection (Zhao et al., 2019). MiR-365-3p can negatively regulate interleukin 6 (*IL6*) gene expression (Xu et al., 2011), a central cytokine during acute phase response and associated with central nervous system protection during viral infections (Pavelko et al., 2003). MiR-146 is decreased when comparing ZIKV+ and RECZIKV + vs CONTROL group has an important role in *IFN signaling*. Wangs et al. have shown that miR-146 was able to suppress *STAT1*-dependent expression of type 1 and 2 interferons during HBV proliferation (Wang et al., 2013). Another important miRNA, miR-199 is decreased in plasma of the ZIKV + group, described as critical during HCV replication as its upregulation is related to increased viral replication (Fornari et al., 2010; Henry et al., 2010). Here, our clustering analysis revealed that when the patients pass from the acute to convalescent phase, their plasma miRNA content is similar to the CONTROL group, despite still having dysregulated miRNAs in common with the ZIKV + group. Computational analysis revealed that *senescence signaling* is a potential canonical pathway modulated by the dysregulated miRNAs observed in ZIKV + patients. Cellular senescence is described as a signaling pathway with dual opposite roles during cellular stress like viral infections. It can induce a proinflammatory phenotype and cell host protection (Baz-Martínez et al., 2016) but also can be used by the pathogen, like viruses, as a strategy to escape from the cellular antiviral system. The built network with targets of DMs from the ZIKV + group showed as a central node the embryonic lethal abnormal vision (ELAVL1), an RNA-binding protein (RBP) that is responsible for increasing the half-life and steady-state levels of different types of mRNAs, including the ones related to apoptosis and rapid inflammatory and stress response. *ELAVL1* mRNA (also named *HUR* or *ELAV1*) was previously shown to be an experimentally validated target of miR-125b-5p (Guo et al., 2009; Shwetha et al., 2018), also with decreased levels in the plasma of ZIKV + patients. The importance of this RNA-binding protein and miR-125 was previously highlighted during *in vitro* HCV infection. MiR-125 downregulation using antagomiRs led to an increase in the ELAV1 protein abundance in the cytoplasm enhancing HCV replication. This may be related to another described function of ELAV1 as an IFNB1 abundance regulator. ELAV1 strongly interacts with IFNB1 that, like most of the cytokines, contains adenylate-uridylate (A/U)-rich elements (ARES) which makes these cytokine mRNAs highly unstable. Based on that, reduced expression of *ELAVL1* downregulated type 1 *IFN* secretion and the first response to viruses (Herdy et al., 2015). In our study, miR-125 was not found to be dysregulated in the RECZIKV + group, and interferon signaling is among the enriched canonical pathways for this group. The top 2 most enriched pathways for RECZIKV+ were *oncostatin M signaling and the role of JAK family kinases* in IL6-*type cytokine signaling*. Both proteins are members of the same family sharing related receptor complexes and mediating communication between the central nervous system and the immune system. Among the targets identified for miR-30a-5p, which is decreased levels in both groups (ZIKV+ and RECZIKV+) compared to CONTROL, JAK1 was found within the *oncostatin signaling pathway*. In response to viral infections, the *JAK/STAT signaling pathway* is essential in the regulation of local inflammation (Ezeonwumelu et al., 2021). Oncostatin was described to play important roles during physiological and pathological conditions by maintaining neural precursor cell homeostasis and having neuroprotective action, respectively (Martins et al., 2019). Among the canonical pathways enriched in the list of shared DM, targets are the ones related to immune response and inflammation. For example, *neuroinflammation*, *toll-like receptor*, *the role of PRRs in recognition of viruses,* and IL-6 *signaling*. Finally, we highlighted the importance and previously described functions of miR-142-3p in the context of viral infections. This microRNA was first described by Chen et al., in 2004 as specifically expressed in embryonic and adult hematopoietic tissues, and is required for hematopoietic lineage development and function (Chen et al., 2004). MiR-142-3p was also shown to target cytokines like IL6 and ITGAV. Importantly, this miRNA interferes in viral replication, as previously shown in ZIKV-infected human umbilical cord mesenchymal stem cell assays (Seong et al., 2020). In addition, it may confer an antiviral defense as reported by Berrien-Elliott et al., 2019 for maintaining homeostasis and function of type I innate lymphoid cells (Berrien-Elliott et al., 2019). Enrichment analysis showed potential canonical pathways regulated by miR-142-3p. Among them, pathways related to endocytic mechanisms such as *clathrin-mediated endocytosis signaling and virus entry via endocytic pathways* indicate that this microRNA can potentially regulate intracellular trafficking and virus entry pathways. Among the highly predicted and experimentally validated targets of miR-142-3p are clathrin, Rac family small GTPase 1 (RAC1), integrin beta 1, and CXADR Ig-like cell adhesion molecule (CAR) and protein kinase C (PKC). The prediction analysis showed that the downregulation of miR-142-3p could be potently induced by a viral infection and will interfere with the endocytic network activating process related to the virus

intracellular trafficking incoming mechanism. Our results showed a major decrease in miRNA levels in plasma infected with ZIKV. Importantly we further validated miR-142-3p decreased levels in a greater number of plasma samples. By identifying the targets of the DMs we listed important pathways potentially modulated by the dysregulated miRNAs. Furthermore, by building DM-target networks we could identify specific central molecules for the acute and recovery phases of ZIKV infection. A general limitation of the present study, given the network and pathway inference approaches, is the requirement of functional experimental validation to reliably infer interactions among nodes of the system. This is a particular obstacle in clinical studies where sample numbers and the ability to perform perturbations are often limited. Here, we present a tangential approach to reconstructing networks combining computational predictions, experimental evidence from large databanks, and literature mining integration. We think that the further study of miRNAs and their target molecules in the context of ZIKV infection may translate into the identification of novel therapeutic targets and biomarkers of recovery.

DATA AVAILABILITY STATEMENT

The original contributions presented in the study are included in the article/**Supplementary Material**, further inquiries can be directed to the corresponding author.

ETHICS STATEMENT

The studies involving human participants were reviewed and approved by the Institutional Review Board from Pontifical Catholic University of Goiás (CEP - Research Ethics Committee), under the protocol number 46073815.9.0000.00370. The patients/participants provided their written informed consent to participate in this study.

AUTHOR CONTRIBUTIONS

Supervision and project administration: LF, EC-N, IP, and SGF; conceptualization: LF and EC-N; methodology and investigation: ACC-S, AD, and LF; formal analysis: ACC-S, AD, VC-C, GMW, and LF; resources: EC-N, SGF, IP, LF, and JK; writing and original draft and visualization: LF, ACC-S, EC-N, SGF, and VC; and review and editing: all authors reviewed the article.

FUNDING

LRPF is a financial support recipient from the Brazilian National Institute of Science and Technology for Vaccines (INCT-Vacinas/CNPq), Fundação de Pesquisa do Estado de Minas Gerais (APQ-03551-18 and APQ 03608-17).

SUPPLEMENTARY MATERIAL

The Supplementary Material for this article can be found online at: https://www.frontiersin.org/articles/10.3389/fgene.2022.857728/full#supplementary-material

Supplementary Table S1 | Clinical characteristics of the study subjects.

Supplementary Table S2 | List of DMs in ZIKV+ vs CONTROL.

Supplementary Table S3 | List of DMs in RECZIKV+ vs CONTROL.

Supplementary Table S4 | List of DMs in common between ZIKV+ and RECZIKV+ .

REFERENCES

Alvarezbuylla, E., Benitez, M., Davila, E., Chaos, A., Espinosasoto, C., and Padillalongoria, P. (2007). Gene Regulatory Network Models for Plant Development. *Curr. Opin. Plant Biol.* 10, 83–91. doi:10.1016/j.pbi.2006.11.008

Azouz, F., Arora, K., Krause, K., Nerurkar, V. R., and Kumar, M. (2019). Integrated MicroRNA and mRNA Profiling in Zika Virus-Infected Neurons. *Viruses* 11, 162. doi:10.3390/v11020162

Barros, J. B. d. S., Silva, P. A. N. d., Koga, R. d. C. R., Gonzalez-Dias, P., Carmo Filho, J. R., Nagib, P. R. A., et al. (2018). Acute Zika Virus Infection in an Endemic Area Shows Modest Proinflammatory Systemic Immunoactivation and Cytokine-Symptom Associations. *Front. Immunol.* 9, 821. doi:10.3389/fimmu.2018.00821

Baz-Martínez, M., Da Silva-Álvarez, S., Rodríguez, E., Guerra, J., El Motiam, A., Vidal, A., et al. (2016). Cell Senescence Is an Antiviral Defense Mechanism. *Sci. Rep.* 6, 37007. doi:10.1038/srep37007

Berrien-Elliott, M. M., Sun, Y., Neal, C., Ireland, A., Trissal, M. C., Sullivan, R. P., et al. (2019). MicroRNA-142 Is Critical for the Homeostasis and Function of Type 1 Innate Lymphoid Cells. *Immunity* 51, 479–490. doi:10.1016/j.immuni.2019.06.016

Campos, G. S., Bandeira, A. C., and Sardi, S. I. (2015). Zika Virus Outbreak, Bahia, Brazil. *Emerg. Infect. Dis.* 21, 1885–1886. doi:10.3201/eid2110.150847

Chen, C.-Z., Li, L., Lodish, H. F., and Bartel, D. P. (2004). MicroRNAs Modulate Hematopoietic Lineage Differentiation. *Science* 303, 83–86. doi:10.1126/science.1091903

De Carvalho, N. S., De Carvalho, B. F., Fugaça, C. A., Dóris, B., and Biscaia, E. S. (2016). Zika Virus Infection during Pregnancy and Microcephaly Occurrence: a Review of Literature and Brazilian Data. *Braz. J. Infect. Dis.* 20, 282–289. doi:10.1016/j.bjid.2016.02.006

Ezeonwumelu, I. J., Garcia-Vidal, E., and Ballana, E. (2021). JAK-STAT Pathway: A Novel Target to Tackle Viral Infections. *Viruses* 13, 2379. doi:10.3390/v13122379

Fornari, F., Milazzo, M., Chieco, P., Negrini, M., Calin, G. A., Grazi, G. L., et al. (2010). MiR-199a-3p Regulates mTOR and C-Met to Influence the Doxorubicin Sensitivity of Human Hepatocarcinoma Cells. *Cancer Res.* 70, 5184–5193. doi:10.1158/0008-5472.can-10-0145

Guo, X., Wu, Y., and Hartley, R. (2009). MicroRNA-125a Represses Cell Growth by Targeting HuR in Breast Cancer. *RNA Biol.* 6, 575–583. doi:10.4161/rna.6.5.10079

Hamel, R., Dejarnac, O., Wichit, S., Ekchariyawat, P., Neyret, A., Luplertlop, N., et al. (2015). Biology of Zika Virus Infection in Human Skin Cells. *J. Virol.* 89, 8880–8896. doi:10.1128/jvi.00354-15

Henry, J. C., Park, J.-K., Jiang, J., Kim, J. H., Nagorney, D. M., Roberts, L. R., et al. (2010). miR-199a-3p Targets CD44 and Reduces Proliferation of CD44 Positive Hepatocellular Carcinoma Cell Lines. *Biochem. Biophys. Res. Commun.* 403, 120–125. doi:10.1016/j.bbrc.2010.10.130

Herdy, B., Karonitsch, T., Vladimer, G. I., Tan, C. S. H., Stukalov, A., Trefzer, C., et al. (2015). The RNA-Binding Protein HuR/ELAVL1 Regulates IFN-β mRNA Abundance and the Type I IFN Response. *Eur. J. Immunol.* 45, 1500–1511. doi:10.1002/eji.201444979

Kirschner, M. B., Kao, S. C., Edelman, J. J., Armstrong, N. J., Vallely, M. P., van Zandwijk, N., et al. (2011). Haemolysis during Sample Preparation Alters microRNA Content of Plasma. *PLoS One* 6, e24145. doi:10.1371/journal.pone.0024145

Kozak, R. A., Majer, A., Biondi, M. J., Medina, S. J., Goneau, L. W., Sajesh, B. V., et al. (2017). MicroRNA and mRNA Dysregulation in Astrocytes Infected with Zika Virus. *Viruses* 9, 297. doi:10.3390/v9100297

Lanciotti, R. S., Kosoy, O. L., Laven, J. J., Velez, J. O., Lambert, A. J., Johnson, A. J., et al. (2008). Genetic and Serologic Properties of Zika Virus Associated with an Epidemic, Yap State, Micronesia, 2007. *Emerg. Infect. Dis.* 14, 1232–1239. doi:10.3201/eid1408.080287

Livak, K. J., and Schmittgen, T. D. (2001). Analysis of Relative Gene Expression Data Using Real-Time Quantitative PCR and the 2−ΔΔCT Method. *Methods* 25, 402–408. doi:10.1006/meth.2001.1262

Louten, J., Beach, M., Palermino, K., Weeks, M., and Holenstein, G. (2015). MicroRNAs Expressed during Viral Infection: Biomarker Potential and Therapeutic Considerations. *Biomark Insights* 10, 25–52. doi:10.4137/BMI.S29512

Martins, K. R., Haas, C. S., Ferst, J. G., Rovani, M. T., Goetten, A. L. F., Duggavathi, R., et al. (2019). Oncostatin M and its Receptors mRNA Regulation in Bovine Granulosa and Luteal Cells. *Theriogenology* 125, 324–330. doi:10.1016/j.theriogenology.2018.11.021

Mestdagh, P., Van Vlierberghe, P., De Weer, A., Muth, D., Westermann, F., Speleman, F., et al. (2009). A Novel and Universal Method for microRNA RT-qPCR Data Normalization. *Genome Biol.* 10, R64. doi:10.1186/gb-2009-10-6-r64

Mitchell, P. S., Parkin, R. K., Kroh, E. M., Fritz, B. R., Wyman, S. K., Pogosova-Agadjanyan, E. L., et al. (2008). Circulating microRNAs as Stable Blood-Based Markers for Cancer Detection. *Proc. Natl. Acad. Sci. U.S.A.* 105, 10513–10518. doi:10.1073/pnas.0804549105

Musso, D., Roche, C., Robin, E., Nhan, T., Teissier, A., and Cao-Lormeau, V.-M. (2015). Potential Sexual Transmission of Zika Virus. *Emerg. Infect. Dis.* 21, 359–361. doi:10.3201/eid2102.141363

Oehler, E., Watrin, L., Larre, P., Leparc-Goffart, I., Lastere, S., Valour, F., et al. (2014). Zika Virus Infection Complicated by Guillain-Barre Syndrome-Ccase Report, French Polynesia, December 2013. *Euro Surveill.* 19, 20720. doi:10.2807/1560-7917.es2014.19.9.20720

Ouyang, X., Jiang, X., Gu, D., Zhang, Y., Kong, S. K., Jiang, C., et al. (2016). Dysregulated Serum MiRNA Profile and Promising Biomarkers in Dengue-Infected Patients. *Int. J. Med. Sci.* 13, 195–205. doi:10.7150/ijms.13996

Pavelko, K. D., Howe, C. L., Drescher, K. M., Gamez, J. D., Johnson, A. J., Wei, T., et al. (2003). Interleukin-6 Protects Anterior Horn Neurons from Lethal Virus-Induced Injury. *J. Neurosci.* 23, 481–492. doi:10.1523/jneurosci.23-02-00481.2003

Seong, R.-K., Lee, J. K., Cho, G. J., Kumar, M., and Shin, O. S. (2020). mRNA and miRNA Profiling of Zika Virus-Infected Human Umbilical Cord Mesenchymal Stem Cells Identifies miR-142-5p as an Antiviral Factor. *Emerging Microbes Infect.* 9, 2061–2075. doi:10.1080/22221751.2020.1821581

Shwetha, S., Sharma, G., Raheja, H., Goel, A., Aggarwal, R., and Das, S. (2018). Interaction of miR-125b-5p with Human Antigen R mRNA: Mechanism of Controlling HCV Replication. *Virus. Res.* 258, 1–8. doi:10.1016/j.virusres.2018.09.006

van Rooij, E. (2011). The Art of microRNA Research. *Circ. Res.* 108, 219–234. doi:10.1161/circresaha.110.227496

Wang, S., Zhang, X., Ju, Y., Zhao, B., Yan, X., Hu, J., et al. (2013). MicroRNA-146a Feedback Suppresses T Cell Immune Function by Targeting Stat1 in Patients with Chronic Hepatitis B. *J.Immunol.* 191, 293–301. doi:10.4049/jimmunol.1202100

Xiong, X., Deng, J., Zeng, C., Jiang, Y., Tang, S., and Sun, X. (2017). MicroRNA-141 Is a Tumor Regulator and Prognostic Biomarker in Human Glioblastoma. *Oncol. Lett.* 14, 4455–4460. doi:10.3892/ol.2017.6735

Xu, Z., Xiao, S.-B., Xu, P., Xie, Q., Cao, L., Wang, D., et al. (2011). miR-365, a Novel Negative Regulator of Interleukin-6 Gene Expression, Is Cooperatively Regulated by Sp1 and NF-κB. *J. Biol. Chem.* 286, 21401–21412. doi:10.1074/jbc.m110.198630

Zanluca, C., Melo, V. C. A. d., Mosimann, A. L. P., Santos, G. I. V. d., Santos, C. N. D. d., and Luz, K. (2015). First Report of Autochthonous Transmission of Zika Virus in Brazil. *Mem. Inst. Oswaldo Cruz* 110, 569–572. doi:10.1590/0074-02760150192

Zhao, L., Zhang, X., Wu, Z., Huang, K., Sun, X., Chen, H., et al. (2019). The Downregulation of MicroRNA Hsa-miR-340-5p in IAV-Infected A549 Cells Suppresses Viral Replication by Targeting RIG-I and OAS2. *Mol. Ther. - Nucleic Acids* 14, 509–519. doi:10.1016/j.omtn.2018.12.014

Conflict of Interest: The authors declare that the research was conducted in the absence of any commercial or financial relationships that could be construed as a potential conflict of interest.

Publisher's Note: All claims expressed in this article are solely those of the authors and do not necessarily represent those of their affiliated organizations, or those of the publisher, the editors, and the reviewers. Any product that may be evaluated in this article, or claim that may be made by its manufacturer, is not guaranteed or endorsed by the publisher.

frontiers | Frontiers in Genetics

ORIGINAL RESEARCH
published: 14 June 2022
doi: 10.3389/fgene.2022.871972

Differentially Expressed Bone Marrow microRNAs Are Associated With Soluble HLA-G Bone Marrow Levels in Childhood Leukemia

Renata Santos Almeida[1†], *Thailany Thays Gomes*[1†], *Felipe Souza Araújo*[1], *Sávio Augusto Vieira de Oliveira*[1], *Jair Figueredo Santos*[1], *Eduardo Antônio Donadi*[2] and *Norma Lucena-Silva*[1,3]*

[1]Laboratory of Immunogenetics, Department of Immunology, Aggeu Magalhães Institute, Oswaldo Cruz Foundation (Fiocruz), Recife, Brazil, [2]Clinical Immunology Division, Department of Medicine, School of Medicine of Ribeirão Preto, University of São Paulo (USP), Ribeirão Preto, Brazil, [3]Laboratory of Molecular Biology, Pediatric Oncology Service, IMIP Hospital, Recife, Brazil

OPEN ACCESS

Edited by:
Ticiana DJ Farias,
University of Colorado, United States

Reviewed by:
Vera Rebmann,
University of Duisburg-Essen, Germany
Sara Alves,
Instituto de Pesquisa Pelé Pequeno Príncipe, Brazil
Francesco Puppo,
University of Genoa, Italy

***Correspondence:**
Norma Lucena-Silva
norma.silva@fiocruz.br

[†]These authors have contributed equally to this work and share first authorship

Specialty section:
This article was submitted to RNA, a section of the journal Frontiers in Genetics

Received: 08 February 2022
Accepted: 15 April 2022
Published: 14 June 2022

Citation:
Almeida RS, Gomes TT, Araújo FS, Oliveira SAVd, Santos JF, Donadi EA and Lucena-Silva N (2022) Differentially Expressed Bone Marrow microRNAs Are Associated With Soluble HLA-G Bone Marrow Levels in Childhood Leukemia. Front. Genet. 13:871972. doi: 10.3389/fgene.2022.871972

HLA-G is a nonclassical histocompatibility class I molecule that plays a role in immune vigilance in cancer and infectious diseases. We previously reported that highly soluble HLA-G (sHLA-G) levels in the bone marrow were associated with a high blood cell count in T-acute lymphoblastic leukemia, a marker associated with a poor prognosis. To understand the posttranscriptional *HLA-G* gene regulation in leukemia, we evaluated the bone marrow microRNA profile associated with the HLA-G bone marrow mRNA expression and sHLA-G bone marrow levels in children exhibiting acute leukemia (B-ALL, T-ALL, and AML) using massively parallel sequencing. Ten differentially expressed miRNAs were associated with high sHLA-G bone marrow levels, and four of them (hsa-miR-4516, hsa-miR-486-5p, hsa-miR-4488, and hsa-miR-5096) targeted *HLA-G*, acting at distinct *HLA-G* gene segments. For qPCR validation, these miRNA expression levels (ΔCt) were correlated with *HLA-G5* and *RREB1* mRNA expressions and sHLA-G bone marrow levels according to the leukemia subtype. The hsa-miR-4488 and hsa-miR-5096 expression levels were lower in B-ALL than in AML, while that of hsa-miR-486-5p was lower in T-ALL than in AML. In T-ALL, hsa-miR-5096 correlated positively with *HLA-G5* and negatively with sHLA-G. In addition, hsa-miR-4516 correlated negatively with sHLA-G levels. In AML, hsa-miR-4516 and hsa-miR-4488 correlated positively with *HLA-G5* mRNA, but the *HLA-G5* negatively correlated with sHLA-G. Our findings highlight the need to validate the findings of massively parallel sequencing since the experiment generally uses few individuals, and the same type of leukemia can be molecularly quite variable. We

Abbreviations: 3′UTR, 3′ untranslated region; 5′ UTR, 5′ untranslated region; ALL, acute lymphoblastic leukemia; AML, acute myeloid leukemia; B-ALL, acute lymphoblastic leukemia of B cells; cDNA, complementary DNA; CRE, cAMP response element–binding protein; Ct, cycle threshold; DE-miRNA, differentially expressed microRNA; FDR, false discovery rate; HLA-G, human leukocyte antigen G; HRE, hypoxia responsive element; ILT2, Ig-like transcript 2; ILT4, Ig-like transcript 4; ISRE, interferon-stimulated response element; KEGG, Kyoto Encyclopedia of Genes and Genomes; KIR2DL4, killer cell immunoglobulin-like receptor, two Ig domains and long cytoplasmic tail 4; LILRB1, leukocyte immunoglobulin-like receptor B1; LILRB1, leukocyte immunoglobulin-like receptor B2; MHC, major histocompatibility complex; miRNA/miR, microRNA; mRNA, messenger RNA; NK, natural killer cells; PCR, polymerase chain reaction; RREB-1, Ras-responsive element-binding protein 1; RT-PCR, reverse transcription polymerase chain reaction; sHLA-G, soluble human leukocyte antigen G; T CD8, leukocyte T cluster differentiation 8; T-ALL, acute lymphoblastic leukemia of T cells.

showed that miRNA's milieu in leukemia's bone marrow environment varies according to the type of leukemia and that the regulation of sHLA-G expression exerted by the same miRNA may act by a distinct mechanism in different types of leukemia.

Keywords: leukemia, HLA-G, microRNA, bone marrow, posttranscriptional regulation, ALL, AML

INTRODUCTION

HLA-G is a nonclassical MHC class I molecule with particular and distinct characteristics when compared with classical molecules, including restricted tissue expression, little gene variability at the coding region, and significant variability at the regulatory regions. HLA-G exhibits immunomodulatory properties rather than antigen presentation function (Castelli et al., 2014; Carosella et al., 2015; Amodio and Gregori, 2020). Several immune system cell functions, such as the cytotoxic effect of NK and T CD8+ cells, antigen presentation by dendritic cells, among others, are negatively regulated due to HLA-G binding to the inhibitory leukocyte ILT2 (LILRB1), ILT4 (LILRB2), and KIR2DL4 receptors (Colonna et al., 1998; Rajagopalan and Long, 1999; Shiroishia et al., 2003, 2006; Yan and Fan, 2005; Donadi et al., 2011; Rouas-Freiss et al., 2014; Amodio and Gregori, 2020).

HLA-G expression has been primarily related to its immunotolerance in pregnancy (Rouas-Freiss et al., 1997; Xu et al., 2020), but differential *HLA-G* levels can also influence the pathogenesis and outcome of infectious and noninfectious diseases (Yan et al., 2009; Rizzo et al., 2008). In cancer, increased HLA-G levels can alter the immunosurveillance mechanism, favoring tumor immune escape (Yan, 2011; Castelli et al., 2014; Rouas-Freiss et al., 2014; Lin and Yan, 2018). High plasma HLA-G (sHLA-G) levels have been associated with immunosuppression and worse prognosis in several hematological malignancies, such as acute and chronic leukemias (Sebti et al., 2003; Gros et al., 2006; Rizzo et al., 2014; Caocci et al., 2017), Hodgkin's lymphoma (Diepstra et al., 2008; Caocci et al., 2016), and diffuse large B-cell lymphoma (Josionek-Kupnicka et al., 2016).

Little attention has been devoted to the role of bone marrow sHLA-G levels in hematological disorders; however, several lines of evidence indicate its relevant contribution. The sHLA-G levels in the non-leukemic bone marrow are higher than in the peripheral blood (Almeida et al., 2018; Cavalcanti et al., 2017). In a previous study conducted by our group, high bone marrow sHLA-G levels were associated with elevated blood cell count in childhood T-cell acute lymphoblastic leukemia (ALL), a criterion related to poor prognosis (Almeida et al., 2018). Bone marrow sHLA-G levels may be regulated by transcriptional and posttranscriptional factors, which may differentially influence the gene expression depending on the *HLA-G* gene polymorphic sites at regulatory regions and on the microenvironment milieu (Castelli et al., 2010; Castelli et al., 2014; Porto et al., 2015). In this context, differential microRNA expression profiles have been associated with different types of leukemia, such as T-cell ALL (T-ALL) (Schotte et al., 2009; Schotte et al., 2011; Wallaert et al., 2017), B-cell ALL (B-ALL) (Schotte et al., 2009; Schotte et al., 2011), and chronic lymphocytic leukemia (CLL) (Calin et al., 2005), which are targets mainly to genes of innate and adaptive immunity (O'Connell et al., 2010; Mehta and Baltimore, 2016; Omar er al., 2019), particularly genes encoding immune checkpoint molecules (Eichmüller et al., 2017; Hirschberger et al., 2018; Omar et al., 2019).

Since, in T-ALL, only high sHLA-G producers are associated with elevated blood cell count (dos Santos Almeida et al., 2018), this study was designed to clarify the relationship between the sHLA-G levels and the microRNA profiles in the bone marrow of untreated ALL patients to unveil some of the posttranscriptional control of HLA-G in leukemia.

MATERIALS AND METHODS

Study Design, Population, and Ethical Considerations

A group of 15 children with ALL (8 B-ALL and 7 T-ALL) aged between 0 and 18 years were considered for the study of differentially expressed microRNA (DE-miRNA) in bone marrow cells according to the marrow stroma sHLA-G levels. For real-time quantitative PCR validation experiments, we compared the levels of DE-miRNA in another group of ALL patients (23 B-ALL and 11 T-ALL). To demonstrate that the effect observed was related to the lymphoid cell type, we also evaluated samples from 31 children with acute myeloid leukemia (AML). We also included a control group with 14 samples from children whose myelogram confirmed the absence of leukemia. The expressions of the *HLA-G5* and *RREB1* target genes were evaluated in the bone marrow cells of 19 children with B-ALL, 8 with T-ALL, and 28 with AML. All patients were referred, diagnosed, and treated at the IMIP Hospital, Recife, Brazil. Bone marrow aspirates were obtained from each patient at admission and submitted for the isolation of mononuclear cell fractioning for leukemia diagnosis confirmation, performed as previously described (Marques et al., 2011). The samples were stored under −80 °C conditions provided by a laboratory deep freezer, which was protected against power outage by an uninterruptible power supply (UPS) and emergency line. All the patients with leukemia presented at least 70% of blasts in the bone marrow. The samples were obtained after the children's legal guardians provided informed consent, approving their participation in the study. The study protocol was previously approved by the local ethics committee (CAAE: #13296913.3.0000.5190 and #0073.0.095.000-10). The patients' (age and sex) and blast (immunophenotype and genetic alterations) features are shown in **Table 1**.

Determination of Soluble HLA-G Levels in Bone Marrow

A sandwich ELISA assay was used to measure the soluble HLA-G (shredded HLA-G1 and HLA-G5 isoforms) levels, following the

TABLE 1 | Characterization of childhood acute leukemia patients.

Features	B-ALL (*n* = 46)		T-ALL (*n* = 16)		AML (*n* = 44)	
Age at diagnosis						
Minimum	0.3		2.7		0.8	
Maximum	15		16		18	
Mean	5.7		8.8		9.2	
Standard deviation	3.3		3.9		5.2	
Sex						
Male	28		15		25	
Female	18		1		19	
Blast immunophenotype						
	Pro-B	1	ETP	1	AML-M0	6
	Pre-B	40	Pre-T	9	AML-M1	4
	Pre-B	3	Cortical-T	2	AML-M2	11
	Transitional-B	1	Mature-T	4	AML-M3	6
	Mature-B	1			AML-M4	2
					AML-M5	8
					AML-M6	4
					AML-M7	3
Blast genetic alterations						
	t (12;21) *ETV6-RUNX1*	5	*SIL/TAL*	1	t (8;21) *RUNX1-RUNX1T1*	5
	t (1;19) *TCF3-PBX1*	2	*HOX11*	0	inv (16) *CBFB/MYH11*	4
	t (9;22) *BCR/ABL*	2	*HOX11L2*	1	t (15;17) *PML-RARA*	4
	t (4;11) *KMT2A-AFF1*	0			t (9;11) *KMT2A-MLLT3*	2
	Negative	37	Negative	14	Negative	29

Note: ETP, Early T-cell precursor.

manufacturer's instructions (BioVendor Laboratory Medicine, Inc., Czech Republic), with the limit of detection of 0.6 Units/mL. Our previous study detected an average of 200 U/mL ± 25 SD (standard deviation) of sHLA-G levels in the bone marrow stroma of healthy children (Almeida et al., 2018). Based on this, patients presenting between 150 and 250 U/mL of sHLA-G levels in the bone marrow stroma, that is, 200 U/mL plus two standard deviations above or below, were defined as the intermediate producers, those presenting with more than 250 U/mL of sHLA-G were high producers, while those who produced less than 150 U/mL were low producers.

MicroRNA Sequencing Analysis

We used the miRNA sequencing database to evaluate the miRNA expression related to the sHLA-G levels in the marrow stroma. Total RNA extraction, quality assessment, library construction, and miRNA sequencing were performed as described previously (Almeida et al., 2019). miRNA sequencing data have been deposited in the ArrayExpress database at EMBL-EBI (www.ebi.ac.uk/arrayexpress) under the accession number E-MTAB-11621. The sequencing analysis included read quality control and contamination assessment using FastQC (https://www.bioinformatics.babraham.ac.uk/projects/fastqc/) and Cutadapt (Martin, 2011) programs considering a Q-score ≥30 and reads with a length ≥ 17 nucleotides. We used Bowtie (http://bowtie-bio.sourceforge.net/index.shtml) for indexing of human reference genome hg38 version, which is deposited in the UCSC Genome Browser (https://genome.ucsc.edu/). The miRDeep2 2.0.0.8 software (Friedländer et al., 2008) was applied for sequence alignment and miRNA identification, considering miRBase release 21 (http://www.mirbase.org/) (Griffiths-Jones et al., 2006; Kozomara and Griffiths-Jones, 2010). Differentially expressed (DE) miRNA profiles were obtained using the edgeR package (Robinson et al., 2010) and the standard analysis and quantile normalization parameters in the R software (https://cran.r-project.org/), considering at least 20 reads in a minimum of 1 sample, a false discovery rate (FDR) ≤0.05, and a log fold change (logFC) cutoff point of 1 or −1. A comparison of the bone marrow miRNA levels between lower versus higher sHLA-G producers was performed. Target prediction of DE-miRNAs was performed using the miRWalk 2.0 (Dweep et al., 2015), and functional annotation was determined by DAVID tools v.6.7 (Huang et al., 2009; Huang et al., 2009), considering the Kyoto Encyclopedia of Genes and Genomes (KEGG) pathways and Gene Ontology (GO) terms: biological process and FAT level, both with Benjamini–Hochberg (BH)–corrected *p*-values ≤ 0.05. The DE-miRNA alignment with the *HLA-G* gene (NG_029039.1) and mRNA sequences (NM_002127.5) was performed using the RNAhybrid v.2.2 tool (Kruger and Rehmsmeier, 2006), considering the essential features for the interaction of the two molecules, that is, Watson and Crick base pairing, few gaps in the interaction, especially on the seed sequence, seed (2–8 miRNA nucleotide), low free energy (≤−20 Kcal), and interaction with target 3′UTR, coding sequence, and promoter region (Castelli et al., 2014).

A search for genes encoding proteins related to *HLA-G* transcription's positive and negative regulation was performed, considering previous studies that describe or review the action of such molecules (Moreau et al., 1999; Gobin et al., 2002; Flajollet

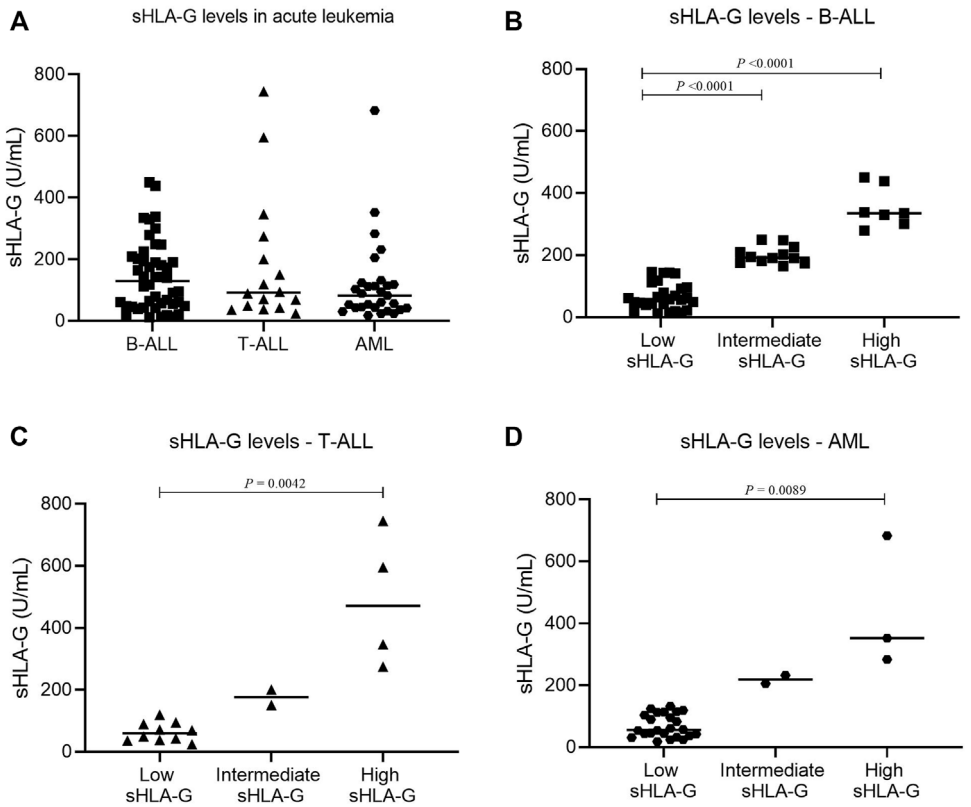

FIGURE 1 | Comparison of sHLA-G levels in the bone marrow stroma of pediatric acute leukemia. **(A)** sHLA-G in B-ALL (square, *n* = 46), T-ALL (triangle, *n* = 16), and AML (hexagon, *n* = 29); **(B)** sHLA-G levels in B-ALL (square: low, *n* = 27; intermediate, *n* = 12; high, *n* = 7); **(C)** sHLA-G levels in T-ALL (triangle: low, *n* = 10; intermediate, *n* = 2; high, *n* = 4); and **(D)** sHLA-G levels in AML (hexagon: low, *n* = 24; intermediate, *n* = 2; high, *n* = 3). For comparison of the three groups, the Kruskal–Wallis test was used followed by Dunn's multiple comparison for two groups.

TABLE 2 | miRNAs differentially expressed between childhood ALL high and low soluble HLA-G producers with FDR ≤0.05.

miRNA	LogFC	FDR
Upregulated in high sHLA-G producers		
hsa-miR-1248	5.427	0.006
hsa-miR-205-5p	5.870	0.014
hsa-miR-3196	3.824	0.035
hsa-miR-4485-3p	5.380	0.006
hsa-miR-4488	5.036	0.013
hsa-miR-4516	3.560	0.028
hsa-miR-451a	3.003	0.014
hsa-miR-4532	3.846	0.014
hsa-miR-486-5p	2.910	0.014
hsa-miR-5096	2.589	0.030

Note: LogFC, fold change in base 2 logarithm; FDR, false discovery rate.

et al., 2009; Castelli et al., 2014; Yaghi et al., 2016). The positive regulators that were considered were *CREB1*, *CREBBP*, *JUN*, *ATF2*, *IRF1*, *HIF1A*, and *IL10*. The negative regulators that were sought were *RREB1*, *HDAC1*, *CTBP1*, and *CTBP2*. We also considered *REST*, *EHMT1*, *ZEB1*, *ZEB2*, *ZNF217*, and *LSD1* genes since the proteins are members of the CTBP core complex (Shi et al., 2003; Shi et al., 2004) and may exert an indirect influence on *HLA-G* expression. All the positive and negative regulators of *HLA-G* those were considered were analyzed for their ability to interact with the differentially expressed miRNAs in this study, according to the miRTarBase v. 8.0, a database of experimentally validated interactions (Chou et al., 2018).

MicroRNA Validation by Reverse Transcription Quantitative Polymerase Chain Reaction Assays

For validation experiments, we selected the four miRNAs most likely to target the *HLA-G* gene (NG_029039.1) and messenger RNA (NM_002127.5) based on the sequence alignment analysis (RNAhybrid v.2.2) (Krûger, Rehmsmeier, 2006). The representative scheme showing the interaction site between *HLA-G* and the four miRNAs selected for validation was constructed using the ApE v2.0.61 software (https://jorgensen.biology.utah.edu/wayned/ape/). The TaqMan Advanced miRNA cDNA Synthesis Kit (Life Technologies, Foster City, California, USA), TaqMan Advanced miRNA Assay (reference: miR-191-5p; targets: miR-5096, miR-4516, miR-4488, miR-486-5p; Life Technologies), and TaqMan Fast Advanced Master Mix

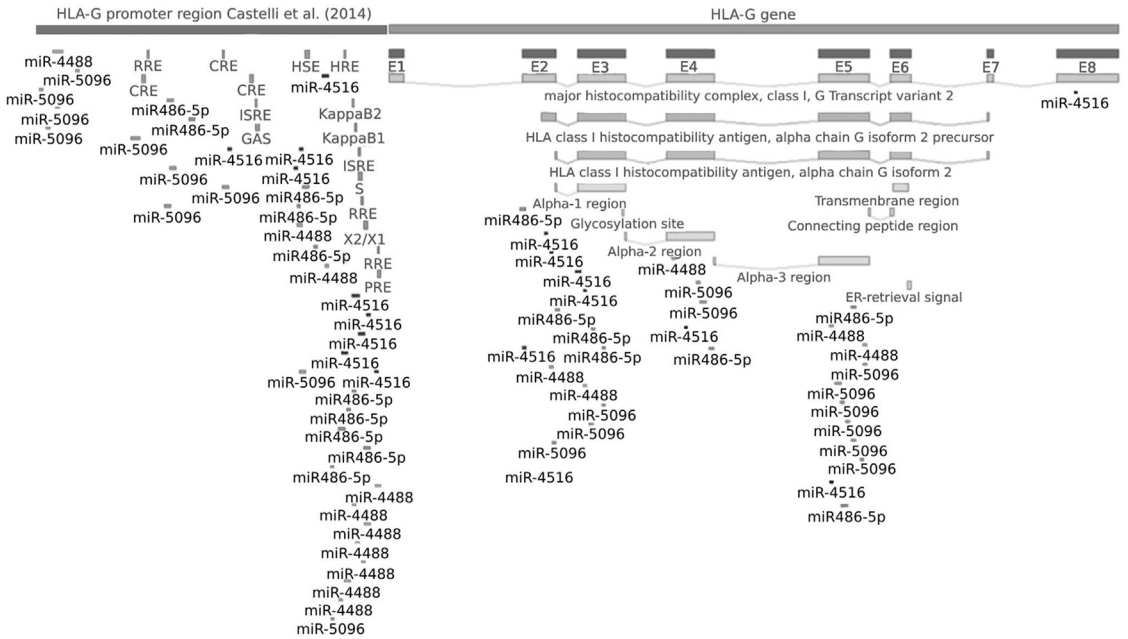

FIGURE 2 | *HLA-G* gene binding sites for hsa-miR-5096, hsa-miR-4516, hsa-miR-486-5p, and hsa-miR-4488. The miRNA cascade in the figure indicates putative binding sites in the target gene. Note: the promoter region was mapped and analyzed as described by Castelli et al. (2014). Coding sequence was considered as described by GenBank (<https://www.ncbi.nlm.nih.gov/nuccore/NG_029039.1>), and exon 8 is considered as the *HLA-G* 3′UTR [5].

TABLE 3 | Positive and negative regulators of *HLA-G* expression potentially targeted by the DE-miRNAs in childhood ALL, encompassing high marrow sHLA-G producers.

	miR-1248	miR-205-5p	miR-3196	miR-4488	miR-4516	miR-451a	miR-4532	miR-486-5p	miR-5096
Positive regulators									
CREB1	X	X	—	—	X	—	—	—	X
CREBBP	X	—	X	X	—	—	—	—	X
JUN	—	X	—	X	—	—	—	—	—
ATF2	X	X	—	—	—	X	—	X	X
IRF1	X	X	—	—	—	—	X	—	X
HIF1A	X	—	—	—	—	—	—	—	—
IL10	—	—	—	—	—	—	—	—	X
Negative regulators									
RREB-1	X	X	X	X	X	—	—	X	X
HDAC1	X	—	—	—	X	—	—	—	X
CTBP1/2	X	X	X	—	X	—	X	X*	X*
REST	X	X	—	—	X	—	—	X	X
EHMT1	—	—	X	X	—	—	—	—	—
ZEB1/2	X	X	—	—	X	—	—	X**	X**
ZnF217	—	—	—	—	X	—	—	X	X

*Note: * only* CTBP2 *was a target of miR-486-5p and miR-5096. ** miR-486-5p putative targets only* ZEB1, *and miR-5096 targets only* ZEB2. *The hsa-miR-4485-3p was not included in the table because it does not target any of the* HLA-G *regulators above.*

(Life Technologies) were used according to the manufacturer's instructions to evaluate the miRNA expression. Reverse transcription PCR (RT-PCR) assays were performed in a SimpliAmp Thermal Cycler (Applied Biosystems, Foster City, California, USA) and quantitative PCR (q-PCR) in a QuantStudio 5 Real-Time System (Applied Biosystems) and 7500 Real-Time System (Applied Biosystems) according to the manufacturer's instructions.

Expression of *HLA-G5* and *RREB1* mRNA by Quantitative Polymerase Chain Reaction

To study the relative expression of *HLA-G5* and *RREB1*, cDNA synthesis was performed from total RNA using the enzyme M-MLV-RT 200 U/μL (Invitrogen, Carlsbad, California, USA) and SimpliAmp Thermal Cycler equipment (Applied Biosystems). *HLA-G5* primers have been described in Gomes et al. (2018), and they were designed to target all *RREB1* isoforms

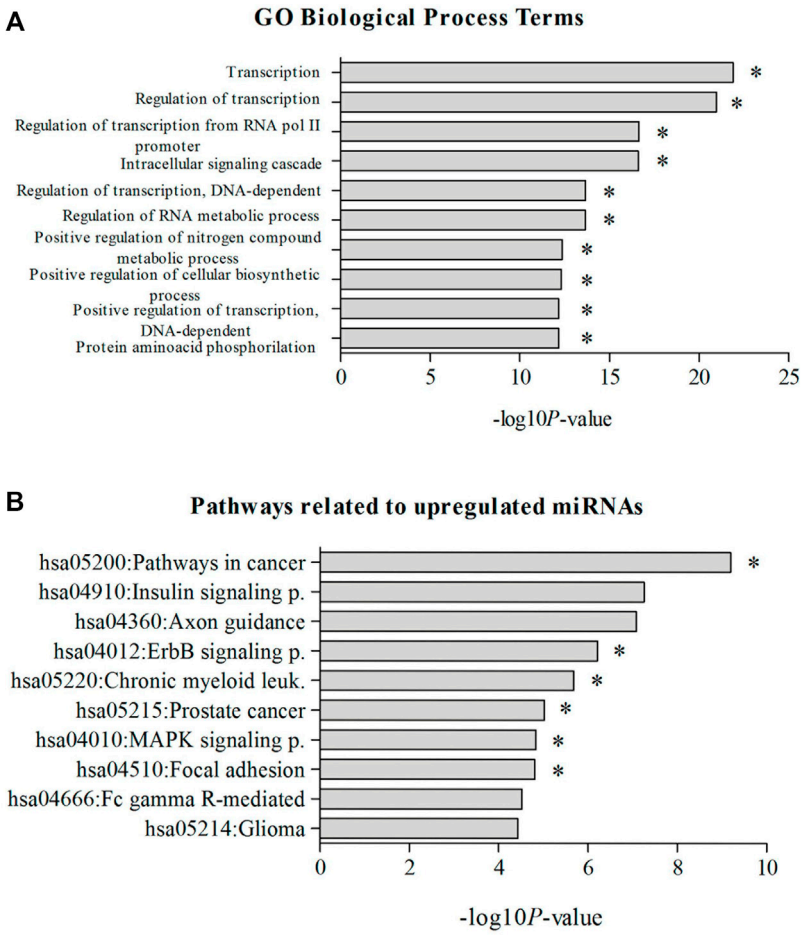

FIGURE 3 | Most significant KEGG pathways. **(A)** GO, biological process terms; **(B)** related to upregulated miRNAs in childhood in ALL patients with high sHLA-G levels. Note: *pathways containing genes coding for positive or negative regulators of *HLA-G* expression. KEGG pathway categories: hsa05200:Pathways in cancer, hsa04910:Insulin signaling pathway, hsa04360:Axon guidance, hsa04012:ErbB signaling pathway, hsa05220:Chronic myeloid leukemia, hsa05215:Prostate cancer, hsa04010:MAPK signaling pathway, hsa04510:Focal adhesion, hsa04666:Fc gamma R–mediated phagocytosis, hsa05214:Glioma. GO, biological process terms: GO:0006350—transcription, GO:0045449—regulation of transcription, GO:0006357—regulation of transcription from RNA polymerase II promoter, GO:0007242—intracellular signaling cascade, GO:0006355—regulation of transcription, DNA dependent, GO:0051252—regulation of RNA metabolic process, GO:0051173—positive regulation of nitrogen compound metabolic process, GO:0031328—positive regulation of cellular biosynthetic process, GO:0045893—positive regulation of transcription, DNA dependent, GO:0006468—protein amino acid phosphorylation.

(RREB-1F: 5′-AAAGATGGTAGAAGACGGG-3′ and RREB-1R: 5′-GTGGGTTATCTGAATGGGTC-3′). Expression was performed using the SYBR Green DNA intercalator (Applied Biosystems).

Statistical Analysis

The normality distribution of the miRNA–mRNA expression was determined using the Shapiro–Wilk and Kolmogorov–Smirnov tests. For comparison between two or three groups, the Mann–Whitney U and Kruskal–Wallis tests were used, respectively. A Spearman's correlation coefficient analysis was performed between miRNA and mRNA expressions. In different experiments, the number of samples may have differed due to the shortage of clinical samples that did not allow all analyses to be performed. The GraphPad Prism V.5.01 (GraphPad Software, Inc.) was used to perform the analyses, considering a significant p-value ≤ 0.05. For miRNA relative expression analysis, ΔCt (cycle threshold) values were determined based on the following equation: ΔCt = Ct (target miRNA) – Ct (reference miRNA). The Ct values were the average duplicates with a standard deviation (SD) ≤ 0.5. The same equation and parameters were used to calculate the mRNA expression, considering *HLA-G5* or *RREB1* as the target gene and *GAPDH* as the reference gene.

RESULTS

Soluble HLA-G Levels in Pediatric Acute Leukemia Patients

Bone marrow sHLA-G levels in childhood AML, T-ALL, and B-ALL showed no statistical differences ($p = 0.3483$). There were

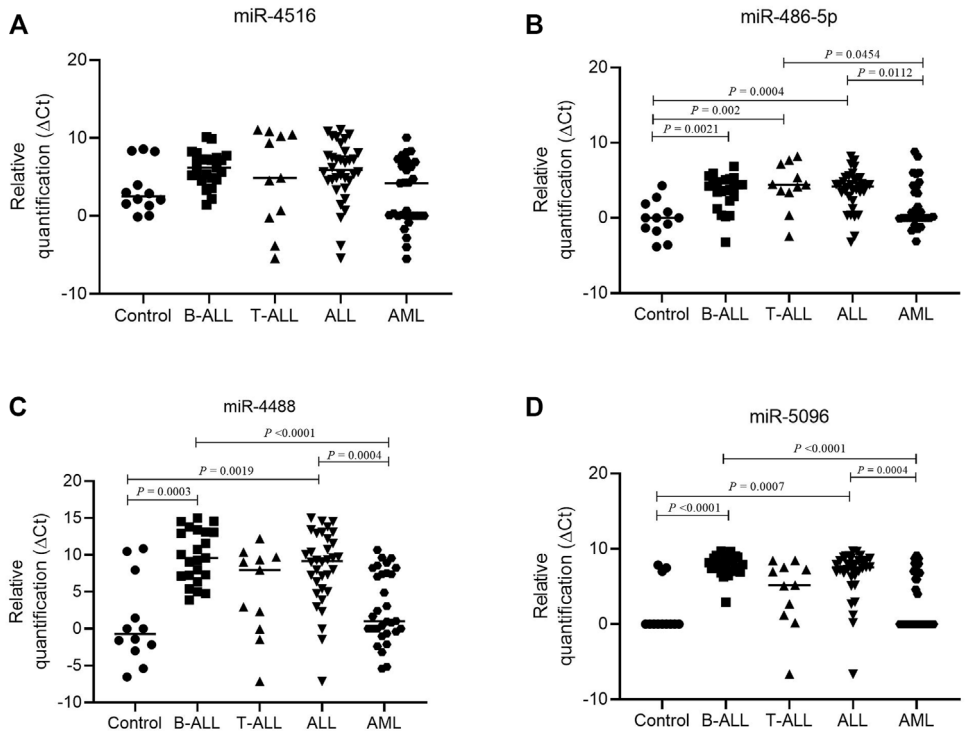

FIGURE 4 | Difference in miRNA expression in lymphoid and myeloid leukemia. **(A)** Relative expression of hsa-miR-4516 in control (circle, *n* = 12), B-ALL (square, *n* = 23), T-ALL (triangle, n = 11), ALL (inverted triangle, *n* = 34), and AML (hexagon, *n* = 31) groups; **(B)** relative expression of hsa-miR-486-5p in control (circle, *n* = 12), B-ALL (square, *n* = 23), T-ALL (triangle, *n* = 11), ALL (inverted triangle, *n* = 34), and AML (hexagon, *n* = 31) groups; **(C)** relative expression of hsa-miR-4488 in control (circle, *n* = 12), B-ALL (square, *n* = 23), T-ALL (triangle, *n* = 11), ALL (inverted triangle, *n* = 34), and AML (hexagon, *n* = 31) groups; and **(D)** relative expression of hsa-miR-5096 in control (circle, *n* = 12), B-ALL (square, *n* = 23), T-ALL (triangle, *n* = 11), ALL (inverted triangle, *n* = 34), and AML (hexagon, *n* = 31) groups. For comparing three or more groups, the Kruskal–Wallis test was used followed by Dunn's multiple comparison for two groups. Note: For delta Ct, the higher the values, the lower the miRNA expression.

low, intermediate, and high sHLA-G producers in each leukemia subtype (**Figure 1**).

Identification of Cellular MicroRNAs Upregulated in High Marrow sHLA-G Producers

The analysis of differentially expressed miRNA profiles in the bone marrow cells of non-treated children with ALL revealed 10 miRNAs upregulated in high sHLA-G producers (logFC >2.0) when compared with low sHLA-G producers (**Table 2**).

Target Prediction of Differentially Expressed MicroRNAs and Functional Annotation

The analysis of target gene prediction with the 10 miRNAs showed 14,518 potential gene targets, of which only the hsa-miR-5096 was predicted as a putative regulator of *HLA-G* mRNA by three different algorithms and, by less number, the hsa-miR-4516, hsa-miR-4488, and hsa-miR-486-5p miRNAs (**Figure 2**). All four miRNAs presented several anchor sites at the promoter and coding regions of the *HLA-G* gene. Some of the binding sites of miRNAs are in transcription factor zones. The cAMP-responsive element (CRE) is a predicted site for hsa-miR-5096 binding; the heat shock element (HSE) for hsa-miR-486-5p; the hypoxia-responsive element (HRE) for hsa-miR-4516 and hsa-miR-4488; the Kappa B1, Kappa B2 (NF-κB responsive element), interferon-stimulated response element (ISRE) module, and the SXY module for hsa-miR-4488, hsa-miR-4516, and hsa-miR-486-5p; and the Ras-responsive element (RRE) and progesterone-responsive element (PRE) for hsa-miRNA-4516 and hsa-miR-4488. The hsa-miR-5096 did not bind to any of these transcription-binding sites. Only the hsa-miR-4516 targets the *HLA-G* 3′ untranslated region at the position covering the +3035 C/T polymorphic site.

The analysis of the miRNA gene targets for functional annotation revealed several biological pathways involving genes already described in the literature that may be positive or negative regulators for the *HLA-G* gene. **Table 3** shows the genes involved in the induction or repression of *HLA-G* transcription and their putative miRNA regulators identified in this study.

Considering the 10 most significant KEGG pathways related to all upregulated miRNAs in high sHLA-G producers, 6 included the genes encoding known positive (*CREB1*, *CREBBP*, *JUN*, and *IL10*) and negative (*CTBP1/2* and *HDAC1*) regulators of *HLA-G* expression (**Figure 3**), as well in other pathways associated with leukemogenesis, namely, hsa04310:Wnt, hsa04660:T-cell receptor, hsa04062:

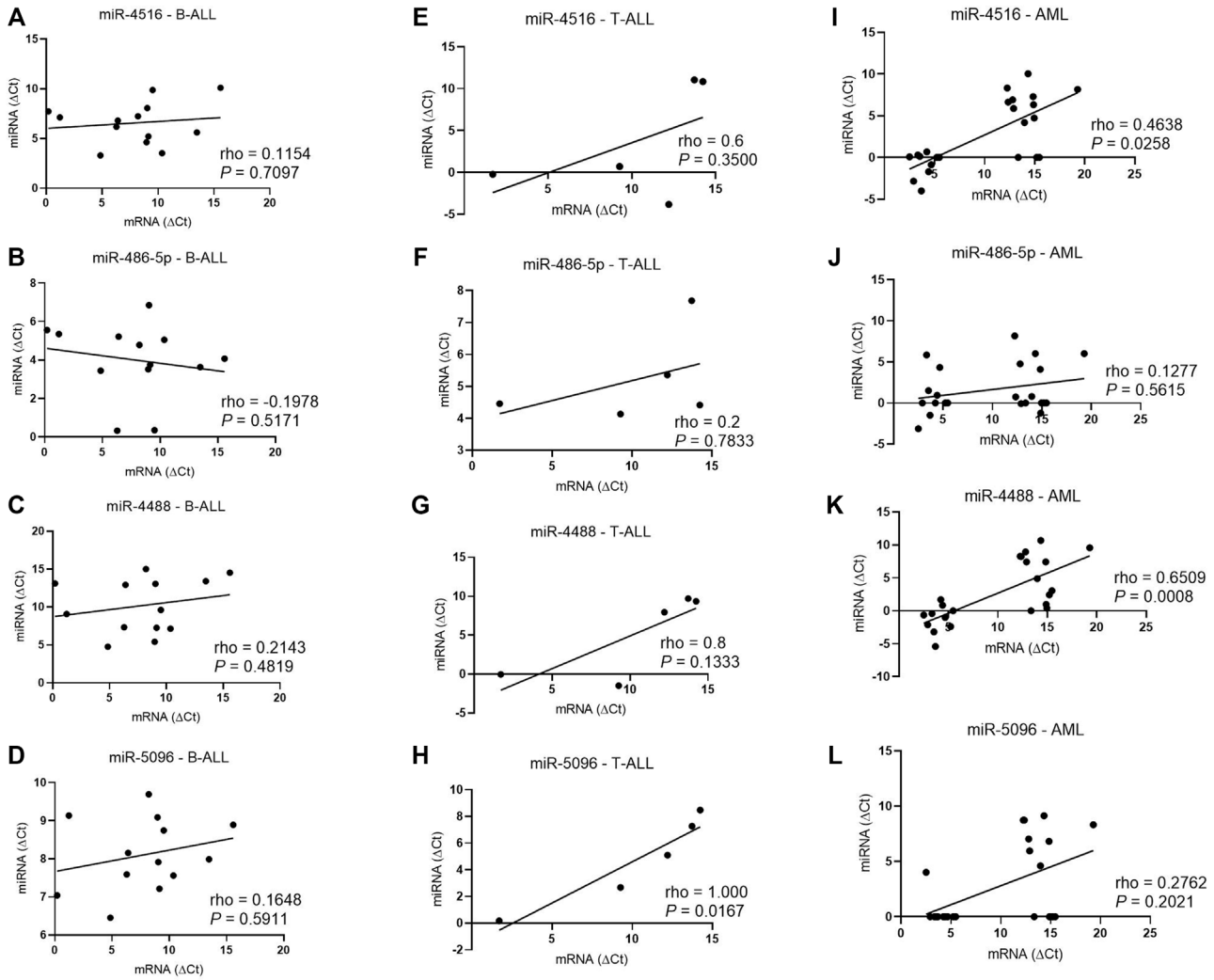

FIGURE 5 | Correlation coefficient analysis between miRNAs and HLA-G5 mRNA levels in the bone marrow from patients with untreated leukemia. **(A)** Correlation coefficient analysis between hsa-miR-4516 and HLA-G5 in B-ALL (n = 13); **(B)** correlation coefficient analysis between hsa-miR-486-5p and HLA-G5 in B-ALL (n = 13); **(C)** correlation coefficient analysis between hsa-miR-4488 and HLA-G5 in B-ALL (n = 13); **(D)** correlation coefficient analysis between hsa-miR-5096 and HLA-G5 in B-ALL (n = 13); **(E)** correlation coefficient analysis between hsa-miR-4516 and HLA-G5 in T-ALL (n = 5); **(F)** correlation coefficient analysis between hsa-miR-486-5p and HLA-G5 in T-ALL (n = 5); **(G)** correlation coefficient analysis between hsa-miR-4488 and HLA-G5 in T-ALL (n = 5); **(H)** correlation coefficient analysis between hsa-miR-5096 and HLA-G5 in T-ALL (n = 5); **(I)** correlation coefficient analysis between hsa-miR-4516 and HLA-G5 in AML (n = 23); **(J)** correlation coefficient analysis between hsa-miR-486-5p and HLA-G5 in AML (n = 23); **(K)** correlation coefficient analysis between hsa-miR-4488 and HLA-G5 in AML (n = 23); and **(L)** correlation coefficient analysis between hsa-miR-5096 and HLA-G5 in AML (n = 23). For the correlation analysis, the Spearman's correlation coefficient was used.

chemokine, hsa04662:B-cell receptor, hsa04330:Notch, and hsa04350:TGF-beta signaling pathways. Most of the statistically significant GO biological processes involved in regulating transcription and cell signaling cascade include inducers (*CREB1*, *CREBBP*, *ATF2*, *JUN*, and *IL10*) and repressors (*RREB1*, *CTBP1/2*, and *HDAC1*) of the *HLA-G* expression (**Figure 3**).

Confirmation of Bone Marrow MicroRNA Expression in Childhood Leukemia

The comparison of the miRNA levels in the bone marrow showed that miR-486-5p, miR-4488, and miR-5096 levels were significantly higher in controls than in ALL, particularly B-ALL, and only miR-486-5p was higher in controls than in T-ALL ($p < 0.05$). No significant differences in miRNA levels were observed between controls and AML bone marrow samples ($p > 0.05$). In addition, the AML samples showed higher miR-4488 and miR-5096 levels than did B-ALL and higher miR-486-5p levels than did T-ALL ($p < 0.05$) (**Figure 4**).

Correlations Between MicroRNAs and *HLA-G5* mRNA Levels

In T-ALL, the hsa-miR-5096 levels correlated positively with the *HLA-G5* mRNA expression (rho = 1; $p = 0.0167$) (**Figure 5**). In myeloid leukemia, the hsa-miR-4516 (rho = 0.4638; $p = 0.0258$) and hsa-miR-4488 (rho = 0.6509, $p = 0.0008$) levels were also

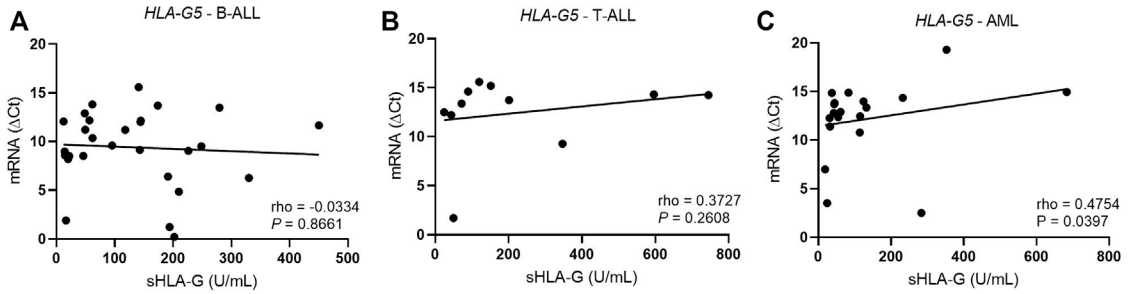

FIGURE 6 | Correlation coefficient analysis between HLA-G5 mRNA and sHLA-G levels in the bone marrow from patients with untreated leukemia. **(A)** Correlation coefficient analysis between HLA-G5 and sHLA-G in B-ALL (n = 28); **(B)** correlation coefficient analysis between HLA-G5 and sHLA-G in T-ALL (n = 11); and **(C)** correlation coefficient analysis between HLA-G5 and sHLA-G in AML (n = 19). For the correlation analysis, the Spearman's correlation coefficient was used.

positively correlated with the *HLA-G5* mRNA levels. However, the increase in *HLA-G5* mRNA expression was translated into a significant decrease in sHLA-G only in myeloid leukemia, with moderate and significant Spearman's coefficient (rho = 0.475; p = 0.0397), but neither in B-ALL nor T-ALL (**Figure 6**). This was assumed considering that the delta Ct values are inversely proportional to the mRNA levels.

In addition, increased hsa-miR-5096 (rho = 0.72; p = 0.0144) and hsa-miR-4516 (rho = 0.67; p = 0.0277) levels (low ΔCt) correlated with decreased sHLA-G protein levels in T-ALL, but only hsa-miR-5096 correlated also with the HLA-G mRNA (**Figure 7**), but only hsa-miR-5096 correlated also with the *HLA-G* mRNA.

For a detailed analysis, the samples were categorized according to the bone marrow miRNA levels in the low or high miRNA level group, and sHLA-G levels in both groups were compared. In T-ALL, patients with high levels of hsa-miR-5096 and miR-4516 had a median sHLA-G value of 46 U/mL, while patients with low levels of miRNA had a median sHLA-G value of 200 U/mL (p = 0.0519). Overall, high miRNA expressions were associated with homogenous low sHLA-G levels, while low miRNA levels were associated with largely variable sHLA-G levels, which contributed to the borderline significance of the differences. In B-ALL, the groups of low and high miRNA levels were not capable of segregating samples with different sHLA-G levels. In AML, the difference between the median value of sHLA-G between the low- and high-miRNA-level groups was not significant (**Figure 8**).

Considering that the *RREB1* gene is a target for the four studied miRNAs and that the RREB-1 protein has three potential binding sites in the *HLA-G* gene promoter, the relationship between the *RREB1* mRNA levels and each miRNA and *HLA-G5* mRNA levels were evaluated. The results revealed that only in B-ALL, the *RREB1* and *HLA-G5* mRNA expressions were positively correlated (rho = 0.5632, p = 0.0018). In addition, only the hsa-miR-4488 correlated positively with *RREB1* mRNA expression (rho = 0.4368, p = 0.0615), but it did not reach significance.

DISCUSSION

In this study, the evaluation of the differential expression profiles of miRNAs in the bone marrow among leukemia patients exhibiting high and low marrow sHLA-G levels envisaged the identification of new regulators of *HLA-G* that may play a role in cancer immunosurveillance (Castelli et al., 2014; Lin and Yan, 2018; Aguagué et al., 2011; Paul et al., 1998). Few or no studies have reported many of the 10 differentially expressed miRNAs as modulators of HLA-G expression. Interestingly, according to the next-generation sequencing analysis, all miRNAs were upregulated in the group of high HLA-G producers, suggesting that these miRNAs target the *HLA-G* gene sequence; however, they do not downregulate *HLA-G* expression. Previous studies focusing on the *TNF* gene (Vasudevan et al., 2007) have shown alternative mechanisms of action of miRNAs, increasing the transcription of the target gene and the expression of target proteins, dependent on the micro-ribonucleoproteins (microRNPs) and gene regions (promoter or coding region), with which miRNAs interact (Vasudevan et al., 2007; Place et al., 2008). The sequence alignment analysis showed that the hsa-miR-5096, hsa-miR-4516, hsa-miR-4488, and hsa-miR-486-5p miRNAs are capable of binding multiple sites at coding and 5′ untranslated region of the *HLA-G* gene and a unique binding site for hsa-miR-4516 at the 3′ untranslated region.

The validation experiments showed that the hsa-miR-4516 levels in the bone marrow did not differ significantly in non-leukemic and leukemia samples. However, the relationship between the high hsa-miR-4516 levels and low sHLA-G protein levels in the bone marrow in T-ALL indicated that the classic mechanism of negative regulation by the miRNA exerted at the 3′UTR of the *HLA-G* gene was active. The correlation coefficient analysis revealed that increased hsa-miR-4516 levels (low delta Ct values) correlated with lower sHLA-G levels. Previously, a study reported the hsa-miR-4516 as a potential regulator of *HLA-G* expression based on *in silico* study, which showed a putative binding between the two molecules but lacked functional studies (Porto et al., 2015). The predicted interaction between hsa-miR-4516 and *HLA-G* occurs at the +3035 polymorphic site of 3′UTR of the *HLA-G* gene, which might affect the hsa-miR-4516–mediated downregulation of *HLA-G* expression. In T-ALL, we also observed that increased hsa-miR-5096 expression levels correlated positively with *HLA-G5* mRNA and negatively with sHLA-G levels. One of the predicted

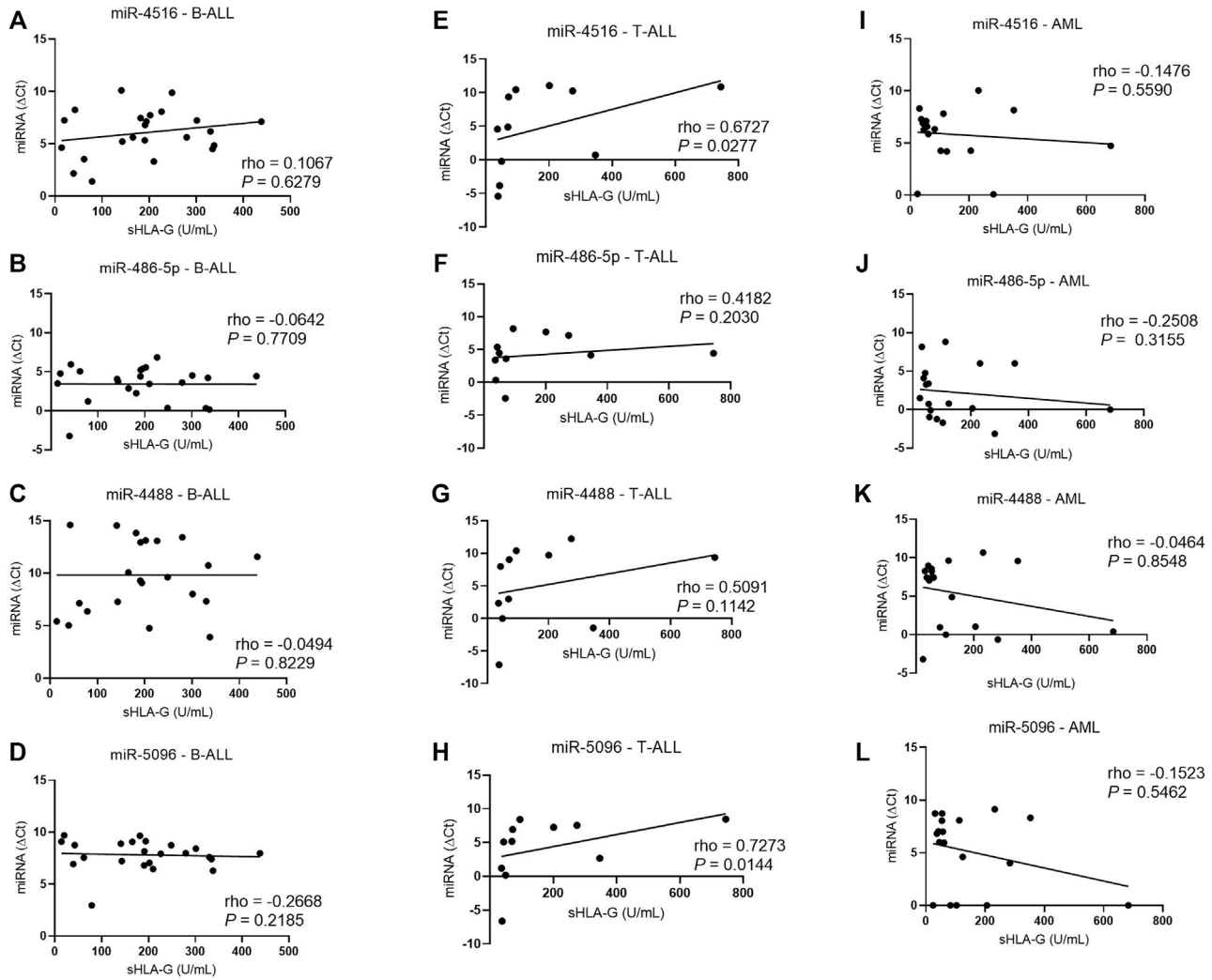

FIGURE 7 | Correlation coefficient analysis between miRNAs expression and sHLA-G levels in the bone marrow from patients with untreated leukemia. **(A)** Correlation between hsa-miR-4516 and sHLA-G in B-ALL ($n = 23$); **(B)** correlation between hsa-miR-486-5p and sHLA-G in B-ALL ($n = 23$); **(C)** correlation between hsa-miR-4488 and sHLA-G in B-ALL ($n = 23$); **(D)** correlation between hsa-miR-5096 and sHLA-G in B-ALL ($n = 23$); **(E)** correlation between hsa-miR-4516 and sHLA-G in T-ALL ($n = 11$); **(F)** correlation between hsa-miR-486-5p and sHLA-G in T-ALL ($n = 11$); **(G)** correlation between hsa-miR-4488 and sHLA-G in T-ALL ($n = 11$); **(H)** correlation between hsa-miR-5096 and sHLA-G in T-ALL ($n = 11$); **(I)** correlation between hsa-miR-4516 and sHLA-G in AML ($n = 18$); **(J)** correlation between hsa-miR-486-5p and sHLA-G in AML ($n = 18$); **(K)** correlation between hsa-miR-4488 and sHLA-G in AML ($n = 18$); and **(L)** correlation between hsa-miR-5096 and sHLA-G in AML ($n = 18$). For the correlation analysis, the Spearman's correlation coefficient was used.

binding sites for the hsa-miR-5096 is the CRE site at the *HLA-G* promoter, which induces gene transcription in response to cAMP (Gobin et al., 2002). The hsa-miR-5096 was reported as a potential tumor suppressor miRNA capable of inhibiting the proliferation, migration, and invasion of breast cancer cells *in vitro* by targeting the SLC7A11 gene, which is related to ferroptosis resistance (Yadav et al., 2021). On the other hand, Thuringer et al. (2017) demonstrated an oncogene role for hsa-miR-5096 whose high expression contributed to increased invasiveness of glioblastoma cells by decreasing Kir4.1 protein levels, a K+ channel involved in the ionic homeostasis in the brain (Thuringer et al., 2017). The hsa-miR-5096 seems to target different genes in distinct cell types and microenvironments with a different action mechanism, which may occur also in leukemia. Similarly, the cell heterogeneity could partially explain the difference between miRNA sequencing results and qPCR experiments. In addition, it should be considered that the sHLA-G protein levels depend on the resultant effect of the negative and positive regulators of the *HLA-G* expression, the own expression of which is regulated by hsa-miR-5096 and hsa-miR-4516.

In B-ALL, we observed a moderate correlation between the *HLA-G* expression and one of its negative regulators, the RREB-1, and apparently, the *RREB1* expression correlated with hsa-miR-4488 levels in the bone marrow. The RREB-1 protein is a well-known repressor of *HLA-G* expression, interacting with the *HLA-G* gene at three different sites in the promoter region (Flajollet

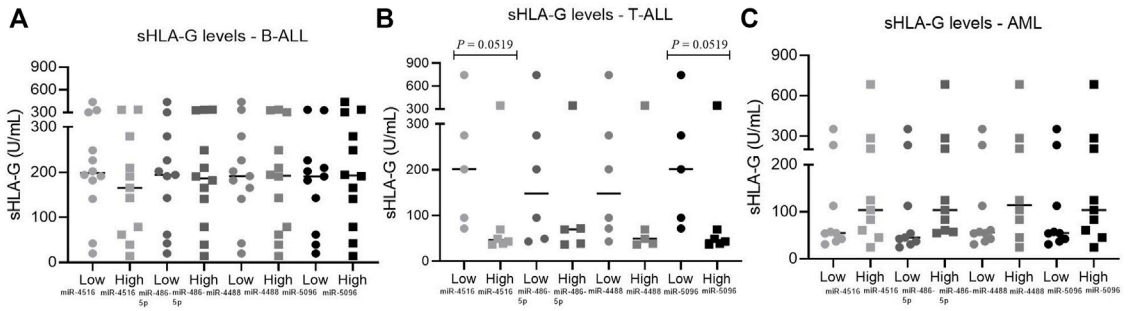

FIGURE 8 | Relationship between sHLA-G with miRNAs expression in leukemic bone marrow. **(A)** Relationship between sHLA-G and miRNAs expression in B-ALL: low miR-4516, $n = 12$; high miR-4516, $n = 11$; low miR-486-5p, $n = 11$, high miR-486-5p, $n = 12$; low miR-4488, $n = 11$, high miR-4488, $n = 12$; low miR-5096, $n = 11$, high miR-5096, $n = 12$; **(B)** relationship between sHLA-G and miRNAs expression in T-ALL: low miR-4516, $n = 5$, high miR-4516, $n = 6$; low miR-486-5p, $n = 6$, high miR-486-5p, $n = 5$; low miR-4488, $n = 6$, high miR-4488, $n = 5$; low miR-5096, $n = 5$, high miR-5096, $n = 6$; **(C)** relationship between sHLA-G and miRNAs expression in AML: low miR-4516, $n = 9$, high miR-4516, $n = 9$; low miR-486-5p, $n = 9$, high miR-486-5p, $n = 9$; low miR-4488, $n = 10$, high miR-4488, $n = 8$; low miR-5096, $n = 9$, high miR-5096, $n = 9$. For comparison of two groups, the Mann–Whitney test was used.

et al., 2009). In addition, it is important to note that RREB-1 acts in a complex with other proteins, HDAC1, CtBP1/2, REST, EHMT1, ZEB1/2, and ZnF217, which are involved in chromatin remodeling and transcription machinery assembly (Delcuve et al., 2012; Barroilhet et al., 2013; Ray et al., 2014; Vitkevičienė et al., 2019) and are also targets for these differentially expressed miRNAs. However, the role of hsa-miR-4488 at the RRE site is unclear, since hsa-miR-4488 regulates the expression of RREB1, which induces the downregulation of *HLA-G* expression by binding to the RRE site. Further studies evaluating the role of miRNA/*RREB1*/*HLA-G* interaction may clarify whether hsa-miR-4488 competes with the RREB-1 factor for the RRE site at the *HLA-G* promoter. Hsa-miR-4488 has been reported with aberrant expression in other cancers, such as colorectal cancer (Zhang et al., 2014) and melanoma (Fattore et al., 2019), and its increased expression has been associated with drug resistance in melanoma cell lines (Fattore et al., 2019). To associate the high hsa-miR-4488 levels in the bone marrow with chemotherapy resistance in T-ALL, a larger casuistic would be necessary.

In AML, the hsa-miR-4488, hsa-miR-486-5p, and hsa-miR-5096 levels in the bone marrow were higher than were in ALL, hsa-miR-4488 and hsa-miR-4516 expressions correlated with *HLA-G5* expression ($p = 0.0008$ and $p = 0.0258$, respectively), and the increased *HLA-G5* expression correlated with low sHLA-G levels, but no miRNA expression correlated with the sHLA-G levels.

Previous studies of extracellular vesicles from breast cancer cells reported that hsa-miR-4488 was negatively correlated to the mitochondrial calcium uniporter and that was related to the suppression of angiogenesis of vascular endothelial cells by acting on *CX3CL1*. Its absence or absent expression appeared to increase angiogenesis and favor metastasis in breast cancer cells (Zheng et al., 2020). This study was the first to report the effect of hsa-miR-4488 in hematological cancer, with a significantly less hsa-miR-4488 level in AML and a much lesser one in ALL when compared to the non-leukemic bone marrow. The hsa-miR-4488 mechanism of action in physiologic and pathologic bone marrow remains unknown.

Besides the high levels of hsa-miR-486-5p in AML when compared to ALL, there was no significant difference between the AML levels and non-leukemic bone marrow levels. The higher miRNA level in non-leukemic bone marrow corroborates the function of hsa-miR-486-5p in the induction of growth and survival of megakaryocyte–erythroid progenitors (Wang et al., 2015). The hsa-miR-486-5p level was reported to be downregulated in the peripheral blood leukocytes in untreated chronic myeloid leukemia (CML) adult patients, which was upregulated after imatinib treatment (Ninawe et al., 2021). Another study showed that high miR-486-5p levels induced apoptosis and caspase-3 activity in leukemic cells by upregulating the *FOXO1* mRNA expression (Liu et al., 2019). On the contrary, another study suggested that hsa-miR-486-5p might be involved in the growth and survival of leukemic cells in AML secondary to Down syndrome, which generally compromises the megakaryocyte–erythroid precursors (Wang et al., 2015). Our casuistries were of children with leukemia, and cases of CML are rare; therefore, the mechanism of action of hsa-miR-486-5p in ALL remains unclear. Is it associated with the reduced number of megakaryocyte–erythroid progenitors observed?

Nine of 10 hsa-miRNAs revealed in this study, namely, hsa-miR-1248, hsa-miR-205-5p, hsa-miR-3196, hsa-miR-4488, hsa-miR-4516, hsa-miR-451a, hsa-miR-4532, hsa-miR-486-5p, and hsa-miR-5096, exhibited the ability to interact with at least one gene (*CREB1*, *CREBBP*, *JUN*, *ATF2*, *IRF1*, *HIF1A*, and *IL10*) coding for a protein involved in the induction of *HLA-G* expression. Moreover, the CREB1, CREBBP, C-Jun, ATF-2, IRF-1, and HIF-1A are well-known proteins that bind to specific promoter sites of the *HLA-G* gene activating its transcription (Gobin et al., 2002; Mouillot et al., 2007; Castelli et al., 2014; Garziera et al., 2017). Soluble mediators, such as IL-10, IFN-β, and IFN-γ cytokines and progesterone hormone, are capable of inducing *HLA-G* expression *via* intracellular signaling pathway; therefore, a possible interaction between miRNAs

mentioned above in these mediators' genes can also decrease the *HLA-G* expression (Moreau et al., 1999; Chu et al., 1999; Lefebvre et al., 1999; Yie et al., 2006).

The resulting effect of all variables directly or indirectly involved in the *HLA-G* expression in physiological and pathological bone marrow is not yet known. Our study added new information on the regulation of HLA-G levels in leukemia. We identified four new miRNA molecules associated with the *HLA-G* expression regulation and its predicted target genes. We showed that some miRNA and target gene levels correlated with the *HLA-G* mRNA and protein levels in the tumor microenvironment. We also showed that the miRNA expression and regulation differed according to the leukemia type.

Future studies in a more extensive series of patients could support the hypothesis that miRNAs' regulation of sHLA-G expression may play a role in the prognosis of acute leukemias, indicating the potential translation of these results in clinical practice, possibly as a new prognosis marker and target for immunotherapy.

DATA AVAILABILITY STATEMENT

The data presented in the study are deposited in the ArrayExpress database at EMBL-EBI (www.ebi.ac.uk/arrayexpress) repository, accession number E-MTAB-11621.

ETHICS STATEMENT

The studies involving human participants were reviewed and approved by CAAE 13296913.3.0000.5190 and #0073.0.095.000-10. Written informed consent to participate in this study was provided by the participants' legal guardian/next of kin.

AUTHOR CONTRIBUTIONS

RA, TG, NL-S, and ED conceived and designed the study, did the formal analysis, and wrote the manuscript. RA, TG, FA, SO, and JS conducted the experimental work. NL-S and ED applied for financial support and managed the project. All the authors contributed to the article and approved the submitted version.

FUNDING

This work was supported by grants from 1) the Brazilian National Council for Scientific and Technological Development (CNPq) (PROEP-IAM2019 #400786/2019-2, #310364/2015-9, and #310892/2019-8 to NL-S and #302060/2019-7 to ED); 2) the CAPES (PROCAD grant #88881-068436/2014-09 and Finance Code 001); and 3) the Foundation for Science and Technology of the State of Pernambuco (FACEPE) (grants APQ-1044-4.01/15 and fellowship #IBPG-0411-2.08/21 to TG).

ACKNOWLEDGMENTS

We thank Viviane Carvalho and Cássia Pereira for their invaluable technical assistance and the Program for Technological Development in Tools for Health (PDTIS-FIOCRUZ).

REFERENCES

Agaugué, S., Carosella, E. D., and Rouas-Freiss, N. (2011). Role of HLA-G in Tumor Escape through Expansion of Myeloid-Derived Suppressor Cells and Cytokinic Balance in Favor of Th2 versus Th1/Th17. *J. Am. Soc. Hematol.* 117 (26), 7021–7031. doi:10.1182/blood-2010-07-294389

Almeida, R. S., Araújo, F. S., Oliveira, S. A. V., Coutinho, L. L., Donadi, E. A., and Lucena-Silva, N. (2018). "Mirnome Analysis of Brazilian Childhood Acute Lymphoblastic Leukemia Reveals an Association of 10 miRNAs with Increased Soluble HLA-G Levels," in *Abstracts from the 50th Congress of the International Society of Paediatric Oncology (SIOP) Kyoto, Japan November 16-19, 2018* (Pediatr: Blood Cancer). doi:10.1002/pbc.27455

Almeida, R. S., Costa E Silva, M., Coutinho, L. L., Garcia Gomes, R., Pedrosa, F., Massaro, J. D., et al. (2019). MicroRNA Expression Profiles Discriminate Childhood T- from B-acute Lymphoblastic Leukemia. *Hematological Oncol.* 37 (1), 103–112. doi:10.1002/hon.2567

Amodio, G., and Gregori, S. (2020). HLA-G Genotype/expression/disease Association Studies: success, Hurdles, and Perspectives. *Front. Immunol.* 11, 1178. doi:10.3389/fimmu.2020.01178

Barroilhet, L., Yang, J., Hasselblatt, K., Paranal, R. M., Ng, S. K., Rauh-Hain, J. A., et al. (2013). C-terminal Binding Protein-2 Regulates the Response of Epithelial Ovarian Cancer Cells to Histone Deacetylase Inhibitors. *Oncogene* 32 (33), 3896–3903. doi:10.1038/onc.2012.380

Calin, G. A., Ferracin, M., Cimmino, A., Di Leva, G., Shimizu, M., Wojcik, S. E., et al. (2005). A MicroRNA Signature Associated with Prognosis and Progression in Chronic Lymphocytic Leukemia. *New Engl. J. Med.* 353 (17), 1793–1801. doi:10.1056/NEJMoa050995

Caocci, G., Greco, M., Arras, M., Cusano, R., Orrù, S., Martino, B., et al. (2017). HLA-G Molecules and Clinical Outcome in Chronic Myeloid Leukemia. *Leuk. Res.* 61, 1–5. doi:10.1016/j.leukres.2017.08.005

Caocci, G., Greco, M., Fanni, D., Senes, G., Littera, R., Lai, S., et al. (2016). HLA-G Expression and Role in Advanced-Stage Classical Hodgkin Lymphoma. *Eur. J. Histochem. EJH* 60 (2). doi:10.4081/ejh.2016.2606

Carosella, E. D., Rouas-Freiss, N., Tronik-Le Roux, D., Moreau, P., and LeMaoult, J. (2015). HLA-G: an Immune Checkpoint Molecule. *Adv. Immunol.* 127, 33–144. doi:10.1016/bs.ai.2015.04.001

Castelli, E. C., Mendes-Junior, C. T., Deghaide, N. H. S., De Albuquerque, R. S., Muniz, Y. C. N., Simões, R. T., et al. (2010). The Genetic Structure of 3′ Untranslated Region of the HLA-G Gene: Polymorphisms and Haplotypes. *Genes Immun.* 11 (2), 134–141. doi:10.1038/gene.2009.74

Castelli, E. C., Veiga-Castelli, L. C., Yaghi, L., Moreau, P., and Donadi, E. A. (20142014). Transcriptional and Posttranscriptional Regulations of the HLA-G Gene. *J. Immunol. Res.* doi:10.1155/2014/734068

Cavalcanti, A., Almeida, R., Mesquita, Z., Duarte, A. L. B. P., Donadi, E. A., and Lucena-Silva, N. (2017). Gene Polymorphism and HLA-G Expression in Patients with Childhood-onset Systemic Lupus Erythematosus: A Pilot Study. *Hla* 90 (4), 219–227. doi:10.1111/tan.13084

Chou, C. H., Shrestha, S., Yang, C. D., Chang, N. W., Lin, Y. L., Liao, K. W., et al. (2018). miRTarBase Update 2018: a Resource for Experimentally Validated microRNA-Target Interactions. *Nucleic Acids Res.* 46 (D1), D296–D302. doi:10.1093/nar/gkx1067

Chu, W., Yang, Y., Geraghty, D. E., and Hunt, J. S. (1999). Interferons Enhance HLA-G mRNA and Protein in Transfected Mouse Fibroblasts. *J. Reprod. Immunol.* 42 (1), 1–15. doi:10.1016/S0165-0378(98)00077-1

Colonna, M., Samaridis, J., Cella, M., Angman, L., Allen, R. L., O'Callaghan, C. A., et al. (1998). Cutting Edge: Human Myelomonocytic Cells Express an Inhibitory Receptor for Classical and Nonclassical MHC Class I Molecules. *J. Immunol.* 160 (7), 3096–3100.

Delcuve, G. P., Khan, D. H., and Davie, J. R. (2012). Roles of Histone Deacetylases in Epigenetic Regulation: Emerging Paradigms from Studies with Inhibitors. *Clin. epigenetics* 4 (1), 1–13. doi:10.1186/1868-7083-4-5

Diepstra, A., Poppema, S., Boot, M., Visser, L., Nolte, I. M., Niens, M., et al. (2008). HLA-G Protein Expression as a Potential Immune Escape Mechanism in Classical Hodgkin's Lymphoma. *Tissue antigens* 71 (3), 219–226. doi:10.1111/j.1399-0039.2008.01005.x

Donadi, E. A., Castelli, E. C., Arnaiz-Villena, A., Roger, M., Rey, D., and Moreau, P. (2011). Implications of the Polymorphism of HLA-G on its Function, Regulation, Evolution and Disease Association. *Cell Mol. Life Sci.* 68 (3), 369–395. doi:10.1007/s00018-010-0580-7

dos Santos Almeida, R., de Luna Ramos, A. M., Luna, C. F., Pedrosa, F., Donadi, E. A., and Lucena-Silva, N. (2018). Cytokines and Soluble HLA-G Levels in Bone Marrow Stroma and Their Association with the Survival Rate of Patients Exhibiting Childhood T-Cell Acute Lymphoblastic Leukemia. *Cytokine* 102, 94–101. doi:10.1016/j.cyto.2017.07.014

Eichmüller, S. B., Osen, W., Mandelboim, O., and Seliger, B. (2017). Immune Modulatory microRNAs Involved in Tumor Attack and Tumor Immune Escape. *JNCI: J. Natl. Cancer Inst.* 109 (10). doi:10.1093/jnci/djx034

Fattore, L., Ruggiero, C. F., Pisanu, M. E., Liguoro, D., Cerri, A., Costantini, S., et al. (2019). Reprogramming miRNAs Global Expression Orchestrates Development of Drug Resistance in BRAF Mutated Melanoma. *Cel Death Differ.* 26 (7), 1267–1282. doi:10.1038/s41418-018-0205-5

Flajollet, S., Poras, I., Carosella, E. D., and Moreau, P. (2009). RREB-1 Is a Transcriptional Repressor of HLA-G. *J. Immunol.* 183 (11), 6948–6959. doi:10.4049/jimmunol.0902053

Friedländer, M. R., Chen, W., Adamidi, C., Maaskola, J., Einspanier, R., Knespel, S., et al. (2008). Discovering microRNAs from Deep Sequencing Data Using miRDeep. *Nat. Biotechnol.* 26 (4), 407–415. doi:10.1038/nbt1394

Garziera, M., Scarabel, L., and Toffoli, G. (20172017). Hypoxic Modulation of HLA-G Expression through the Metabolic Sensor HIF-1 in Human Cancer Cells. *J. Immunol. Res.* doi:10.1155/2017/4587520

Gobin, S. J., Biesta, P., de Steenwinkel, J. E., Datema, G., and Van den Elsen, P. J. (2002). HLA-G Transactivation by cAMP-Response Element-Binding Protein (CREB): An Alternative Transactivation Pathway to the Conserved Major Histocompatibility Complex (MHC) Class I Regulatory Routes. *J. Biol. Chem.* 277 (42), 39525–39531. doi:10.1074/jbc.M112273200

Gomes, R. G., de Brito, C. A. A., Martinelli, V. F., Dos Santos, R. N., dos Santos Gomes, F. O., Peixoto, C. A., et al. (2018). HLA-G Is Expressed in Intestinal Samples of Ulcerative Colitis and Crohn's Disease Patients and HLA-G5 Expression Is Differentially Correlated with TNF and IL-10 Cytokine Expression. *Hum. Immunol.* 79 (6), 477–484. doi:10.1016/j.humimm.2018.03.006

Griffiths-Jones, S., Grocock, R. J., Van Dongen, S., Bateman, A., and Enright, A. J. (2006). miRBase: microRNA Sequences, Targets and Gene Nomenclature. *Nucleic Acids Res.* 34 (Suppl. l_1), D140–D144. doi:10.1093/nar/gkj112

Gros, F., Sebti, Y., de Guiber, S., Branger, B., Bernard, M., Fauchet, R., et al. (2006). Soluble HLA-G Molecules Are Increased during Acute Leukemia, Especially in Subtypes Affecting Monocytic and Lymphoid Lineages. *Neoplasia* 8 (3), 223–230. doi:10.1593/neo.05703

Hirschberger, S., Hinske, L. C., and Kreth, S. (2018). MiRNAs: Dynamic Regulators of Immune Cell Functions in Inflammation and Cancer. *Cancer Lett.* 431, 11–21. doi:10.1016/j.canlet.2018.05.020

Huang, D. W., Sherman, B. T., and Lempicki, R. A. (2009). Bioinformatics Enrichment Tools: Paths toward the Comprehensive Functional Analysis of Large Gene Lists. *Nucleic Acids Res.* doi:10.1093/nar/gkn923

Huang, D. W., Sherman, B. T., and Lempicki, R. A. (2009). Systematic and Integrative Analysis of Large Gene Lists Using DAVID Bioinformatics Resources. *Nat. Protoc.* 4, 44–57. doi:10.1038/nprot.2008.211

Jesionek-Kupnicka, D., Bojo, M., Prochorec-Sobieszek, M., Szumera-Ciećkiewicz, A., Jabłońska, J., Kalinka-Warzocha, E., et al. (2016). HLA-G and MHC Class II Protein Expression in Diffuse Large B-Cell Lymphoma. *Archivum immunologiae et therapiae experimentalis* 64 (3), 225–240. doi:10.1007/s00005-015-0372-8

Kozomara, A., and Griffiths-Jones, S. (2010). miRBase: Integrating microRNA Annotation and Deep-Sequencing Data. *Nucleic Acids Res.* 39 (Suppl. l_1), D152–D157. doi:10.1093/nar/gkq1027

Krüger, J., and Rehmsmeier, M. (2006). RNAhybrid: microRNA Target Prediction Easy, Fast and Flexible. *Nucleic Acids Res.* 34 (Suppl. l_2), W451–W454. doi:10.1093/nar/gkl243

Lefebvre, S., Moreau, P., Guiard, V., Ibrahim, E. C., Adrian-Cabestre, F., Menier, C., et al. (1999). Molecular Mechanisms Controlling Constitutive and IFN-γ-Inducible HLA-G Expression in Various Cell Types. *J. Reprod. Immunol.* 43 (2), 213–224. doi:10.1016/S0165-0378(99)00035-2

Lin, A., and Yan, W. H. (2018). Heterogeneity of HLA-G Expression in Cancers: Facing the Challenges. *Front. Immunol.*, 2164. doi:10.3389/fimmu.2018.02164

Liu, H., Ni, Z., Shi, L., Ma, L., and Zhao, J. (2019). MiR-486-5p Inhibits the Proliferation of Leukemia Cells and Induces Apoptosis through Targeting FOXO1. *Mol. Cell. probes* 44, 37–43. doi:10.1016/j.mcp.2019.02.001

Marques, E. A. L. V., Neves, L., Fonseca, T. C., Lins, M. M., Pedrosa, F., and Lucena-Silva, N. (2011). Molecular Findings in Childhood Leukemia in Brazil: High Frequency of MLL-ENL Fusion/t (11; 19) in Infant Leukemia. *J. Pediatr. hematology/oncology* 33 (6), 470–474. doi:10.1097/MPH.0b013e3181fb8f61

Martin, M. (2011). Cutadapt Removes Adapter Sequences from High-Throughput Sequencing Reads. *Embnet. Journal* 17 (1), 10–12. doi:10.14806/ej.17.1.200

Mehta, A., and Baltimore, D. (2016). MicroRNAs as Regulatory Elements in Immune System Logic. *Nat. Rev. Immunol.* 16 (5), 279–294. doi:10.1038/nri.2016.40

Moreau, P., Adrian-Cabestre, F., Menier, C., Guiard, V., Gourand, L., Dausset, J., et al. (1999). IL-10 Selectively Induces HLA-G Expression in Human Trophoblasts and Monocytes. *Int. Immunol.* 11 (5), 803–811. doi:10.1093/intimm/11.5.803

Mouillot, G., Marcou, C., Zidi, I., Guillard, C., Sangrouber, D., Carosella, E. D., et al. (2007). Hypoxia Modulates HLA-G Gene Expression in Tumor Cells. *Hum. Immunol.* 68 (4), 277–285. doi:10.1016/j.humimm.2006.10.016

Ninawe, A., Guru, S. A., Yadav, P., Masroor, M., Samadhiya, A., Bhutani, N., et al. (2021). miR-486-5p: a Prognostic Biomarker for Chronic Myeloid Leukemia. *ACS omega* 6(11), 7711–7718. doi:10.1021/acsomega.1c00035

Nückel, H., Rebmann, V., Dürig, J., Dührsen, U., and Grosse-Wilde, H. (2005). HLA-G Expression Is Associated with an Unfavorable Outcome and Immunodeficiency in Chronic Lymphocytic Leukemia. *Blood* 105 (4), 1694–1698. doi:10.1182/blood-2004-08-3335

O'connell, R. M., Rao, D. S., Chaudhuri, A. A., and Baltimore, D. (2010). Physiological and Pathological Roles for microRNAs in the Immune System. *Nat. Rev. Immunol.* 10 (2), 111–122. doi:10.1038/nri2708

Omar, H. A., El-Serafi, A. T., Hersi, F., Arafa, E. S. A., Zaher, D. M., Madkour, M., et al. (2019). Immunomodulatory MicroRNAs in Cancer: Targeting Immune Checkpoints and the Tumor Microenvironment. *FEBS J.* 286 (18), 3540–3557. doi:10.1111/febs.15000

Paul, P., Rouas-Freiss, N., Khalil-Daher, I., Moreau, P., Riteau, B., Le Gal, F. A., et al. (1998). HLA-G Expression in Melanoma: a Way for Tumor Cells to Escape from Immunosurveillance. *Proc. Natl. Acad. Sci.* 95 (8), 4510–4515. doi:10.1073/pnas.95.8.4510

Place, R. F., Li, L. C., Pookot, D., Noonan, E. J., and Dahiya, R. (2008). MicroRNA-373 Induces Expression of Genes with Complementary Promoter Sequences. *Proc. Natl. Acad. Sci.* 105 (5), 1608–1613. doi:10.1073/pnas.0707594105

Porto, I. O., Mendes-Junior, C. T., Felício, L. P., Georg, R. C., Moreau, P., Donadi, E. A., et al. (2015). MicroRNAs Targeting the Immunomodulatory HLA-G Gene: a New Survey Searching for microRNAs with Potential to Regulate HLA-G. *Mol. Immunol.* 65 (2), 230–241. doi:10.1016/j.molimm.2015.01.030

Rajagopalan, S., and Long, E. O. (1999). A Human Histocompatibility Leukocyte Antigen (HLA)-G–specific Receptor Expressed on All Natural Killer Cells. *J. Exp. Med.* 189 (7), 1093–1100. doi:10.1084/jem.189.7.1093

Ray, S. K., Li, H. J., Metzger, E., Schüle, R., and Leiter, A. B. (2014). CtBP and Associated LSD1 Are Required for Transcriptional Activation by NeuroD1 in Gastrointestinal Endocrine Cells. *Mol. Cell. Biol.* 34 (12), 2308–2317. doi:10.1128/mcb.01600-13

Rizzo, R., Audrito, V., Vacca, P., Rossi, D., Brusa, D., Stignani, M., et al. (2014). HLA-G Is a Component of the CLL Escape Repertoire to Generate Immune

Suppression: Impact of HLA-G 14 Bp (Rs66554220) Polymorphism. *Haematologica*. doi:10.3324/haematol.2013.095281

Rizzo, R., Hviid, T. V. F., Govoni, M., Padovan, M., Rubini, M., Melchiorri, L., et al. (2008). HLA-G Genotype and HLA-G Expression in Systemic Lupus Erythematosus: HLA-G as a Putative Susceptibility Gene in Systemic Lupus Erythematosus. *Tissue antigens* 71 (6), 520–529. doi:10.1111/j.1399-0039.2008.01037.x

Robinson, M. D., McCarthy, D. J., and Smyth, G. K. (2010). edgeR: a Bioconductor Package for Differential Expression Analysis of Digital Gene Expression Data. *Bioinformatics* 26, 139–140. doi:10.1093/bioinformatics/btp616

Rouas-Freiss, N., Gonçalves, R. M. B., Menier, C., Dausset, J., and Carosella, E. D. (1997). Direct Evidence to Support the Role of HLA-G in Protecting the Fetus from Maternal Uterine Natural Killer Cytolysis. *Proc. Natl. Acad. Sci.* 94 (21), 11520–11525. doi:10.1073/pnas.94.21.11520

Rouas-Freiss, N., Moreau, P., LeMaoult, J., and Carosella, E. D. (20142014). The Dual Role of HLA-G in Cancer. *J. Immunol. Res.* doi:10.1155/2014/359748

Schotte, D., Chau, J. C. K., Sylvester, G., Liu, G., Chen, C., Van Der Velden, V. H. J., et al. (2009). Identification of New microRNA Genes and Aberrant microRNA Profiles in Childhood Acute Lymphoblastic Leukemia. *Leukemia* 23 (2), 313–322. doi:10.1038/leu.2008.286

Schotte, D., Moqadam, F. A., Lange-Turenhout, E. A. M., Chen, C., Van IJcken, W. F. J., Pieters, R., et al. (2011). Discovery of New microRNAs by Small RNAome Deep Sequencing in Childhood Acute Lymphoblastic Leukemia. *Leukemia* 25 (9), 1389–1399. doi:10.1038/leu.2011.105

Sebti, Y., Le Friec, G., Pangault, C., Gros, F., Drénou, B., Guilloux, V., et al. (2003). Soluble HLA-G Molecules Are Increased in Lymphoproliferative Disorders. *Hum. Immunol.* 64 (11), 1093–1101. doi:10.1016/j.humimm.2003.08.345

Shi, Y., Lan, F., Matson, C., Mulligan, P., Whetstine, J. R., Cole, P. A., et al. (2004). Histone Demethylation Mediated by the Nuclear Amine Oxidase Homolog LSD1. *Cell* 119 (7), 941–953. doi:10.1016/j.cell.2004.12.012

Shi, Y., Sawada, J. I., Sui, G., Affar, E. B., Whetstine, J. R., Lan, F., et al. (2003). Coordinated Histone Modifications Mediated by a CtBP Co-repressor Complex. *Nature* 422 (6933), 735–738. doi:10.1038/nature01550

Shiroishi, M., Kuroki, K., Ose, T., Rasubala, L., Shiratori, I., Arase, H., et al. (2006). Efficient Leukocyte Ig-like Receptor Signaling and crystal Structure of Disulfide-Linked HLA-G Dimer. *J. Biol. Chem.* 281 (15), 10439–10447. doi:10.1074/jbc.M512305200

Shiroishi, M., Tsumoto, K., Amano, K., Shirakihara, Y., Colonna, M., Braud, V. M., et al. (2003). Human Inhibitory Receptors Ig-like Transcript 2 (ILT2) and ILT4 Compete with CD8 for MHC Class I Binding and Bind Preferentially to HLA-G. *Proc. Natl. Acad. Sci.* 100 (15), 8856–8861. doi:10.1073/pnas.1431057100

Thuringer, D., Chanteloup, G., Boucher, J., Pernet, N., Boudesco, C., Jego, G., et al. (2017). Modulation of the Inwardly Rectifying Potassium Channel Kir4. 1 by the Pro-invasive miR-5096 in Glioblastoma Cells. *Oncotarget* 8 (23), 37681. doi:10.18632/oncotarget.16949

Vasudevan, S., Tong, Y., and Steitz, J. A. (2007). Switching from Repression to Activation: microRNAs Can Up-Regulate Translation. *Science* 318 (5858), 1931–1934. doi:10.1126/science.1149460

Vitkevičienė, A., Skiauterytė, G., Žučenka, A., Stoškus, M., Gineikienė, E., Borutinskaitė, V., et al. (20192019). HDAC and HMT Inhibitors in Combination with Conventional Therapy: a Novel Treatment Option for Acute Promyelocytic Leukemia. *J. Oncol.* doi:10.1155/2019/6179573

Wallaert, A., Van Loocke, W., Hernandez, L., Taghon, T., Speleman, F., and Van Vlierberghe, P. (2017). Comprehensive miRNA Expression Profiling in Human T-Cell Acute Lymphoblastic Leukemia by Small RNA-Sequencing. *Scientific Rep.* 7 (1), 1–8. doi:10.1038/s41598-017-08148-x

Wang, L. S., Li, L., Li, L., Chu, S., Shiang, K. D., Li, M., et al. (2015). MicroRNA-486 Regulates normal Erythropoiesis and Enhances Growth and Modulates Drug Response in CML Progenitors. Blood. *J. Am. Soc. Hematol.* 125 (8), 1302–1313. doi:10.1182/blood-2014-06-581926

Xu, X., Zhou, Y., and Wei, H. (2020). Roles of HLA-G in the Maternal-Fetal Immune Microenvironment. *Front. Immunol.* 11, 592010. doi:10.3389/fimmu.2020.592010

Yadav, P., Sharma, P., Sundaram, S., Venkatraman, G., Bera, A. K., and Karunagaran, D. (2021). SLC7A11/xCT Is a Target of miR-5096 and its Restoration Partially Rescues miR-5096-Mediated Ferroptosis and Anti-tumor Effects in Human Breast Cancer Cells. *Cancer Lett.* 522, 211–224. doi:10.1016/j.canlet.2021.09.033

Yaghi, L., Poras, I., Simoes, R. T., Donadi, E. A., Tost, J., Daunay, A., et al. (2016). Hypoxia Inducible Factor-1 Mediates the Expression of the Immune Checkpoint HLA-G in Glioma Cells through Hypoxia Response Element Located in Exon 2. *Oncotarget* 7 (39), 63690–63707. doi:10.18632/oncotarget.11628

Yan, W. H., and Fan, L. A. (2005). Residues Met76 and Gln79 in HLA-G α1 Domain Involved in KIR2DL4 Recognition. *Cel Res.* 15 (3), 176–182. doi:10.1038/sj.cr.7290283

Yan, W. H. (2011). HLA-G Expression in Cancers: Potential Role in Diagnosis, Prognosis and Therapy. Endocrine, Metabolic & Immune Disorders-Drug Targets (Formerly Current Drug Targets-Immune. *Endocr. Metab. Disord.* 11 (1), 76–89. doi:10.2174/187153011794982059

Yan, W. H., Lin, A., Chen, B. G., and Chen, S. Y. (2009). Induction of Both Membrane-Bound and Soluble HLA-G Expression in Active Human Cytomegalovirus Infection. *J. Infect. Dis.* 200 (5), 820–826. doi:10.1086/604733

Yie, S. M., Li, L. H., Li, G. M., Xiao, R., and Librach, C. L. (2006). Progesterone Enhances HLA-G Gene Expression in JEG-3 Choriocarcinoma Cells and Human Cytotrophoblasts *In Vitro*. *Hum. Reprod.* 21 (1), 46–51. doi:10.1093/humrep/dei305

Zhang, J., Luo, X., Li, H., Deng, L., and Wang, Y. (20142014). Genome-wide Uncovering of STAT3-Mediated miRNA Expression Profiles in Colorectal Cancer Cell Lines. *Biomed. Res. Int.* doi:10.1155/2014/187105

Zheng, X., Lu, S., He, Z., Huang, H., Yao, Z., Miao, Y., et al. (2020). MCU-dependent Negative Sorting of miR-4488 to Extracellular Vesicles Enhances Angiogenesis and Promotes Breast Cancer Metastatic Colonization. *Oncogene* 39 (46), 6975–6989. doi:10.1038/s41388-020-01514-6

Conflict of Interest: The authors declare that the research was conducted in the absence of any commercial or financial relationships that could be construed as a potential conflict of interest.

Publisher's Note: All claims expressed in this article are solely those of the authors and do not necessarily represent those of their affiliated organizations, or those of the publisher, the editors, and the reviewers. Any product that may be evaluated in this article, or claim that may be made by its manufacturer, is not guaranteed or endorsed by the publisher.

frontiers | Frontiers in Genetics

ORIGINAL RESEARCH
published: 24 June 2022
doi: 10.3389/fgene.2022.875939

Upregulated miRNAs on the *TP53* and *RB1* Binding Seedless Regions in High-Risk HPV-Associated Penile Cancer

*Jenilson da Silva[1], Carla Cutrim da Costa[2], Ingryd de Farias Ramos[3], Ana Carolina Laus[4], Luciane Sussuchi[4], Rui Manuel Reis[4], André Salim Khayat[5,6], Luciane Regina Cavalli[7] and Silma Regina Pereira[8]**

[1]Postgraduate Program in Health Science, Federal University of Maranhão, São Luís, Brazil, [2]Degree in Biological Sciences, Department of Biology, Federal University of Maranhão, São Luís, Brazil, [3]Postgraduate Program in Oncology and Medical Sciences, Federal University of Pará, Belém, Brazil, [4]Molecular Oncology Research Center, Barretos Cancer Hospital, Barretos, Brazil, [5]Oncology Research Center, Federal University of Pará, Belém, Brazil, [6]Institute of Biological Sciences, Federal University of Pará, Belém, Brazil, [7]Research Institute Pelé Pequeno Príncipe, Faculdades Pequeno Príncipe, Curitiba, Brazil, [8]Laboratory of Genetics and Molecular Biology, Department of Biology, Federal University of Maranhão, São Luís, Brazil

OPEN ACCESS

Edited by:
Ticiana D. J. Farias,
University of Colorado, United States

Reviewed by:
Hin Fung Tsang,
Hong Kong Adventist Hospital, Hong Kong SAR, China
Natasha Andressa Jorge,
Leipzig University, Germany
Gilda Alves Brown,
Rio de Janeiro State University, Brazil

***Correspondence:**
Silma Regina Pereira
silma.pereira@ufma.br

Specialty section:
This article was submitted to RNA, a section of the journal Frontiers in Genetics

Received: 14 February 2022
Accepted: 26 May 2022
Published: 24 June 2022

Citation:
da Silva J, da Costa CC, de Farias Ramos I, Laus AC, Sussuchi L, Reis RM, Khayat AS, Cavalli LR and Pereira SR (2022) Upregulated miRNAs on the TP53 and RB1 Binding Seedless Regions in High-Risk HPV-Associated Penile Cancer. Front. Genet. 13:875939. doi: 10.3389/fgene.2022.875939

Cancer development by the human papillomavirus (HPV) infection can occur through the canonical HPV/p53/RB1 pathway mediated by the E2/E6/E7 viral oncoproteins. During the transformation process, HPV inserts its genetic material into host Integration Sites (IS), affecting coding genes and miRNAs. In penile cancer (PeCa) there is limited data on the miRNAs that regulate mRNA targets associated with HPV, such as the *TP53* and *RB1* genes. Considering the high frequency of HPV infection in PeCa patients in Northeast Brazil, global miRNA expression profiling was performed in high-risk HPV-associated PeCa that presented with *TP53* and *RB1* mRNA downregulated expression. The miRNA expression profile of 22 PeCa tissue samples and five non-tumor penile tissues showed 507 differentially expressed miRNAs: 494 downregulated and 13 upregulated (let-7a-5p, miR-130a-3p, miR-142-3p, miR-15b-5p miR-16-5p, miR-200c-3p, miR-205-5p, miR-21-5p, miR-223-3p, miR-22-3p, miR-25-3p, miR-31-5p and miR-93-5p), of which 11 were identified to be in HPV16-IS and targeting *TP53* and *RB1* genes. One hundred and thirty-one and 490 miRNA binding sites were observed for *TP53* and *RB1*, respectively, most of which were in seedless regions. These findings suggest that up-regulation of miRNA expression can directly repress *TP53* and *RB1* expression by their binding sites in the non-canonical seedless regions.

Keywords: penile cancer, tumor suppressor repression, miRNA, HPV, *TP53*, *Rb1*

INTRODUCTION

The *TP53* gene is known as the "sentinel gene" due to its ability to identify cell damage and to coordinate complex mechanisms to mediate cell repair, protecting genome stability and, consequently, cell homeostasis. Therefore, it is not surprising that *TP53* tumor suppressor is the most frequently mutated gene in human tumors. Most of the alterations described are missense mutations, whereby the protein loses its primary function, or it acquires oncogenetic functions (Datta et al., 2017; Wang and Sun, 2017; Sammons et al., 2020). In addition, the p53 mutant protein

may also facilitate the adaptation of tumor cells to the disadvantageous environment that arises as the tumor grows (Mantovani et al., 2019).

The association between human papillomavirus (HPV) and some cancers, including cervical, head and neck, vulvar, anorectal, and penile squamous cell carcinomas (SCC), is well characterized by the canonical mechanism involving the HPV oncogenes E6 and E7 and p53 and RB1 proteins (de Martel et al., 2017). During the transformation process, HPV inserts its genetic material into host human integration sites (IS), which have been identified in regions harboring cancer-related genes, as well as in regions presenting copy number alterations (CNAs) (Busso-Lopes et al., 2015; Macedo et al., 2020; Pinatti et al., 2021). Indeed, integration of DNA-copy number alterations and other omics data have shown that DNA methylation, mRNA, and miRNA expressions alterations affect coding-genes and miRNAs located within or near the HPV common integration sites (Barzon et al., 2014; Groves and Coleman, 2018; Rosa et al., 2019; Pinatti et al., 2021).

In the last decade, it has been also demonstrated that the wild-type p53 protein plays primarily its role as a transcription factor by regulating a large network of protein-coding genes and non-coding RNAs, including miRNAs, both inducing or repressing their targets (Hermeking, 2012; Fischer, 2017). In addition, the p53 protein regulates miRNA processing, primarily through its central DNA-binding domain, a target site of most cancer-specific mutations. Interestingly, miRNAs can also regulate p53 expression by matching in the seed region into the 3′UTR of *TP53* mRNA, directly inducing the repression of *TP53* or its regulators (Hermeking, 2012; Hermeking et al., 2014). Although several tumor-specific alterations in the p53-miRNA network have been described in different cancers (Hermeking, 2012; Datta et al., 2019), there is no data on miRNAs targeting of *TP53* gene in HPV-associated penile cancer.

PeCa is a rare carcinoma in developed countries, but it presents higher incidence rates in South America, Asia, and Africa, where limited economic and social conditions play a large impact leading to delay in diagnosis, and treatment initiation. In Brazil, specifically in the Northeast region that is particularly affected by low socio-economic conditions and educational levels and high frequency of HPV infection, presents a high incidence of PeCa, with patients presenting additional comorbidities, which contributes to a high incidence of mortality rates (Macedo et al., 2020; Silva et al., 2021) However, even in countries that are not impacted by major economic limitations, the incidence and mortality rates of PeCa has increased, mainly among younger patients (Hansen et al., 2018). Hence, the increased occurrence of PeCa, irrespectively of the countries' socioeconomic conditions, has suggested that HPV infection is possibly the main triggering mechanism for tumor development, in addition to poor hygiene of the genital region, phimosis, uncircumcision, and chronic inflammation (Christodoulidou et al., 2015; Kidd et al., 2017; Adashek et al., 2019).

PeCa treatment options are limited. No effective target therapy is available, mainly due to the scarcity of knowledge on the molecular pathways involved in the development and progression of these tumors. Limited data is available on the role and mechanisms of miRNA deregulation in PeCa, including those that disrupt miRNAs targets that regulate critical genes associated with the action of HPV, such as the *TP53* and *RB1* genes. Considering the high frequency of HPV infection in patients with advanced PeCa in Maranhão State, in Northeast of Brazil, in the present study miRNAs expression analysis was performed in high-risk HPV-associated PeCa with *TP53* and *RB1* mRNA downregulated expression, as previously reported by our group in >80 and 60% of the patients, respectively (Macedo et al., 2020).

This study opens the opportunity to better understand the role of *TP53* and *RB1* transcriptional regulators in HPV-associated penile carcinomas and brings much needed knowledge on the molecular tumorigenesis of this still-neglected tumor.

MATERIALS AND METHODS

Sample Cohort

Fresh PeCa chemotherapy-naive surgical resection tissue specimens were obtained from 22 patients from the Aldenora Hospital, São Luís, Maranhão, Brazil. These patients are a subset of a larger cohort of 37 patients previously investigated for HPV *status*, gene, and protein expression for *TP53* and *RB1* (Macedo et al., 2020). All the samples were collected under patients' written informed consent, approved by the Research Ethics Committee on Humans from the Federal University of Maranhão and by the National Research Ethics Commission (CONEP-Brazil, CAAE: 46371515.5.0000.5087). Tumor and adjacent non-tumor tissues, sampled from 2 cm distant from the tumor site after histopathological assessment, were obtained before any cancer treatment. At the time of the sample collection, the patients had no history of other cancers or sexually transmitted diseases.

The clinical and histopathological variables were obtained from patients' medical records. The mean age of the patients at diagnosis was 64.22 ± 15.63 years, ranging from 32 to 85 years old. The patients declared themselves smokers (41%) and alcoholics (45.5%). All tumors were classified as squamous cell carcinoma (SCC), and the condylomatous and keratinized histological subtypes localized mostly in the glans, corpus cavernosum, and corpus spongiosum were the most frequent, 45.4 and 36.4%, respectively. Tumor grades II and III were the most frequent, present in 54.5 and 27.3% of the patients, respectively. Lymphatic and perineural invasion were positive in 18.2 and 22.8% of the patients, who presented mostly ulcerated lesions (68.2% of the cases), followed by vegetative (18.2%) and verrucous (13.6%). Penectomy (partial and total) was performed in 95.4% of the patients. The primary tumor of each patient was positive for HPV by Nested-PCR and DNA sequencing, as described in Macedo *et al.* In this subset, the multiple infections were detected in 50.0% of the cases. The HPV16 genotype was the most frequent (72.2%), followed by the 74 (16.6%), 30, 59 and 66 (11%, each) genotypes. Genotypes found in lower frequencies were 6, 18, 30, 35, 44, 53, 58, and 73 (**Supplementary Table S1**). Four cases were positive for HPV, but not genotyped since the samples did not have sufficient DNA for Nested-PCR and/or DNA sequencing analysis. **Table 1** and

TABLE 1 | Clinical-histopathological profile of patients diagnosed with HPV positive penile carcinoma (n = 22).

Variable	Number (%)	Variable	Number (%)
1. Histological subtype		5. Lesion	
Condylomatous	10 (45.4%)	Ulcerated	15 (68.2%)
Keratinized PeCa	8 (36.4%)	Vegetative	4 (18.2%)
Mixed	4 (18.2%)	Verrucous	3 (13.6%)
2. Tumor size		6. Tumor site	
0.6–2.0	4 (18.2%)	Glans	9 (40.9%)
2.1–5.0	15 (68.2%)	Glans and foreskin	7 (31.8%)
5.1—10.0	3 (13.6%)	Foreskin	2 (9.1%)
3. Tumor stage		Glans, foreskin and other areas	4 (18.2%)
pT1	6 (27.3%)	7. Surgery type	
pT2	9 (40.9%)	Preserved penis	1 (4.5)
pT3	7 (31.8%)	Partial penectomy	16 (72.7%)
4. Tumor grade		Radical penectomy	5 (22.7%)
I	4 (18.2%)	8. Phimosis occurrence	
II	12 (54.5%)	Yes	8 (36.3%)
III	6 (27.3%)	No	9 (41.0%)
—	—	No information	5 (22.7%)

Supplementary Table S1 present the detailed patients' clinical-histopathological information.

Considering our previous study (Macedo et al., 2020) in which we have demonstrated *TP53* and *RB1* down-regulated expression at both mRNA (by real-time PCR) and protein (by immunohistochemistry) levels (86 and 65% of the cases, respectively), in this study, we investigated the possible mechanisms by which these genes might be repressed in HPV-associated PeCa. For that, a subset of 22 tumors was evaluated for differential miRNA expression in relation to adjacent non-tumor tissues (n = 5). Fifteen of the 22 tumors have data on the expression of *TP53* and *RB1* (73 and 69% of the tumors are underexpressed, respectively) (**Supplementary Table S1**). Subsequently, prediction miRNAs binding sites analysis were performed in the *TP53* and *RB1* gene, followed by a search for molecular pathways potentially involved in penile carcinogenesis in HPV-positive patients.

Global miRNA Expression Analysis

Total RNA from 22 PeCa tumors and five adjacent non-tumor tissues was isolated using the TRIzol protocol (Invitrogen Carlsbad, CA, United States). RNA concentration and quality were tested by measuring the 260/280 and 260/230 ratios using the Nanodrop 2001 spectrophotometer (Willington, DE, United States). Expression of miRNAs was determined using the *nCounter® Human v.3 miRNA expression* platform (*Nanostring Technologies™*, Seattle, Wa, United States), which contains human probes from miRBase v.22 (http://www.mirbase.org) targeting 827 human miRNAs, six positive controls, eight negative controls, three positive binding controls, three negative binding controls, five internal reference genes (*ACTB*, *B2M*, *GAPDH*, *RPL19,* and *RPL0*) and five miRNA controls (ath-miR- 159a, cel-miR-248, cel-miR-254, osa-miR-414, and osa-miR-442) as previously reported at the Molecular Oncology Research Center (Pessôa-Pereira et al., 2020; Causin et al., 2021). The raw data were pre-processed and exported as RCC files. The raw data of the study, as well as the clinical information of the patients are available for access from the *Gene Expression Omnibus* (GEO), under registration GSE197121.

Differential miRNA Expression Analysis

The raw data were normalized and analyzed using the ROSALIND® Nanostring platform (https://rosalind.onramp.bio/). Adjacent non-tumor tissues distant 2 cm for the primary tumor were used as control. Read distribution percentages, identity heatmaps, and sample MDS plots were generated as part of the QC step. The normalization was conducted following the background subtraction based on POS_A probes correction factors (positive control normalization and codeset normalization). For both steps, the geometric mean of each probeset was used to create a normalization factor. The fold changes, p-values for comparisons were calculated using the t-test method ($p \leq 0.05$). p-value adjustment was performed using the Benjamini–Hochberg ($p \leq 0.01$) method to estimate false discovery rates (FDR). The clustering of miRNAs for the final heatmap was constructed using the PAM (Partitioning Around Medoids) through a method using the FPC R library (Hennig, 2020) that takes into account the direction and type of all signals in a pathway, the position, function, and type of each miRNA identified. Fold change (≥2 for miRNAs upregulated and ≤-2 for miRNAs downregulated), p-value and adjusted p-value were used as selection criteria for miRDE.

Prediction of miRNA Binding Sites in the *TP53* and *RB1* Gene Sequences

The *STarMir* software (Kanoria et al., 2016) was used to identify the miRNAs binding regions in *TP53* and *RB1* genes (CLIP-data). The construction design and nucleic acid fold of *STarMir* are obtained from the *Mfold* package (Zuker, 2003) and *Sfold* which contains the *Srna* module (Ding et al., 2004). *Sfold* applies a two-step model for hybridization between mRNA and miRNA. In this model, hybridization of the miRNA-target occurs at an accessible target site and then the hybrid elongates to form the complete

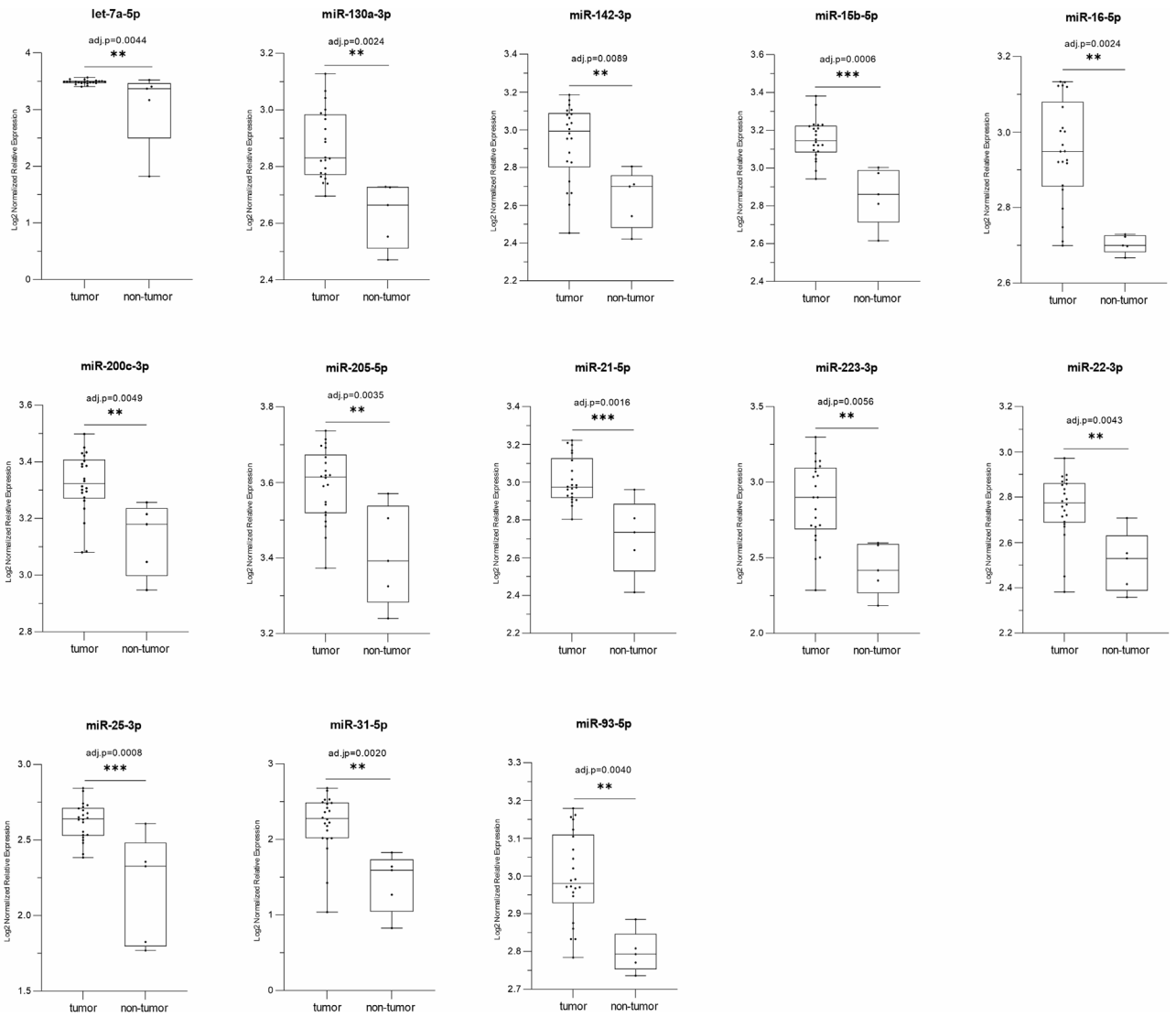

FIGURE 1 | The box-plots represent a comparison of the relative expression levels of the 13 miRDE upregulated in tumors ($n = 22$) versus normal tissue ($n = 5$); $p \leq 0.05$ by *t*-test and adj.-p ≤ 0.01 by Benjamini–Hochberg; $^{*}p \leq 0.05$, $^{**}p \leq 0.01$ and $^{***}p \leq 0.001$.

miRNA-target duplex. The minimum free energy of hybridization was obtained from the RNA*hybrid* tool (Rehmsmeier et al., 2004; Long et al., 2007). Only interactions in "seed" and "seedless" regions with LogitProb values ≥0.5; $\Delta G_{hybrid} \leq -10.00$ and site-access ≥ 0.4 were considered.

Pathway's Enrichment Analysis

Pathway's enrichment analysis was performed by miRPath v.3 - DIANA TOOLS software (Vlachos et al., 2015) using the Tarbase prediction algorithm and considering the *p*-value threshold ≤0.05. The generated pathways are part of the *Kyoto Encyclopedia of Genes and Genomes* (KEGG). The *TP53* and *RB1* genes were used as filters to generate KEGG pathways. The *'pathways union'* function was used to generate the related top pathways, considering the *p*-value threshold ≤0.05 and enrichment analysis method by Fisher's Exact Test.

RESULTS

Overexpressed miRNAs Targeting TP53 and RB1 in Penile Cancer Patients

Differential miRNA expression analysis was performed in the 22 PeCa tissues. The global miRNA expression profile of these tumors showed 507 differentially expressed miRNAs (miRDE) compared to a group of five adjacent non-tumor penile tissues. Among these miRDE, 494 (97.4%) miRNAs were downregulated and 13 (2.6%) upregulated (**Figure 1**; **Table 2**). Considering the previously detected lower *TP53* mRNA expression (85.7% (12/14) and lower protein expression in 87.5% (14/16) of these cases (Macedo et al., 2020), we further investigated the up-regulated miRNAs in the subset of 22 tumors, of which 73% were downregulated. The miRDEs let-7a-5p, miR-130a-3p, miR-15b-5p, miR-21-5p, and miR-25-3p were overexpressed in

TABLE 2 | Thirteen differentially expressed miRNAs observed upregulated in the PeCa patients, and their respective chromosomal location and HPV integration sites (presented by miRNA number).

miRNAs	Cytoband	Start—Stop (bp)	Integration site HPV (genotype)[a]	miRNA expression	Frequency (%)	Log2FC	*p*-Value	Adj.-*p*
let-7a-5p	9q22.32	96,938,234–96,938,325	yes, (16.18)	upregulated	100.0	2.2266	0.0019	0.0044
miR-130a-3p	11q12.1	57,641,198–57,641,286	yes, (16)	upregulated	100.0	1.1603	0.0008	0.0024
miR-142-3p	17q22	58,331,222–58,331,327	yes, (16)	upregulated	86.4	1.4576	0.0054	0.0089
miR-15b-5p	3q25.33	160,404,588–160,404,685	yes, (16)	upregulated	100.0	1.6509	0.0000	0.0006
miR-16-5p	13q14.2	50,623,109–50,623,197	yes, (16)	upregulated	95.5	1.2512	0.0008	0.0024
miR-200c-3p	12p13.31	6,963,694–6,963,771	no	upregulated	95.5	1.2541	0.0023	0.0049
miR-205-5p	1q32.2	209,428,820–209,432,384	yes, (16.18)	upregulated	95.5	1.4610	0.0013	0.0035
miR-21-5p	17q23.1	59,841,262–59,841,342	yes, (16.18)	upregulated	100.0	1.4629	0.0004	0.0016
miR-223-3p	Xq12	66,018,870–66,018,979	no	upregulated	95.5	2.0222	0.0028	0.0056
miR-22-3p	17p13.3	1,617,197–1,617,281	yes, (16)	upregulated	91.0	1.0605	0.0018	0.0043
miR-25-3p	7q22.1	100,093,560–100,093,643	yes, (16)	upregulated	100.0	1.5448	0.0001	0.0008
miR-31-5p	9p21.3	21,512,114–21,512,184	yes, (16)	upregulated	91.0	2.0012	0.0006	0.0020
miR-93-5p	7q22.1	99,691,391–99,691,470	yes, (16)	upregulated	95.5	1.0525	0.0016	0.0040

[a]*Data obtained from HPVBase (Kumar Gupta and Kumar, 2015) and VISDB (Tang et al., 2020).*

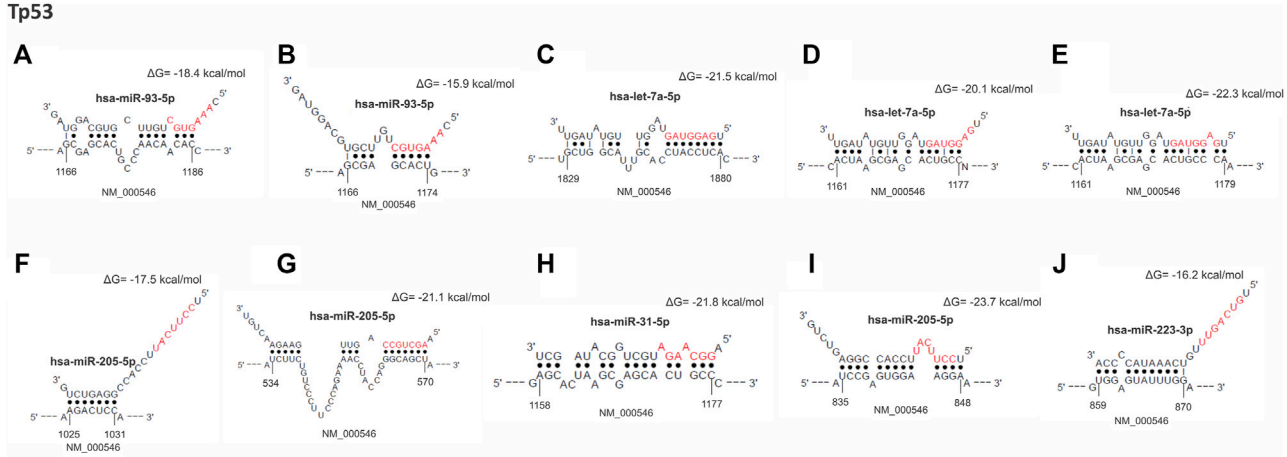

FIGURE 2 | From **(A–J)**, hybrid mRNA (*TP53*)—miRNA upregulated. The upper and lower sequences represent the miRNA in the 3′-5′ sense and 5′-3′ sense hybridization sites in the mRNA, repectively. The numbers at the ends of the mRNA show the starting and ending position of the hybridization sites. Dots between the sequences indicate the paired nucleotides. Nucleotides in red mark the "seed" sequence in miRNA. The energy resulting from the hybridization was calculated by the RNA*hybrid* algorithm.

100% of cases. Interestingly, 84.6% (n = 11) of miRDEs were found to be located at HPV integration sites. The HPV integration sites were identified as target regions of the oncogenic HPV16 genotype, the most frequently detected genotype in our study cohort (**Supplementary Table S1**).

Figure 1 Relative expression of thirteen miRNAs upregulated (tumor vs. non-tumor) in the PeCa studied.

Prediction of miRNA binding sites revealed that all 13 up-regulated miRNAs targeted the *TP53* gene, acting as negative regulators of this tumor suppressor gene expression. We found 131 target sites for these miRNAs: 98.5% in the non-canonical seedless regions and two in the seed regions (**Supplementary Table S2**). Interestingly, *TP53* presents 129 seedless sites, in which all 13 differentially expressed miRNAs could bind. The coding region presented the highest number of target seedless regions with 81/129 sites (62.8%), followed by 3′UTR with 32/129 sites (24.8%) and 5′UTR with 16/129 sites (12.4%). Bindings in the gene seed regions were observed to occur with miR-22-3p and let-7a-5p and both interactions were of 8mer-type. The binding between let-7a-5p and *TP53* occurred in a canonical 3′UTR region, while the binding of miR-22-3p occurred in a non-canonical coding region (site position: 534–570 (bp); seed position: 564–570 (bp). This region is highly conserved (site conservation = 0.963 and seed conservation = 0.933). Our

TABLE 3 | Top 10 miRNA binding regions identified in TP53 and RB1 genes.

miRNA	Site position[a]	LogitProb[b]	Region	ΔG_{hybrid}[c]	ΔG_{total}[d]	Site access[e]	Site consv[f]	Site location[g]
Binding regions in TP53								
miR-93-5p	1,166–1,174	0.864	CDS	−15.900	−15.316	0.714	0.959	0.820
miR-93-5p	1,166–1,186	0.848	CDS	−18.400	−18.018	0.805	0.981	0.820
let-7a-5p	1829–1850	0.835	3′UTR[h]	−21.500	−12.736	0.631	0.001	0.357
let-7a-5p	1,161–1,177	0.831	CDS	−20.100	−19.630	0.767	0.900	0.816
let-7a-5p	1,161–1,179	0.808	CDS	−22.300	−21.904	0.783	0.910	0.816
miR-205-5p	1,025–1,031	0.787	CDS	−17.500	−10.665	0.602	0.997	0.701
miR-22-3p	534–570	0.762	CDS[i]	−21.100	2.9490	0.448	0.963	0.285
miR-31-5p	1,158–1,177	0.755	CDS	−21.800	-16.974	0.667	0.912	0.813
miR-205-5p	835–848	0.755	CDS	−23.700	-13.153	0.442	0.907	0.540
miR-223-3p	859–870	0.727	CDS	−16.200	-6.7460	0.421	0.803	0.560
Binding regions in RB1								
let-7a-5p	2,506–2,517	0.953	CDS[i]	−18.100	−16.708	0.823	0.999	0.840
miR-130a-3p	2,529–2,537	0.917	CDS	−17.100	−11.446	0.708	1.000	0.848
miR-31-5p	4,704–4,721	0.912	3′UTR	−20.100	−17.244	0.651	1.000	0.963
let-7a-5p	4,686–4,712	0.911	3′UTR	−22.100	−17.127	0.608	0.999	0.953
miR-31-5p	4,704–4,719	0.899	3′UTR	−18.700	−16.076	0.627	1.000	0.963
miR-31-5p	4,704–4,717	0.898	3′UTR	−17.200	−14.545	0.672	1.000	0.963
let-7a-5p	4,686–4,719	0.896	3′UTR	−20.700	−14.420	0.573	1.000	0.953
miR-130a-3p	2,529–2,534	0.892	CDS	−15.900	−10.778	0.646	1.000	0.848
miR-142-3p	2002–2026	0.883	CDS	−18.500	−12.601	0.692	0.847	0.659
let-7a-5p	562–571	0.878	CDS	−15.500	−14.118	0.846	0.957	0.142

[a]*Start and end position of the target region (site) predicted to be bound by miRNA.*
[b]*Probability of the site being an miRNA binding site as predicted by our nonlinear logistic model.*
[c]*A measure of stability for miRNA:target hybrid as computed by RNAhybrid.*
[d]*A measure of the total energy change of the hybridization.*
[e]*A measure of structural accessibility as computed by the average probability of a nucleotide being single-stranded (i.e., unpaired) for the nucleotides in the predicted binding site.*
[f]*Conservation score by the PhastCons program for the binding site.*
[g]*Relative starting location of the predicted binding site along the length of the sequence (e.g., for 3′′ UTR, 0 indicates the 5′′ end of the UTR, and one corresponds to the 3′′ end).*
[h]*"seed" region in 3′UTR ("seed" position: 1843–1849, binding: 8mer).*
[i]*"seed" region in CDS ("seed" position: 564–570, binding: 8mer).*

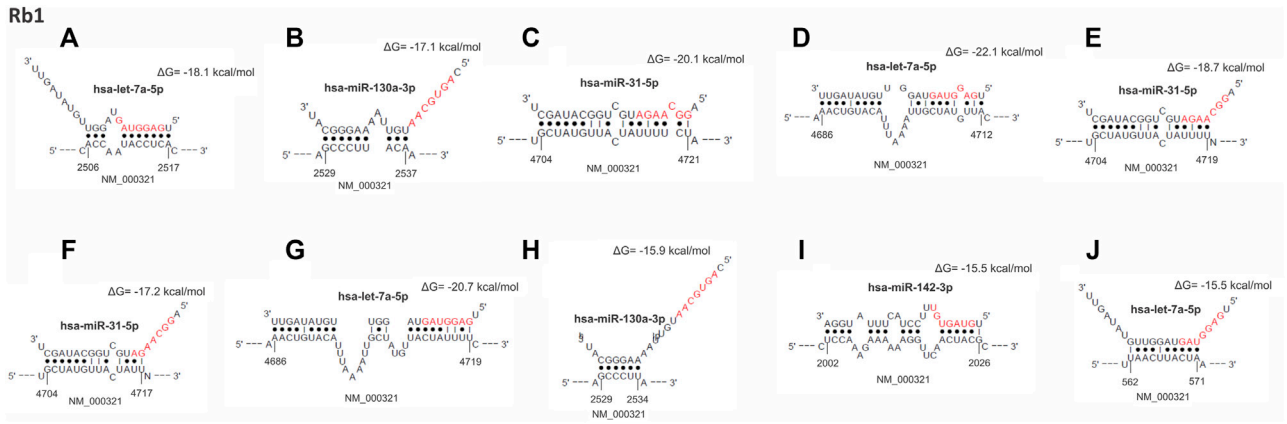

FIGURE 3 | From **(A–J)**, hybrid mRNA (RB1)—miRNA upregulated. The upper and lower sequences represent the miRNA in the 3′-5′ sense and 5′-3′ sense hybridization sites in the mRNA, respectively. The numbers at the ends of the mRNA show the starting and ending position of the hybridization sites. Dots between the sequences indicate the paired nucleotides. Nucleotides in red mark the "seed" sequence in miRNA. The energy resulting from the hybridization was calculated by the RNA*hybrid* algorithm.

analysis also revealed that miR-93-5p and let-7a-5p can bind to a higher number of seedless regions, 21 and 20 predicted binding sites, respectively, while miR-15b-5p, miR-16-5p, miR-223-5p, miR-22-5p, and miR-31-5p bind to a lower number of regions, i.e., five predicted sites for each. Considering the size of the *TP53* mRNA (2,591 bp; transcript variant 1, NCBI Reference Sequence:

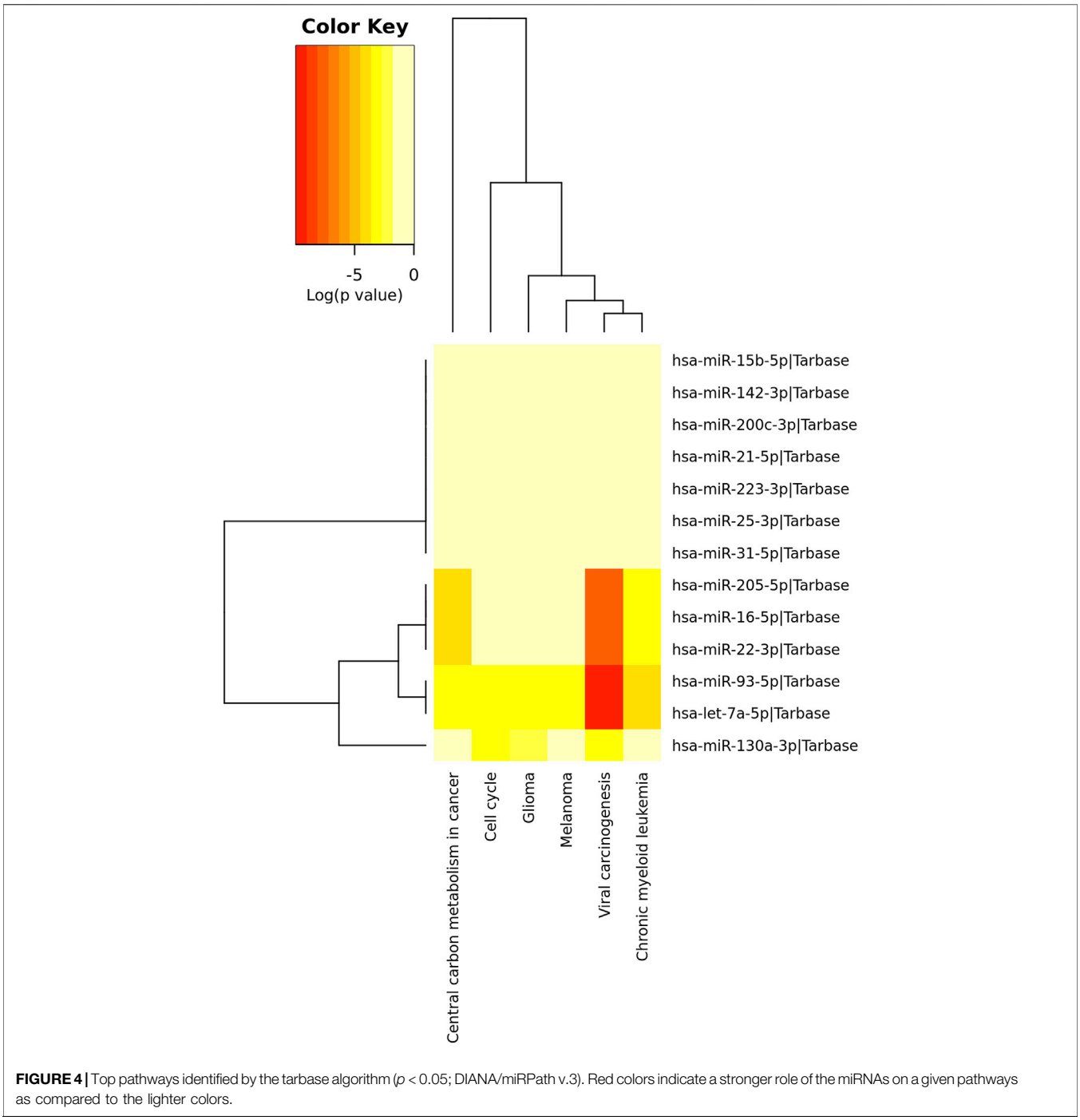

FIGURE 4 | Top pathways identified by the tarbase algorithm ($p < 0.05$; DIANA/miRPath v.3). Red colors indicate a stronger role of the miRNAs on a given pathways as compared to the lighter colors.

NM_000546.5) we observed that the 1,000–1073bp, 2,500–2580bp, and 835–899bp intervals are miRNA binding hotspots regions, harboring a total of 22, 16 and 14 sites, respectively. **Figure 2**; **Table 3** show the ten main binding sites observed in the *TP53* gene.

Figure 2 Top 10 miRNAs binding site regions identified in the *TP53* gene.

The lower expression of *RB1* gene was also found in 69% of the tumors. Interestingly, we observed that the thirteen overexpressed miRNAs that down-regulated *TP53* also regulated *RB1* expression (**Figure 3**). A total of 490 miRNA binding sites were identified for *RB1* (**Supplementary Table S3**), of which 477 (97.3%) were located in the non-canonical seedless regions, while 13 (2.7%) were in the seed regions. Bindings in the seed regions occurred with seven overexpressed miRNAs (miR-93-5p, let-7a-5p, miR-25-3p, miR-130a-3p, miR-200c-3p, miR-205-5p, and miR-142-3p), most of which were 7mer-A1 (46.2%). Other binding sites identified in the seed regions were offset-6mer

TABLE 4 | Top six molecular pathways involving overexpressed miRNAs targeting *TP53* and *RB1* genes.

KEGG Pathway	*p*-Value pathway	miRNAs name	Target gene	*p*-Value interaction
Viral carcinogenesis (hsa05203)	$<1.00 \times 10^{-325}$	let-7a-5p	*TP53* and *RB1*	1.16×10^{-10}
		miR-130a-3p	*RB1*	0.0039733
		miR-16-5p	*TP53*	6.44×10^{-08}
		miR-205-5p	*TP53*	6.44×10^{-08}
		miR-22-3p	*TP53*	6.44×10^{-08}
		miR-93-5p	*TP53* and *RB1*	1.16×10^{-10}
Central carbon metabolism in cancer (hsa05230)	3.39×10^{-06}	let-7a-5p	*TP53*	0.0011443
		miR-16-5p	*TP53*	0.0005629
		miR-205-5p	*TP53*	0.0005629
		miR-22-3p	*TP53*	0.0005629
		miR-93-5p	*TP53*	0.0011443
Chronic myeloid leukemia (hsa05220)	1.33×10^{-05}	let-7a-5p	*TP53* and *RB1*	0.0005998
		miR-16-5p	*TP53*	0.0041602
		miR-205-5p	*TP53*	0.0041602
		miR-22-3p	*TP53*	0.0041602
		miR-93-5p	*TP53* and *RB1*	0.0005998
Glioma (hsa05214)	0.0064303	let-7a-5p	*TP53* and *RB1*	0.0017756
		miR-130a-3	*RB1*	0.0105785
		miR-93-5p	*TP53* and *RB1*	0.0017756
Melanoma (hsa05218)	0.0120334	let-7a-5p	*TP53* and *RB1*	0.0041201
		miR-93-5p	*TP53* and *RB1*	0.0041201
Cell cycle (hsa04110)	0.0224147	let-7a-5p	*TP53* and *RB1*	0.0038093
		miR-130a-3	*RB1*	0.0014269
		miR-93-5p	*TP53* and *RB1*	0.0038093

(23.0%), 6mer, and 7mer-m8 (15.4%, each) (**Supplementary Table S2A**). The *RB1* gene also presented the highest number of miRNA target sites in seedless regions (490 in total), in which all 13 differentially expressed miRNAs can bind. The *RB1* coding region also had the highest number of seedless regions (57.0%), followed by 3′UTR (42.4%) and 5′UTR (0.6%). The miRNA let-7a-5p showed the highest number of seedless bindings (77 predicted sites), followed by miR-93-5p (74 predicted sites). The miRNAs presenting a smaller number of regions were miR-16-5p, miR-205-5p, miR-223-3p (22 predicted sites, each) and miR-22-3p (19 predicted sites). The *RB1* gene also presented hotspots regions where several miRNAs can bind. The intervals between 2,202–2297pb and 1906–1997 pb house a total of 21, and 19 sites, respectively (NCBI Reference Sequence: NM_000321.3). **Table 3** shows the top 10 binding sites in *RB1*.

Figure 3 Top 10 miRNAs binding site regions identified in the *RB1* gene.

Molecular Pathways

KEGG pathway analysis was performed to identify the involvement of the 13 upregulated miRNAs above in disease and signaling pathways. This analysis revealed a total of 13 KEGG pathways (**Supplementary Table S3**), of which the top was: viral carcinogenesis (hsa05203) (p=$<1.00 \times 10^{-325}$), central carbon metabolism in cancer (hsa05230) ($p = 3.39 \times 10^{-06}$), chronic myeloid leukemia (hsa05220) ($p = 1.33 \times 10^{-05}$), glioma (hsa05214) ($p = 0.0064$), melanoma (hsa05218) ($p = 0.0120$) and cell cycle (hsa04110) ($p = 0.0224$) (**Figure 4**; **Table 4**).

Figure 4 Unsupervised hierarchical grouping of the 13 miRNAs differentially expressed and top related pathways.

DISCUSSION

It is well known that the integration of the human papillomavirus (HPV) can occur at or near cancer-related genes (Durst et al., 1987). However, it is not completely understood the mechanisms by which the HPV virus controls its integration into the host cell genome and the molecular consequences that ultimately lead to the development and progression of the HPV infected tumors. Studies have used high-performance technologies to identify virus integration sites in the host genome to better understand the molecular alterations that occur in the host cell, leading to the loss of its genomic stability (Akagi et al., 2014; Bodelon et al., 2016; Liu et al., 2016; Gao et al., 2017; Rosa et al., 2019). The most well-known example is the canonical HPV/*TP53*/*RB1* signaling pathway initiated by the viral E2 disruption. This leads to the loss of the negative feedback control of the viral oncoproteins E6 and E7, mediating ubiquitination and degradation of the p53 and pRb proteins, respectively (Squarzanti et al., 2018). Other authors proposed that HPV integration also directly causes activation of oncogenes or inactivation of tumor suppressors, as reported in HPV-related squamous cell carcinomas (Parfenov et al., 2014; Hu et al., 2015).

In our previous study, we showed downregulated mRNA expression of the *TP53* and *RB1* genes in 86 and 65% of high-

risk HPV-associated PeCa, respectively. In the present subset of cases, we evaluated miRNAs' expression, and observed that 73 and 69% were downregulated for both genes, respectively, suggesting the existence of other regulatory mechanisms in addition to the canonical HPV/*TP53*/*RB1* pathway (Macedo et al., 2020). Although not all the cases presented with expression alterations in these genes, these results were recently corroborated by Furuya *et al.*, who also described *TP53* reduced expression levels in penile tumors.

Compared to other cancers (Santos et al., 2018; Datta et al., 2019; Hussen et al., 2021; Liu et al., 2021), few studies have described epigenetic events in penile tumors, whether evaluating miRNAs (Zhang et al., 2015; Hartz et al., 2016; Kuasne et al., 2017; Peta et al., 2017; Ayoubian et al., 2021; Furuya et al., 2021) or by evaluating methylation patterns (Feber et al., 2015; Kuasne et al., 2015; Marchi et al., 2017). Changes by both mechanisms could justify the downregulation of *TP53* and *RB1*, however only *RB1* has been reported to be hypermethylated (Marchi et al., 2017). Additionally, as most pathogenic variants of these genes have been described in coding regions, the mRNA downregulation of *TP53* and *RB1* does not appear to be due to mutations (Feber et al., 2016; Wang et al., 2019; Chahoud et al., 2021). Furthermore, few studies have evaluated patients' cohorts with a high incidence of HPV infection, remaining poorly known the impact of HPV infection in disrupting mRNA/miRNA networks in penile tumors (Zhang et al., 2015; Hartz et al., 2016; Kuasne et al., 2017; Ayoubian et al., 2021; Furuya et al., 2021). In the present study, our main goal was to determine whether altered miRNAs expression could be associated with the down-regulation of the *TP53* and *RB1* expression in the etiopathogenesis of HPV-associated PeCa. This goal is of critical relevance to these particular virus associated with infected tumors, considering that the patient cohort investigated, from the State of Maranhão in Northeastern Brazil, is characterized by advanced PeCa and a high rate of HPV infection (>90%), as we reported previously (Coelho et al., 2018; Macedo et al., 2020). In addition, this study can provide useful information to target HPV-specific molecular pathways in human cancers.

In the present study, all patients were tested for HPV by nested-PCR followed by DNA sequencing. Using two highly sensitive methods we successfully detected HPV infection in 100% of men with PeCa, all of them with high-risk subtypes. Despite the high HPV prevalence in all human populations, occurring as hundreds of types, subtypes, and variants, many of them are not associated with cancer. On the other hand, it is well established the correlation between high-risk HPV and severe dysplasia, *in situ* and invasive cancer, usually as monoclonal lesions due to clonal selection from less advanced precursors (Pontén and Guo, 1998). This may explain why we were able to detect HPV in 100% of the primary tumor since all of them presented high-risk genotypes.

It is well established that p53 regulates the expression of both protein-coding genes and non-coding RNAs (Hermeking, 2012; Fischer, 2017). *TP53*-regulated miRNAs can mediate tumor suppression in response to cellular stress; similarly, the expression and activity of p53 can also be under the control of miRNAs (Hermeking, 2012). More than 20 miRNAs have been described to directly regulate p53 via canonical bindings (seed) in 3′UTR (reviewed by Liu et al., 2017). Down regulation of *TP53* through seed sequences induce phenotypes that are consistent with loss of p53 function, such as reduced apoptosis, cellular senescence, increased invasion, and growth of tumor cells (Hermeking, 2012; Deng and Sui, 2013; Hermeking et al., 2014). Despite the increasing number of miRNAs that form the TP53 mRNA/miRNAs interaction network, there is no information on *TP53*-repressor miRNAs in HPV-associated PeCa. Our data revealed a total of 507 differentially expressed miRNA (miRDE) between the tumor and non-tumor tissue of HPV-infected PeCa patients, of which 494 were downregulated and 13 were upregulated. Among the 13 miRDE upregulated, five (let-7a-5p, miR-130a-3p, miR-15b-5p, miR-21-5p and miR-25-3p) were found overexpressed in 100% of the tumors analyzed. Moreover, miR-130a-3p, miR-15b-5p and miR-31-5p were predicted as novel regulator for *TP53* gene; while miR-142-3p, miR-200c-3p, miR-205-5p, miR-223-3p, miR-22-3p, miR-25-3p and miR-31-5p for *RB1*.

Several studies have shown up-regulated expression of these miRNAs in several types of tumors. Overexpression of let-7a-5p has been observed in HCV-related cirrhosis (Petkevich et al., 2021) and liver cancer and ovarian cancer, where it presents a non-invasive diagnostic potential (Liu et al., 2021). Corroborating our data, some studies have also suggested that *TP53* is a target of let-7a-5p (Balakrishnan et al., 2014; Pillai et al., 2014; Nunez Lopez et al., 2019; Zhou et al., 2019). MiR-130a-3p is recognized as a miRNA with tumor suppressor action (Kong et al., 2018; Song et al., 2021), that may act directly (Causin et al., 2021) or indirectly (Hu et al., 2021) in cancer progression. On the other hand, miR-15b-5p has generally been described to act on cell proliferation mechanisms, such as the ones involving the *LATS2* (Liu et al., 2020), *BCL-2* (Zhang et al., 2015), and *PTPN4*/*STAT3* pathways (Liu et al., 2020).

Interestingly, down-regulation of *TP53* by miR-25 resulted in a decrease in apoptosis in HCT116 colon cancer cells, A549 cells, NSCLC, and multiple myeloma cells (Kumar et al., 2011). In lung cancer, miR-25 was observed to promote cell proliferation and also inhibit apoptosis by down-regulating the expression of the *MOAP1*/*TP53* axis genes (Wu et al., 2015). Moreover, recent evidence shows that miR-25-3p may also act with LncRNAs on a *LINC00858*/miR-25/*SMAD7* axis modulating *TP53*-wild expression in colorectal carcinoma (Zhan et al., 2020). (Wang et al., 2021) also observed that exosomal miR-25-3p induced cell proliferation and resistance to temozolomide in glioblastoma through down-regulation of *FBXW7*, promoting c-Myc and cyclin E expression. MiR-21-5p, also observed up-regulated in this study, was shown by (Huang et al., 2021) to negatively regulate the tumor suppressor *PDCD4* and cause resistance to by Osimertinib by interfering with MEK/ERK signaling.

These results are in concordance with the suppressive effect of these miRNAs in the HPV-related genes observed in PeCa in the present study. Our computational analysis revealed that *TP53* and *RB1* have 131 and 490 target sites for the 13 upregulated miRNAs, respectively. The highest number of miRNA binding sites were identified in coding regions, and not in UTR regions, as reported by

(Hafner et al., 2010) Furthermore, 98.5 and 97.3% of the sites in *TP53* and *RB1*, respectively, are in non-canonical seedless regions, presenting high levels of complementarity and conservation. Although most miRNA targets have sites that are perfectly complementary to the seed region, it has been shown that miRNAs can directly interact with seedless binding sequences, even improving their function (Shin et al., 2010). (Lal et al., 2009) for example, presented evidence of cell proliferation control by miR-24 in the *E2F2/MYC* axis through seedless binding in the 3′UTR region. (Park et al., 2017). also showed that destabilization of miRNAs targets is dramatically increased when binding occurs in non-canonical seedless regions. Therefore, we propose that the 13 miRNAs overexpressed in PeCa directly repress *TP53* and *RB1* by silencing their messenger RNA at different binding sites, especially in non-canonical seedless regions.

Although a unique miRNA may have a pivotal role in a particular pathway, most miRNAs act targeting multiple mRNAs, affecting the same or several gene pathways. Considering the 13 upregulated miRNAs, we predicted six main pathways by the enrichment analysis. Viral carcinogenesis (hsa05203), in which *TP53* and *RB1* act, was the main pathway affected ($p < 1.00 \times 10\text{-}325$). MiR-205-5p, miR-16-5p, miR-22-3p, miR-93-5p, let-7a-5p, and miR-130a-3p were involved in most of the pathways affected. Glioma and cell cycle pathways, in addition to viral carcinogenesis, were previously shown to be regulated by other miRNAs identified in cytobands affected by CNVs in the same population from Maranhão State (Silva et al., 2021). Thus, these current findings reinforce the involvement of these pathways in HPV-associated penile tumorigenesis.

It is worth highlighting that 84.6% of miRDE were observed to be located in HPV integration sites (HPV-IS), including the five miRDE overexpressed in 100% of cases (sites at 3q25.33, 7q22.1, 9q22.32, 11q12.1, and 17q23.1). Several viruses mediate tumorigenesis by expressing viral oncogenes or activating host oncogenes through the integration of viral DNA into the human genome (Lee and Dutta, 2009; Tuna and Amos, 2017). We have recently shown that chromosomal regions with gene copy number alterations (CNA) are present in HPV-IS, such as 2p12-p11.2 and 14q32.33 (observed in 100% of PeCa patients), which can also affect the expression of miRNAs located in these regions (Macedo et al., 2020; Silva et al., 2021). These regions were also described in other HPV-associated tumors (Wentzensen et al., 2004; Kumar Gupta and Kumar, 2015; Holmes et al., 2016; Liu et al., 2016). This data shows the close connection of CNAs and miRNA deregulation located in HPV-IS. Altogether, our present data, support that miRNAs located in HPV-IS can directly repress genes related to HPV infection, such as *TP53* and *RB1*, highlighting HPV insertion as one of the factors that trigger epigenetic mechanisms.

CONCLUSION

In this study, we suggest that the HPV-related genes, *TP53* and *RB1*, are directly down-regulated by 13 miRNAs located in high-risk HPV integration sites, notably for the HPV16 subtype, present in 72% of the PeCa patients studied. Considering that the expression and activity of *TP53* and *RB1* can be under the control of miRNAs, our findings provide a new understanding of the role of high-risk HPV infection in penile tumorigenesis through an epigenetic mechanism.

DATA AVAILABILITY STATEMENT

The datasets presented in this study can be found in online repositories. The names of the repository/repositories and accession number(s) can be found below: https://www.ncbi.nlm.nih.gov/geo/, GSE197121.

ETHICS STATEMENT

The studies involving human participants were reviewed and approved by Research Ethics Committee on Humans from the Federal University of Maranhão and by the National Research Ethics Commission (CONEP-Brazil, CAAE: 46371515.5.0000.5087). The patients/participants provided their written informed consent to participate in this study.

AUTHOR CONTRIBUTIONS

Conceptualization, SP and JS; Methodology, SP, JS, RR, AL, LS, and CC; Formal Analysis, SP, AK, IF, and JS; Investigation, JS and SP; Resources, SP and AK; Writing—Original Draft Preparation, SP and JS; Writing—Review and Editing, SP and LC; Visualization, LC and AK; Supervision, SP; Project Administration, SP; Funding Acquisition, SP and AK.

FUNDING

This research was funded by Fundação de Amparo à Pesquisa e ao Desenvolvimento Científico e Tecnológico do Maranhão (FAPEMA)—Grant number IECT-05551/18 and Uniscience—nanoString miRNA Grant for SP, and by Comissão de Aperfeiçoamento de Pessoal do Nível Superior (CAPES; code 001) and for providing scholarship for JS. "The APC was funded by PROPESP-FEDERAL UNIVERSITY OF PARÁ".

SUPPLEMENTARY MATERIAL

The Supplementary Material for this article can be found online at: https://www.frontiersin.org/articles/10.3389/fgene.2022.875939/full#supplementary-material

REFERENCES

Adashek, J. J., Necchi, A., and Spiess, P. E. (2019). Updates in the Molecular Epidemiology and Systemic Approaches to Penile Cancer. *Urologic Oncol. Seminars Orig. Investigations* 37 (7), 403–408. doi:10.1016/j.urolonc.2019.04.012

Akagi, K., Li, J., Broutian, T. R., Padilla-Nash, H., Xiao, W., Jiang, B., et al. (2014). Genome-wide Analysis of HPV Integration in Human Cancers Reveals Recurrent, Focal Genomic Instability. *Genome Res.* 24 (2), 185–199. doi:10.1101/gr.164806.113

Ayoubian, H., Heinzelmann, J., Hölters, S., Khalmurzaev, O., Pryalukhin, A., Loertzer, P., et al. (2021). MiRNA Expression Characterizes Histological Subtypes and Metastasis in Penile Squamous Cell Carcinoma. *Cancers* 13 (6), 1480. doi:10.3390/cancers13061480

Balakrishnan, I., Yang, X., Brown, J., Ramakrishnan, A., Torok-Storb, B., Kabos, P., et al. (2014). Genome-Wide Analysis of miRNA-mRNA Interactions in Marrow Stromal Cells. *Stem Cells* 32 (3), 662–673. doi:10.1002/stem.1531

Barzon, L., Cappellesso, R., Peta, E., Militello, V., Sinigaglia, A., Fassan, M., et al. (2014). Profiling of Expression of Human Papillomavirus-Related Cancer miRNAs in Penile Squamous Cell Carcinomas. *Am. J. Pathology* 184 (12), 3376–3383. doi:10.1016/j.ajpath.2014.08.004

Bodelon, C., Untereiner, M. E., Machiela, M. J., Vinokurova, S., and Wentzensen, N. (2016). Genomic Characterization of Viral Integration Sites in HPV-Related Cancers. *Int. J. Cancer* 139 (9), 2001–2011. doi:10.1002/ijc.30243

Busso-Lopes, A. F., Marchi, F. A., Kuasne, H., Scapulatempo-Neto, C., Trindade-Filho, J. C. S., de Jesus, C. M. N., et al. (2015). Genomic Profiling of Human Penile Carcinoma Predicts Worse Prognosis and Survival. *Cancer Prev. Res.* 8 (2), 149–156. doi:10.1158/1940-6207.CAPR-14-0284

Causin, R. L., da Silva, L. S., Evangelista, A. F., Leal, L. F., Souza, K. C. B., Pessôa-Pereira, D., et al. (2021). MicroRNA Biomarkers of High-Grade Cervical Intraepithelial Neoplasia in Liquid Biopsy. *BioMed Res. Int.* 2021, 1–9. doi:10.1155/2021/6650966

Chahoud, J., Gleber-Netto, F. O., McCormick, B. Z., Rao, P., Lu, X., Guo, M., et al. (2021). Whole-exome Sequencing in Penile Squamous Cell Carcinoma Uncovers Novel Prognostic Categorization and Drug Targets Similar to Head and Neck Squamous Cell Carcinoma. *Clin. Cancer Res.* 27 (9), 2560–2570. doi:10.1158/1078-0432.CCR-20-4004

Christodoulidou, M., Sahdev, V., Houssein, S., and Muneer, A. (2015). Epidemiology of Penile Cancer. *Curr. Problems Cancer* 39 (3), 126–136. doi:10.1016/j.currproblcancer.2015.03.010

Coelho, R. W. P., Pinho, J. D., Moreno, J. S., Garbis, D. V. e. O., do Nascimento, A. M. T., Larges, J. S., et al. (2018). Penile Cancer in Maranhão, Northeast Brazil: the Highest Incidence Globally? *BMC Urol.* 18 (1), 50. doi:10.1186/s12894-018-0365-0

Datta, A., Das, P., Dey, S., Ghuwalewala, S., Ghatak, D., Alam, S. K., et al. (2019). Genome-Wide Small RNA Sequencing Identifies MicroRNAs Deregulated in Non-small Cell Lung Carcinoma Harboring Gain-Of-Function Mutant P53. *Genes* 10 (11), 852. doi:10.3390/genes10110852

Datta, A., Ghatak, D., Das, S., Banerjee, T., Paul, A., Butti, R., et al. (2017). p53 Gain-of-function Mutations Increase Cdc7-dependent Replication Initiation. *EMBO Rep.* 18 (11), 2030–2050. doi:10.15252/embr.201643347

de Martel, C., Plummer, M., Vignat, J., and Franceschi, S. (2017). Worldwide Burden of Cancer Attributable to HPV by Site, Country and HPV Type. *Int. J. Cancer* 141 (4), 664–670. doi:10.1002/ijc.30716

Deng, G., and Sui, G. (2013). Noncoding RNA in Oncogenesis: A New Era of Identifying Key Players. *Ijms* 14 (9), 18319–18349. doi:10.3390/ijms140918319

Ding, Y., Chan, C. Y., and Lawrence, C. E. (2004). Sfold Web Server for Statistical Folding and Rational Design of Nucleic Acids. *Nucleic Acids Res.* 32, W135–W141. doi:10.1093/nar/gkh449

Dürst, M., Croce, C. M., Gissmann, L., Schwarz, E., and Huebner, K. (1987). Papillomavirus Sequences Integrate Near Cellular Oncogenes in Some Cervical Carcinomas. *Proc. Natl. Acad. Sci. U.S.A.* 84 (4), 1070–1074. doi:10.1073/pnas.84.4.1070

Feber, A., Arya, M., de Winter, P., Saqib, M., Nigam, R., Malone, P. R., et al. (2015). Epigenetics Markers of Metastasis and HPV-Induced Tumorigenesis in Penile Cancer. *Clin. Cancer Res.* 21 (5), 1196–1206. doi:10.1158/1078-0432.CCR-14-1656

Feber, A., Worth, D. C., Chakravarthy, A., de Winter, P., Shah, K., Arya, M., et al. (2016). *CSN1* Somatic Mutations in Penile Squamous Cell Carcinoma. *Cancer Res.* 76 (16), 4720–4727. doi:10.1158/0008-5472.CAN-15-3134

Fischer, M. (2017). Census and Evaluation of P53 Target Genes. *Oncogene* 36 (28), 3943–3956. doi:10.1038/onc.2016.502

Furuya, T. K., Murta, C. B., Murillo Carrasco, A. G., Uno, M., Sichero, L., Villa, L. L., et al. (2021). Disruption of miRNA-mRNA Networks Defines Novel Molecular Signatures for Penile Carcinogenesis. *Cancers* 13 (19), 4745. doi:10.3390/cancers13194745

Gao, G., Johnson, S. H., Vasmatzis, G., Pauley, C. E., Tombers, N. M., Kasperbauer, J. L., et al. (2017). Common Fragile Sites (CFS) and Extremely Large CFS Genes Are Targets for Human Papillomavirus Integrations and Chromosome Rearrangements in Oropharyngeal Squamous Cell Carcinoma. *Genes Chromosom. Cancer* 56 (1), 59–74. doi:10.1002/gcc.22415

Groves, I. J., and Coleman, N. (2018). Human Papillomavirus Genome Integration in Squamous Carcinogenesis: what Have Next-Generation Sequencing Studies Taught Us? *J. Pathol.* 245 (1), 9–18. doi:10.1002/path.5058

Hafner, M., Landthaler, M., Burger, L., Khorshid, M., Hausser, J., Berninger, P., et al. (2010). Transcriptome-wide Identification of RNA-Binding Protein and MicroRNA Target Sites by PAR-CLIP. *Cell.* 141 (1), 129–141. doi:10.1016/j.cell.2010.03.009

Hansen, B. T., Orumaa, M., Lie, A. K., Brennhovd, B., and Nygård, M. (2018). Trends in Incidence, Mortality and Survival of Penile Squamous Cell Carcinoma in Norway 1956-2015. *Int. J. Cancer* 142 (8), 1586–1593. doi:10.1002/ijc.31194

Hartz, J. M., Engelmann, D., Fürst, K., Marquardt, S., Spitschak, A., Goody, D., et al. (2016). Integrated Loss of miR-1/miR-101/miR-204 Discriminates Metastatic from Nonmetastatic Penile Carcinomas and Can Predict Patient Outcome. *J. Urology* 196 (2), 570–578. doi:10.1016/j.juro.2016.01.115

Hennig, C. (2020). Fpc: Flexible Procedures for Clustering. Fpc: Flexible Procedures for Clustering. AvaliableAt: https://CRAN.R-project.org/package=fpc (Accessed August 5, 2021).

Hermeking, H. (2012). MicroRNAs in the P53 Network: Micromanagement of Tumour Suppression. *Nat. Rev. Cancer* 12 (9), 613–626. doi:10.1038/nrc3318

Hermeking, H., Rokavec, M., Li, H., and Jiang, L. (2014). The p53/microRNA Connection in Gastrointestinal Cancer. *Ceg* 395, 395. doi:10.2147/CEG.S43738

Holmes, A., Lameiras, S., Jeannot, E., Marie, Y., Castera, L., Sastre-Garau, X., et al. (2016). Mechanistic Signatures of HPV Insertions in Cervical Carcinomas. *npj Genomic Med.* 1 (1), 16004. doi:10.1038/npjgenmed.2016.4

Hu, W., Zheng, X., Liu, J., Zhang, M., Liang, Y., and Song, M. (2021). MicroRNA MiR-130a-3p Promotes Gastric Cancer by Targeting Glucosaminyl N-Acetyl Transferase 4 (GCNT4) to Regulate the TGF-B1/smad3 Pathway. *Bioengineered* 12 (2), 11634–11647. doi:10.1080/21655979.2021.1995099

Hu, Z., Zhu, D., Wang, W., Li, W., Jia, W., Zeng, X., et al. (2015). Genome-wide Profiling of HPV Integration in Cervical Cancer Identifies Clustered Genomic Hot Spots and a Potential Microhomology-Mediated Integration Mechanism. *Nat. Genet.* 47 (2), 158–163. doi:10.1038/ng.3178

Huang, W.-C., Yadav, V. K., Cheng, W.-H., Wang, C.-H., Hsieh, M.-S., Huang, T.-Y., et al. (2021). The MEK/ERK/miR-21 Signaling Is Critical in Osimertinib Resistance in EGFR-Mutant Non-small Cell Lung Cancer Cells. *Cancers* 13 (23), 6005. doi:10.3390/cancers13236005

Hussen, B. M., Ahmadi, G., Marzban, H., Fard Azar, M. E., Sorayyayi, S., Karampour, R., et al. (2021). The Role of HPV Gene Expression and Selected Cellular MiRNAs in Lung Cancer Development. *Microb. Pathog.* 150, 104692. doi:10.1016/j.micpath.2020.104692

Kanoria, S., Rennie, W., Liu, C., Carmack, C. S., Lu, J., and Ding, Y. (2016). STarMir Tools for Prediction of microRNA Binding Sites. *Methods Mol. Biol.* 1490, 73–82. doi:10.1007/978-1-4939-6433-8_6

Kidd, L. C., Chaing, S., Chipollini, J., Giuliano, A. R., Spiess, P. E., and Sharma, P. (2017). Relationship between Human Papillomavirus and Penile Cancer-Implications for Prevention and Treatment. *Transl. Androl. Urol.* 6 (5), 791–802. doi:10.21037/tau.2017.06.27

Kong, X., Zhang, J., Li, J., Shao, J., and Fang, L. (2018). MiR-130a-3p Inhibits Migration and Invasion by Regulating RAB5B in Human Breast Cancer Stem Cell-like Cells. *Biochem. Biophysical Res. Commun.* 501 (2), 486–493. doi:10.1016/j.bbrc.2018.05.018

Kuasne, H., Barros-Filho, M. C., Busso-Lopes, A., Marchi, F. A., Pinheiro, M., Muñoz, J. J. M., et al. (2017). Integrative miRNA and mRNA Analysis in Penile Carcinomas Reveals Markers and Pathways with Potential Clinical Impact. *Oncotarget* 8 (9), 15294–15306. doi:10.18632/oncotarget.14783

Kuasne, H., Cólus, I. M. d. S., Busso, A. F., Hernandez-Vargas, H., Barros-Filho, M. C., Marchi, F. A., et al. (2015). Genome-wide Methylation and Transcriptome Analysis in Penile Carcinoma: Uncovering New Molecular Markers. *Clin. Epigenet* 7 (1), 46. doi:10.1186/s13148-015-0082-4

Kumar Gupta, A., and Kumar, M. (2015). HPVbase - a Knowledgebase of Viral Integrations, Methylation Patterns and microRNAs Aberrant Expression: As Potential Biomarkers for Human Papillomaviruses Mediated Carcinomas. *Sci. Rep.* 5 (1), 12522. doi:10.1038/srep12522

Kumar, M., Lu, Z., Takwi, A. A. L., Chen, W., Callander, N. S., Ramos, K. S., et al. (2011). Negative Regulation of the Tumor Suppressor P53 Gene by microRNAs. *Oncogene* 30 (7), 843–853. doi:10.1038/onc.2010.457

Lal, A., Navarro, F., Maher, C. A., Maliszewski, L. E., Yan, N., O'Day, E., et al. (2009). miR-24 Inhibits Cell Proliferation by Targeting E2F2, MYC, and Other Cell-Cycle Genes via Binding to "Seedless" 3′UTR MicroRNA Recognition Elements. *Mol. Cell.* 35 (5), 610–625. doi:10.1016/j.molcel.2009.08.020

Lee, Y. S., and Dutta, A. (2009). MicroRNAs in Cancer. *Annu. Rev. Pathol. Mech. Dis.* 4 (1), 199–227. doi:10.1146/annurev.pathol.4.110807.092222

Liu, J., Yoo, J., Ho, J. Y., Jung, Y., Lee, S., Hur, S. Y., et al. (2021). Plasma-derived Exosomal miR-4732-5p Is a Promising Noninvasive Diagnostic Biomarker for Epithelial Ovarian Cancer. *J. Ovarian Res.* 14 (1), 59. doi:10.1186/s13048-021-00814-z

Liu, J., Zhang, C., Zhao, Y., and Feng, Z. (2017). MicroRNA Control of P53. *J. Cell. Biochem.* 118 (1), 7–14. doi:10.1002/jcb.25609

Liu, X., Dong, Y., and Song, D. (2020a). Inhibition of microRNA-15b-5p Attenuates the Progression of Oral Squamous Cell Carcinoma via Modulating the PTPN4/STAT3 Axis. *Cmar* Vol. 12, 10559–10572. doi:10.2147/CMAR.S272498

Liu, Y., Lu, Z., Xu, R., and Ke, Y. (2016). Comprehensive Mapping of the Human Papillomavirus (HPV) DNA Integration Sites in Cervical Carcinomas by HPV Capture Technology. *Oncotarget* 7 (5), 5852–5864. doi:10.18632/oncotarget.6809

Liu, Z.-J., Liu, S.-H., Li, J.-R., Bie, X.-C., and Zhou, Y. (2020b). MiR-15b-5b Regulates the Proliferation of Prostate Cancer PC-3 Cells via Targeting LATS2. *Cmar* Vol. 12, 10669–10678. doi:10.2147/CMAR.S266421

Long, D., Lee, R., Williams, P., Chan, C. Y., Ambros, V., and Ding, Y. (2007). Potent Effect of Target Structure on microRNA Function. *Nat. Struct. Mol. Biol.* 14 (4), 287–294. doi:10.1038/nsmb1226

Macedo, J., Silva, E., Nogueira, L., Coelho, R., Silva, J., Santos, A., et al. (2020). Genomic Profiling Reveals the Pivotal Role of hrHPV Driving Copy Number and Gene Expression Alterations, Including mRNA Downregulation of *TP53* and *RB1* in Penile Cancer. *Mol. Carcinog.* 59 (6), 604–617. doi:10.1002/mc.23185

Mantovani, F., Collavin, L., and Del Sal, G. (2019). Mutant P53 as a Guardian of the Cancer Cell. *Cell. Death Differ.* 26 (2), 199–212. doi:10.1038/s41418-018-0246-9

Marchi, F. A., Martins, D. C., Barros-Filho, M. C., Kuasne, H., Busso Lopes, A. F., Brentani, H., et al. (2017). Multidimensional Integrative Analysis Uncovers Driver Candidates and Biomarkers in Penile Carcinoma. *Sci. Rep.* 7 (1), 6707. doi:10.1038/s41598-017-06659-1

Nunez Lopez, Y. O., Retnakaran, R., Zinman, B., Pratley, R. E., and Seyhan, A. A. (2019). Predicting and Understanding the Response to Short-Term Intensive Insulin Therapy in People with Early Type 2 Diabetes. *Mol. Metab.* 20, 63–78. doi:10.1016/j.molmet.2018.11.003

Parfenov, M., Pedamallu, C. S., Gehlenborg, N., Freeman, S. S., Danilova, L., Bristow, C. A., et al. (2014). Characterization of HPV and Host Genome Interactions in Primary Head and Neck Cancers. *Proc. Natl. Acad. Sci. U.S.A.* 111 (43), 15544–15549. doi:10.1073/pnas.1416074111

Park, J. H., Shin, S.-Y., and Shin, C. (2017). Non-canonical Targets Destabilize microRNAs in Human Argonautes. *Nucleic Acids Res.* 45, 1569–1583. doi:10.1093/nar/gkx029

Pessôa-Pereira, D., Evangelista, A. F., Causin, R. L., da Costa Vieira, R. A., Abrahão-Machado, L. F., Santana, I. V. V., et al. (2020). MiRNA Expression Profiling of Hereditary Breast Tumors from BRCA1- and BRCA2-Germline Mutation Carriers in Brazil. *BMC Cancer* 20 (1), 143. doi:10.1186/s12885-020-6640-y

Peta, E., Cappellesso, R., Masi, G., Sinigaglia, A., Trevisan, M., Grassi, A., et al. (2017). Down-regulation of microRNA-146a Is Associated with High-Risk Human Papillomavirus Infection and Epidermal Growth Factor Receptor Overexpression in Penile Squamous Cell Carcinoma. *Hum. Pathol.* 61, 33–40. doi:10.1016/j.humpath.2016.10.019

Petkevich, A. A., Abramov, A. A., Pospelov, V. I., Malinina, N. A., Kuhareva, E. I., Mazurchik, N. V., et al. (2021). Exosomal and Non-exosomal miRNA Expression Levels in Patients with HCV-Related Cirrhosis and Liver Cancer. *Oncotarget* 12 (17), 1697–1706. doi:10.18632/oncotarget.28036

Pillai, M. M., Gillen, A. E., Yamamoto, T. M., Kline, E., Brown, J., Flory, K., et al. (2014). HITS-CLIP Reveals Key Regulators of Nuclear Receptor Signaling in Breast Cancer. *Breast Cancer Res. Treat.* 146 (1), 85–97. doi:10.1007/s10549-014-3004-9

Pinatti, L. M., Gu, W., Wang, Y., Elhossiny, A., Bhangale, A. D., Brummel, C. V., et al. (2021). SearcHPV: A Novel Approach to Identify and Assemble Human Papillomavirus-Host Genomic Integration Events in Cancer. *Cancer* 127 (19), 3531–3540. doi:10.1002/cncr.33691

Pontén, J., and Guo, Z. (1998). Precancer of the Human Cervix. *Cancer Surv.* 32, 201–229.

Rehmsmeier, M., Steffen, P., Höchsmann, M., and Giegerich, R. (2004). Fast and Effective Prediction of microRNA/target Duplexes. *RNA* 10 (10), 1507–1517. doi:10.1261/rna.5248604

Rosa, M. N., Evangelista, A. F., Leal, L. F., De Oliveira, C. M., Silva, V. A. O., Munari, C. C., et al. (2019). Establishment, Molecular and Biological Characterization of HCB-514: A Novel Human Cervical Cancer Cell Line. *Sci. Rep.* 9 (1), 1913. doi:10.1038/s41598-018-38315-7

Sammons, M. A., Nguyen, T.-A. T., McDade, S. S., and Fischer, M. (2020). Tumor Suppressor P53: From Engaging DNA to Target Gene Regulation. *Nucleic Acids Res.* 48 (16), 8848–8869. doi:10.1093/nar/gkaa666

Santos, J., Peixoto da Silva, S., Costa, N., Gil da Costa, R., and Medeiros, R. (2018). The Role of MicroRNAs in the Metastatic Process of High-Risk HPV-Induced Cancers. *Cancers* 10 (12), 493. doi:10.3390/cancers10120493

Shin, C., Nam, J.-W., Farh, K. K.-H., Chiang, H. R., Shkumatava, A., and Bartel, D. P. (2010). Expanding the MicroRNA Targeting Code: Functional Sites with Centered Pairing. *Mol. Cell.* 38 (6), 789–802. doi:10.1016/j.molcel.2010.06.005

Silva, J. d., Nogueira, L., Coelho, R., Deus, A., Khayat, A., Marchi, R., et al. (2021). HPV-associated Penile Cancer: Impact of Copy Number Alterations in miRNA/mRNA Interactions and Potential Druggable Targets. *Cbm* 32, 147–160. doi:10.3233/CBM-210035

Song, G.-L., Xiao, M., Wan, X.-Y., Deng, J., Ling, J.-D., Tian, Y.-G., et al. (2021). MiR-130a-3p Suppresses Colorectal Cancer Growth by Targeting Wnt Family Member 1 (WNT1). *Bioengineered* 12 (1), 8407–8418. doi:10.1080/21655979.2021.1977556

Squarzanti, D. F., Sorrentino, R., Landini, M. M., Chiesa, A., Pinato, S., Rocchio, F., et al. (2018). Human Papillomavirus Type 16 E6 and E7 Oncoproteins Interact with the Nuclear P53-Binding Protein 1 in an *In Vitro* Reconstructed 3D Epithelium: New Insights for the Virus-Induced DNA Damage Response. *Virol. J.* 15 (1), 176. doi:10.1186/s12985-018-1086-4

Tang, D., Li, B., Xu, T., Hu, R., Tan, D., Song, X., et al. (2020). VISDB: A Manually Curated Database of Viral Integration Sites in the Human Genome. *Nucleic Acids Res.* 48 (D1), D633–D641. doi:10.1093/nar/gkz867

Tuna, M., and Amos, C. I. (2017). Next Generation Sequencing and its Applications in HPVassociated Cancers. *Oncotarget* 8 (5), 8877–8889. doi:10.18632/oncotarget.12830

Vlachos, I. S., Zagganas, K., Paraskevopoulou, M. D., Georgakilas, G., Karagkouni, D., Vergoulis, T., et al. (2015). DIANA-miRPath v3.0: Deciphering microRNA Function with Experimental Support. *Nucleic Acids Res.* 43 (W1), W460–W466. doi:10.1093/nar/gkv403

Wang, J., Li, T., and Wang, B. (2021). Exosomal Transfer of miR-25-3p P-romotes the P-roliferation and T-emozolomide R-esistance of G-lioblastoma C-ells by T-argeting FBXW7. *Int. J. Oncol.* 59 (2), 64. doi:10.3892/ijo.2021.5244

Wang, X., and Sun, Q. (2017). *TP53* Mutations, Expression and Interaction Networks in Human Cancers. *Oncotarget* 8 (1), 624–643. doi:10.18632/oncotarget.13483

Wang, Y., Wang, K., Chen, Y., Zhou, J., Liang, Y., Yang, X., et al. (2019). Mutational Landscape of Penile Squamous Cell Carcinoma in a Chinese Population. *Int. J. Cancer* 145 (5), 1280–1289. doi:10.1002/ijc.32373

Wentzensen, N., Vinokurova, S., and Doeberitz, M. v. K. (2004). Systematic Review of Genomic Integration Sites of Human Papillomavirus Genomes in Epithelial Dysplasia and Invasive Cancer of the Female Lower Genital Tract. *Cancer Res.* 64 (11), 3878–3884. doi:10.1158/0008-5472.CAN-04-0009

Wu, T., Chen, W., Kong, D., Li, X., Lu, H., Liu, S., et al. (2015). MiR-25 Targets the Modulator of Apoptosis 1 Gene in Lung Cancer. *Carcin* 36 (8), 925–935. doi:10.1093/carcin/bgv068

Zhan, J., Tong, J., and Fu, Q. (2020). Long Non-coding RNA LINC00858 P-romotes TP53-wild-type C-olorectal C-ancer P-rogression by R-egulating the microRNA-25-3p/SMAD7 axis. *Oncol. Rep.* 43, 1267–1277. doi:10.3892/or.2020.7506

Zhang, L., Wei, P., Shen, X., Zhang, Y., Xu, B., Zhou, J., et al. (2015a). MicroRNA Expression Profile in Penile Cancer Revealed by Next-Generation Small RNA Sequencing. *Plos One* 10 (7), e0131336. doi:10.1371/journal.pone.0131336

Zhang, Y., Huang, F., Wang, J., Peng, L., and Luo, H. (2015b). MiR-15b Mediates Liver Cancer Cells Proliferation through Targeting BCL-2. *Int. J. Clin. Exp. Pathol.* 7, 15677–15683.

Zhou, X., Zhang, Z., and Liang, X. (2019). Regulatory Network Analysis to Reveal Important miRNAs and Genes in Non-small Cell Lung Cancer. *Cell. J.* 21 (4), 459–466. doi:10.22074/cellj.2020.6281

Zuker, M. (2003). Mfold Web Server for Nucleic Acid Folding and Hybridization Prediction. *Nucleic Acids Res.* 31 (13), 3406–3415. doi:10.1093/nar/gkg595

Conflict of Interest: The authors declare that the research was conducted in the absence of any commercial or financial relationships that could be construed as a potential conflict of interest.

Publisher's Note: All claims expressed in this article are solely those of the authors and do not necessarily represent those of their affiliated organizations, or those of the publisher, the editors and the reviewers. Any product that may be evaluated in this article, or claim that may be made by its manufacturer, is not guaranteed or endorsed by the publisher.

frontiers | Frontiers in Genetics

ORIGINAL RESEARCH
published: 30 June 2022
doi: 10.3389/fgene.2022.865472

MicroRNAs miR-142-5p, miR-150-5p, miR-320a-3p, and miR-4433b-5p in Serum and Tissue: Potential Biomarkers in Sporadic Breast Cancer

*Tamyres Mingorance Carvalho[1], Guillermo Ortiz Brasil[1], Tayana Schultz Jucoski[1], Douglas Adamoski[1,2], Rubens Silveira de Lima[3], Cleverton C. Spautz[3], Karina Furlan Anselmi[3], Patricia Midori Murobushi Ozawa[1,4], Iglenir João Cavalli[1], Jaqueline Carvalho de Oliveira[1], Daniela Fiori Gradia[1] and Enilze Maria de Souza Fonseca Ribeiro[1]**

[1]Laboratory of Human Cytogenetics and Oncogenetics, Postgraduate Program in Genetics, Department of Genetics, Federal University of Paraná (UFPR), Curitiba, Brazil, [2]Brazilian Biosciences National Laboratory (LNBio), Brazilian Center for Research in Energy and Materials (CNPEM), Sao Paulo, Brazil, [3]Breast Disease Center, Hospital Nossa Senhora das Graças, Curitiba, Brazil, [4]Department of Cell and Developmental Biology, Vanderbilt University School of Medicine, Nashville, TN, United States

OPEN ACCESS

Edited by:
William C. Cho, QEH, Hong Kong SAR, China

Reviewed by:
Ehsan Nazemalhosseini-Mojarad, Shahid Beheshti University of Medical Sciences, Iran
Magali Espinosa, Instituto Nacional de Medicina Genómica (INMEGEN), Mexico

***Correspondence:**
Enilze Maria de Souza Fonseca Ribeiro
eribeiro@ufpr.br

Specialty section:
This article was submitted to RNA, a section of the journal Frontiers in Genetics.

Received: *29 January 2022*
Accepted: *16 May 2022*
Published: *30 June 2022*

Citation:
Carvalho TM, Brasil GO, Jucoski TS, Adamoski D, Lima RSd, Spautz CC, Anselmi KF, Ozawa PMM, Cavalli IJ, Carvalho de Oliveira J, Gradia DF and Ribeiro EMdSF (2022) MicroRNAs miR-142-5p, miR-150-5p, miR-320a-3p, and miR-4433b-5p in Serum and Tissue: Potential Biomarkers in Sporadic Breast Cancer. Front. Genet. 13:865472. doi: 10.3389/fgene.2022.865472

Breast cancer (BC) is a heterogeneous disease, and establishing biomarkers is essential to patient management. We previously described that extracellular vesicle–derived miRNAs (EV-miRNAs) miR-142-5p, miR-150-5p, miR-320a, and miR-4433b-5p in serum discriminated BC from control samples, either alone or combined in a panel. Using these previously described markers, we intend to evaluate whether the same markers identified in EVs are also potential biomarkers in tissue and serum. Expression analysis using RT-qPCR was performed using serum of 67 breast cancer patients (BC-S), 19 serum controls (CT), 83 fresh tumor tissues (BC-T), and 29 adjacent nontumor tissue samples (NT). In addition, analysis from The Cancer Genome Atlas (TCGA) data (832 BC-T and 136 NT) was performed. In all comparisons, we found concordant high expression levels of miR-320a and miR-4433b-5p in BC-S compared to CT in both EVs and cell-free miRNAs (cf-miRNAs). Although miR-150-5p and miR-142-5p were not found to be differentially expressed in serum, panels including these miRNAs improved sensitivity and specificity, supporting our previous findings in EVs. Fresh tissue and data from the TCGA database had, in most comparisons, an opposite behavior when compared to serum and EVs: lower levels of all miRNAs in BC-T than those in NT samples. TCGA analyses revealed reduced expression levels of miR-150-5p and miR-320a-3p in BC-T than those in NT samples and the overexpression of miR-142-5p in BC-T, unlike our RT-qPCR results from tissue in the Brazilian cohort. The fresh tissue analysis showed that all miRNAs individually could discriminate between BC-T and NT in the Brazilian cohort, with high sensitivity and sensibility. Furthermore, combining panels showed higher AUC values and improved sensitivity and specificity. In addition, lower levels of miR-320a-3p in serum were associated with poor overall survival in BC Brazilian patients. In summary, we observed that miR-320a and miR-4433b-5p distinguished BC from controls with high specificity and sensibility, regardless of the sample source. In addition, lower levels of miR-150-5p and higher levels of miR-142-5p were statistically significant biomarkers in tissue,

according to TCGA. When combined in panels, all combinations could distinguish BC patients from controls. These results highlight a potential application of these miRNAs as BC biomarkers.

Keywords: breast cancer, miR-142-5p, miR-150-5p, miR-320a, miR-4433b-5p, biomarkers

1 INTRODUCTION

Breast cancer (BC) is the most common malignancy and the second leading cause of death by cancer in women worldwide (Sung et al., 2021). Only in 2020, more than 2 million females had developed the disease, and the occurrence of 66,000 new cases is expected in each year of the triene 2020–2022 in Brazil (INCAdeda.S, 2019). As a heterogeneous disease, different classifications for BC have been proposed, mainly based on histology and risk factors but since the 2000s also based on gene expression. Perou et al. (2000) proposed that the phenotypic variety of BC might be accompanied by a distinct gene expression and described the first molecular classification subdividing tumors expressing hormonal receptors (estrogen and progesterone), overexpressing HER2 oncoprotein, and with the basal phenotype (Perou et al., 2000). This classification was validated and expanded (Sørlie et al., 2001; Farmer et al., 2005; Prat et al., 2013) and adapted to clinical practice by a partly corresponding immunohistochemical (IHC) classification (Goldhirsch et al., 2013). Currently, the molecular classification based on IHC defines four subgroups using four markers, estrogen receptor (ER), progesterone receptor (PR), HER2 expression, and the proliferation marker Ki-67. The subgroups are luminal A (LA), luminal B (LB), HER2 enriched, and triple-negative breast cancer (TNBC). Although the TNBC subgroup is considered a single entity on IHC, it is a very heterogeneous group that reflects on treatment decisions (Marra et al., 2020).

Personalized medicine has been the ultimate goal of current oncology management. Accuracy in the tumor characterization and prediction of patient prognosis based on tumor biology improves the opportunity for target treatments. A better characterization of the genomic landscape, the application of omics technologies, and novel clinical trials will pave the way toward personalized anticancer treatments in breast cancer. Despite the efforts and advances, the morbidity and mortality of BC remain high (INCA, 2019). In this scenario, a deep understanding of BC molecular characteristics is essential to develop new biomarkers for early detection and classification, positively impacting diagnosis, treatment, and effectiveness of controlling this neoplasia.

A class of molecules that have been described to play a significant role in cancer is the microRNAs (miRNAs). miRNAs are small non-coding RNAs that regulate gene expression in biological processes (Ambros, 2004; Bartel, 2009; Ramassone et al., 2018), and their deregulation can lead to cancer development (Rupaimoole and Slack, 2017; Adhami et al., 2018; Mandujano-Tinoco et al., 2018). Several studies suggest that miRNAs can become helpful biomarkers to monitor cancer progression and prognosis (Wang et al., 2016; Adhami et al., 2018; Ozawa et al., 2020a; Hong et al., 2020), but the potential of miRNAs in BC patients remains uncertain. Recently, miR-875 and miR-103a-3p were found as potential prognostic markers in BC patients. Nonetheless, the number of evaluated patients was quite limited, in addition to the absence of a second validation cohort (Liu H. et al., 2022; Liu et al., 2022 X.). Combined circulating miRNAs were validated to accurately distinguish BC patients and subtypes from controls (Kim et al., 2021a; Zhang et al., 2021a; Li et al., 2022b), and to screen BC patients associated with mammography (Zou et al., 2021a; 2022a), highlighting the relevance of the panel's studies.

Interestingly, a recent study from our group found that lower levels of miR-150-5p, miR-142-5p, and miR-320a in extracellular vesicles from patient serum are associated with advanced tumor grades and larger tumor size (Ozawa et al., 2020b). The authors also identified that a panel comprising miR-142-5p, miR-320a, and miR-4433b-5p could distinguish BC patients from controls with high sensitivity and specificity (Ozawa et al., 2020b). To assess if these miRNAs can also be used as biomarkers in different types of samples, we analyzed the expression of these miRNAs in tumor tissue and cell-free miRNAs (cf-miRNAs) in serum.

2 MATERIALS AND METHODS

This study was approved by the Ethical Committee in Research from the Health Sciences Unit of the Federal University of Paraná (UFPR) (CAAE 19870319.3.0000.0102). All individuals signed a written informed consent form.

2.1 Sample Characterization

2.1.1. Fresh Tumor Samples and Serum

We included 30 breast tumor tissues (BC-T) and 29 nontumor adjacent tissues (NT) collected during surgery at the Hospital Nossa Senhora das Graças (Curitiba, Southern Brazil). We also collected peripheral blood (BC-S) from 67 patients before surgery in BD Vacutainer® SST™ II Advance tubes, and we further processed the blood to obtain serum. The tissue samples were stored in RNA Stabilizing Solution (RNAlater®—Invitrogen) until processing. In addition, we collected control serum samples (CT) from 19 healthy volunteers at the Federal University of Parana. We excluded controls younger than 50 years or with a previous personal or familial history of cancer and patients with previously neoadjuvant chemotherapy. We obtained clinical and histopathological information about the immunohistochemical markers, age at diagnosis, cancer or death events, histological classification and grade of tumor, the presence or absence of axillary lymph node metastasis, and tumor size from the patient's medical reports (**Table 1**). The classification was based on Goldhirsch et al. (2013).

TABLE 1 | Clinicopathological data obtained from the TCGA database and clinical reports of breast cancer patients.

	TCGA			Brazilian cohort*			
	NT	**LA**	**BLBC**	**NT**	**LA**	**TNBC**	**CT**
N	75	250#	83	29	56	27	19
Median age	57.21 ± 15.67	58 ± 13.4	55 ± 13.06	55 ± 14.86	61 ± 13.13	54 ± 16.11	55 ± 14.86
Survival data, ¥	1913 ± 1,046	1812 ± 1,304	1759 ± 1,061	n.i.	16/26	10/26	n.i.
Menopausal status, £							
Pre-	17/53	64/227	14/78	n.i	10/56	10/27	2/19
Post-	35/53	155/227	58/78	n.i	46/56	17/27	17/19
Peri-	1/53	8/227	6/78	n.i			
Tumor size							
≤20 mm	--	n.i.	n.i.	15/28	10/22	8/13	--
>20 mm	--	n.i.	n.i.	13/28	12/22	5/13	--
Histological classification							
Infiltrating ductal	--	168/250	73/83	--	34/56	25/27	--
Infiltrating lobular	--	54/250	2/83	--	8/56	1/27	--
Mixed ductal and lobular	--	11/250	1/83	--	8/56	0	--
Others †	--	17/250	7/83	--	6/56	1/27	--
Histological grade							
I, IA, IB	--	66/248	12/81	--	5/24	0	--
II, IIA, IIB	--	132/248	60/81	--	19/24	3/12	--
III, IIIA, IIIB, IIIC	--	46/248	9/81	--	0	9/12	--
IV, X	--	6/248	0/81	--	0	0	--
Metastatic axillary lymph node							
POS	38/69	121/232	26/77	7/28	5/47	10/22	--
NEG	31/69	111/232	51/77	21/28	42/47	12/22	--

N, number of all patients included in the study for each group. (*) The Brazilian cohort includes all the patients who have at least one of the studied samples—serum (BC-S = 67; CT = 19) or tissue (BC-T = 30; NT = 29). NT, adjacent non-tumor tissue; LA, luminal A; TNBC, triple-negative breast cancer; CT, serum samples of controls; BLBC, basal-like breast cancer; (--), not applicable; and (n.i.), not informed. (£) menopausal status of Brazilian patients was estimated based on the age of patients, and patients with peri- and post-menopausal statuses are grouped (≥50). (¥) Survival data for TCGA are represented as days to death, while the Brazilian cohort is the number of patients with data about cancer or death events. (†) includes mucinous carcinoma, tubular carcinoma, medullary carcinoma, and metaplastic carcinoma. Numbers in each parameter differ due to the lack of information for some patients. (#) LA group from the TCGA database includes four male samples, which have been removed from posterior analyses.

2.1.2 TCGA

We evaluated the tissue expression profile in a second cohort using data from 822 samples with miRNA mature strand expression RNA-seq extracted from "The Cancer Genome Atlas" (TCGA) database, from TCGA BRCA cohort version 2017-09-08. TCGA data were obtained as log2 (RPM+1) and converted to fold change (FC). We further processed the data according to adjusted p-value < 0.05 and false discovery rate (FDR) < 0.05.

TCGA data contained the following clinicopathological parameters: age of diagnosis, histological classification, grade and size of the tumor, and the presence or absence of axillary lymph node metastasis, in addition to days to death and overall survival information (**Table 1**). We selected for analysis the intrinsic subtypes luminal A (LA) ($n = 250$) and basal-like breast carcinoma (BLBC) ($n = 83$) on TCGA samples and nontumor samples. We identified the target miRNAs using the unique identification of mature miRNAs (MIMAT ID). The selected miRNAs were as follows: miR-142-5p (MIMAT0000433), miR-150-5p (MIMAT0000451), miR-320a-3p (MIMAT0000510), and miR-4433b-5p (MIMAT0030413) on tumor (BC-T) and nontumor samples (NT). We accessed clinical and histopathological information and performed differential expression analyses comparing NT and BC-T samples in addition to the intrinsic subtypes LA and BLBC.

2.2 Sample Processing

We stored all tumor samples in RNA Stabilizing Solution until further processing. We centrifuged the blood samples at 700 g for 10 min to obtain serum. For RNA extraction from tissue, we used the miRNeasy kit (Qiagen, Hilden, Germany), while for RNA from serum, we used the MagMAX™ Total Nucleic Acid Isolation Kit (Thermo Fisher Scientific, Waltham, United States), both according to the manufacturer's instructions. We then evaluated the quality parameters using the spectrophotometer *NanoDrop 2000* (Thermo Fisher Scientific, Waltham, United States) and stored samples at −80°C until further processed.

2.3 RT-qPCR

We performed reverse transcription–quantitative polymerase chain reactions (RT-qPCRs) using a TaqMan MicroRNA Reverse Transcription Kit (Thermo Fisher Scientific, Waltham, United States). Briefly, for a final volume of 20 µl, 10 ng of total RNA extracted was mixed with 1.25 mM dNTPs, 3.75 U/µl of MultiScribe™ Reverse Transcriptase, 1x of Reverse Transcription Buffer, 0.25 U/µl of RNase inhibitor, and 0.125x of each primer—has-miR-142-5p (ID: 002248), has-miR-150-5p (ID: 000473), has-miR-320a (ID: 002277), and has-miR-4433b-5p (ID: 466345_mat). The mixture was submitted to cycles of 25 °C for 10 min, then 37 °C for 2 h, and 85 °C for 5 min on an Eppendorf 5331 MasterCycler Gradient Thermal Cycler (Eppendorf, DE). Next, cDNA samples were diluted at 1:5, and 2.25 µl of this mix was added to 1x TaqMan Universal PCR Master Mix II (no UNG) for a final volume of 5 µl in 384-well plates. Triplicates were performed for each sample, and

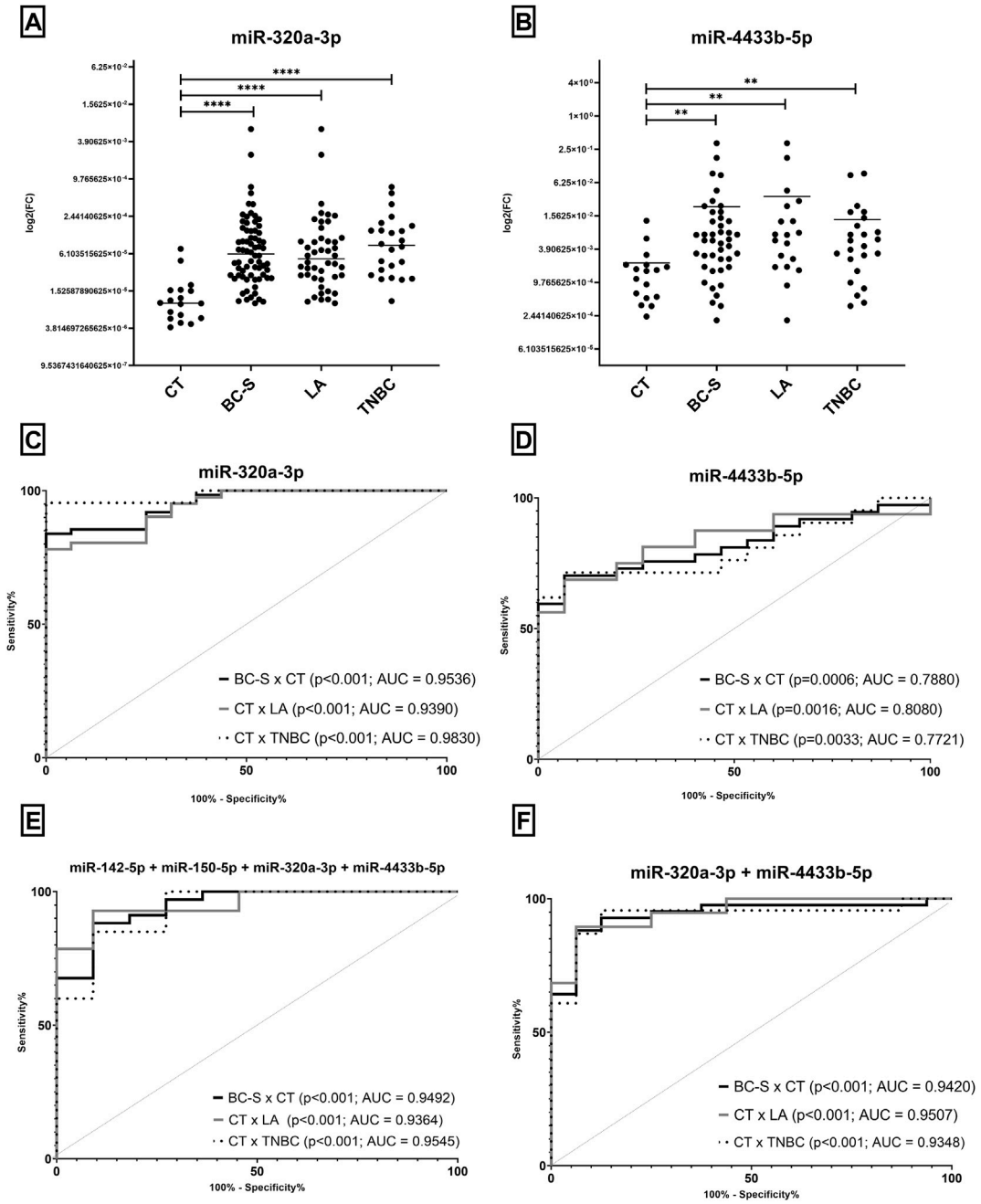

FIGURE 1 | Expression levels of miRNAs by RT-qPCR in serum samples and potential of cf-miRNAs to discriminate BC and subtypes (LA and TNBC) from CT. Expression levels of miRNAs **(A)** miR-320a-3p and **(B)** miR-4433b-5p in BC-S and subtypes (LA and TNBC) and CT. After outlier removal, each dot represents one sample. ROC curves for BC-S diagnosis and prognosis in Brazilian samples **(C–F)**, comparing BC-S to CT (black), CT to LA (gray), and CT to TNBC (dotted). ROC curves were performed to evaluate miR-320a-3p **(C)** or miR-4433b-5p **(D)** individually **(F)** or in combination with all miRNAs in a completed panel **(E)**. ROC = receiver operating characteristic; AUC, area under the curve; CT, serum controls; BC-S, breast cancer serum samples; LA, luminal A; and TNBC, triple-negative breast cancer. (**) $p = 0.001$ and (****) $p < 0.0001$.

the median was used for analysis. qPCR was performed using the ViiA 7 Real-Time PCR System (Applied Biosystems, United States) with the following protocol: 50 °C for 5 min, 95 °C for 10 min, and 40 cycles of 95 °C for 15 s, 55 °C for 30 s, and 60 °C for 30 s. The BT-474 ductal carcinoma cell line was used as a calibrator sample among plates. We used the expression of the small-nucleolar RNA RNU48 as the endogenous control. The $2^{-\Delta\Delta Cq}$ method was used to estimate the miRNA expression level using the QuantStudio Real-Time PCR Software v1.3 (Thermo Fisher Scientific, Waltham, United States).

2.4 Statistical Analysis

We converted TCGA data obtained as log2 (RPM+1) to fold change (FC). We used the $2^{-\Delta\Delta Cq}$ to calculate the FC values for qPCR analysis. We tested normality using the Shapiro–Wilk normality test and the D'Agostino & Pearson omnibus test in GraphPad Prism 8 (GraphPad Software Inc., United States). We adopted nonparametric tests for data that did not pass either test. We compared groups using the unpaired *t* test, the Mann–Whitney test, or the Kruskal–Wallis test as fitting, followed by Dunn's multiple comparisons test. We evaluated clinicopathological differences between groups that allow evaluation by presence/absence using Fisher's exact test (SISA *quantitative skills*). Based on days to death and the presence/absence of death event, we calculated overall survival (OS), comparing low or high expression of each miRNA through log-rank (Mantel–Cox) and the Gehan–Breslow–Wilcoxon tests. We used GraphPad Prism 8 (GraphPad Software Inc., United States) to calculate individual receiver operating characteristic (ROC) curves based on FC values. For combined ROC curves, we performed a binary logistic regression analysis using IBM SPSS Statistics 26.0 (IBM SPSS Statistics Inc., Armonk, NY, United States), and we determined the cutoff, sensitivity, and specificity by Youden's index (higher sensitivity + specificity).

3 RESULTS

3.1 miR-320a-3p and miR-4433b-5p Are Overexpressed in Serum Samples and Discriminate Patients From Controls, Especially When Combined in Panels

We analyzed four miRNAs in 53 serum samples of breast cancer patients (BC-S) and 19 CT. We found higher levels of miR-320a-3p and miR-4433b-5p in BC-S and BC subtypes (LA and TNBC) than in CT (**Figures 1A,B**). Both miRNAs discriminate BC-S and its subtypes compared to CT with high sensitivity and specificity, either alone or combined in a panel (**Figures 1C–F**). Interestingly, miR-320a-3p discriminates TNBC to CT with AUC = 0.9830 (**Figure 1C**). Although miR-150-5p and miR-142-5p revealed no DE in BC-S samples when combined in panels, both miRNAs improved the discrimination of BC-S (including subtypes) from CT samples with high sensitivity and specificity (**Figure 1E**). No difference was observed in the miRNA expression associated with age, histological grade, size of the tumor, or axillary lymph node status.

3.2 In Tissue Samples, Lower Levels of miRNAs Discriminate Tumors From Non-Tumor Samples

In contrast to what we observed in serum, we observed lower expression levels of the four evaluated miRNAs in tissues in BC-T than in NT samples (**Figures 2A–D**). This trend is also true when we compared tissue sample and serum from the same patient; while miR-320a-3p and miR-4433b-5p were higher in BC than CT in serum, we observed in tissue an opposite trend (**Figures 2E,F**). We also found higher expression of all miRNAs in NT than LA subtype and overexpression of miR-320a and miR-4433b-5p in NT samples compared to that in TNBC (**Figures 2A–D**). High or low expression of the miRNAs was not correlated with the clinicopathological parameters evaluated.

We performed ROC curve analysis to investigate the diagnostic potential of miRNAs for BC-T and subtype differentiation. We noticed high sensitivity and specificity by all miRNAs to discriminate BC-T from NT. Of note, a panel combining miR-320a-3p and miR-4433b-5p showed improved values for AUC when comparing BC-T patients to NT, with 100% sensitivity (**Table 2**).

In addition, all the studied miRNAs distinguished LA or TNBC from NT samples, except for miR-150-5p, which only differentiated the LA group. Finally, it is interesting to note that the highest values of AUC in panels include miR-320a-3p, even though other combinations were just as suitable (**Table 2**).

3.3 Lower Expression Levels of miR-320a-3p in Serum Associated With Poor Overall Survival in the BC Brazilian Cohort

We divided the patients into two groups based on their miRNA median expression to evaluate the influence of these miRNAs on the disease-specific survival of the Brazilian cohort. We compared the high or low expression to the event of death/survival and days to death. We observed that lower expression levels of miR-320a-3p in serum samples were associated with poor overall survival when compared to the group with higher levels (**Figure 3**).

3.4 Differential Expression of miRNAs in BC Samples From TCGA Database

We analyzed data from a total of 822 TCGA samples. Although the median age did not differ among the groups, we observed that 63.6% of BC-T patients had post-menopausal status, compared to 46.7% in the control group. Most BLBC was represented by infiltrating ductal carcinoma (88%), unlike LA, which revealed heterogeneous histology. In addition, we found about a quarter of LA patients with early BC histological grade (stage I), compared to 14.81% on BLBC. In addition, BLBC presented a higher axillary lymph node metastasis frequency than LA (64.4% vs. 44.4%, respectively) (**Table 1**).

Similar to the results described for the Brazilian cohort, miR-150-5p, miR-320a-3p, and miR-4433b-5p were downregulated in BC-T samples. On the other hand, tumor and non-tumor comparisons from the TCGA database revealed the overexpression of miR-142-5p in BC-T samples. When analyzing BC subtypes, we observed the overexpression of miR-142-5p and miR-150-5p comparing BLBC *versus* LA. In addition, miR-142-5p showed a higher expression in both BLBC and LA subtypes than in NT samples. On the other hand, we found a reduced expression of miR-150-5p and miR-4433b-5p in the LA subtype compared to that in NT samples. The miRNAs miR-320a-3p and miR-4433b-5p showed no difference between

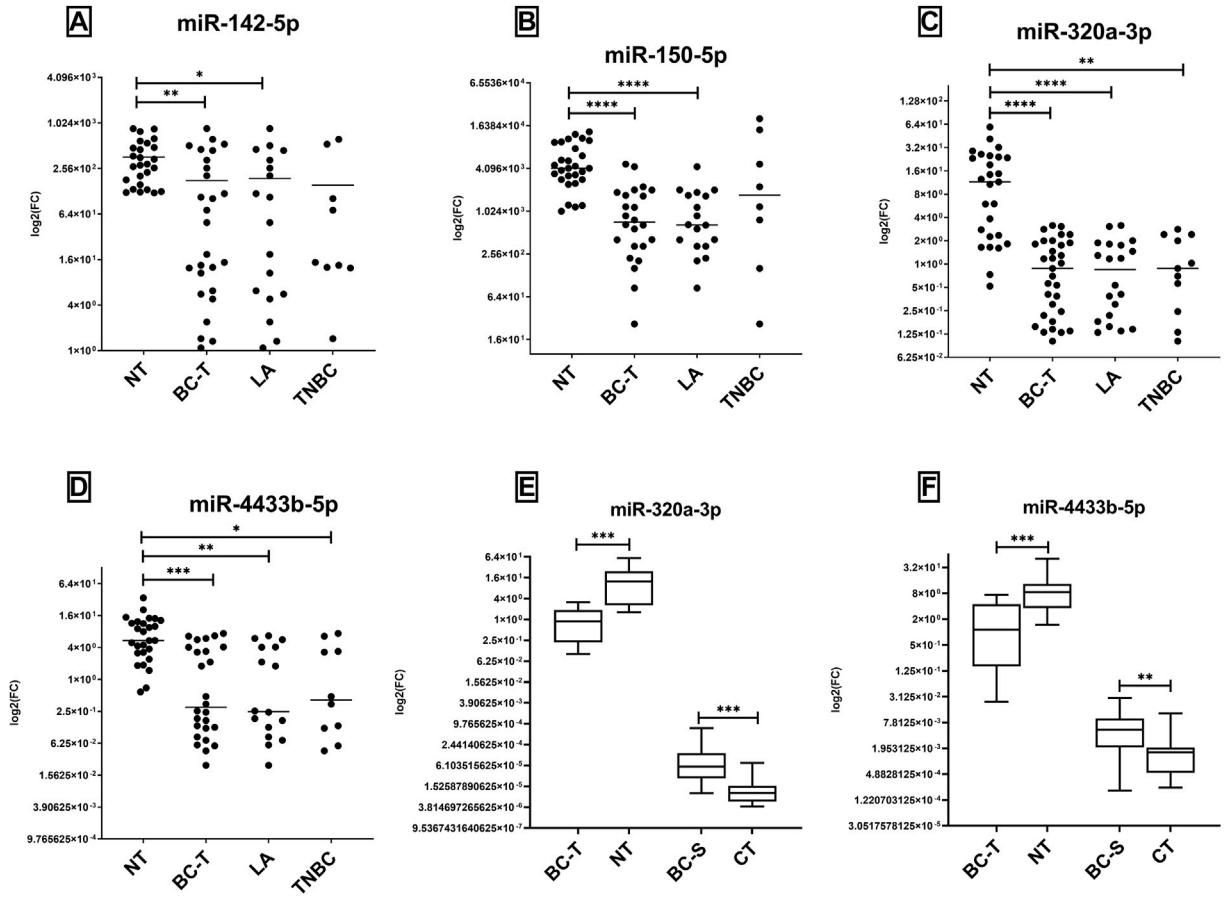

FIGURE 2 | Expression levels of miR-142-5p, miR-150-5p, miR-320a, and miR-4433b-5p on fresh tissue samples. miR-142-5p, miR-150-5p, miR-320a, and miR-4433b-5p evaluated by RT-qPCR in tissue samples **(A–D)**, and the comparison between serum and tissue expression in matched samples **(E,F)**. **(A–D)** Levels of expression were evaluated in NT and BC-T samples; BC-T samples comprised LA and TNBC subtypes, and the expression of all miRNAs was evaluated. After outlier removal, each dot represents one sample in the tissue group. NT samples showed overexpression of all miRNAs evaluated compared to BC-T **(A)** and LA samples. **(E,F)** BC-S and BC-T were evaluated as matched pairs from patients with both samples to all miRNAs ($n = 16$). NT and CT were also compared but not paired. Inverse directions were found between miRNA expression comparing BC-S (high) and BC-T (low). BC-T, breast cancer tissue samples; NT, non-tumor samples; BC-S, breast cancer serum samples; LA, luminal A; TNBC, triple-negative breast cancer; and CT, controls. (*) $p = 0.01$; (**) $p = 0.001$; (***) $p = 0.0001$; and (****) $p < 0.0001$.

BC subtypes (**Figure 4**). The expression of all miRNAs was neither correlated with overall survival nor with the clinicopathological parameters evaluated.

3.5 The Complete Panel Improved the Diagnostic Value of miRNAs in TCGA Samples

We performed ROC curve analysis to investigate the diagnostic value of miRNAs in TCGA samples. In fact, we found that high levels of miR-142-5p distinguished NT from BC-T, as well as from BC subtypes, with high sensitivity and specificity. Although significant, we observed that the AUC values for miR-150-5p, miR-320a-3p, and miR-4433b-5p were below 0.7 (**Table 3**). Nonetheless, unlike what we described in the Brazilian cohort (**Table 2**), in TCGA data, we observed that the complete panel with all four miRNAs studied improved the diagnostic potential of biomarkers in all comparisons performed (**Table 3**).

3.6 miRNA Expression Levels Showed an Opposite Direction in Serum (Cell-Free and EVs) Compared to Tissue Samples

We compared the expression levels of all miRNAs in serum and tissue samples (both by TCGA and by RT-qPCR) with our previous results in EVs (Ozawa et al., 2020c). We found the same expression pattern in serum samples compared to our earlier findings in EVs and an opposite expression pattern in TCGA data and fresh tissue samples for most comparisons. There were a few exceptions, mainly for miR-142-5p (**Table 4**). In addition, we found miR-320a and miR-4433b-5p with a higher expression in TNBC than in CT samples, contrasting with our previous results.

TABLE 2 | Data about receiver operating characteristic (ROC) curves to investigate the diagnostic potential of miRNAs on Brazilian tissue samples.

Comparison	miRNA	AUC	Sensitivity	Specificity	*p*-value
NT x BC	miR-142-5p	0.7434	66.67	96.15	0.0005
	miR-150-5p	0.8108	91.67	85.71	<0.0001
	miR-320a-3p	0.9009	74.19	81.48	<0.0001
	miR-4433b-5p	0.8462	65.38	81.48	<0.0001
	miR-150-5p + miR-320a-3p panel	0.8929	100.0	67.86	<0.0001
	miR-142-5p + miR-320a-3p panel	0.7232	89.29	46.43	0.0041
	miR-320a-3p + miR4433b-5p	**0.9121**	**100.0**	**78.57**	**< 0.0001**
	miR-142-5p + miR-320a-3p + miR-4433b-5p panel	0.9084	100.0	78.57	<0.0001
	miR-150-5p + miR-320a-3p + miR-4433b-5p panel	0.9075	100.0	78.57	<0.0001
	miRNAs complete panel*	0.8982	78.57	100.0	<0.0001
NT x LA	miR-142-5p	0.7368	61.11	100.0	0.0063
	miR-150-5p	0.8797	94.44	85.71	<0.0001
	miR-320a	**0.9125**	**70.00**	**92.59**	**< 0.0001**
	miR-4433b-5p	0.8482	68.75	81.48	0.0001
	miR-150-5p + miR-320a-3p panel	0.9079	89.29	78.95	<0.0001
	miR-142-5p + miR-320a-3p + miR-4433b-5p panel	0.9082	78.57	100.0	<0.0001
	miR-150-5p + miR-320a-3p + miR-4433b-5p panel	0.9056	78.57	100.0	<0.0001
	miRNAs complete panel*	0.8929	78.57	100.0	<0.0001
NT x TNBC	miR-142-5p	0.7571	77.78	100.0	0.0170
	miR-150-5p	0.6473	--	--	0.2092
	miR-320a	0.8799	63.64	92.59	0.0003
	miR-4433b-5p	0.8429	60.00	88.89	0.0015
	miR-150-5p + miR-320a-3p panel	0.9152	92.86	75.00	0.0004
	miR-142-5p + miR-320a-3p + miR-4433b-5p panel	0.9008	78.57	100.0	0.0003
	miR-150-5p + miR-320a-3p + miR-4433b-5p panel	**0.9241**	**75.00**	**100.0**	**0.0003**
	miRNAs complete panel*	0.9240	75.00	100.0	0.0003

(*): The four miRNAs were evaluated together. In bold and underlined are the highest AUC values for the group comparison. Only AUC>0.7 is presented, except for NT x TN, using miR-150-5p. Sensitivity and specificity are presented as percentages (%). BC, breast cancer; NT, adjacent non-tumor tissue; LA, luminal A; TNBC, triple-negative breast cancer; and (--) not evaluated.

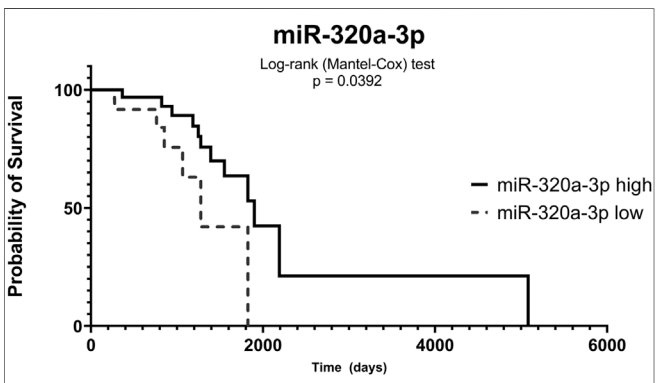

FIGURE 3 | Low expression of miR-320a-3p in serum is correlated with poor overall survival. The serum samples of breast cancer patients (BC-S) were divided into groups based on miR-320a-3p expression levels (high—straight line; low—dotted line). Time was evaluated in days and probability in percentage (%) of survival.

For miR-142-5p, we found no differential expression in serum. According to the TCGA database, we found higher levels in BC-T than in NT, but in fresh tissue from Brazilian samples, we found an opposite expression pattern. IN addition to that, following Ozawa's findings, miR-142-5p could discriminate BC-T from NT samples (AUC >0.7) with sensitivity and specificity. In addition, by combining panels, the diagnostic potential was improved.

4 DISCUSSION

The value of miRNAs as cancer biomarkers has been studied and discussed for some time, and an increasing number of cancer-associated miRNAs have been identified, including in BC (Bao et al., 2019; Li et al., 2020; Jang et al., 2021). The potential diagnostics of circulating miRNAs, especially from exosomes (EV-miRNAs), has already been discussed (Liu et al., 2019; Ozawa et al., 2020b, 2020a). In addition, other non-coding RNAs (nc-RNAs) are emerging as potential biomarkers as long non-coding RNAs (Gradia et al., 2017; Barazetti et al., 2021; Mathias et al., 2021) and circular RNAs (circ-RNAs) (Qian et al., 2018; Ameli-Mojarad et al., 2021; de Palma et al., 2022). Ameli-Mojarad et al. (2021) showed a higher expression of circRNAs in BC tissues than in adjacent tissues. So, we have a world of new molecules to explore, and the combination of them in different panels must be considered.

Combining circulating miRNAs in panels shows improvement in the diagnosis and prognosis potential. Recently, Turkistani et al. (2021) found that panels of deregulated miRNAs showed a discriminatory potential based on TNBC tumor size, lymph node metastasis, and recurrence status of the disease. Recently, miR-875 and miR-103a-3p were described as potential prognostic markers in BC patients. Nonetheless, the number of evaluated patients was quite limited, in addition to the absence of a second validation cohort (Liu H. et al., 2022; Liu et al., 2022 X.). Combined circulating miRNAs were validated to accurately distinguish BC patients and subtypes from controls (Kim

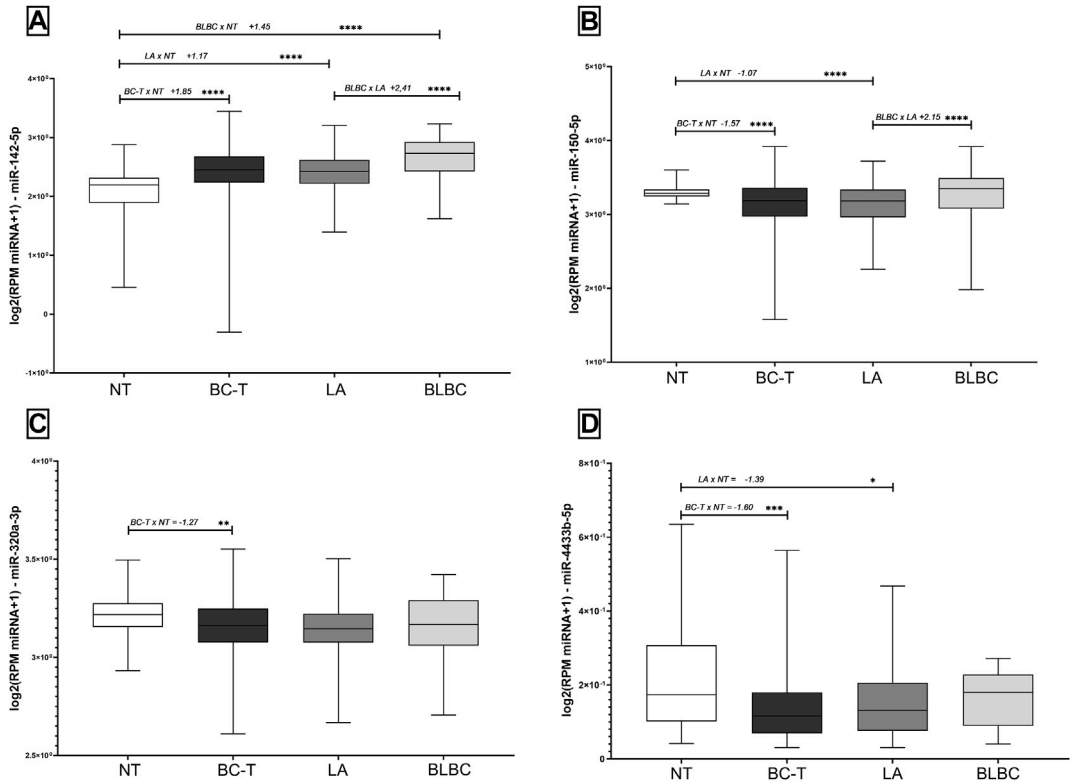

FIGURE 4 | Expression levels of miR-142-5p, miR-150-5p, miR-320a-3p, and miR-4433b-5p in tissue samples according to the TCGA database. Expression levels of **(A)** miR-142-5p, **(B)** miR-150-5p, **(C)** miR-320a-3p, and **(D)** miR-4433b-5p in BC-T and subtypes (LA and BLBC) and NT. Fold change between the two groups compared and the order of comparisons were indicated before the FC and *p* values. NT, non-tumor samples; BC-T, breast cancer tissue samples; LA, luminal A; BLBC, basal-like breast cancer; and FC, fold change. (*) $p < 0.01$; (**) $p = 0.001$; (***) $p = 0.0001$; and (****) $p < 0.0001$.

TABLE 3 | Data about receiver operating characteristic (ROC) curves to investigate the diagnostic potential of miRNAs on TCGA samples.

Comparison	miRNA	AUC	Sensitivity	Specificity	*p*-value
NT x BC	miR-142-5p	0.7532	65.86	76.00	<0.0001
	miR-150-5p + miR-142-5p panel	0.9317	88.76	86.67	<0.0001
	miR-142-5p + miR-320a-3p panel	0.7681	52.07	89.33	<0.0001
	miRNAs complete panel*	**0.9345**	**87.68**	**90.67**	< **0.0001**
NT x LA	miR-142-5p	0.7371	62.40	76.00	<0.0001
	miR-150-5p + miR-320a-3p panel	0.7458	69.60	70.67	<0.0001
	miR-150-5p + miR-142-5p panel	0.9179	84.80	86.67	<0.0001
	miR-142-5p + miR-320a-3p panel	0.7738	72.00	72.00	<0.0001
	miRNAs complete panel*	**0.9266**	**85.20**	**90.67**	< **0.0001**
NT x BLBC	miR-142-5p	0.8671	72.29	93.33	<0.0001
	miR-150-5p + miR-142-5p panel	0.9680	93.90	92.00	<0.0001
	miR-142-5p + miR-320a-3p panel	0.8694	70.73	92.00	<0.0001
	miRNAs complete panel*	**0.9689**	**93.90**	**92.00**	< **0.0001**
LA x BLBC	miR-142-5p	0.7220	72.29	67.60	<0.0001
	miR-150-5p + miR-142-5p panel	0.7711	68.67	78.80	<0.0001
	miR-142-5p + miR-320a-3p panel	0.7274	59.04	80.80	<0.0001
	miRNAs complete panel*	**0.7728**	**63.86**	**80.80**	< **0.0001**

Only AUC>0.7 is presented. In bold and underlined are the highest AUC values for the group comparison. (*): the four miRNAs were evaluated together. Sensitivity and specificity are presented as percentage (%). BC, breast cancer; NT, non-tumor tissue; LA, luminal A; and BLBC, basal-like breast cancer.

et al., 2021b; Zhang et al., 2021b; Li et al., 2022b) and to screen BC patients associated with mammography (Zou et al., 2021b; 2022b), highlighting the relevance of panel studies. A recent study found that a panel comprising four EV-miRNAs (miR-9, miR-16, miR-21, and miR-429) presented high sensitivity to discriminate BC subtypes of the early stages of the disease.

TABLE 4 | Comparison of the expression level and performance of miR-142-5p, miR-150-5p, miR-320a, and miR-4433b-5p in tissue and serum samples (cell-free miRNAs and EVs).

	TCGA	Fresh tissue	Serum samples	EV-miRNAs#
BC x CT				
miR-142-5p	high, AUC = 0.7532	low, AUC = 0.7434	n.s.	high, AUC = 0.7964
miR-150-5p	low, AUC = 0.6552	low, AUC = 0.8108	n.s.	n.s.
miR-320a	low, AUC = 0.6219	low, AUC = 0.9009	high, AUC = 0.9536	high, AUC = 0.8063
miR-4433b-5p	low, AUC = 0.6772	low, AUC = 0.8462	high, AUC = 0.8198	high, AUC = 0.7964
miR-142-5p + miR-320a	low, AUC = 0.7681	low, AUC = 0.7232	high, AUC = 0.9468	high, AUC = 0.9410
miR-142-5p + miR-320a + miR-4433b-5p	low, AUC = 0.6796	low, AUC = 0.9075	high, AUC = 0.9429	high, AUC = 0.8387
LA x CT				
miR-142-5p	high, AUC = 0.7371	low, AUC = 0.7368	n.s.	high, AUC = 0.9180
miR-150-5p	low, AUC = 0.6852	low, AUC = 0.8797	n.s.	n.s.
miR-320a	low, AUC = 0.6695	low, AUC = 0.9125	high, AUC = 0.9390	high, AUC = 0.8828
miR-4433b-5p	low, AUC = 0.6279	low, AUC = 0.8482	high, AUC = 0.8375	high, AUC = 0.8672
miR-142-5p + miR-320a-3p	high, AUC = 0.7738	low, AUC = 0.9082	high, AUC = 0.9667	high, AUC = 0.9410
TNBC/BLBC x CT				
miR-142-5p	high, AUC = 0.8671	n.s.	n.s.	n.s.
miR-150-5p	n.s.	n.s.	n.s.	n.s.
miR-320a	n.s.	low, AUC = 0.8799	high, AUC = 0.9830	n.s.
miR-4433b-5p	n.s.	low, AUC = 0.8429	high, AUC = 0.8063	n.s.
LA x TNBC/BLBC				
miR-142-5p	low, AUC = 0.7220	n.s.	n.s.	high, AUC = 0.9208
miR-150-5p	low, AUC = 0.6322	n.s.	n.s.	high, AUC = 0.8667
miR-320a	n.s.	n.s.	n.s.	n.s.
miR-4433b-5p	n.s.	n.s.	n.s.	n.s.

#EV-miRNAs were evaluated by Ozawa (2020). Only the data that were comparable between the two studies are presented. AUC, area under the curve; n. s, not significant; BC, breast cancer; CT, control samples; LA, luminal A; TNBC, triple-negative breast cancer; and BLBC, basal-like breast cancer.

Interestingly, these miRNAs were chosen using the TCGA database (Kim et al., 2021b), drawing attention to the relevance of candidate validation, especially when combined in panels.

A previous study from our group showed the potential of an EV-miRNA panel including miR-142-5p, miR-150-5p, and miR-320a discriminating BC patients from controls with 93.33% sensitivity and 68.75% specificity. In addition, miR-142-5p levels were associated with clinicopathological parameters, such as bigger tumor size, higher stage, and presence of lymph node metastasis (Ozawa et al., 2020b). Aiming to investigate if these miRNAs also have a good performance as biomarkers in different types of samples, we performed a dual sample analysis strategy: TCGA database in tissue and RT-qPCR of miR-142-5p, miR-150-5p, miR-320a, and miR-4433b-5p in tissue and serum samples.

In this work, we found higher levels of miR-320a and miR-4433b-5p in BCS and in the LA subtype than in CT, similar to Ozawa's results (Ozawa et al., 2020b). In addition, the panel including miR-142-5p, miR-320a, and miR-4433b-5p discriminated BC patients from controls with likewise high sensitivity and specificity. In contrast, lower expression levels of miR-150-5p, miR-320a-3p, and miR-4433b-5p were observed in BC-T than in NT samples, both by TCGA and RT-qPCR analyses of our Brazilian cohort. These miRNAs showed potential diagnostic value in the Brazilian cohort to discriminate BCT from NT samples with higher sensitivity and specificity, either alone or combined in panels. This potential was also observed in TCGA samples, especially in the panel including all four miRNAs (**Table 4**).

Discussing our results, the dysregulation of miR-320a has been previously described in breast cancer, with an increased expression, suggesting it as a biomarker for invasive disease (Yang et al., 2014). However, its anti-oncogenic potential has also been studied before (Lü et al., 2015; Wang et al., 2015; Yu et al., 2016). Interestingly, in this study, we found significantly low expression levels of miR-320a in BC, both by TCGA and RT-qPCR, strengthening the potential of this miRNA as a biomarker for BC. In fact, miR-320a-3p showed that it could significantly discriminate BC-T from NT tissue (AUC = 0.9009), and this AUC value can be improved when combining miR-320a-3p in panels with other miRNAs. In addition, miR-320a-3p differentiates LA or TNBC subtypes from NT in the Brazilian cohort. In serum, we observed that high levels of miR-320a-3p in BC-S compared to controls can effectively distinguish these groups with higher sensitivity and specificity, according to our previous findings in EV-miRNAs (Ozawa et al., 2020c). Indeed, we found lower levels of miR-320a-3p on BC-S associated with poor overall survival in the Brazilian cohort, highlighting its potential as a diagnostic biomarker.

The literature regarding miR-4433b-5p is quite limited but indicates a trend for its association with cancer. Wu et al. (2019) observed a reduction in BCR-ABL mRNA through miR-4433 regulation. Ozawa et al. (2020b) found that miR-4433-5p, which was also part of the miRNA panel to distinguish LA from CT samples, was overexpressed in BC patients compared to that in CT. We noticed reduced levels of this miRNA in BCT compared to those in NT samples both by RT-qPCR and TCGA, and it showed high sensitivity and specificity as a BC biomarker. In addition, a combined panel including miR-4433b-5p and miR-320a-3p

improved their diagnostic potential. Interestingly, we observed increased expression levels of miR-4433b-5p in serum similar to what was found in EVs (Ozawa et al., 2020c). These results indicate a potential involvement of miR-4433b-5p in mediating cell-to-cell communication in BC.

We found no differential expression of miR-142-5p and miR-150-5p in serum, contrasting with our previous EV results (Ozawa et al., 2020b) (**Table 4**). Tissue samples showed reduced expression of both miRNAs in BC-T and LA subtype compared to that in NT samples. Our RT-qPCR experiments showed a lower expression level of miR-142-5p in BCT samples, but the TCGA database showed overexpression of this miRNA. Likewise, the cancer literature about miR-142-5p is controversial, including in BC. Overexpression of miR-142-5p was previously found in BC tissue and was also associated with increased tumor size and metastasis, suggesting that miR-142-5p could be a possible target therapy for BC (Xu and Wang, 2018; Yu et al., 2019). On the other hand, a recent study found miR-142-5p acting as a tumor suppressor in BC, inhibiting cell invasion and migration by targeting DNMT1 (Li et al., 2022a). Lower levels of miR-142-5p in BC were also found to be negatively correlated with circWAC, another type of non-coding RNA (Wang et al., 2021).

Some authors found a reduced expression of miR-142 in BC samples but in a mature miRNA generated from the 3p arm of the precursor (miR-142-3p) (Mansoori et al., 2019; Ma et al., 2020; Xu et al., 2020). Nonetheless, we found miR-142-5p as a potential diagnostic biomarker in the Brazilian cohort, with a reduced expression in BC compared to that in NT samples. We also found lower levels of miR-142-5p in the LA subtype than in the BLBC according to TCGA samples and higher levels of this miRNA in the LA subtype than in the TNBC according to studied EV-miRNA samples (**Table 4**). When miR-142-5p was combined in panels in the Brazilian cohort, the diagnostic potential and sensitivity improved, similar to what was described for EVs (Ozawa et al., 2020c).

TNBC is a heterogeneous group of tumors and comprises at least six different subtypes, including basal-like breast carcinoma (BLBC) (Millikan et al., 2008; Garmpis et al., 2020; Marra et al., 2020). In our study, similar to what was described for TNBC (Bou Zerdan et al., 2022; Derakhshan and Reis-Filho, 2022), BLBC comprised mainly of infiltrating ductal carcinoma, presenting higher metastatic axillary lymph nodes than the LA subtype.

miR-150 seems to be involved in the tumorigenesis and development of a few solid tumors, but the role of this miRNA remains controversial (Wang et al., 2016; Kim et al., 2017; Koshizuka et al., 2018; Xiao et al., 2019). Some studies found that overexpression of miR-150-5p could inhibit apoptosis and increase EMT and cancer progression (Huang et al., 2013; Lu et al., 2019). However, miR-150-5p′ targets were previously associated with cancer growth and metastatic events (Jiang et al., 2019; Wang et al., 2019; Jia et al., 2021), while miR-150-5p overexpression has been described to be associated with reduced tumor aggressiveness. Similarly, the overexpression of miR-150-5p in BC cells has already been associated with decreased proliferation, invasion, and migration properties (Hu et al., 2019; Jiang et al., 2019; Jia et al., 2021). In our study, TCGA analysis showed that BLBC had an overexpression of miR-150-5p compared to that of LA. In the Brazilian cohort, we found reduced expression levels of miR-150-5p in the LA subtype compared to those in NT samples (AUC = 0.8797). In addition, the diagnostic potential of miR-150-5p improved when combined in panels, especially with miR-320-3p (AUC = 0.9079), suggesting these miRNAs as potential biomarkers to identify the LA subtype.

In summary, the present study showed high expression of miR-320a-3p and miR-4433b-5p in serum from BC patients, in accordance with our previous results on EVs. In contrast, we found reduced levels of miR-142-5p, miR-150-5p, miR-320a-3p, and miR-4433b-5p in tumor tissues from BC patients. Nevertheless, all miRNAs discriminated BC and LA subtypes from NT tissue with high sensitivity and sensibility. In serum samples, we observed that miR-320a-3p and miR-4433b-5p could distinguish BC and LA from CT. In addition, the different combinations of miRNAs in panels improved the diagnostic potential of BC patients and subtypes compared to that of controls. Finally, we found lower levels of miR-320a-3p associated with poor overall survival. Overall, we suggest that the studied miRNAs have potential as diagnostic biomarkers for BC when compared to that for controls and discriminate the LA subtypes. The small number of patients in this study is a limitation, and additional studies in larger samples and also testing new combinations of miRNAs and other classes of ncRNAs will be needed to address the role of these miRNAs in BC tumorigenesis and progression and their use to access the diagnostic, classification, and prognosis.

DATA AVAILABILITY STATEMENT

The datasets presented in this study can be found in online repositories. The names of repository/repositories and accession number(s) can be found in the main article.

ETHICS STATEMENT

The studies involving human participants were reviewed and approved by Comitê de Ética do Setor de Ciências da Saúde, Universidade Federal do Paraná. The patients/participants provided their written informed consent to participate in this study.

AUTHOR CONTRIBUTIONS

TC, TJ, ER, DG, and JCO designed the study. TC and GB performed RT-qPCR experiments. TC and TJ obtained and analyzed data from TCGA samples. DA, JCO, and DG supervised TCGA analyses, experimental processes, and statistical analyses. RL, CS, and KA provided the tissue and serum samples and the histopathological information about Brazilian patients. PO performed and analyzed EV experiments and revised the manuscript. TC wrote the draft of

the manuscript. ER supervised the project and revised the manuscript. All authors reviewed and agreed to the final version of the manuscript.

FUNDING

This study was partially funded by PRONEX (116/2018) and PPSUS (036/2017)—Fundação Araucária-CNPq-MS. Scholarships to TC, GB, and TJ were provided by the Coordenação de Aperfeiçoamento de Pessoal de Nível Superior—Brasil (CAPES)—Finance Code 001.

ACKNOWLEDGMENTS

We thank all breast cancer patients who donated samples to this study. We also thank M. Sc. Ana Luiza Mattana for helping with sample processing. We thank M. Sc. Bernardo Zoehler for suggestions and assistance with statistical analysis.

REFERENCES

Adhami, M., Haghdoost, A. A., Sadeghi, B., and Malekpour Afshar, R. (2018). Candidate miRNAs in Human Breast Cancer Biomarkers: a Systematic Review. *Breast Cancer* 25, 198–205. doi:10.1007/s12282-017-0814-8

Ambros, V. (2004). The Functions of Animal microRNAs. *Nature* 431, 350–355. doi:10.1038/nature02871

Ameli-Mojarad, M., Ameli-Mojarad, M., Nourbakhsh, M., and Nazemalhosseini-Mojarad, E. (2021). Circular RNA Hsa_circ_0005046 and Hsa_circ_0001791 May Become Diagnostic Biomarkers for Breast Cancer Early Detection. *J. Oncol.* 2021, 1–7. doi:10.1155/2021/2303946

Bao, C., Lu, Y., Chen, J., Chen, D., Lou, W., Ding, B., et al. (2019). Exploring Specific Prognostic Biomarkers in Triple-Negative Breast Cancer. *Cell Death Dis.* 10, 807. doi:10.1038/s41419-019-2043-x

Barazetti, J. F., Jucoski, T. S., Carvalho, T. M., Veiga, R. N., Kohler, A. F., Baig, J., et al. (2021). From Micro to Long: Non-coding RNAs in Tamoxifen Resistance of Breast Cancer Cells. *Cancers* 13, 3688. doi:10.3390/CANCERS13153688

Bartel, D. P. (2009). MicroRNAs: Target Recognition and Regulatory Functions. *Cell* 136, 215–233. doi:10.1016/j.cell.2009.01.002

Bou Zerdan, M., Ghorayeb, T., Saliba, F., Allam, S., Bou Zerdan, M., Yaghi, M., et al. (2022). Triple Negative Breast Cancer: Updates on Classification and Treatment in 2021. *Cancers* 14, 1253. doi:10.3390/CANCERS14051253

de Palma, F. D. E., Salvatore, F., Pol, J. G., Kroemer, G., and Maiuri, M. C. (2022). Circular RNAs as Potential Biomarkers in Breast Cancer. *Biomedicines* 10, 725. doi:10.3390/BIOMEDICINES10030725

Derakhshan, F., and Reis-Filho, J. S. (2022). Pathogenesis of Triple-Negative Breast Cancer. *Annu. Rev. Pathol. Mech. Dis.* 17, 181–204. doi:10.1146/ANNUREV-PATHOL-042420-093238

Farmer, P., Bonnefoi, H., Becette, V., Tubiana-Hulin, M., Fumoleau, P., Larsimont, D., et al. (2005). Identification of Molecular Apocrine Breast Tumours by Microarray Analysis. *Oncogene* 24, 4660–4671. doi:10.1038/sj.onc.1208561

Garmpis, N., Damaskos, C., Garmpi, A., Nikolettos, K., Dimitroulis, D., Diamantis, E., et al. (2020). Molecular Classification and Future Therapeutic Challenges of Triple-Negative Breast Cancer. *Vivo* 34, 1715–1727. doi:10.21873/invivo.11965

Goldhirsch, A., Winer, E. P., Coates, A. S., Gelber, R. D., Piccart-Gebhart, M., Thürlimann, B., et al. (2013). Personalizing the Treatment of Women with Early Breast Cancer: Highlights of the St Gallen International Expert Consensus on the Primary Therapy of Early Breast Cancer 2013. *Ann. Oncol.* 24, 2206–2223. doi:10.1093/ANNONC/MDT303

Gradia, D., Mathias, C., Coutinho, R., Cavalli, I., Ribeiro, E., and de Oliveira, J. (2017). Long Non-coding RNA TUG1 Expression Is Associated with Different Subtypes in Human Breast Cancer. *ncRNA* 3, 26. doi:10.3390/NCRNA3040026

Hong, H.-C., Chuang, C.-H., Huang, W.-C., Weng, S.-L., Chen, C.-H., Chang, K.-H., et al. (2020). A Panel of Eight microRNAs Is a Good Predictive Parameter for Triple-Negative Breast Cancer Relapse. *Theranostics* 10, 8771–8789. doi:10.7150/THNO.46142

Hu, X., Liu, Y., Du, Y., Cheng, T., and Xia, W. (2019). Long Non-coding RNA BLACAT1 Promotes Breast Cancer Cell Proliferation and Metastasis by miR-150-5p/CCR2. *Cell Biosci.* 9, 1–9. doi:10.1186/s13578-019-0274-2

Huang, S., Chen, Y., Wu, W., Ouyang, N., Chen, J., Li, H., et al. (2013). MiR-150 Promotes Human Breast Cancer Growth and Malignant Behavior by Targeting the Pro-apoptotic Purinergic P2X7 Receptor. *PLoS ONE* 8, e80707. doi:10.1371/journal.pone.0080707

INCAdeda, S. (2019). *Estimativa 2020 : incidência de câncer no Brasil/Instituto Nacional de Câncer José Alencar Gomes da Silva*. – Rio de Janeiro: INCA.

Jang, J., Kim, Y., Kang, K., Kim, K., Park, Y., and Kim, C. (2021). Multiple microRNAs as Biomarkers for Early Breast Cancer Diagnosis. *Mol. Clin. Oncol.* 14, 1–9. doi:10.3892/mco.2020.2193

Jia, H., Wu, D., Zhang, Z., and Li, S. (2021). Regulatory Effect of the MAFG-AS1/miR-150-5p/MYB axis on the Proliferation and Migration of Breast Cancer Cells. *Int. J. Oncol.* 58, 33–44. doi:10.3892/ijo.2020.5150

Jiang, M., Qiu, N., Xia, H., Liang, H., Li, H., and Ao, X. (2019). Long Non-coding RNA FOXD2-AS1/miR-150-5p/PFN2 axis Regulates Breast Cancer Malignancy and Tumorigenesis. *Int. J. Oncol.* 54, 1043–1052. doi:10.3892/ijo.2019.4671

Kim, M. W., Park, S., Lee, H., Gwak, H., Hyun, K. A., Kim, J. Y., et al. (2021a). Multi-miRNA Panel of Tumor-derived Extracellular Vesicles as Promising Diagnostic Biomarkers of Early-stage Breast Cancer. *Cancer Sci.* 112, 5078–5087. doi:10.1111/CAS.15155

Kim, M. W., Park, S., Lee, H., Gwak, H., Hyun, K. A., Kim, J. Y., et al. (2021b). Multi-miRNA Panel of Tumor-derived Extracellular Vesicles as Promising Diagnostic Biomarkers of Early-stage Breast Cancer. *Cancer Sci.* 112, 5078–5087. doi:10.1111/CAS.15155

Kim, T. H., Jeong, J.-Y., Park, J.-Y., Kim, S.-W., Heo, J. H., Kang, H., et al. (2017). miR-150 Enhances Apoptotic and Anti-tumor Effects of Paclitaxel in Paclitaxel-Resistant Ovarian Cancer Cells by Targeting Notch3. *Oncotarget* 8, 72788. doi:10.18632/oncotarget.20348

Koshizuka, K., Hanazawa, T., Kikkawa, N., Katada, K., Okato, A., Arai, T., et al. (2018). Antitumor miR-150-5p and miR-150-3p Inhibit Cancer Cell Aggressiveness by Targeting SPOCK1 in Head and Neck Squamous Cell Carcinoma. *Auris Nasus Larynx* 45, 854–865. doi:10.1016/j.anl.2017.11.019

Li, H., Li, H.-H., Chen, Q., Wang, Y.-Y., Fan, C.-C., Duan, Y.-Y., et al. (2022a). miR-142-5p Inhibits Cell Invasion and Migration by Targeting DNMT1 in Breast Cancer. *Oncol. Res.* 28, 885–897. doi:10.3727/096504021X16274672547967

Li, J., Guan, X., Fan, Z., Ching, L.-M., Li, Y., Wang, X., et al. (2020). Non-invasive Biomarkers for Early Detection of Breast Cancer. *Cancers* 12, 1–8. doi:10.3390/cancers12102767

Li, X., Tang, X., Li, K., and Lu, L. (2022b). Evaluation of Serum MicroRNAs (miR-9-5p, miR-17-5p, and miR-148a-3p) as Potential Biomarkers of Breast Cancer. *BioMed Res. Int.* 2022, 1–8. doi:10.1155/2022/9961412

Liu, H., Bian, Q.-Z., Zhang, W., and Cui, H.-B. (2022a). Circulating microRNA-103a-3p C-ould B-e a D-iagnostic and P-rognostic B-iomarker for B-reast C-ancer. *Oncol. Lett.* 23, 1792. doi:10.3892/OL.2021.13156

Liu, Q., Peng, F., and Chen, J. (2019). The Role of Exosomal Micrornas in the Tumor Microenvironment of Breast Cancer. *Ijms* 20, 1–27. doi:10.3390/ijms20163884

Liu, X., Liu, M., Ma, H., Wang, J., and Zheng, Y. (2022b). miR-875 Serves as A Candidate Biomarker for Detection and Prognosis and Is Correlated with PHH3 Index Levels in Breast Cancer Patients. *Clin. Breast Cancer* 22, e199–e205. doi:10.1016/J.CLBC.2021.06.008

Lü, M., Ding, K., Zhang, G., Yin, M., Yao, G., Tian, H., et al. (2015). MicroRNA-320a Sensitizes Tamoxifen-Resistant Breast Cancer Cells to Tamoxifen by Targeting ARPP-19 and ERRγ*. *Sci. Rep.* 5, 1–10. doi:10.1038/srep08735

Lu, Q., Guo, Z., and Qian, H. (2019). Role of microRNA-150-5p/SRCIN1 axis in the P-rogression of B-reast C-ancer. *Exp. Ther. Med.* 17, 2221. doi:10.3892/etm.2019.7206

Ma, T., Liu, H., Liu, Y., Liu, T., Wang, H., Qiao, F., et al. (2020). USP6NL Mediated by LINC00689/miR-142-3p Promotes the Development of Triple-Negative Breast Cancer. *BMC Cancer* 20, 1–12. doi:10.1186/s12885-020-07394-z

Mandujano-Tinoco, E. A., García-Venzor, A., Melendez-Zajgla, J., and Maldonado, V. (2018). New Emerging Roles of microRNAs in Breast Cancer. *Breast Cancer Res. Treat.* 171, 247–259. doi:10.1007/s10549-018-4850-7

Mansoori, B., Mohammadi, A., Gjerstorff, M. F., Shirjang, S., Asadzadeh, Z., Khaze, V., et al. (2019). miR-142-3p Is a Tumor Suppressor that Inhibits Estrogen Receptor Expression in ER-positive Breast Cancer. *J. Cell Physiol.* 234, 16043–16053. doi:10.1002/jcp.28263

Marra, A., Trapani, D., Viale, G., Criscitiello, C., and Curigliano, G. (2020). Practical Classification of Triple-Negative Breast Cancer: Intratumoral Heterogeneity, Mechanisms of Drug Resistance, and Novel Therapies. *npj Breast Cancer* 6 (1 6), 1–16. doi:10.1038/s41523-020-00197-2

Mathias, C., Muzzi, J. C. D., Antunes, B. B., Gradia, D. F., Castro, M. A. A., and Carvalho de Oliveira, J. (2021). Unraveling Immune-Related lncRNAs in Breast Cancer Molecular Subtypes. *Front. Oncol.* 11, 1–16. doi:10.3389/FONC.2021.692170

Millikan, R. C., Newman, B., Tse, C.-K., Moorman, P. G., Conway, K., Smith, L. V., et al. (2008). Epidemiology of Basal-like Breast Cancer. *Breast Cancer Res. Treat.* 109, 123–139. doi:10.1007/s10549-007-9632-6

Ozawa, P. M. M., Jucoski, T. S., Vieira, E., Carvalho, T. M., Malheiros, D., and Ribeiro, E. M. D. S. F. (2020a). Liquid Biopsy for Breast Cancer Using Extracellular Vesicles and Cell-free microRNAs as Biomarkers. *Transl. Res.* 223, 40–60. doi:10.1016/j.trsl.2020.04.002

Ozawa, P. M. M., Vieira, E., Lemos, D. S., Souza, I. L. M., Zanata, S. M., Pankievicz, V. C., et al. (2020b). Identification of miRNAs Enriched in Extracellular Vesicles Derived from Serum Samples of Breast Cancer Patients. *Biomolecules* 10, 150. doi:10.3390/biom10010150

Perou, C. M., Sørlie, T., Eisen, M. B., van de Rijn, M., Jeffrey, S. S., Rees, C. A., et al. (2000). Molecular Portraits of Human Breast Tumours. *Nature* 406, 747–752. doi:10.1038/35021093

Prat, A., Cheang, M. C. U., Martín, M., Parker, J. S., Carrasco, E., Caballero, R., et al. (2013). Prognostic Significance of Progesterone Receptor-Positive Tumor Cells within Immunohistochemically Defined Luminal A Breast Cancer. *Jco* 31, 203–209. doi:10.1200/JCO.2012.43.4134

Qian, L., Yu, S., Chen, Z., Meng, Z., Huang, S., and Wang, P. (2018). The Emerging Role of circRNAs and Their Clinical Significance in Human Cancers. *Biochimica Biophysica Acta (BBA) - Rev. Cancer* 1870, 247–260. doi:10.1016/j.bbcan.2018.06.002

Ramassone, A., Pagotto, S., Veronese, A., and Visone, R. (2018). Epigenetics and microRNAs in Cancer. *Ijms* 19, 459. doi:10.3390/ijms19020459

Rupaimoole, R., and Slack, F. J. (2017). MicroRNA Therapeutics: Towards a New Era for the Management of Cancer and Other Diseases. *Nat. Rev. Drug Discov.* 16, 203–222. doi:10.1038/nrd.2016.246

Sørlie, T., Perou, C. M., Tibshirani, R., Aas, T., Geisler, S., Johnsen, H., et al. (2001). Gene Expression Patterns of Breast Carcinomas Distinguish Tumor Subclasses with Clinical Implications. *Proc. Natl. Acad. Sci. U. S. A.* 98, 10869. doi:10.1073/pnas.191367098

Sung, H., Ferlay, J., Siegel, R. L., Laversanne, M., Soerjomataram, I., Jemal, A., et al. (2021). Global Cancer Statistics 2020: GLOBOCAN Estimates of Incidence and Mortality Worldwide for 36 Cancers in 185 Countries. *CA A Cancer J. Clin.* 71, 209–249. doi:10.3322/caac.21660

Turkistani, S., Sugita, B. M., Fadda, P., Marchi, R., Afsari, A., Naab, T., et al. (2021). A Panel of miRNAs as Prognostic Markers for African-American Patients with Triple Negative Breast Cancer. *BMC Cancer* 21, 1–16. doi:10.1186/s12885-021-08573-2

Wang, B., Yang, Z., Wang, H., Cao, Z., Zhao, Y., Gong, C., et al. (2015). MicroRNA-320a Inhibits Proliferation and Invasion of Breast Cancer Cells by Targeting RAB11A. *Am. J. Cancer Res.* 5, 2719–2729.

Wang, J., Chen, J., and Sen, S. (2016). MicroRNA as Biomarkers and Diagnostics. *J. Cell. Physiol.* 231, 25–30. doi:10.1002/jcp.25056

Wang, L., Zhou, Y., Jiang, L., Lu, L., Dai, T., Li, A., et al. (2021). CircWAC Induces Chemotherapeutic Resistance in Triple-Negative Breast Cancer by Targeting miR-142, Upregulating WWP1 and Activating the PI3K/AKT Pathway. *Mol. Cancer* 20, 1–15. doi:10.1186/S12943-021-01332-8

Wang, Z., Wang, P., Cao, L., Li, F., Duan, S., Yuan, G., et al. (2019). Long Intergenic Non-coding RNA 01121 Promotes Breast Cancer Cell Proliferation, Migration, and Invasion via the miR-150-5p/HMGA2 Axis. *Cmar* 11, 10859–10870. doi:10.2147/CMAR.S230367

Wu, H., Yin, J., Ai, Z., Li, G., Li, Y., and Chen, L. (2019). Overexpression of miR-4433 by Suberoylanilide Hydroxamic Acid Suppresses Growth of CML Cells and Induces Apoptosis through Targeting Bcr-Abl. *J. Cancer* 10, 5671–5680. doi:10.7150/jca.34972

Xiao, G., Wang, P., Zheng, X., Liu, D., and Sun, X. (2019). FAM83A-AS1 Promotes Lung Adenocarcinoma Cell Migration and Invasion by Targeting miR-150-5p and Modifying MMP14. *Cell Cycle* 18, 2972–2985. doi:10.1080/15384101.2019.1664225

Xu, T., He, B. S., Pan, B., Pan, Y. Q., Sun, H. L., Liu, X. X., et al. (2020). MiR-142-3p Functions as a Tumor Suppressor by Targeting RAC1/PAK1 Pathway in Breast Cancer. *J. Cell Physiol.* 235, 4928–4940. doi:10.1002/jcp.29372

Xu, W., and Wang, W. (2018). MicroRNA-142-5p Modulates Breast Cancer Cell Proliferation and Apoptosis by Targeting Phosphatase and Tensin Homolog. *Mol. Med. Rep.* 17, 7529–7536. doi:10.3892/mmr.2018.8812

Yang, H., Yu, J., Wang, L., Ding, D., Zhang, L., Chu, C., et al. (2014). MiR-320a Is an Independent Prognostic Biomarker for Invasive Breast Cancer. *Oncol. Lett.* 8, 1043–1050. doi:10.3892/ol.2014.2298

Yu, J., Wang, J.-G., Zhang, L., Yang, H.-P., Wang, L., Ding, D., et al. (2016). MicroRNA-320a Inhibits Breast Cancer Metastasis by Targeting Metadherin. *Oncotarget* 7, 38612–38625. doi:10.18632/oncotarget.9572

Yu, W., Li, D., Zhang, Y., Li, C., Zhang, C., and Wang, L. (2019). MiR-142-5p Acts as a Significant Regulator through Promoting Proliferation, Invasion, and Migration in Breast Cancer Modulated by Targeting SORBS1. *Technol. Cancer Res. Treat.* 18, 153303381989226–11. doi:10.1177/1533033819892264

Zhang, K., Wang, Y.-Y., Xu, Y., Zhang, L., Zhu, J., Si, P.-C., et al. (2021a). A Two-miRNA Signature of Upregulated miR-185-5p and miR-362-5p as a Blood Biomarker for Breast Cancer. *Pathology - Res. Pract.* 222, 153458. doi:10.1016/J.PRP.2021.153458

Zhang, K., Wang, Y.-Y., Xu, Y., Zhang, L., Zhu, J., Si, P.-C., et al. (2021b). A Two-miRNA Signature of Upregulated miR-185-5p and miR-362-5p as a Blood Biomarker for Breast Cancer. *Pathology - Res. Pract.* 222, 153458. doi:10.1016/J.PRP.2021.153458

Zou, R., Loke, S. Y., Tan, V. K.-M., Quek, S. T., Jagmohan, P., Tang, Y. C., et al. (2021a). Development of a microRNA Panel for Classification of Abnormal Mammograms for Breast Cancer. *Cancers* 13, 2130. doi:10.3390/CANCERS13092130

Zou, R., Loke, S. Y., Tan, V. K.-M., Quek, S. T., Jagmohan, P., Tang, Y. C., et al. (2021b). Development of a microRNA Panel for Classification of Abnormal Mammograms for Breast Cancer. *Cancers* 13, 2130. doi:10.3390/CANCERS13092130

Zou, R., Loke, S. Y., Tang, Y. C., Too, H.-P., Zhou, L., Lee, A. S. G., et al. (2022a). Development and Validation of a Circulating microRNA Panel for the Early Detection of Breast Cancer. *Br. J. Cancer* 126, 472–481. doi:10.1038/S41416-021-01593-6

Zou, R., Loke, S. Y., Tang, Y. C., Too, H.-P., Zhou, L., Lee, A. S. G., et al. (2022b). Development and Validation of a Circulating microRNA Panel for the Early Detection of Breast Cancer. *Br. J. Cancer* 126, 472–481. doi:10.1038/S41416-021-01593-6

Conflict of Interest: The authors declare that the research was conducted in the absence of any commercial or financial relationships that could be construed as a potential conflict of interest.

frontiers | Frontiers in Genetics

TYPE Original Research
PUBLISHED 10 August 2022
DOI 10.3389/fgene.2022.887477

OPEN ACCESS

EDITED BY
Gabriel Adelman Cipolla,
Federal University of Paraná, Brazil

REVIEWED BY
Lin Zhang,
China University of Mining and Technology, China
Ryoma Yoneda,
Saitama Medical University, Japan

*CORRESPONDENCE
Yang Liu,
sunny301x@sina.com

SPECIALTY SECTION
This article was submitted to RNA, a section of the journal Frontiers in Genetics

RECEIVED 01 March 2022
ACCEPTED 29 June 2022
PUBLISHED 10 August 2022

CITATION
Zhang M, Zhang J and Liu Y (2022), Comprehensive analysis of molecular features, prognostic values, and immune landscape association of m6A-regulated immune-related lncRNAs in smoking-associated lung squamous cell carcinoma.
Front. Genet. 13:887477.
doi: 10.3389/fgene.2022.887477

Comprehensive analysis of molecular features, prognostic values, and immune landscape association of m6A-regulated immune-related lncRNAs in smoking-associated lung squamous cell carcinoma

Meng Zhang[1,2], Jian Zhang[1,2] and Yang Liu[1,2]*

[1]School of Medicine, Nankai University, Tianjin, China, [2]Department of Thoracic Surgery, The First Medical Centre, Chinese PLA General Hospital, Beijing, China

Lung squamous cell carcinoma (LUSC) is the second most common histopathological subtype of lung cancer, and smoking is the leading cause of this type of cancer. However, the critical factors that directly affect the survival rate and sensitivity to immunotherapy of smoking LUSC patients are still unknown. Previous studies have highlighted the role of N6-methyladenosine (m6A) RNA modification, the most common epigenetic modification in eukaryotic species, together with immune-related long non-coding RNAs (lncRNAs) in promoting the development and progression of tumors. Thus, elucidating m6A-modified immune lncRNAs in LUSC patients with smoking history is vital. In this study, we described the expression and mutation features of the 24 m6A-related regulators in the smoking-associated LUSC cohort from The Cancer Genome Atlas (TCGA) database. Then, two distinct subtypes based on the expression levels of the prognostic m6A-regulated immune lncRNAs were defined, and differentially expressed genes (DEGs) between the subtypes were identified. The distributions of clinical characteristics and the tumor microenvironment (TME) between clusters were analyzed. Finally, we established a lncRNA-associated risk model and exhaustively clarified the clinical features, prognosis, immune landscape, and drug sensitivity on the basis of this scoring system. Our findings give insight into potential mechanisms of LUSC tumorigenesis and development and provide new ideas in offering LUSC patients with individual and effective immunotherapies.

KEYWORDS

M6A, immune lncRNA, prognosis, tumor microenvironment, smoking, squamous cell lung carcinoma

Introduction

Lung cancer, one of the leading causes of cancer death all over the world, also has a higher morbidity than other cancer types, seriously imperiling people's health and lives nowadays. Many key issues have been identified and considered to be closely related to the tumorigenesis of lung cancer, such as smoking, environmental pollution, occupational exposure, and, especially, some genetic factors (Goldstraw et al., 2011). Lung squamous cell carcinoma (LUSC) is the most common histopathological subtype after lung adenocarcinoma (LUAD), accounting for nearly 30% of patients who are diagnosed with lung cancer (Socinski et al., 2018). It is worth mentioning that smoking is the leading cause of LUSC, and most patients with this kind of cancer have a clear history of smoking (Alexandrov et al., 2016). One research focusing on non-smoking lung cancer in Eastern Asia revealed that smoking-related and non-smoking-related lung cancers were quite different, and they were likely to show different responses to targeted therapies (Chen et al., 2020a). In addition, numerous studies have found that smoking could profoundly influence the tumor microenvironment (TME) and lung microbiome, promoting the progression and metastasis of lung cancer (Desricha rd et al., 2018). To have a better understanding of LUSC, much research and clinical trials were dedicated to revealing the molecular mechanisms of the cancer and putting forward some effective measures to decrease the mortality of the disease both in prevention and treatment aspects, including early screening and some particular therapy methods like immunotherapy (Pan et al., 2021). Although these measures may achieve a certain effect in some degree, the 5-year overall survival rate does not markedly improve, especially for these advanced or poorly differentiated tumors. For these reasons, it is necessary to build an effective and accurate risk model to predict the prognosis of LUSC patients with smoking history.

N6-methyladenosine (m6A) RNA modification is a current hotspot in the cancer research area. Although it was first discovered as early as the 1970s, further research was significantly limited by the detection and research techniques those days, and studies on this kind of epigenetic modification have been stagnant for a long time (Wang et al., 2014). With the development of high-throughput sequencing, colorimetry, and liquid chromatography–mass spectrometry techniques (specific techniques including MeRIP-seq, miCLIP-seq, SCARLET, and LC-MS/MS), RNA methylation attracted people's attention again, and it has now been shown that more than half of the nucleic acid methylation modifications belong to m6A modification. By interacting with various functional proteins, m6A modification can affect the processing of almost all kinds of RNA molecules in multiple species, such as messenger RNA (mRNA; splicing, subcellular localization, polyadenylation, translation, and degradation), small non-coding RNA, and transporter RNA (tRNA) (Cantara et al., 2011; Liu and Jia, 2014; Alarcon et al., 2015; Zhang and Jia, 2018). In addition, according to previous studies, many biological processes such as tissue development, circadian rhythm regulation, DNA damage response, gender determination, and the development and progression of various diseases, especially of tumors, were closely regulated by this sort of epigenetic modification (Lence et al., 2016; Xiang et al., 2017; Zhao et al., 2017; Kasowitz et al., 2018; Tong et al., 2018). Further studies have illuminated that several enzymes or proteins were directly involved in the m6A RNA modification process, and then, these proteins could be divided into three categories based on their special structural features and functions: 1. methyltransferase (writers): a complex composed of multiple subunits to modify m6A methylation on RNA, including a core complex consisting of METTL3 (catalytic subunit) and METTL14 and several subunits that can increase the activity and specificity of the complex, such as WTAP, RBM15, KIAA1429, ZC3H13, and RBM15B; 2. m6A-binding proteins (readers): playing a biological function by recognizing and binding m6A methylation marks on RNA, including YTHDF family of proteins (YTHDF1-3), YTHDC1, YTHDC2, HNRNPC, HNRNPA2B1, EIF3A, and IGF2BPs; 3. demethylases: only two demethylases, FTO and ALKBH5, have been identified so far, which can remove the m6A methyl group from the modulated RNA, although they may exhibit different demethylation activities in a specific tissue or reaction environment (Jiang et al., 2021).

Long non-coding RNAs (lncRNAs), as one of the most important kinds of non-coding RNAs, are longer than 200 nucleotides in length but are not translated into proteins (Esteller, 2011). Although structurally similar to mRNAs, lncRNAs still have some special and unique features such as low conservation, high abundance, and timing specificity. With the development of high-throughput sequencing technology, it is believed that more lncRNAs will be discovered, and their biological functions in diseases, especially in tumorigenesis, will also be elucidated in a new way. Recent research studies have shown that lncRNAs could also undergo m6A methylation modification ultimately affecting their stability, subcellular localization, and local structure, resulting in the alteration of their biological regulatory functions (Chen et al., 2020b). Moreover, lncRNAs were also reported to be involved in the processes of immune response in multiple cancers (Hu et al., 2019). Thus, whether immune-related lncRNAs could be modulated by m6A modification and promote tumor progression in LUSC needs further studies.

TME refers to the inner environment in which tumor cells arise and live. A variety of cells including tumor cells, fibroblasts, immune and inflammatory cells, along with the intercellular substance, microvessels, and immune-associated biological molecules infiltrating in this region, together make up the TME (Liu et al., 2021). In recent years, increasing research has concentrated on the impact of the dynamic changes and related factors of the TME on tumorigenesis and progression of

tumors, and multiple mechanisms underlying the TME-promoting tumor development have been exhaustively clarified (Ringquist et al., 2021). As the TME can profoundly influence the progression and strategies of immune therapies for cancer patients, several algorithms based on RNA-seq data to evaluate the composition of immune-related cells in the TME have been developed, including TIMER, CIBERSORT, EPIC, MCP-counter, and ESTIMATE (Xu et al., 2021).

As presented earlier, m6A RNA modification, immune-related lncRNA, and dynamic changes in TME components occupy important positions in the development and progression of tumors. Whether the immune-related lncRNAs regulated by m6A regulators can significantly affect the prognosis of smoking-associated LUSC patients in a coordinated manner through the TME mechanisms deserves further studies, although several comprehensive and systematic studies have demonstrated these complicated relationships in LUAD patients (Zhang et al., 2021; Zheng et al., 2021; Zhou and Gao, 2021). Despite much research existing in the field of LUAD, the study of LUSC in this area has obviously not received enough attention. Although surgery for early LUSC can achieve good therapeutic results, advanced patients do not have many appropriate treatment options on the grounds that this kind of tumor is particularly resistant to radiochemotherapy. Owing to the reasons mentioned earlier, immunotherapy combined with chemotherapy has become the first-line treatment for advanced LUSC patients. Thus, exploring the role of m6A RNA methylation in the immune response of LUSC patients will help develop better immunotherapy strategies.

In this study, we first described the expression profiles and mutation characteristics of the 24 m6A-related proteins in the smoking-associated LUSC cohort from The Cancer Genome Atlas (TCGA) database. Second, lncRNAs that were closely co-expressed with immune genes and m6A regulators were identified. Then, these LUSC patients were classified into different molecular subtypes based on the expression levels of the selected lncRNAs. Gene subtypes were then set up according to the differentially expressed genes (DEGs) of the previously established molecular subtypes. Finally, we established a lncRNA-associated signature as a prognostic model and exhaustively clarified the immune landscape on the basis of this scoring system, aiming to provide insight into the potential immune mechanisms of LUSC tumorigenesis and predicting the prognosis and response of immunotherapy for smoking-associated LUSC patients.

Materials and methods

Patients and datasets

The LUSC patients with definite smoking history, including reformed and current smokers in TCGA database, were enrolled in this study. All patients' information, including RNA-seq data (exhibited as fragments per kilobase million, FPKM), corresponding clinical information (age, gender, TNM (tumor node metastasis classification) stage, T (tumor), N (node), M (metastasis), smoking history, overall survival, and survival state), and single nucleotide variation data, was obtained from TCGA database website (https://portal.gdc.cancer.gov/), totalizing 49 normal and 473 tumor samples. LUSC samples with no complete follow-up information were excluded to reduce the statistical bias. The copy number variation (CNV) data on TCGA-LUSC samples were collected from Xena functional genomics explorer (https://xenabrowser.net/).

Identification of m6A-regulated immune LncRNAs in the smoking-associated TCGA-LUSC cohort

A total of 24 genes were found to act as, in light of previous studies, m6A regulators, including eight writers (*METTL3*, *METTL14*, *METTL16*, *WTAP*, *VIRMA*, *ZC3H13*, *RBM15*, and *RBM15B*), 14 readers (*YTHDC1*, *YTHDC2*, *YTHDF1*, *YTHDF2*, *YTHDF3*, *HNRNPC*, *FMR1*, *LRPPRC*, *HNRNPA2B1*, *IGF2BP1*, *IGF2BP2*, *IGF2BP3*, *RBMX*, and *EIF3A*), and two erasers (*FTO* and *ALKBH5*). For this reason, we extracted the expression matrix of the 24 m6A-related genes and lncRNAs in the smoking-associated TCGA-LUSC cohorts. The Pearson correlation coefficients were calculated to access the co-expression correlation between the 24 m6A-related genes and lncRNAs. LncRNAs that met the threshold of |Pearson correlation coefficients| > 0.30 and $p < 0.001$ were considered to be m6A-related lncRNAs. Furthermore, immune-related genes were obtained from IMMPORT (https://www.immport.org/home) and InnateDB (https://www.innatedb.ca/) websites. The co-expression relationship between the immune-related genes and lncRNAs was calculated by Pearson analysis, and lncRNAs with |Pearson correlation coefficients| > 0.40 and $p < 0.001$ were regarded as immune-related lncRNAs. Intersections of the two lncRNA sets were defined as m6A-regulated immune lncRNAs.

Unsupervised consensus clustering analysis

To identify the molecular subgroups that were mediated by the expression patterns of m6A-related immune lncRNAs or DEGs in the smoking-associated LUSC cohort, the "ConsensusClusterPlus" package of R software (version 3.6.2) was utilized for unsupervised consensus clustering analysis (50 repetitions and 0.8 pItem). The cumulative distribution function (CDF) curve and consensus matrix were combined to find the most suitable k value that could provide a more

representative clustering model for LUSC patients. The differences in gene expressions, clinical characteristics (age, gender, TNM stage, T, N, and smoking history), and prognosis between the classified subgroups were evaluated using the Wilcoxon test, chi-squared test, and Kaplan–Meier survival curves, respectively.

Tumor microenvironment analysis

To evaluate the degree of infiltration of immune cells in different subgroups, we employed the ESTIMATE method to calculate the immune and stromal scores and estimate scores for each patient in the smoking-associated LUSC cohort with the help of "estimate" R package. After the risk score model was constructed, several common algorithms like EPIC, TIMER, MCP-counter, and XCELL were performed to compare the differences of infiltrating levels of immune cells between the high- and low-risk groups. The immune infiltration data on the TCGA-LUSC cohort were downloaded from the TIMER2.0 database (http://timer.cistrome.org/). In addition, we also estimated the expression of a series of immune checkpoint molecules and IFN-related genes using the Wilcoxon test in different subgroups as a necessary supplement for the immune cell infiltration analysis. The "maftools" R package was used to describe the mutation information of the top 20 genes with the highest mutation frequency in high- and low-risk groups.

Functional enrichment analysis for DEGs between different clusters

The DEGs between the classified clusters were identified by means of the "limma" R package (adjusted p-value < 0.001), and the expression profile of these DEGs was then extracted from previously downloaded RNA-seq data. To further explore the involved biological processes and signal pathways of modules that were most relevant to risk scores, Gene Ontology (GO) and Kyoto Encyclopedia of Genes and Genomes (KEGG) analyses were carried out utilizing the "clusterProfiler" package of R software with the p-value < 0.05 as the significant threshold.

Hub gene identification

The protein–protein interaction (PPI) network of these prognostic DEGs, which were identified by univariate Cox regression analysis, was constructed with the help of the STRING database (https://string-db.org/). Then, the network was enrolled in Cytoscape software (version 3.7.2), and cytoHubba plug-in was downloaded to calculate the top 10 hub genes by means of the "Degree" algorithm.

Construction of the risk score model in the smoking-associated TCGA-LUSC cohort

By virtue of the previously identified m6A-related lncRNAs, a risk score model was constructed as follows. First, univariate Cox regression analysis was utilized to screen lncRNAs that were significantly associated with the overall survival (OS) of patients from the smoking-associated TCGA-LUSC cohort. Then, lncRNAs with the p-value < 0.05 in the univariate Cox regression analysis were further subjected to multivariate Cox regression analysis to identify the ones that could independently affect the prognosis of LUSC patients. Finally, a 12-lncRNA signature model for prognostic prediction in this cohort was successfully established based on the expression levels and corresponding coefficients of the selected lncRNAs. The risk score of each patient in the cohort was calculated by the following equation: risk score = $\sum_{i=1}^{12}(\beta i * Exp i)$. In this formula, βi meant the coefficient derived from multivariate Cox regression, and $Exp i$ referred to the expression levels of the 12 lncRNAs in this model. Furthermore, all samples in the cohort were assigned to high- or low-risk groups according to their risk score with the median value as the cutoff value.

Survival analysis and evaluation of the risk model

As the patients in the smoking-associated TCGA-LUSC cohort have been divided into high- and low-risk groups, we drew the Kaplan–Meier survival curves of the two groups with the help of "survival" and "survMiner" packages of R software, and the log-rank test was used to evaluate the survival difference between the two groups with $p < 0.05$ as the significant threshold. To access the exactitude of the risk model we have built, the receiver operating characteristic (ROC) curve was displayed and the area under the curve (AUC) was calculated by means of the "timeROC" R package. In addition, the "timeROC" package and "compare" function were utilized to contrast the AUC of the risk score with other clinical features at 1 year ($p < 0.05$ as significant).

Independence assessment and stratification analysis of the risk model

The clinical characteristics and expression profiles of the 12 lncRNAs in high- and low-risk groups were exhibited as a heat map by virtue of the "pheatmap" R package. In addition, to make sure that the risk score of LUSC patients, which was calculated by the 12 lncRNA-related signature in this study, could act as an independent prognostic factor when compared to other traditional clinical features, univariate and multivariate Cox regression analyses were successively performed using OS as the dependent variable, while five potential prognostic factors,

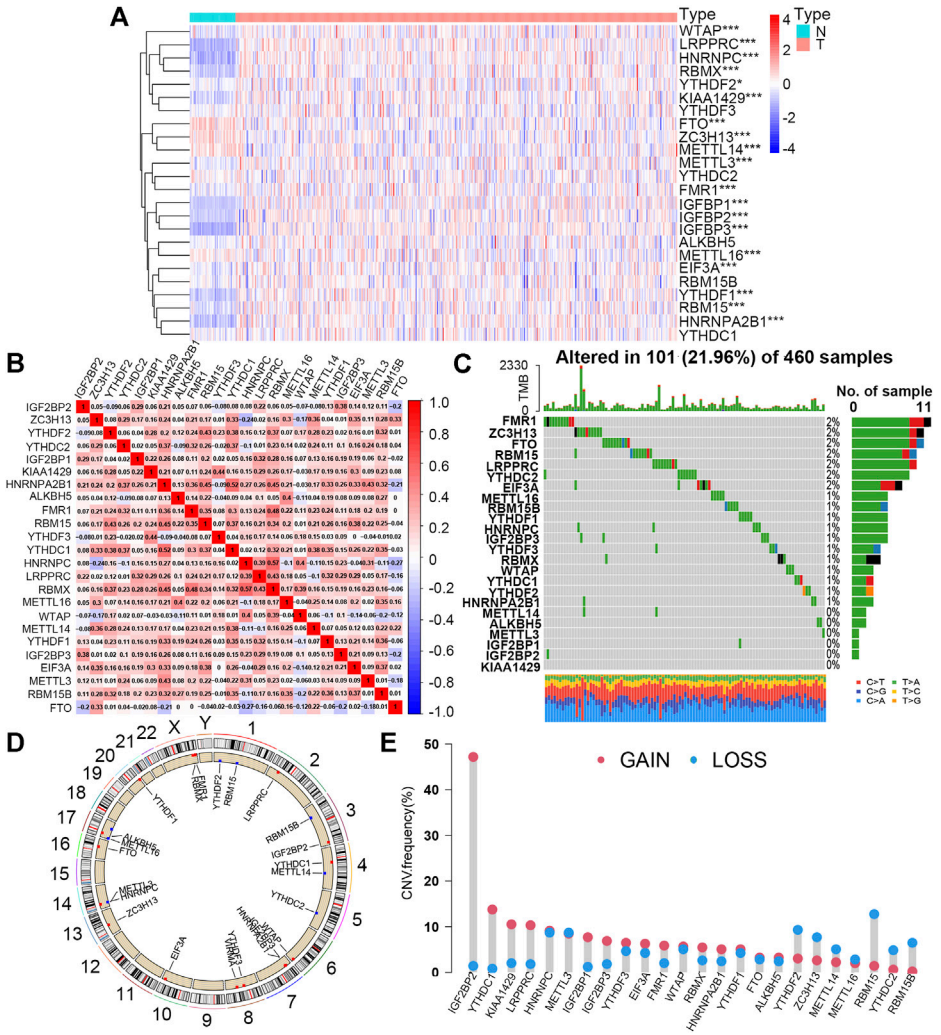

FIGURE 1
Expression levels and mutation features of 24 m6A regulators in the smoking-associated LUSC cohort from TCGA database. **(A)** Expression differences of 24 m6A regulators between normal (N) (n = 49) and tumor (T) (n = 473) samples (*$p < 0.05$; ***$p < 0.001$). **(B)** Expression correlation analysis of 24 m6A regulators in the smoking-associated LUSC cohort. Red and blue refer to positive and negative correlation, respectively. **(C)** Somatic mutation types and frequency of 24 m6A regulators in 460 LUSC samples with smoking history. **(D)** Locations and CNV types of 24 m6A genes on 24 different chromosomes. Red and blue refer to the increased and decreased CNV types, respectively. **(E)** CNV frequency of 24 m6A regulators in the smoking-associated LUSC cohort. Red and blue refer to the increased and decreased CNV types, respectively.

namely, smoking history, age, gender, TNM stage, and risk score, were incorporated in Cox regression analyses as independent variables. Furthermore, based on the results of multivariate Cox regression analysis, stratification analysis was carried out to further investigate whether the risk model would also have prognostic efficiency under the stratified clinical features that had been proven to be significantly associated with OS and acted as an independent prognostic factor for LUSC patients in this cohort. Moreover, for the classified high- and low-risk groups, gene set enrichment analysis (GSEA), which could provide a better assistance in searching for the potential downstream pathways and investigating the possible mechanisms underlying the association between risk score and prognosis, was performed by means of GSEA 4.0.3 software.

Building and assessment of the nomogram

Subsequently, a nomogram was successfully developed using the independent risk factors derived from the multivariate Cox regression analysis in this cohort. The survival possibility at 1, 3, and 5 years from diagnosis of a given LUSC patient could be concisely predicted by putting these concerned factors independently affecting patients' survival into this

comprehensive scoring system. In addition, in order to assess the specificity, accuracy, and discriminative ability of the established nomogram, we drew a calibration curve with those three time points by making use of the "rms" package of R software.

Drug sensitivity analysis

To provide references for the treatment of LUSC patients based on our established risk scoring system, we assessed the 50% inhibitive concentration (IC50) of a series of common chemotherapeutic drugs for patients in low- and high-risk groups using "pRRophetic" R package. $p < 0.05$ was considered to indicate significant differences between the two groups.

Results

Expression and mutation features of 24 m6A regulators in the smoking-associated LUSC cohort

The detailed workflow of the present study is shown in Supplementary Figure S1. A total of 24 m6A regulators were incorporated into this study, and the expression levels of most of these proteins between the normal (49) and tumor (473) sample groups showed significant differences. According to the heat map (Figure 1A), 15 m6A regulators (YTHDF2, FMR1, METTL3, EIF3A, WTAP, RBM15, VIRMA, IGF2BP2, RBMX, YTHDF1, IGF2BP1, HNRNPA2B1, IGF2BP3, HNRNPC, and LRPPRC) were upregulated, and only 4 regulators (METTL16, METTL14, FTO, and ZC3H13) were downregulated in tumor samples compared to controls. In addition, five proteins (YTHDC2, YTHDC1, YTHDF3, RBM15B, and ALKBH5) had no significant distinction between the two groups. This result demonstrated that m6A regulators might play a vital role in tumorigenesis and progression for LUSC patients with smoking history. Furthermore, we observed that more than 80% of m6A regulators displayed a positive correlation with each other, suggesting that these proteins would have a common mode of action in regulating this kind of epigenetic modification of RNA (Figure 1B).

For the study of mutation characteristics, we first explored the frequency and types of somatic mutations of the 24 m6A regulators. During this analysis, 101 (21.96%) of the 460 samples with mutation information were found to possess mutations and 18 (75%) out of the 24 m6A regulators were mutated with the frequency varying from 1% to 2% (Figure 1C). Then, we analyzed the CNV of the 24 m6A regulators in the LUSC cohort. The CNV of the 24 m6A regulators and their positions on different chromosomes were visualized as the circos plot (Figure 1D). Figure 1E shows that IGF2BP2, YTHDC1, KIAA1429 (VIRMA), and LRPPRC had the most notable increases in copy number alterations, while RBM15, RBM15B, YTHCD2, YTHDF2, and ZC3H13 owned the decreased CNV, which was basically consistent with the expression changes between normal and tumor sample groups. The expression levels of the 24 m6A regulators between the TP53 wild and mutated groups were further compared and nine of them (37.5%) showing higher levels in the TP53 mutated group than that in the wild group, implying that mutated TP53 might promote the expression of these m6A-related genes (Supplementary Figure S2A).

The prognostic values of the 24 m6A regulators in this LUSC cohort were estimated by univariate Cox regression analysis. However, none of them had a significant effect on the overall survival of patients, and the results suggested that m6A regulators might play a role *via* their downstream modulated lncRNAs (Supplementary Figure S2B).

Identification of m6A-related immune lncRNAs

According to the criteria described previously, a total of 1,177 m6A-related lncRNAs and 2,885 immune-related lncRNAs were screened out. The intersection of the aforementioned two sets included 1,030 lncRNAs that were finally defined as m6A-related immune ones (Figure 2A). To further explore lncRNAs that could significantly affect the prognosis of smoking-associated LUSC patients, univariate Cox regression analysis was carried out, and 22 lncRNAs were identified as exhibiting prognostic values. Forest plot further revealed that eight of these prognostic lncRNAs were protective factors, with patients with higher expression exhibiting better prognosis (Supplementary Figure S3A). The expression profiles of 22 lncRNAs were extracted from RNA-seq data for further studies.

Identification of m6A clusters based on m6A-related immune lncRNAs

To investigate whether the identified m6A-regulated immune-related lncRNAs could influence the prognosis and other clinical features of smoking-associated LUSC patients in a coordinated way, we performed unsupervised consensus clustering analysis by using the expression matrix of 22 prognostic lncRNAs previously identified by univariate Cox regression. According to the consensus matrix, we selected k = 2 as the optimal clustering parameter and divided these patients into two m6A clusters named cluster A (147 cases) and cluster B (319 cases) (Figure 2B). The Kaplan–Meier survival curve showed that the prognosis of patients in cluster A was significantly better than that in cluster B (Figure 2C). We further evaluated the differences in lncRNA expression levels

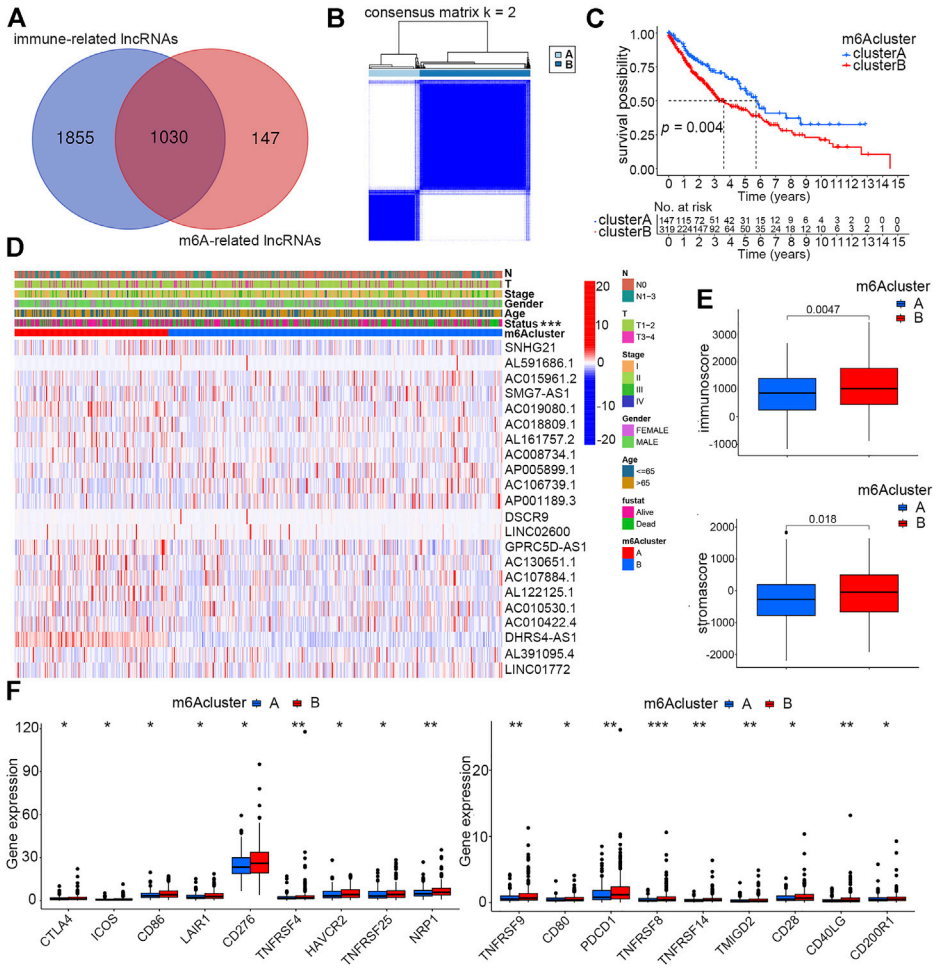

FIGURE 2
Identification of two distinct m6A clusters and differences of their clinical and immune features. **(A)** Identification of immune-related lncRNAs regulated by m6A regulators. **(B)** Two distinct m6A clusters were determined based on m6A-regulated immune-related lncRNAs *via* unsupervised consensus clustering analysis. **(C)** Overall survival differences between m6A clusters A and B by Kaplan–Meier survival analysis. Log-rank $p = 0.004$. **(D)** Differences of clinical features and expression profiles of m6A-regulated immune-related lncRNAs between clusters A and B (***$p < 0.001$) **(E)** Differences of immune and stroma scores by ESTIMATE analysis of smoking-associated LUSC samples between m6A clusters A and **B**. **(F)** Differences of expression levels of immune checkpoint molecules between m6A clusters A and B (*$p < 0.05$, **$p < 0.01$, and ***$p < 0.001$).

and clinical features between the two clusters. According to the heatmap, expression levels of the 22 m6A-regulated immune-related lncRNAs were quite different between the two clusters. In addition, the survival status also showed a distinct distribution characteristic, which was consistent with the previous survival analysis (Figure 2D).

As the TME could directly or indirectly influence patient survival by regulating immune infiltration, our study further concentrated on investigating whether immune-related factors play a crucial role in causing different clinical performance of the two clusters. ESTIMATE analysis suggested that patients in cluster B had higher immune and stromal scores than patients in cluster A (Figure 2E). Much research has reported that high infiltration of immune cells, especially adaptive immune cells like activated $CD4^+$ T cells and $CD8^+$ T cells, could effectively promote the ability of the immune system of eliminating tumor cells, thereby inhibiting tumor growth (Tekpli et al., 2019). In this study, we speculated that it was the high stromal cell infiltration that counteracted the anti-cancer effects of immune cells, accounting for the reasons why patients in cluster B with higher immune scores exhibited poorer prognosis. Another factor directly affecting patient's prognosis and sensitivity to immunotherapy is immune checkpoint proteins. We evaluated the expression levels of 18 immune checkpoint molecules between the two clusters, and the result showed that all these proteins, including PDCD1 and CTLA4, had higher expression in cluster B patients (Figure 2F).

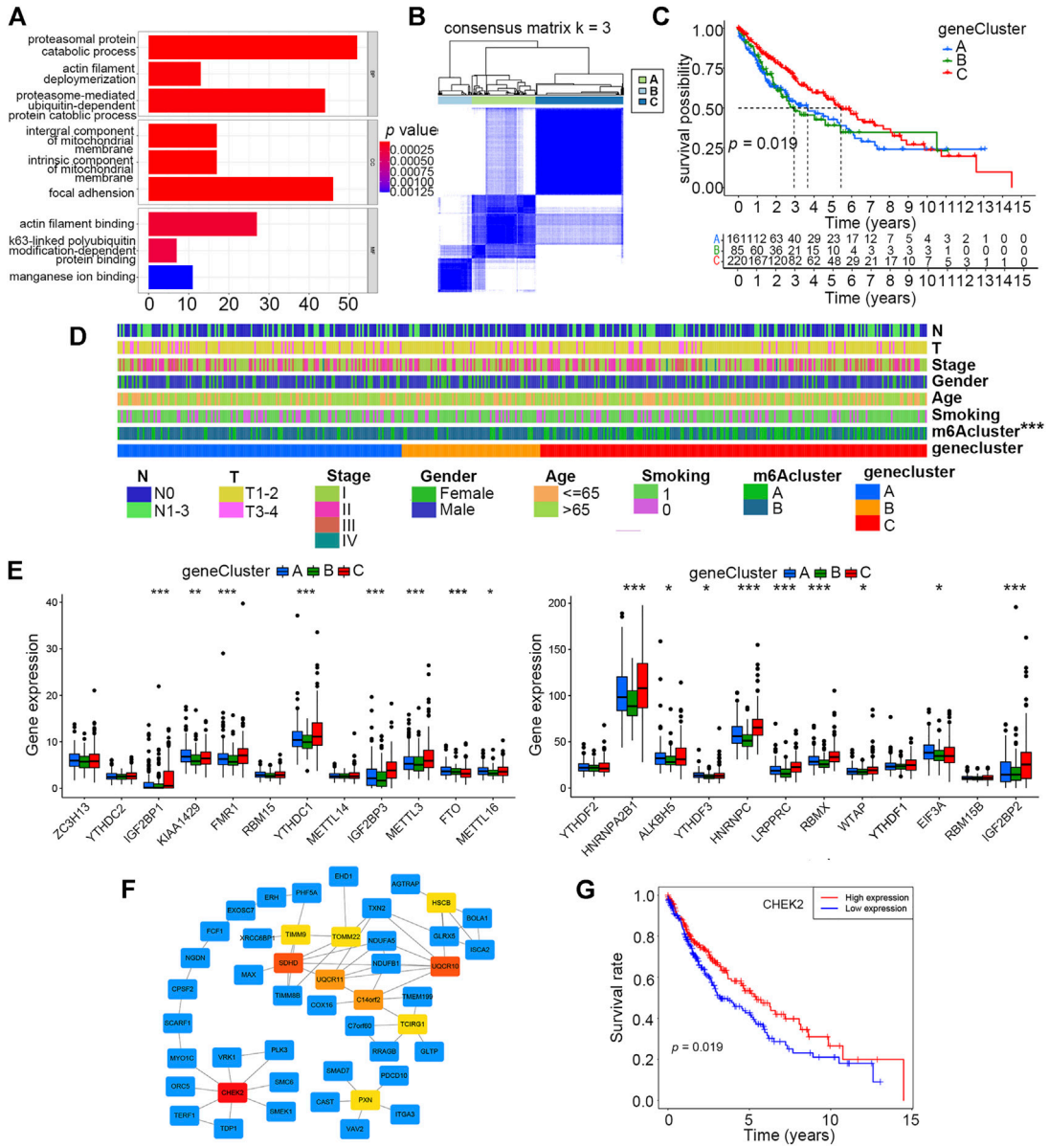

FIGURE 3
Identification of three distinct gene clusters based on DEGs of m6A clusters A and **B**. **(A)** Enrichment analysis of 1814 DEGs of m6A clusters A and B by GO. **(B)** Identification of three distinct gene clusters based on 230 prognostic DEGs of m6A clusters A and B *via* unsupervised consensus clustering analysis. **(C)** Overall survival differences among m6A clusters A, B, and C by Kaplan–Meier survival analysis. Log-rank $p = 0.019$. **(D)** Differences in clinical characteristics and m6A clusters among gene clusters A, B, and **C**. **(E)** Differences in expression levels of 24 m6A regulators among gene clusters A, B, and C (*$p < 0.05$, **$p < 0.01$, and ***$p < 0.001$). **(F)** Hub gene identification among DEGs by Cytoscape software and the Degree algorithm. The top 10 hub genes are marked from pale yellow to deep red, and the darker the color, the more important it is. The other related genes are labeled blue. **(G)** Overall survival differences between high and low expression levels of CHEK2 in the smoking-associated LUSC cohort by Kaplan–Meier analysis. Log-rank $p = 0.019$.

Identification of gene clusters based on DEGs

As the aforementioned categorized clusters have been evidenced to be closely associated with patient prognosis, we further explored the potential mechanisms by functional enrichment analysis using DEGs between the two clusters. By means of the "limma" R package, a total of 1814 DEGs were identified, and their expression profiles combined with relevant clinical information were extracted from original data. GO analysis revealed that DEGs were more likely to be enriched in adhesion- and metabolism-related processes or pathways,

which were previously deemed to be closely correlated with tumor progression (Figure 3A).

To get a better understanding of how these DEGs could have an impact on prognosis, we conducted unsupervised consensus clustering analysis based on the expression profiles of 230 prognostic DEGs singled out by univariate Cox regression, and three distinct gene clusters, A, B, and C, were finally identified (Figure 3B). The prognosis of patients in cluster C was better than that of those in clusters A and B, according to the Kaplan–Meier survival curve (Figure 3C). Furthermore, the distributions of clinical characteristics, including the m6A cluster, among these three clusters were further analyzed. The result showed that the m6A cluster, but not other clinical characteristics, differed among these three gene clusters (Figure 3D). By evaluating the expression levels of the 24 m6A regulators, we found that 17 of them (70.8%) were differentially expressed among the three gene clusters, and most of these differentially expressed regulators had higher expression levels in cluster C than that in the other two clusters (Figure 3E).

Hub gene identification

The top 10 hub genes among these DEGs were identified by means of Cytoscape software, and CHEK2 was ranked as the most important one using the "Degree" algorithm (Figure 3F). We further explored the prognostic value of CHEK2 in this smoking-associated LUSC cohort, and the result showed that patients with a higher CHEK2 expression were more likely to exhibit better overall survival (Figure 3G).

Establishment and validation of a risk score model

As described earlier, 22 of these m6A-related lncRNAs in the smoking-associated TCGA-LUSC cohort were significantly associated with survival prognosis. Subsequently, multivariate Cox regression analysis was performed for these prognosis-related lncRNAs. As a result, 12 lncRNAs were selected to construct a risk signature for LUSC patients. The risk score of each patient could be calculated by the linear combination of the expression value of 12 lncRNAs weighted by their coefficients as follows: risk score = (−0.2264 × expression value of SNHG21) + (0.0458 × expression value of AL591686.1) + (0.8498 × expression value of SMG7-AS1) + (0.4858 × expression value of AC018809.1) + (1.3643 × expression value of AC008734.1) + (0.3552 × expression value of AP005899.1) + (0.1272 × expression value of LINC02600) + (−1.3126 × expression value of AC130651.1) + (−0.7355 × expression value of AC107884.1) + (−0.3529 × expression value of AL122125.1) + (1.2541 × expression value of AC010530.1) + (−0.7161 × expression value of AC010422.4). According to the formula, AL591686.1, SMG7-AS1, AC018809.1, AC008734.1, AP005899.1, AC010530.1, and LINC02600, which exhibited positive coefficients in the risk signature, would predict a poor prognostic ending for those with high expression levels of these lncRNAs. Meanwhile, the other lncRNAs with negative coefficients were regarded as protective factors and higher expression levels of these lncRNAs often indicated a longer overall survival. Patients were assigned to high- or low-risk groups based on the median value of risk scores. According to the risk plot, the risk score model could effectively separate patients with unique survival status into different risk groups, in which the high-risk group had more deceased patients than the low-risk group. Moreover, seven lncRNAs featured with positive coefficients had low expression levels in high-risk group patients, while the remaining five lncRNAs showed opposite expression patterns (Figure 4A). The Kaplan–Meier survival curve suggested that the overall survival of patients in the high-risk group was significantly worse than those in the low-risk group (p-value < 0.05) (Figure 4B). In order to validate the specificity and sensitivity of the established risk model, we depicted the ROC curve and calculated the AUC under different conditions. Figure 4C shows that the risk score had a higher AUC value than other clinical features like age, gender, and TNM stage at 1 year (p-value < 0.05), indicating that this scoring system was superior to others in assessing the prognosis of patients. Moreover, the AUC values under 1, 2 and 3 years were 0.686, 0.670, and 0.699, respectively (Figure 4D). Finally, a Sankey diagram was drawn to describe the relationship of patients in distinct m6A clusters with gene clusters, risk scores, and survival status (Figure 4E).

To have a better understanding of the expression features of the 12 lncRNAs involved in the risk model and their correlation with m6A regulators, we first evaluated their expression levels between normal and tumor sample groups, and all of them were abnormally expressed according to the heatmap (Supplementary Figure S3B). Further analysis demonstrated that there were significant correlations between m6A regulators and the expression of 12 lncRNAs (Supplementary Figure S3C). Another Sankey diagram was depicted to clarify the relationship of the 12 lncRNAs with distinct m6A regulators and risk types (Supplementary Figure S3D).

Independent prognostic and stratified analysis of the risk model

For the sake of evaluating whether the constructed risk scoring system could predict the prognosis as an independent factor, we performed univariate and multivariate Cox regression analyses by putting risk scores together with other clinical features, including smoking history (reformed smoking vs. current smoking), age (≤ 65 years vs. > 65 years), gender (female vs. male), and TNM stage (I vs. II vs. III vs. IV) into

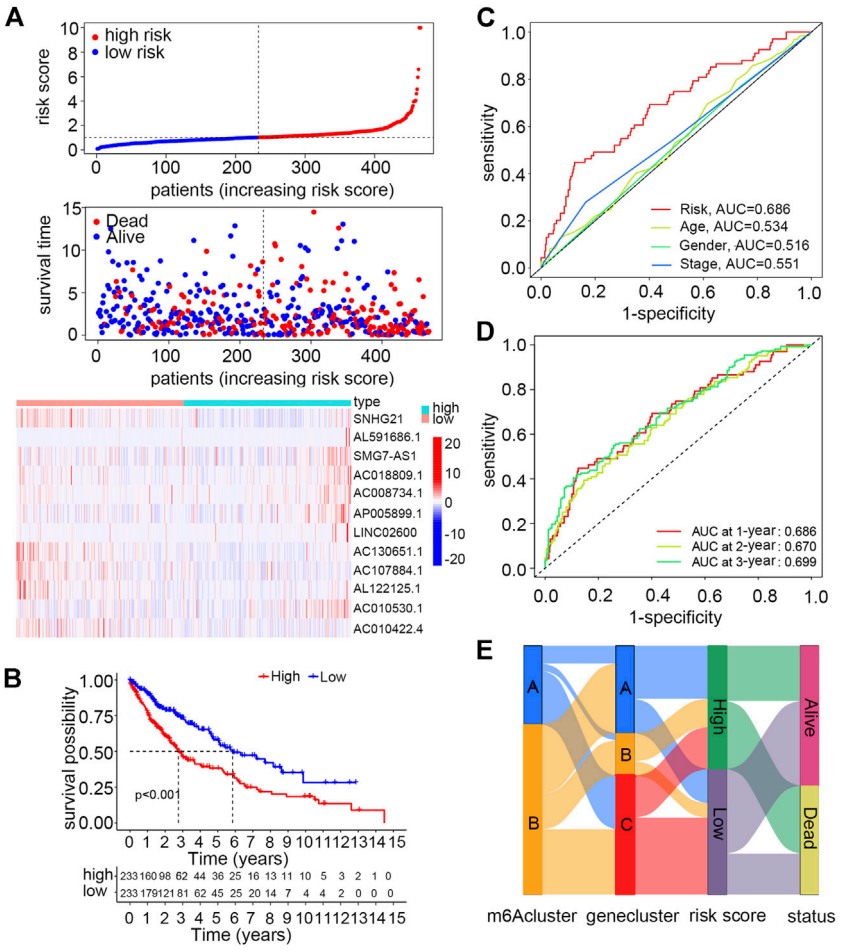

FIGURE 4
Construction and validation of a risk model using m6A-regulated immune-related lncRNAs for smoking-associated LUSC patients. **(A)** Distribution of the risk score and survival status and the expression levels of m6A-regulated immune-related lncRNAs between high- and low-risk groups. **(B)** Overall survival differences between high- and low-risk groups by Kaplan–Meier analysis. Log-rank $p < 0.001$ **(C)** ROC curves and AUC values of the risk score to compare the sensitivity and specificity of the risk score and other clinical features at 1 year. **(D)** ROC curves and AUC values of the risk score at 1, 2, and 3 years. **(E)** Sankey diagram of patients in distinct m6A clusters corresponding to different gene clusters, risk groups, and survival status.

each analysis. The result suggested that risk score, age and smoking history, but not gender and TNM stage, are risk factors that could independently affect patient prognosis (Figures 5A,B). Furthermore, for age and smoking status, which have been proven to be independent risk factors *via* multivariate Cox regression analysis, we performed stratified analysis by dividing them into two diverse subgroups. Patients with high scores under all these stratified conditions, including age (≤ 65 and >65 years old) and smoking history (reformed smoking and current smoking), presented poorer prognosis than low-score patients (Figures 5C,D).

For the constructed risk score model, we explored the relationship of risk scores with two different kinds of categorized clusters and clinical features, including smoking history, age, gender, TNM stage, T, N, and survival status. Among these factors, the m6A cluster, gene cluster, survival status, and age were distributed differently between low- and high-risk groups (Figure 5E). In detail, patients with features of m6A cluster A, gene cluster C, and age ≤ 65 years old were more likely to exhibit lower risk scores (Figure 5F).

GSEA analysis of the risk score groups

GSEA analysis was performed to explore potentially activated pathways in low- and high-risk groups. In the high-risk group, we found many enriched immune-related pathways such as “antigen processing and presentation,” “cytokine–cytokine receptor interaction,” “leukocyte transendothelial migration,” “chemokine signaling pathway,” “natural killer cell-mediated

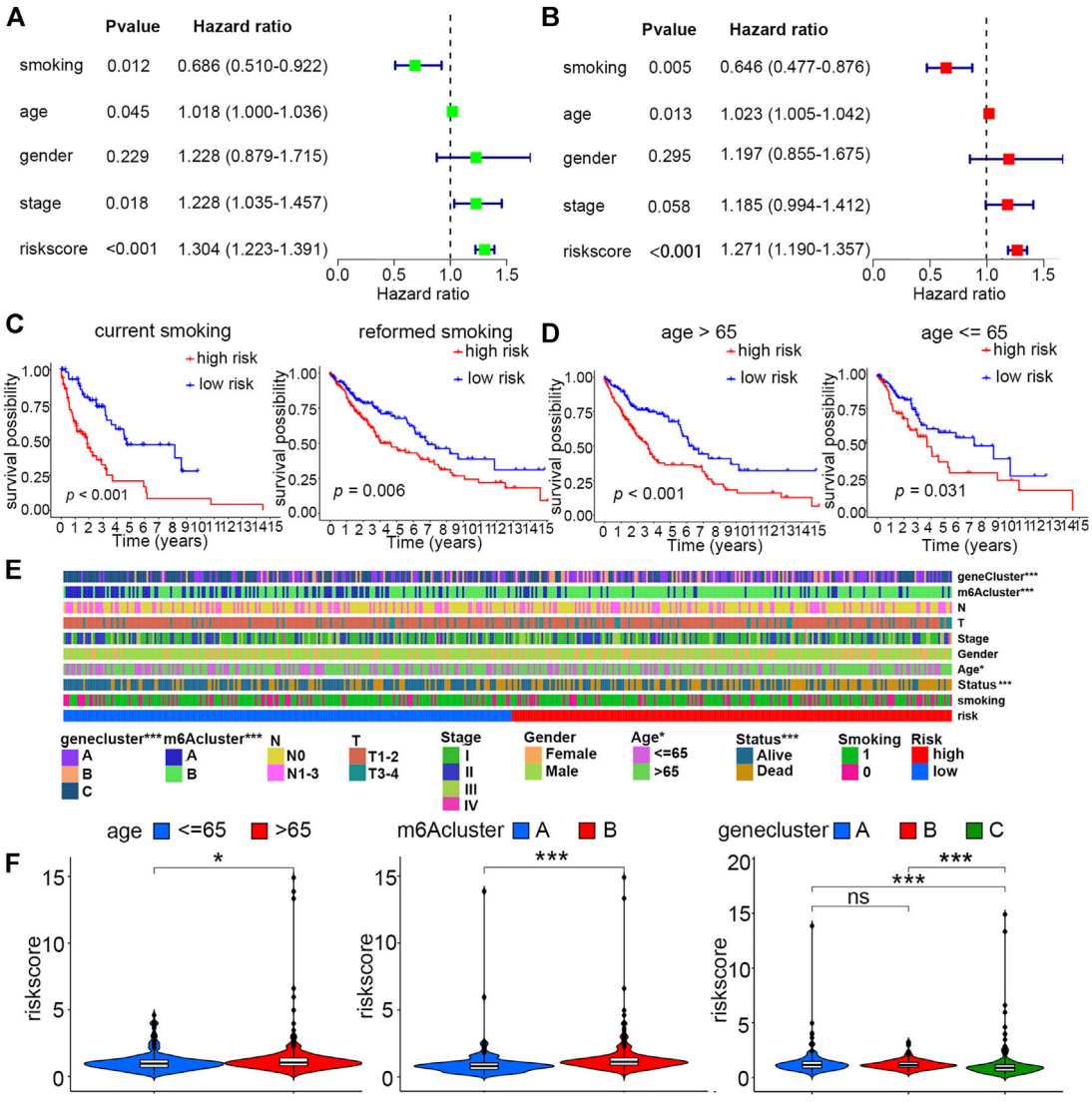

FIGURE 5
Independent prognostic and stratified analyses of the risk model. **(A)** Univariate and **(B)** multivariate Cox regression analyses of risk score and other clinical features. **(C)** Kaplan–Meier curves of high- and low-risk groups with stratified smoking history. **(D)** Kaplan–Meier curves of high- and low-risk groups with stratified age. **(E)** Differences in clinical characteristics, m6A clusters, and gene clusters between high- and low-risk groups (*p < 0.05; ***p < 0.001) **(F)** Distribution of the risk score between age, m6A cluster, and gene cluster subgroups (*p < 0.05; ***p < 0.001).

cytotoxicity," and "toll-like receptor signaling pathway." However, there were only five pathways that were enriched in the low-risk group, like "basal transcription factors" and "RNA degradation" (Supplementary Figure S4).

Correlation analysis of risk scores with immune infiltration and immunotherapy

Three different algorithms, including TIMER, xCell, and MCP-counter, were utilized to assess and compare the immune infiltration levels in high- and low-risk groups. These algorithms suggested that the infiltration levels of immune cells like $CD4^+$ T cells, $CD8^+$ T cells, NK cells, and macrophage cells, as well as some kinds of stromal cells such as endothelial cells and cancer-associated fibroblasts, were positively correlated with risk scores (Figure 6A). Moreover, an analysis aiming to explore the correlation of risk scores with immune checkpoints was performed, and the result showed that patients in the high-risk score group had elevated expression levels of most of these important biomarkers in spite of no significant expression difference of PDL1 between the two groups (Figure 6B,

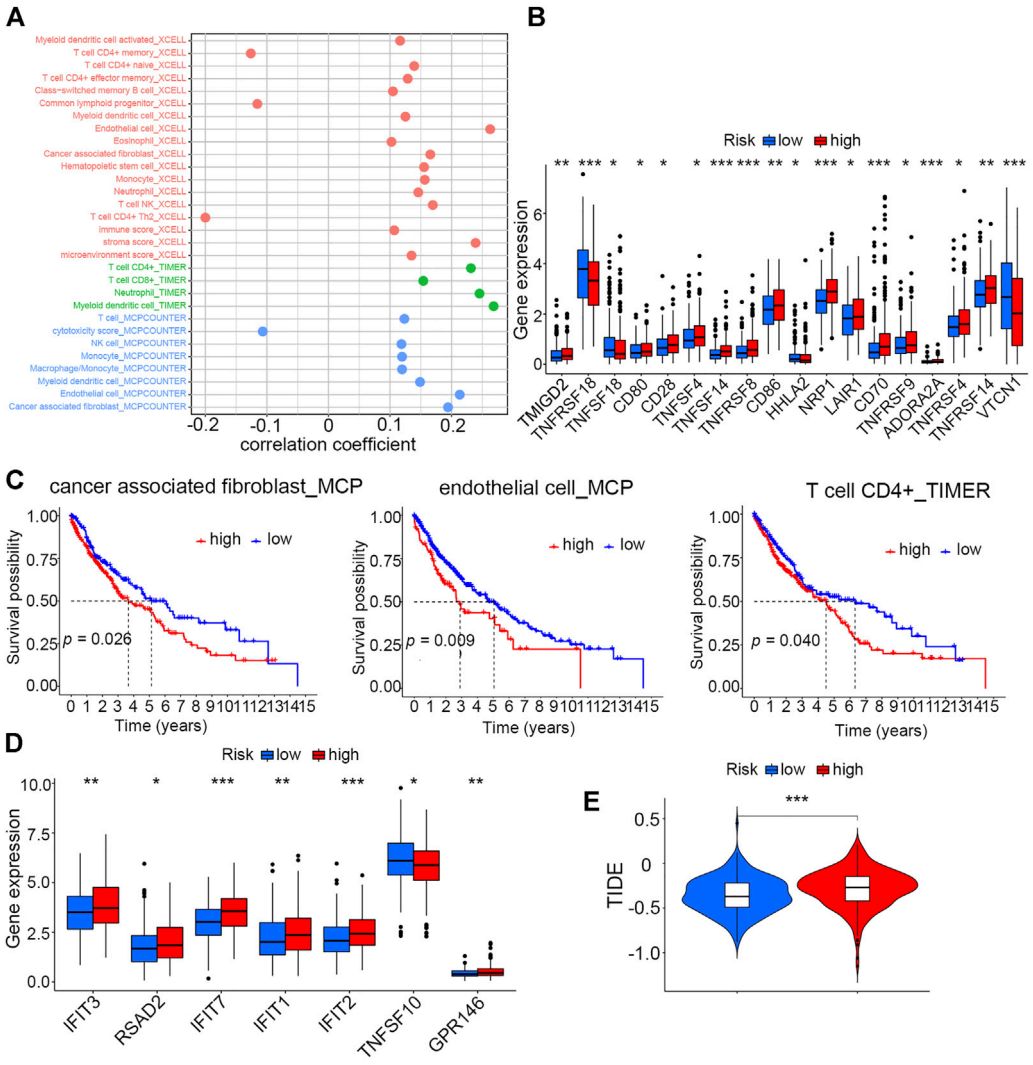

FIGURE 6
Correlation analysis of risk scores with the TME and immunotherapy **(A)** Correlation analysis of the risk score with infiltration levels of immune cells by three different algorithms. **(B)** Differences in expression levels of immune checkpoint molecules between high- and low-risk groups (*p < 0.05, **p < 0.01, and ***p < 0.001). **(C)** Kaplan–Meier analysis of cancer-associated fibroblasts, endothelial cells (MCP), and CD4$^+$ T cells (TIMER) between high- and low-risk groups. **(D)** Differences in expression levels of seven IFN-related genes between high- and low-risk groups (*p < 0.05, **p < 0.01, and ***p < 0.001). **(E)** Tumor immune dysfunction and exclusion (TIDE) analysis to predict the sensitivity of patients in high- and low-risk groups to immunotherapy (***p < 0.001).

Supplementary Figure S5A). Then, we evaluated the survival prognosis of patients under the different infiltration levels of stromal and immune T cells. The high infiltration levels of both the endothelial cells and cancer-associated fibroblasts using MCP-counter and xCell algorithms indicated poor prognosis (Figure 6C, Supplementary Figure S5B). However, patients with high CD4$^+$ T-cell infiltration had worse overall survival than those with low infiltration (Figure 6C). As interferon (IFN) has been proven to be crucial in regulating tumor progression, we compared the expression levels of seven IFN-related genes between the high- and low-risk groups. Most of these IFN-related genes showed higher levels in the high-risk group than in the low-risk group (Figure 6D). In addition, the mutation information of the top 20 genes with the highest alteration frequencies in the two risk groups was visualized as the waterfall plot (Supplementary Figure S5C,D).

Given that the two risk groups had distinct immune characteristics, Tumor Immune Dysfunction and Exclusion (TIDE) was analyzed to compare the sensitivity of high- and low-score patients to immunotherapy. The result demonstrated that the high-risk group with higher TIDE scores was more likely to resist immunotherapy compared to the low-risk group (Figure 6E).

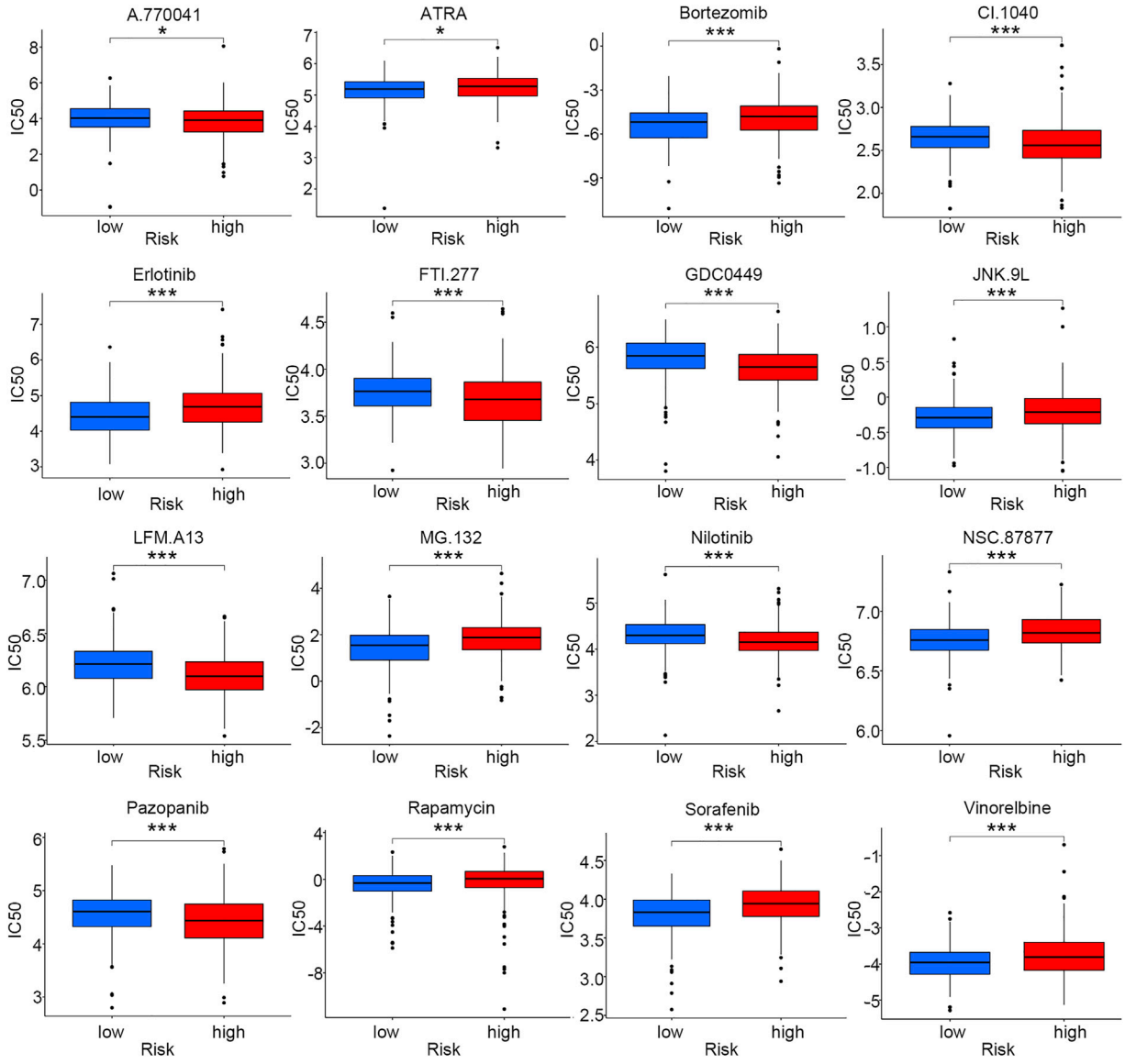

FIGURE 7
Drug sensitivity comparison for smoking-associated LUSC patients between low- and high-risk groups (*$p < 0.05$; ***$p < 0.001$).

Drug sensitivity analysis based on the risk score model

As chemotherapy and targeted therapy have become the most important treatment for LUSC patients, identifying the subgroup of patients that was sensitive to specific drugs could promote their therapeutic effectiveness. Sixteen commonly used anti-tumor drugs were incorporated into this study to be evaluated in each risk group. According to Figure 7, the low-risk group was more likely to respond to ATRA, bortezomib, erlotinib, JNK.9L, MG.132, NSC.87877, rapamycin, sorafenib, and vinorelbine, while the high-risk group was more sensitive to A.770041, CI.1040, FTI.277, GDC0449, LFM. A13, nilotinib, and pazopanib.

Construction and evaluation of the nomogram

In order to conveniently predict the survival prognosis of LUSC patients, we constructed a nomogram by incorporating the risk score and two other prognostic risk factors, namely, age and smoking history, into this predictor (Figure 8A). By means of this nomogram, the survival possibility of a specific patient under 1, 3,

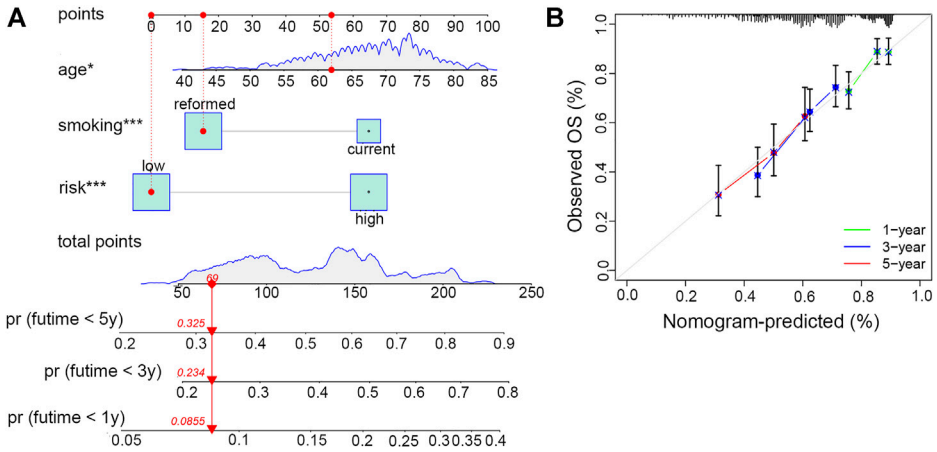

FIGURE 8
Establishment and evaluation of the clinical nomogram. **(A)** Nomogram to predict the survival possibility of smoking-associated LUSC patients at 1, 3, and 5 years. **(B)** Calibration curves to validate the prediction efficiency of the nomogram at 1, 3, and 5 years.

and 5-years could be forecasted. The calibration curve revealed that the predicted overall survival of patients was basically the same as the observed outcome, indicating the high precision of this prediction model (Figure 8B).

Discussion

m6A RNA methylation, which is considered to be the most common epigenetic modification in eukaryotic species, participates in the occurrence and progression of tumors in multiple ways (Jiang et al., 2021). In the present study, we first described the expression profiles and mutation features of 24 m6A regulators in LUSC patients with smoking history. As none of them could significantly affect the prognosis, we speculated that these regulators might act in a coordinated manner *via* modulating methylation levels on downstream RNA molecules, and the results were further verified by their expression correlation analysis. Until now, only one research concerning m6A regulators in LUSC has reported that the hypoxia-mediated high expression of YTHDF2, an important m6A reader, could predict a worse prognosis of LUSC, which was basically consistent with our conclusion (Xu et al., 2022).

To better understand whether m6A-regulated downstream lncRNAs could affect prognosis of patients with LUSC through immune regulatory mechanisms, we picked out m6A-regulated immune-related lncRNAs for further studies. Interestingly, 87.51% (1,030/1,177) of m6A-regulated lncRNAs were considered immune-related, which further validated our hypothesis that m6A RNA modification is deeply involved in immune-related processes. Accumulating evidence suggested that lncRNAs could directly or indirectly regulate the immune response and facilitate the occurrence of immune escape of cancer cells *via* a variety of mechanisms. Peng et al. (2022) have reported that lipopolysaccharides could effectively facilitate immune escape of hepatocellular carcinoma cells by regulating m6A modification on MIR155HG lncRNA to upregulate the PDL1 expression. However, the impact of m6A modification of lncRNAs on immune response in LUSC and the associated mechanisms have not yet been reported by experimental studies.

Unsupervised consensus clustering has become a routine method to divide samples into several typical molecular subgroups based on the expression levels of genes of interest. Gu et al. (2021) classified LUSC samples into different groups by directly incorporating m6A regulators into this clustering model. However, the research did not provide details on the differences of prognosis, immune landscape, and other information among those three distinct groups. In this study, we found that clusters categorized on the basis of m6A-regulated immune-related lncRNAs not only had different distributions of clinical outcomes and features but also represented diverse tumor microenvironment landscapes. Furthermore, we also demonstrated that m6A-regulated immune-related lncRNAs may have profound influence on clinical characteristics of LUSC patients, and the underlying mechanisms might involve changes in the tumor microenvironment. In particular, we also found that patients in the cluster featured with poor prognosis had high levels of immune and stromal scores and overexpressed immune checkpoint molecules. Thus, m6A-regulated immune-related lncRNAs could cooperate and be used as predictors of prognosis and immune response of patients with LUSC.

The risk model is a common method for predicting clinical outcomes of cancer patients. When previous studies concerning

to LUSC directly brought m6A regulators into the model, the predictive effects were often unsatisfactory (Li and Zhan, 2020). In the present study, we established a risk model by means of 12 m6A-regulated immune-related lncRNAs selected by univariate and multivariate Cox regression analyses. In particular, all the lncRNA expression levels, clinical features, prognosis, TME landscapes, and drug sensitivities varied between the two risk groups. Thus, our risk model not only had a certain degree of clinical prediction significance but also provided guidance for personalized treatment in terms of immune-related mechanisms.

We noticed that the infiltration levels of $CD4^+$ T cells, $CD8^+$ T cells, NK cells, cancer-associated fibroblasts, and endothelial cells increased with the elevation of risk scores. Growing evidence has accumulated that $CD4^+$ and $CD8^+$ T cells are important in proinflammatory response and anticancer immunity, leading to a more favorable clinical outcome (Schneider et al., 2021). However, we did not observe such prognosis in patients with high risk scores because of the following possible reasons. First, most infiltrating T cells in tumors might stay in a dysfunctional state, and these "exhausted" T effectors may have lost their inhibitory control of cancers in spite of high infiltration levels (Chen and Mellman, 2017). Second, existing evidence indicated that the stroma cells, like cancer-associated fibroblasts, could directly interact with T cells, suppressing the immune response *via* immune checkpoint activation (Lakins et al., 2018).

Previous studies have categorized tumors into three different immune subtypes including the inflamed phenotype, immune-excluded phenotype, and immune-desert phenotype based on infiltration levels of immune cells and expression degrees of checkpoint proteins (Chen and Mellman, 2017). Although we could not draw a conclusion as to which kind of immune phenotype that the cluster or risk group belongs to, we could still get some enlightenment from this classification system for giving patients individual immunotherapy strategies on the basis of our risk model. According to the TIDE analysis, patients in the high-risk score group were more likely to resist the immunotherapy of checkpoint inhibitors. As only fresh "exhausted" T cells were partly sensitive to PD1/PDL1 inhibitors and "hyperexhausted" T cells might be totally unrecoverable under immunotherapies, PD1/PDL1 blockade combined with other methods that enhanced the efficiency of immunotherapy would be important for this group of patients. Moreover, according to the KEYNOTE-407 study, patients with advanced LUSC could still benefit from pembrolizumab combined with chemotherapy, regardless of positive or negative PDL1 expression (Zhao and Wang, 2020). Our study revealed that there was no significant difference in the PDL1 expression level between high- and low-risk groups.

There were some limitations to our research. First, we only included TCGA-LUSC cohort into the present study. As most expression profiles of LUSC patients published in the GEO database were derived from a microarray, we could not get all the expression data on lncRNAs. Thus, additional retrospective studies with complete lncRNA information and large-scale prospective studies are needed to validate the efficiency of our risk model. Second, as all the information on these prognostic lncRNAs involved in our risk model was obtained from a public database, it is necessary to determine their expression and mutation in newly collected clinical samples and further validate their biological functions through *in vitro* and *in vivo* experiments. Third, lncRNAs have been reported to be involved in tumor immunosuppression through multiple mechanisms and both endogenous and exosome-carried lncRNAs could play an important role in such a process. The present risk model incorporated 12 m6A-regulated immune-related lncRNAs and whether these prognostic lncRNAs could be specially targeted and thus reverse the suppressive TME need further research. Finally, the specific molecular mechanisms of how the risk model could predict the TME remain unclear and need further studies.

In conclusion, the present study comprehensively analyzed the value of m6A-regulated immune-related lncRNAs in predicting clinical features, prognosis, and the tumor microenvironment for LUSC patients with a clear smoking history. Thus, our findings could provide new ideas in giving better clinical decisions and personalized immunotherapy for these patients.

Data availability statement

The original contributions presented in the study are included in the article/Supplementary Material; further inquiries can be directed to the corresponding author.

Ethics statement

The studies involving human participants were reviewed and approved by the Ethics Committee of the General Hospital of PLA. The patients/participants provided their written informed consent to participate in this study.

Author contributions

ZM and LY designed the study. ZM and ZJ collated the data and drafted the manuscript. All authors read and approved the final manuscript.

Funding

This study was supported by grants from the National Natural Science Foundation of China (21876205).

Conflict of interest

The authors declare that the research was conducted in the absence of any commercial or financial relationships that could be construed as a potential conflict of interest.

Publisher's note

All claims expressed in this article are solely those of the authors and do not necessarily represent those of their affiliated organizations, or those of the publisher, the editors, and the reviewers. Any product that may be evaluated in this article, or claim that may be made by its manufacturer, is not guaranteed or endorsed by the publisher.

Supplementary material

The Supplementary Material for this article can be found online at: https://www.frontiersin.org/articles/10.3389/fgene.2022.887477/full#supplementary-material

References

Alarcon, C. R., Lee, H., Goodarzi, H., Halberg, N., and Tavazoie, S. F. (2015). N6-methyladenosine marks primary microRNAs for processing. *Nature* 519 (7544), 482–485. doi:10.1038/nature14281

Alexandrov, L. B., Ju, Y. S., Haase, K., Van Loo, P., Martincorena, I., Nik-Zainal, S., et al. (2016). Mutational signatures associated with tobacco smoking in human cancer. *Science* 354 (6312), 618–622. doi:10.1126/science.aag0299

Cantara, W. A., Crain, P. F., Rozenski, J., McCloskey, J. A., Harris, K. A., Zhang, X., et al. (2011). The RNA modification database, RNAMDB: 2011 update. *Nucleic Acids Res.* 39 (Database issue), D195–D201. doi:10.1093/nar/gkq1028

Chen, D. S., and Mellman, I. (2017). Elements of cancer immunity and the cancer-immune set point. *Nature* 541 (7637), 321–330. doi:10.1038/nature21349

Chen, Y. J., Roumeliotis, T. I., Chang, Y. H., Chen, C. T., Han, C. L., Lin, M. H., et al. (2020). Proteogenomics of non-smoking lung cancer in East Asia delineates molecular signatures of pathogenesis and progression. *Cell* 182 (1), 226–244. doi:10.1016/j.cell.2020.06.012

Chen, Y., Lin, Y., Shu, Y., He, J., and Gao, W. (2020). Interaction between N(6)-methyladenosine (m(6)A) modification and noncoding RNAs in cancer. *Mol. Cancer* 19 (1), 94. doi:10.1186/s12943-020-01207-4

Desrichard, A., Kuo, F., Chowell, D., Lee, K. W., Riaz, N., Wong, R. J., et al. (2018). Tobacco smoking-associated alterations in the immune microenvironment of squamous cell carcinomas. *J. Natl. Cancer Inst.* 110 (12), 1386–1392. doi:10.1093/jnci/djy060

Esteller, M. (2011). Non-coding RNAs in human disease. *Nat. Rev. Genet.* 12 (12), 861–874. doi:10.1038/nrg3074

Goldstraw, P., Ball, D., Jett, J. R., Le Chevalier, T., Lim, E., Nicholson, A. G., et al. (2011). Non-small-cell lung cancer. *Lancet* 378 (9804), 1727–1740. doi:10.1016/S0140-6736(10)62101-0

Gu, C., Shi, X., Qiu, W., Huang, Z., Yu, Y., Shen, F., et al. (2021). Comprehensive analysis of the prognostic role and mutational characteristics of m6A-related genes in lung squamous cell carcinoma. *Front. Cell Dev. Biol.* 9, 661792. doi:10.3389/fcell.2021.661792

Hu, Q., Ye, Y., Chan, L. C., Li, Y., Liang, K., Lin, A., et al. (2019). Oncogenic lncRNA downregulates cancer cell antigen presentation and intrinsic tumor suppression. *Nat. Immunol.* 20 (7), 835–851. doi:10.1038/s41590-019-0400-7

Jiang, X., Liu, B., Nie, Z., Duan, L., Xiong, Q., Jin, Z., et al. (2021). The role of m6A modification in the biological functions and diseases. *Signal Transduct. Target. Ther.* 6 (1), 74. doi:10.1038/s41392-020-00450-x

Kasowitz, S. D., Ma, J., Anderson, S. J., Leu, N. A., Xu, Y., Gregory, B. D., et al. (2018). Nuclear m6A reader YTHDC1 regulates alternative polyadenylation and splicing during mouse oocyte development. *PLoS Genet.* 14 (5), e1007412. doi:10.1371/journal.pgen.1007412

Lakins, M. A., Ghorani, E., Munir, H., Martins, C. P., and Shields, J. D. (2018). Cancer-associated fibroblasts induce antigen-specific deletion of CD8 (+) T Cells to protect tumour cells. *Nat. Commun.* 9 (1), 948. doi:10.1038/s41467-018-03347-0

Lence, T., Akhtar, J., Bayer, M., Schmid, K., Spindler, L., Ho, C. H., et al. (2016). m(6 A modulates neuronal functions and sex determination in Drosophila. *Nature* 540 (7632), 242–247. doi:10.1038/nature20568

Li, N., and Zhan, X. (2020). Identification of pathology-specific regulators of m(6)A RNA modification to optimize lung cancer management in the context of predictive, preventive, and personalized medicine. *EPMA J.* 11 (3), 485–504. doi:10.1007/s13167-020-00220-3

Liu, H., Zhao, H., and Sun, Y. (2021). Tumor microenvironment and cellular senescence: Understanding therapeutic resistance and harnessing strategies. *Semin. Cancer Biol.* doi:10.1016/j.semcancer.2021.11.004

Liu, J., and Jia, G. (2014). Methylation modifications in eukaryotic messenger RNA. *J. Genet. Genomics* 41 (1), 21–33. doi:10.1016/j.jgg.2013.10.002

Pan, Y., Han, H., Labbe, K. E., Zhang, H., and Wong, K. K. (2021). Recent advances in preclinical models for lung squamous cell carcinoma. *Oncogene* 40 (16), 2817–2829. doi:10.1038/s41388-021-01723-7

Peng, L., Pan, B., Zhang, X., Wang, Z., Qiu, J., Wang, X., et al. (2022). Lipopolysaccharide facilitates immune escape of hepatocellular carcinoma cells via m6A modification of lncRNA MIR155HG to upregulate PD-L1 expression. *Cell Biol. Toxicol.* doi:10.1007/s10565-022-09718-0

Ringquist, R., Ghoshal, D., Jain, R., and Roy, K. (2021). Understanding and improving cellular immunotherapies against cancer: From cell-manufacturing to tumor-immune models. *Adv. Drug Deliv. Rev.* 179, 114003. doi:10.1016/j.addr.2021.114003

Schneider, E., Winzer, R., Rissiek, A., Ricklefs, I., Meyer-Schwesinger, C., Ricklefs, F. L., et al. (2021). CD73-mediated adenosine production by CD8 T cell-derived extracellular vesicles constitutes an intrinsic mechanism of immune suppression. *Nat. Commun.* 12 (1), 5911. doi:10.1038/s41467-021-26134-w

Socinski, M. A., Obasaju, C., Gandara, D., Hirsch, F. R., Bonomi, P., Bunn, P. A., Jr., et al. (2018). Current and emergent therapy options for advanced squamous cell lung cancer. *J. Thorac. Oncol.* 13 (2), 165–183. doi:10.1016/j.jtho.2017.11.111

Tekpli, X., Lien, T., Rossevold, A. H., Nebdal, D., Borgen, E., Ohnstad, H. O., et al. (2019). An independent poor-prognosis subtype of breast cancer defined by a distinct tumor immune microenvironment. *Nat. Commun.* 10 (1), 5499. doi:10.1038/s41467-019-13329-5

Tong, J., Flavell, R. A., and Li, H. B. (2018). RNA m(6)A modification and its function in diseases. *Front. Med.* 12 (4), 481–489. doi:10.1007/s11684-018-0654-8

Wang, X., Lu, Z., Gomez, A., Hon, G. C., Yue, Y., Han, D., et al. (2014). N6-methyladenosine-dependent regulation of messenger RNA stability. *Nature* 505 (7481), 117–120. doi:10.1038/nature12730

Xiang, Y., Laurent, B., Hsu, C. H., Nachtergaele, S., Lu, Z., Sheng, W., et al. (2017). RNA m(6)A methylation regulates the ultraviolet-induced DNA damage response. *Nature* 543 (7646), 573–576. doi:10.1038/nature21671

Xu, P., Hu, K., Zhang, P., Sun, Z. G., and Zhang, N. (2022). Hypoxia-mediated YTHDF2 overexpression promotes lung squamous cell carcinoma progression by activation of the mTOR/AKT axis. *Cancer Cell Int.* 22 (1), 13. doi:10.1186/s12935-021-02368-y

Xu, Q., Xu, H., Deng, R., Wang, Z., Li, N., Qi, Z., et al. (2021). Multi-omics analysis reveals prognostic value of tumor mutation burden in hepatocellular carcinoma. *Cancer Cell Int.* 21 (1), 342. doi:10.1186/s12935-021-02049-w

Zhang, C., and Jia, G. (2018). Reversible RNA modification N(1)-methyladenosine (m(1)A) in mRNA and tRNA. *Genomics Proteomics Bioinforma.* 16 (3), 155–161. doi:10.1016/j.gpb.2018.03.003

Zhang, L., Luo, Y., Cheng, T., Chen, J., Yang, H., Wen, X., et al. (2021). Development and validation of a prognostic N6-methyladenosine-related immune gene signature for lung adenocarcinoma. *Pharmgenomics. Pers. Med.* 14, 1549–1563. doi:10.2147/PGPM.S332683

Zhao, B. S., Roundtree, I. A., and He, C. (2017). Post-transcriptional gene regulation by mRNA modifications. *Nat. Rev. Mol. Cell Biol.* 18 (1), 31–42. doi:10.1038/nrm.2016.132

Zhao, X., and Wang, J. (2020). KEYNOTE-407: New hope for the treatment of lung squamous cell carcinoma. *Transl. Lung Cancer Res.* 9 (2), 418–420. doi:10.21037/tlcr.2020.03.12

Zheng, J., Zhao, Z., Wan, J., Guo, M., Wang, Y., Yang, Z., et al. (2021). N-6 methylation-related lncRNA is potential signature in lung adenocarcinoma and influences tumor microenvironment. *J. Clin. Lab. Anal.* 35 (11), e23951. doi:10.1002/jcla.23951

Zhou, B., and Gao, S. (2021). Comprehensive analysis of clinical significance, immune infiltration and biological role of m(6)A regulators in early-stage lung adenocarcinoma. *Front. Immunol.* 12, 698236. doi:10.3389/fimmu.2021.698236

Frontiers in Genetics

Highlights genetic and genomic inquiry relating to all domains of life The most cited genetics and heredity journal, which advances our understanding of genes from humans to plants and other model organisms. It highlights developments in the function and variability of the genome, and the use of genomic tools.

Discover the latest Research Topics

See more →

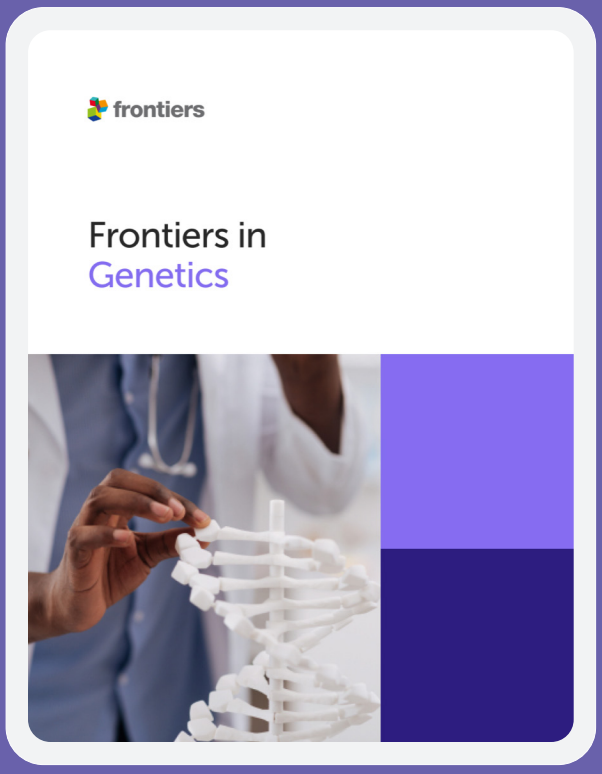

Frontiers

Avenue du Tribunal-Fédéral 34
1005 Lausanne, Switzerland
frontiersin.org

Contact us

+41 (0)21 510 17 00
frontiersin.org/about/contact